VIETNAM ATOMIC ENERGY COMMISSION

The ANNUAL REPORT for 2008

Hanoi, 12-2009

VIETNAM ATOMIC ENERGY COMMISSION

The ANNUAL REPORT for 2008

Editorial board:

Porf. Vuong Huu Tan, Chief Editor
Dr. Le Van Hong
Mr. Nguyen Hoang Anh
Ms. Dang Thi Hong
Mr. Nguyen Trong Trang

Hanoi, 12 - 2009

The VAEC Annual Report for 2008 has been prepared as an account of works carried out at VAEC for the period 2008. Many results presented in the report have been obtained in collaboration with scientists from national and overseas universities and research institutions.

The ANNUAL REPORT for 2008
Edited by
Vietnam Atomic Energy Commission
59 Ly Thuong Kiet, Hanoi
Vietnam
Chairman: Prof. Dr Vuong Huu Tan
Tel: +84-4-9422756
Fax: +84-4-9424133

This report is available from:

Training and Information Division
Dept. of Planning and R&D Management
Vietnam Atomic Energy Commission
59 Ly Thuong Kiet, Hanoi
Vietnam
Tel: +84-4-9423591
Fax: +84-4-9424133
E-mail: hq.vaec@hn.vnn.vn
infor.vaec@hn.vnn.vn

CONTENTS

Preface

The research activities of the Vietnam Atomic Energy Commission (VAEC) during the period from 1 January to 31 December 2008 are presented in this Report. The research activities are focused on the following fields:

1. Nuclear Physics;
2. Reactor Physics, Reactors and Nuclear Power;
3. Instrumentation;
4. Industrial Applications;
5. Applications in Ecology, Environment and Geology;
6. Applications in Biology, Agriculture and Medicine;
7. Radiation Protection and Radioactive Waste Management;
8. Radiation Technology;
9. Radiochemistry and Materials Science;
10. Computation and Other Related Topics.

The total number of permanent staff working at the VAEC as December 31, 2008 was 744 including the clerical service staff. The VAEC was funded from the Government with the amount to 68.266 billion VN Dong for FY 2008. The international support for the VAEC activities is committed to over 3.87 million USD including equipment, staff training and expert services.

Main results of fundamental and applied research implemented in the year were presented in 93 scientific articles, reports and contributions published in many journals, proceedings of conferences, etc. These results were obtained on the basic of the technical cooperation projects (14 VIE projects, 22 RAS projects), the research contracts with the IAEA (16 RCs), the research contracts with the Government, the Ministry of Science, Technology, Vietnam Atomic Energy Commission and the National Program for Fundamental Research (totally 85).

During the time of year 2008, in the VAEC there were 3 graduated in Ph.D. courses; about 210 people have been trained abroad in the fields of nuclear science and technology.

Prof. Dr. Vuong Huu Tan

Chairman, VAEC

1. Contributions

1.1 - Nuclear Physics

THE QUARK-MESON COUPLING MODEL BEYOND THE MEAN FIELD THEORY

Nguyen Tuan Anh, Tran Huu Phat, Le Viet Hoa and Nguyen Van Long

Institute for Nuclear Science and Technology, VAEC

Abstract: A explicit quark model, based on quark degrees of freedom, with quarks coupled to their scalar and vector condensates. The model describes nuclear matter as non-overlapping nucleon bags bound by the self-consistent exchange of scalar and vector mesons, that produces a mechanism for saturation. We obtain a new expression of effective nucleon mass, which depends on the scalar density factor. Finally, we compare this model with the four-quark model for nuclear matter.

1. Introduction

The general success of nuclear physics strongly suggests that nucleons and mesons are the appropriate degrees of freedom for the description of the nucleus at low energy. However, the success of the quark model in explaining the elementary particle phenomenology leaves little room to another interpretation than the nucleon is made out of three quarks. To incorporate the composite nature of the nucleon without losing the successful phenomenology of QHD, Guichon and others [1] constructed a simple generalization of QHD [2], in which the point-line nucleon was replaced by a bag and the sigma and omega mesons coupled to the confined quarks. Technically, the expression for the energy of nuclear matter in the Guichon model is identical to that in QHD. The only place that the internal structure of the nucleon enters is in the equation for the mean scalar field, where the sigma-nucleon coupling constant is replaced by derivation of the effective nucleon mass to sigma field. The other success of the Guichon model is to lead to a reasonable value for the nuclear incompressibility.

In this paper, let us assume that infinite nuclear matter at moderate density is a uniform distribution of nucleons interacting through the exchange of mesons which are coupled directly to the quarks. The mesons are created by quark-antiquark condensates, in the following, they will be treated as the mean fields. We intend to study here nuclear matter at finite temperature beyond the mean field approximation.

This paper is organized as follows. In section 2, we recapitulate the model for nuclear matter at finite temperature. In section 3, we calculate numerical the model. Finally, in section 4, we summarize the results as obtained in this model, discuss its relation with the four-quark model [3] and present an outlook.

2. The Model for Nuclear Matter

If we adopt the static spherical bag model to describe the quark structure of one nucleon located at origin of the coordinates, the Lagrangian for the four-quark model written by the Nambu-Jona-Lasinio -like form,

$$L = [\overline{\psi}^q (i\gamma^\mu \partial_\mu - m_q)\psi^q - \frac{1}{4} G^a_{\mu\nu} G^{a\mu\nu}]\theta_V + \frac{G_s^{q2}}{2}(\overline{\psi}^q \psi^q)^2 - \frac{G_v^{q2}}{2}(\overline{\psi}^q \gamma^\mu \psi^q)^2, \qquad (1)$$

where m_q is the current quark mass, G_s^q and G_v^q are the corresponding quark constants, $G_{\mu\nu}$ is the tensor of gluon field, and θ is a step function, $\theta_V = \theta(R-r)$, R is the bag radius.

After bosonization

$$\boldsymbol{\sigma} = \frac{g_\sigma^q}{m_\sigma^2}\overline{\psi}^q\psi^q, \qquad \boldsymbol{\omega}_\mu = \frac{g_\omega^q}{m_\omega^2}\overline{\psi}^q\gamma_\mu\psi^q, \tag{2}$$

we have

$$L = \left[\overline{\psi}^q(i\gamma^\mu\partial_\mu - m_q)\psi^q - B\right]\theta_V + g_\sigma^q\overline{\psi}^q\boldsymbol{\sigma}\psi^q - g_\omega^q\overline{\psi}^q\gamma^\mu\boldsymbol{\omega}_\mu\psi^q - \frac{1}{2}m_\sigma^2\sigma^2 + \frac{1}{2}m_\omega^2\omega^2, \tag{3}$$

where $G_s^q = g_\sigma^q/m_\sigma, G_v^q = g_\omega^q/m_\omega$, m_σ and m_ω are the corresponding meson masses.

In this model, nuclear matter is described in terms of non-overlapping MIT bags, and the quarks inside the bags interact directly with the scalar and vector meson fields, where, the motion of the quarks is highly relativistic and typically they move much faster than the nucleon in the medium. Thus it is reasonable to assume that the quarks always have sufficient time to adjust their motion as the nucleon responds to the medium it is in so that they stay in the lowest energy state.

Supposing that there exist condensates in medium,

$$B = \frac{1}{4}\langle G_{\mu\nu}^a G^{a\mu\nu}\rangle, \quad \sigma = \langle\boldsymbol{\sigma}\rangle = \frac{g_\sigma^q}{m_\sigma^2}\langle\overline{\psi}^q\psi^q\rangle, \quad \omega_0 = \delta_{0\mu}\langle\boldsymbol{\omega}_\mu\rangle = \frac{g_\omega^q}{m_\omega^2}\delta_{0\mu}\langle\overline{\psi}^q\gamma_\mu\psi^q\rangle, \tag{4}$$

where B plays a role as the bag parameter. Thus the quark equation of motion reads as

$$[i\gamma^\mu\partial_\mu - g_\omega^q\gamma^0\omega_0 - (m_q - g_\sigma^q\sigma)]\psi^q = 0. \tag{5}$$

The normalized solution for a quark in the s-state in the bag is given by

$$\psi_\alpha^q(\vec{r},t) = \frac{N_\alpha}{\sqrt{4\pi}}e^{-i\varepsilon_q t/R}\begin{pmatrix} j_0(xr/R) \\ i\beta_q\ \vec{\sigma}.\hat{r}\ j_1(xr/R)\end{pmatrix}\chi_q\ \theta(R-r), \tag{6}$$

where

$$\varepsilon_q = \Omega_q + g_\omega^q\omega R, \quad \beta_q = \sqrt{\frac{\Omega_q - m_q^* R}{\Omega_q + m_q^* R}}, \quad N_0^{-2} = 2R^3 j_0^2(x)[\Omega_q(\Omega_q - 1) + m_q^* R/2]/x^2, \tag{7}$$

with $\Omega_q = \sqrt{x_a^2 + (m_q^* R)^2}$, $m_q^* = m_q - g_\sigma^q\sigma$, χ_q the quark Pauli spinor. The eigen-frequency, x, of this lowest mode in medium is determined by the boundary condition at the bag surface, $j_0(x) = \beta_q j_1(x)$.

The energy of the nucleon bag is

$$E_{bag} = \sum_q n_q\frac{\Omega_q}{R} - \frac{z_0}{R} + \frac{4}{3}\pi R^3 B, \tag{8}$$

where z_0 ia a parameter accounting for the zero-point energy, n_q is the number of the quark and antiquark inside the bag,

$$n_q = n_c[n_q^+ + n_q^-], \qquad n_c = 3 = 3\sum_q [n_q^+ - n_q^-], \qquad n_q^\pm = [e^{\varepsilon_q^\pm/R\mp\mu_q)/T} + 1]^{-1}, \quad (9)$$

with $n_q^\pm$ the thermal distribution functions for the quark and antiquark, correspondingly.

After subtracting spurious center-of-mass motion inside the bag, the effective mass of the nucleon bag at rest is given as

$$M_N^* = \sqrt{E_{bag}^2 - \Sigma_q \langle p_{c.m.}^2 \rangle}, \qquad \Sigma_q \langle p_{c.m.}^2 \rangle = \Sigma_q n_q (x_q/R)^2. \quad (10)$$

The bag radius R is then obtained through

$$\frac{\partial M_N^*}{\partial R} = 0. \quad (11)$$

At finite temperature, the quarks inside the bag can be thermally excited to higher angular momentum states. However, for simplicity, we shall still assume the bag describing the nucleon to be spherical with radius R which is now temperature dependent.

The thermodynamic grand potential for the model beyond the mean field theory is

$$V = \frac{m_\sigma^2}{2}\sigma^2 - \frac{m_\omega^2}{2}\omega_0^2 + \frac{2}{\pi^2}\int_0^\infty p^2 dp\left[2E_p^* + T\ln(n_p^{*+} n_p^{*-})\right]$$
$$- \frac{4}{(2\pi)^4}\frac{g_s^2}{m_\sigma^2}\int_0^\infty k^2 dk \int_0^\infty p^2 dp[(n_p^{*+} - n_p^{*-})(n_k^{*+} - n_k^{*-}) + \frac{M_p^* M_k^*}{E_p^* E_k^*}(n_p^{*+} + n_p^{*-})(n_k^{*+} + n_k^{*-})]$$

$$- \frac{8}{(2\pi)^4}\frac{g_v^2}{m_\omega^2}\int_0^\infty k^2 dk \int_0^\infty p^2 dp[(n_p^{*+} - n_p^{*-})(n_k^{*+} - n_k^{*-}) - \frac{2M_p^* M_k^*}{E_p^* E_k^*}(n_p^{*+} + n_p^{*-})(n_k^{*+} + n_k^{*-})]. \quad (12)$$

Hence, we obtain the total energy density at finite temperature T and at finite baryon density ρ_B

$$E = V + TS + \mu\rho_B = \frac{m_\sigma^2}{2}\sigma^2 - \frac{m_\omega^2}{2}\omega_0^2 + \frac{2}{\pi^2}\int_0^\infty k^2 dk\, E_k^*(n_p^{*+} + n_p^{*-}) + \frac{2}{\pi^2}\int_0^\infty k^2 dk\, \Sigma_0 (n_p^{*+} - n_p^{*-})$$

$$- \frac{4}{(2\pi)^4}\frac{g_s^2}{m_\sigma^2}\int_0^\infty k^2 dk \int_0^\infty p^2 dp[(n_p^{*+} - n_p^{*-})(n_k^{*+} - n_k^{*-}) + \frac{M_p^* M_k^*}{E_p^* E_k^*}(n_p^{*+} + n_p^{*-})(n_k^{*+} + n_k^{*-})]$$

$$- \frac{8}{(2\pi)^4}\frac{g_v^2}{m_\omega^2}\int_0^\infty k^2 dk \int_0^\infty p^2 dp[(n_p^{*+} - n_p^{*-})(n_k^{*+} - n_k^{*-}) - \frac{2M_p^* M_k^*}{E_p^* E_k^*}(n_p^{*+} + n_p^{*-})(n_k^{*+} + n_k^{*-})],$$

where the entropy density is

$$S = -\frac{2}{\pi^2}\int_0^\infty k^2 dk[\frac{\mu^*}{T}(n_k^{*+} - n_k^{*-}) - \frac{E_k^*}{T}(n_k^{*+} + n_k^{*-}) + \frac{2E_k^*}{T} + \ln(n_k^{*+} n_k^{*-})]$$
$$= -\frac{2}{\pi^2}\int_0^\infty k^2 dk[n_k^{*+}\ln(n_k^{*+}) + (1 - n_k^{*+})\ln(1 - n_k^{*+}) + n_k^{*-}\ln(n_k^{*-}) + (1 - n_k^{*-})\ln(1 - n_k^{*-})],$$

and the baryon density is

$$\rho_B = \frac{2}{\pi^2}\int_0^\infty k^2 dk\ (n_k^{*+} - n_k^{*-}), \qquad n_k^{*\pm} = [e^{(E_k^* \mp \mu^*)/T} + 1]^{-1}, \tag{13}$$

with $n_k^{*\pm}$ the effective thermal distribution functions for the baryon and antibaryon, respectively, $E_k^* = [k^{*2} + M_N^{*2}]^{1/2}$ is the effective nucleon energy and μ^* is the effective baryon chemical potential.

The pressure is the negative of V, and after integration by parts, reduces to the familiar expression

$$P = \frac{m_\sigma^2}{2}\sigma^2 - \frac{m_\omega^2}{2}\omega_0^2 + \frac{2}{3\pi^2}\int_0^\infty dk\ \frac{k^4}{E_k^*}(n_p^{*+} + n_p^{*-})$$

$$- \frac{4}{(2\pi)^4}\frac{g_s^2}{m_\sigma^2}\int_0^\infty k^2 dk \int_0^\infty p^2 dp[(n_p^{*+} - n_p^{*-})(n_k^{*+} - n_k^{*-}) + \frac{M_p^* M_k^*}{E_p^* E_k^*}(n_p^{*+} + n_p^{*-})(n_k^{*+} + n_k^{*-})]$$

$$- \frac{8}{(2\pi)^4}\frac{g_v^2}{m_\omega^2}\int_0^\infty k^2 dk \int_0^\infty p^2 dp[(n_p^{*+} - n_p^{*-})(n_k^{*+} - n_k^{*-}) - \frac{2M_p^* M_k^*}{E_p^* E_k^*}(n_p^{*+} + n_p^{*-})(n_k^{*+} + n_k^{*-})].$$

The vector mean field ω is determined through

$$\left(\frac{\partial E}{\partial \omega_0}\right)_{R,\rho_S} = 0,\ i.e. \omega_0 = \frac{g_v \rho_B}{m_\omega^2}, \tag{14}$$

where $g_v = 3g_\omega^q$. And the scalar mean field σ is fixed by

$$\left(\frac{\partial E}{\partial \sigma}\right)_{R,\rho_B} = 0,\ i.e. \sigma = \frac{g_s}{m_\sigma^2} C(\sigma)\rho_s, \qquad \rho_s = \frac{2}{\pi^2}\int_0^\infty k^2 dk\ \frac{M^*}{E_k^*}(n_p^{*+} + n_p^{*-}), \tag{15}$$

where the scalar factor is

$$C(\sigma) = -(\frac{\partial M^*}{\partial \sigma})/g_s, \qquad \left(\frac{\partial M^*}{\partial \sigma}\right)_R = -g_\sigma^q \frac{E_{bag}}{M^*}\sum_q n_q[(1 - \frac{\Omega_q}{E_{bag}R})S(\sigma) + \frac{m_q^*}{E_{bag}}], \tag{16}$$

for B constant $B = B_0$, $g_s = 3g_\sigma^q S(0)$, and scalar density of the nucleon bag in matter is

$$S(\sigma) = \int d\vec{r}\ \overline{\psi}^q \psi^q = \frac{\Omega_q/2 + m_q^* R(\Omega_q - 1)}{\Omega_q(\Omega_q - 1) + m_q^* R/2}. \tag{17}$$

3. Numerical results

First at all, we consider at zero temperature. B_0, z_0, several values of the radius R, the scalar and vector coupling g_σ^q and g_ω^q are fitted to the saturation density and binding energy for nuclear matter, and some calculated properties of nuclear matter at saturation density are listed in Table 1.

The scalar density factor $C(\sigma)$ is shown in Fig. 1 as a function of the scalar field strength for three bag radii. We see that it is much smaller than unity and that the dependence on the bag radius is not strong. Also our effective nucleon mass plotted in

Fig. 2 shows that their dependence on the bag radius is rather weak. The binding energy with results of QHD are shown in Fig. 3. One of the successes of the model is that the nuclear compressibility, K, is well reproduced the experimentally required values $K = 180:\ 325$ MeV, whereas QHD tends to overestimate it significantly. The energy per baryon for nuclear matter is shown in Fig. 4, where nucleon volume effects are considered. The three curves correspond to the nucleon radius $R = 0, 0.6$ fm and 0.75 fm, respectively. The inclusion of finite volume effects makes the EOS for nuclear matter harder and generates a strong repulsive interaction between nucleons.

Tab 1. $B_0^{1/4}$ and z_0 corresponding to several values of the bag radius and the current quark mass. The effective nucleon mass, M_N^*, the nuclear compressibility, K, are quoted in MeV. The bottom row is for QHD. We take $m_\sigma = 550$ MeV, $m_\omega = 783$, and $M_N = 939$ MeV.

m_q (MeV)		0			5			10		QHD
R_B (fm)	0.6	0.8	1.0	0.6	0.8	1.0	0.6	0.8	1.0	
$B^{1/4}$ (MeV)	211.3	170.3	144.1	210.9	170.0	143.8	210.5	169.6	143.5	
z_0	3.987	3.273	2.559	4.003	3.295	2.587	4.020	3.317	2.614	
$g_s^2/4\pi$	6.86	6.17	5.66	6.89	6.20	5.70	6.91	6.23	5.74	7.29
$g_v^2/4\pi$	9.18	7.79	6.76	9.24	7.85	6.84	9.28	7.92	6.92	10.8
M_N^*	730	756	774	729	754	773	728	753	772	522
K	293	278	266	295	280	267	295	281	269	540

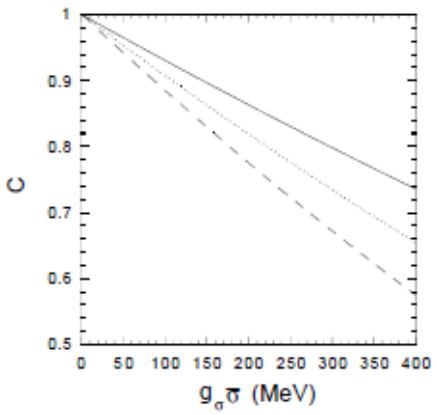

Fig. 1. Scalar density factor $C(\sigma)$ as a function of $g_\sigma\sigma$ ($m_q = 5$ MeV). The solid, dotted and dashed curves show for $R = 0.6, 0.8$ and 1.0 fm, respectively.

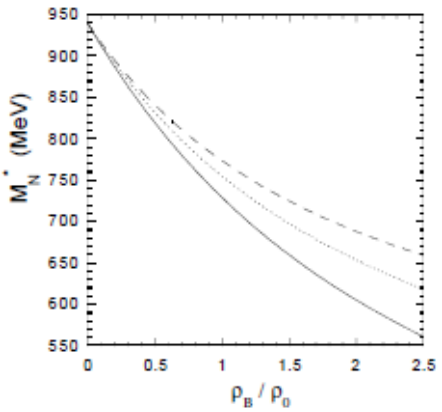

Fig. 2. Effective nucleon mass M_N^* as a function of ρ_B ($m_q = 5$ MeV). The solid, dotted and dashed curves show for $R = 0.6, 0.8$ and 1.0 fm, respectively.

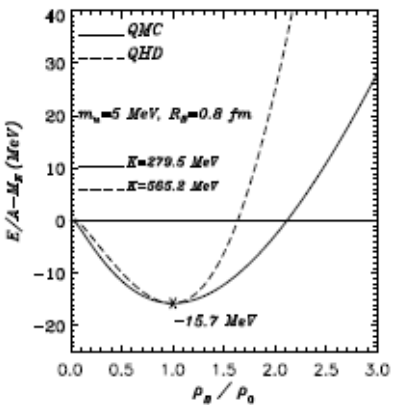

Fig. 3. Binding energy per nucleon by the quark-meson coupling (QMC) (the solid line) and quantum hadron dynamics (QHD) (the dashed line).

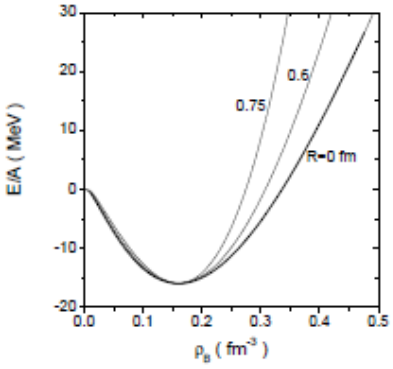

Fig. 4. The energy per baryon of nuclear matter versus baryon density. The radius of the nucleon is chosen to be 0, 0.6 fm and 0.75 fm, respectively.

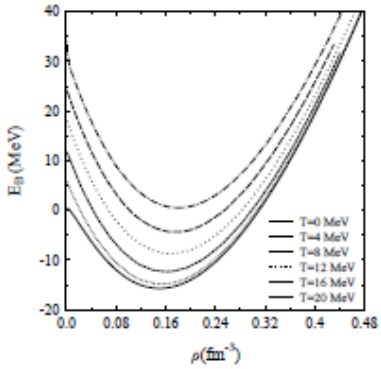

Fig. 5. Binding energy per nucleon E_B as a function of nuclear matter density, ρ_B, at temperatures T = 0, 4, 8, 12, 16 and 20 MeV.

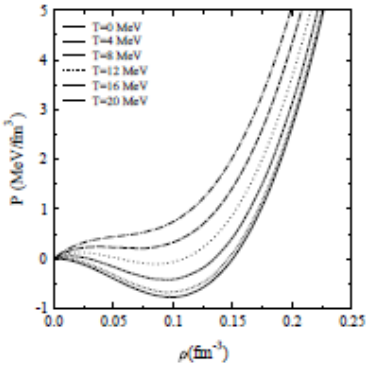

Fig. 6. Pressure P as a function of nuclear matter density, ρ_B, for symmetric matter at temperatures T = 0, 4, 8, 12, 16 and 20 MeV respectively.

At finite temperature, we plot the energy per baryon as a function of the baryon density in Fig. 5 for symmetric nuclear matter, for temperatures 0, 4, 8, 12, 16 and 20 MeV. As expected, this function at zero temperature has a minimum at the nuclear matter saturation density, ρ_0, corresponding to a binding energy of .15.7 MeV. As the temperature increases the minimum shifts towards higher densities. This may be understood from the fact that to compensate for the larger kinetic energy a larger value of ρ is needed to give the minimum. For larger densities the nuclear repulsion effects take over and again energy increases. For higher temperatures, the minimum of the curves become positive, as in the usual non-linear QHD model.

The possible existence of a liquid-gas phase transition is determined by the pressure. We plot this quantity as a function of the baryon density, ρ, for low temperatures in Fig. 6 for symmetric nuclear matter. At zero temperature, the pressure decreases with density, reaches a minimum, then increases and passes through $P = 0$ at $\rho = \rho_0$, where the binding energy per nucleon is a minimum. A decrease of the pressure with density corresponds to a negative compressibility, $K = 9(\partial P/\partial\rho)$, and is a sign of mechanical instability. As the temperature increases the region of mechanical instability decreases. At $T = 17.7$ MeV, the pocket disappears. This corresponds to the critical temperature defined by $(\partial P/\partial\rho)_{T,y_p} = 0$, $(\partial^2 P/\partial\rho^2)_{T,y_p} = 0$, above which the liquid-gas phase transition is continuous. It is comparable to the values for the critical temperature obtained with Skyrme interactions or relativistic models.

4. Conclusion and Outlook

We now summarize the results and conclusions of the present work. We would like to stress the successful generalization of the this model opens a tremendous number of opportunities for further work. Although there are a number of important ways in which this model could be extended, the present model can be applied to all the problems for which QHD has proven so attractive, with very little extra effort. We have

studied symmetric nuclear matter at finite temperature using the quark-meson coupling model which incorporates explicitly quark degrees of freedom. The mean effective fields σ and ω are determined from the minimization of the thermodynamical potential, and the temperature dependent effective bag radius was calculated from the minimization of the effective mass of the nucleon mass of the bag. The thermal contributions of the quarks, which are absent in the QHD model, are dominant and lead to a rise of the effective nucleon mass at finite temperature. In the present calculation, the effective radius of the nucleon bag shrinks with increase of the temperature. The equation of state as derived here is softer than the ones obtained within the non-linear QHD model for all temperatures. The region of mechanical instability decreases with the increase of T .

In the simple QMC model, the bag parameter B is taken as constant B_0 corresponding to the bag parameter for a free nucleon. The nuclear medium effects are taken into account in the modified QMC model. At the end, we show the relation between the modified QMC model with the four quark model for nuclear matter [3].

Actual calculations using a relativistic oscillator in an external field, where the spurious center-of-mass motion is very small, thus the effective nucleon mass is obtain

$$M_N^* = n_c\sqrt{(m_q^* + \frac{V}{3}B)^2 + \frac{z_0^2}{R^2} + \frac{2VB}{3}0[\langle p_{c.m.}\rangle^2] - 2\frac{\Omega z_0}{R^2} - 2\frac{VB}{3}\frac{z_0}{R}};\ \ n_c(m_q^* + \frac{V}{3}B).$$

Comparing this equation with the expression of the effective nucleon mass of the four-quark model for nuclear matter [3],

$$M_q^{*QC} = m_q - \frac{g_\sigma^{q2}}{m_\sigma^2}\langle\overline{\psi}^q\psi^q\rangle_{med.} + \frac{g_\sigma^{q2}}{m_\sigma^2}\langle\overline{\psi}^q\psi^q\rangle_{vac.},$$

we obtain

$$M_N^{*QMC} = n_c M_q^{*QC},$$

$$\frac{V}{3}B = \frac{g_\sigma^{q2}}{m_\sigma^2}\langle\overline{\psi}^q\psi^q\rangle_{vac.} = \frac{g_\sigma^{q2}}{m_\sigma^2}\frac{2n_c}{\pi^2}\int_0^\Lambda k^2 dk\,\frac{M_q^*}{E_k^*},$$

where Λ is the momentum cutoff.

Hence, we realize that the four-quark model for nuclear matter is similar to the modified quark-meson coupling model, where the bag parameter depends on the medium, in this case, it connects to the effective nucleon mass in the medium.

References

[1]. P. A. Guichon, Phys. Lett. B200 (1988) 235; P. A. Guichon, K. Saito, E. N. Rodionov, and A. W. Thomas, Nucl. Phys. **A601**, 349 (1996); K. Saito, K. Tsushima, and A. W. Thomas, Phys. Rev. **C55**, 2637 (1997); P. G. Blunden and G. A. Miller, Phys. Rev. **C54**, 359 (1996); X. Jin and B. K. Jenning, Phys. Rev. **C54**, 1427 (1996); G. Krein, A. W. Thomas, and K. Tsushima, Nucl. Phys. **A650**, 313 (1999).

[2]. R. J. Furnstahl and D. B. Serot, Comments Nucls. Part. Phys. 2, A23 (2000); D. B. Serot and J. D. Walecka, nucl-th/0010031; P. D. Serot and J. D. Walecka, Adv. Nucl. Phys., **16** (1985) 1; P. D. Serot and J. D. Walecka, Int. J. Mod. Phys. **E6** (1997) 515; M. Müller and B. D. Serot, Phys. Rev. **C52** (1995) 2072; M.

Nakano, A. Hasegawa, H. Kouno and K. Koide, Phys. Rev. **C49** (1994) 3061; **C49** (1994) 3076; Tran Huu Phat and Nguyen Tuan Anh , Il Nuovo cimento **A110** (1997) 475, and Il Nuovo cimento **A110** (1997) 839.

[3]. Tran Huu Phat, Nguyen Tuan Anh and Le Viet Hoa, Adv. Natur. Sci. **5** (2004) 33; Tran Huu Phat, Nguyen Tuan Anh and Le Viet Hoa, Nucl. Phys. **A722** (2003) 548c; Tran Huu Phat, Nguyen Tuan Anh, Nguyen Van Long, Le Viet Hoa, Proceedings of the 7th National Conference on Nuclear Science and Technology, August 30-31 (2007), Danang City, Vietnam.

Papers Published In Relation To The Project

On the quark-meson coupling model beyond the mean-field approximation, Submitted to journal Communication in Physics, 2008.

APPLICATION OF R-MATRIX THEORY TO DEVELOP A COMPUTER CODE FOR CALCULATIONS OF NEUTRON CAPTURE CROSS SECTION AND ANALYSIS OF RESONANCE PARAMETERS IN RESOLVE RESONANCE REGION

Pham Ngoc Son, Nguyen Canh Hai, Tran Tuan Anh, Nguyen Xuan Hai
Ho Huu Thang, Phu Chi Hoa and Vuong Huu Tan

Nuclear Research Institute, Dalat, Vietnam

Abstract: The R-matrix theory of nuclear reaction has been applied to develop a computer code for calculation of radioactive capture cross section and analysis of resonance parameters in resolve resonance energy region. The code was develop with computer language C++, and named as *"CrossComp"*. The theoretical models and techniques used in CrossComp are multilevel Reich-Moore approximation, Doppler broadening estimation with Free Gas Model and none linear multi-parameter least squares fit. The code was tested by make some comparison between the present calculated values and data from Jendl3.3, which present a well agreement results. As an illustration, the new experimental data of resonance parameters of nuclide La-139, reported by R. Terlizzi 2007, were used for calculation of radioactive capture cross sections in energy range from 10eV to 9keV.

I. Introduction

Nuclear data are fundamental to the development and application of all nuclear sciences and technologies [1]. Measured neutron capture cross sections data for most of nuclides are currently necessary for the calculations of neutron transport, the assessments of the reactor safety, the investigations of high-burn-up core characteristics, the decay heat power predictions, and for the nuclear transmutation study. In resonance energy region, neutron capture cross sections are special important for the study on the nuclear structure and nuclear reaction mechanism. However, the experimental data are not directly used for applications. The data should be processed to obtain a set of suitable resonance parameters of which, the applicable cross section data would be reproduced by a theoretical model of nuclear reaction. An analysis code for neutron cross-section data in the is often include of three main aspects [2], including an appropriate theoretical model for calculation of cross sections, correction procedures for experimental conditions such as Doppler broadening, multi-scattering, shelf shielding, and a fitting procedure to analysis the resonance parameters which give the "best" fit of theoretical to experimental values.

In this report, we introduce the preliminary development of a new computer code, called "*CrossComp*", for calculation of neutron cross sections and resonance parameter analysis in energy range of resolved resonances.

II. Objective

The main objective of the project is to provide an appropriate computer code for calculation and analysis of neutron capture cross sections in resolve resonance region.

III. Contents

The main contents of the project are as following: (i) to study on the R-matrix theory of nuclear reaction, Doppler broadening of resonance peaks at a given temperature condition, and fitting data procedure for determination of resonance parameters, (ii) to develop a C++ code for calculation and analysis of neutron capture cross sections in resolve resonance region, basis on R-matrix theory, (iii) to calculate the resonance neutron capture cross sections of nuclide ^{139}La by applied the present code with new experimental values of resonance parameters, reported in [3].

IV. Methods

The Reich-Moore approximation to R-matrix theory of E. P. Wigner and L. Eisenbud [4,5] has been applied to develop the present code (CrossComp). The free gas model for calculation of Doppler broadening cross section, and the Levenberg-Marquardt iterative method for none linear multi-parameter least squares fit procedure are used in the sub functions of CrossComp. The code has been tested by comparison of the present calculated values with evaluated data from Jendl3.3 [6].

V. Results and discussion

A c++ code called "CrossComp" for neutron resonance capture cross section calculation has been developed. The window interface of CrossComp is introduced in Figure 1. The results of comparison between calculated values from CrossComp and evaluated data from Jenndl3.3 is shown in Figure 2, which all most reproduce the same data in resonance region. The behavior of Doppler broadening cross section at different temperature of 0^{o}K, 10^{o}K, 100^{o}K and 300^{o}K, for resonance at 72.3eV of ^{139}La, is presented in Figure 3. The new experimental values of resonance parameters, reported by R. Terlizzi [3], were introduced into calculation for neutron resonance capture cross section of nuclide ^{139}La by using the code CrossComp. The calculated results are shown in Figures 4 and 5, in compare with data from Jendl3.3 and Endf/B6, in which some significantly different were observed, especially in energy region higher than 4keV.

Acknowledgments

The authors would like to express their thanks to the Vietnam Atomic Energy Commission (VAEC) and the Dalat Nuclear Research Institute (DNRI) for their great encouragement and financial support for this work.

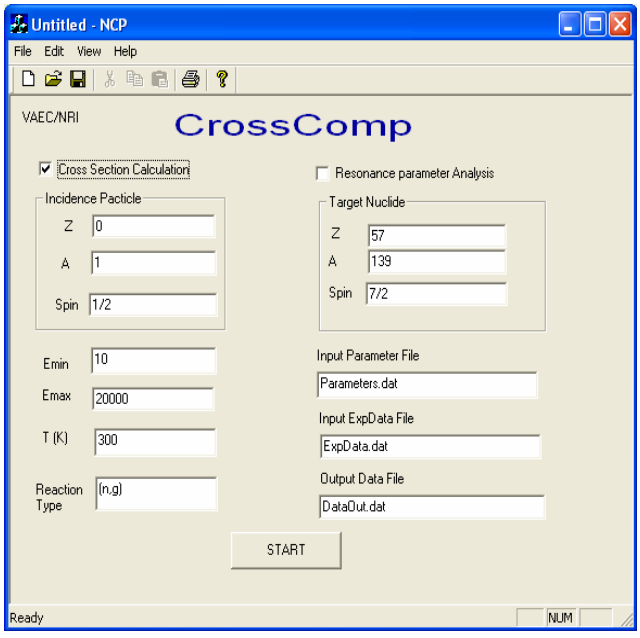

Fig. 1. The window interface of the computer code CrossComp.

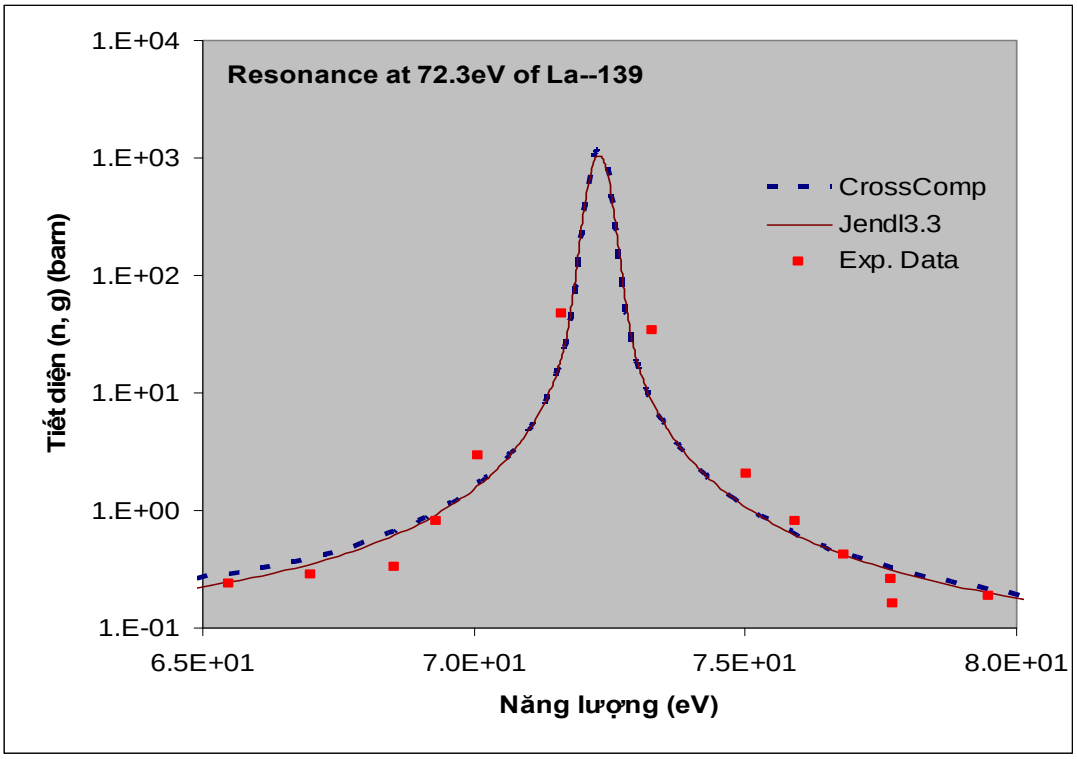

Fig. 2. The results of comparison between calculated values from Cross Comp and evaluated data from Jenndl3.3.

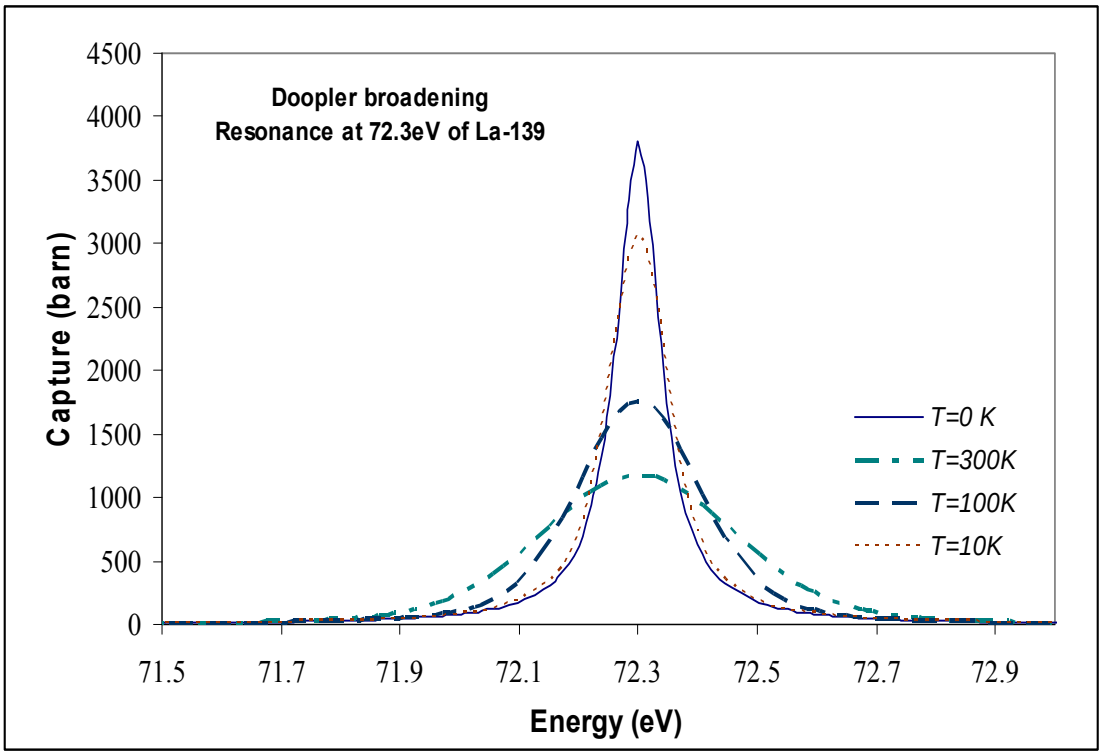

Fig. 3. The behavior of Doppler broadening cross section at different temperature for resonance at 72.3eV of ^{139}La, calculated using the code Cross Comp

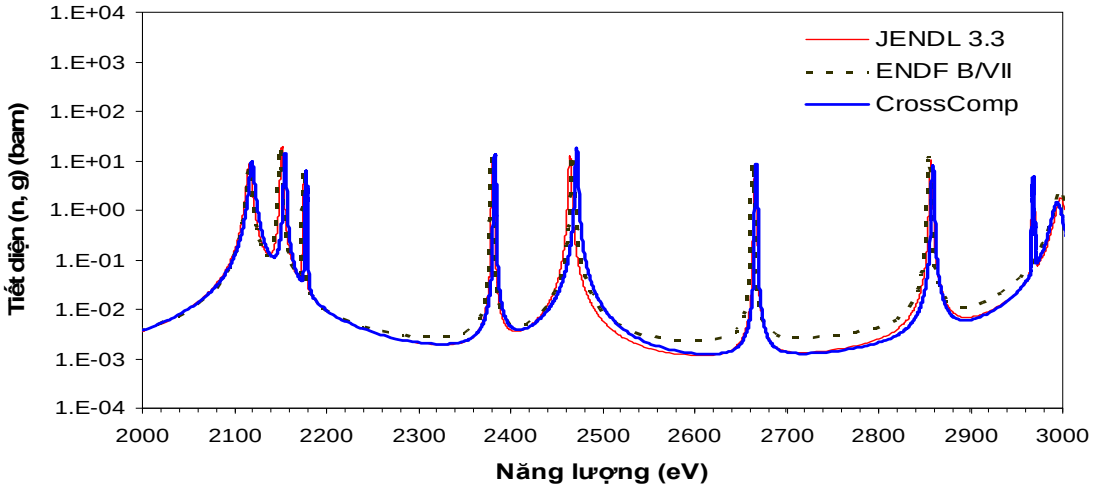

Fig. 4. Results of calculation for neutron resonance capture cross section of ^{139}La, energy range from 2keV to 3keV.

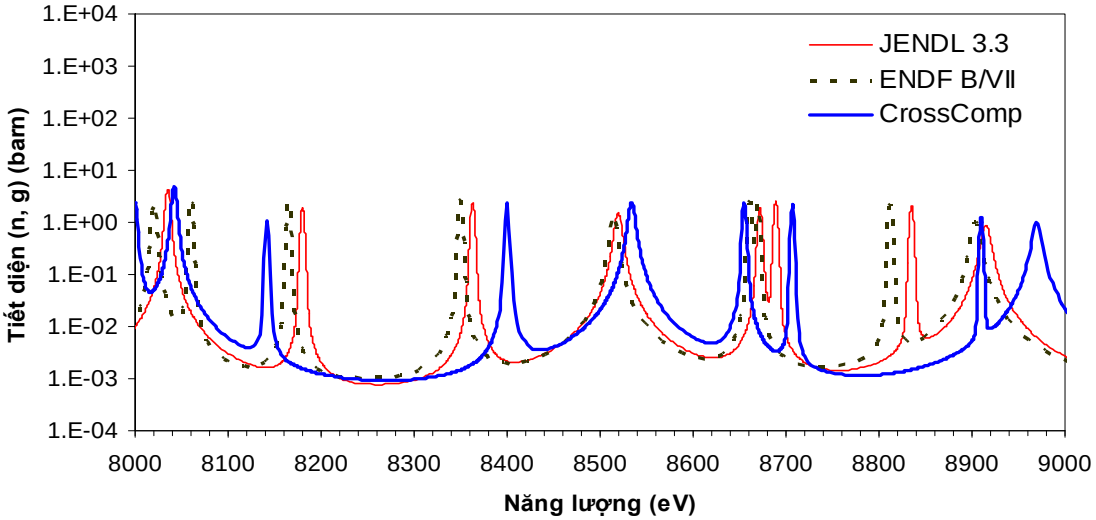

*Fig. 5***.** Results of calculation for neutron resonance capture cross section of ^{139}La, energy range from 8keV to 9keV.

Papers to be published

1. Vương Hữu Tấn, Phạm Ngọc Sơn, "Introduction to CrossComp: a computer code for analysis of neutron resonance cross section", under prepare to submit to Nuclear Science and Technology (NST), November 2009.

References

[1]. F. H. Fröhner, *Evaluation and Analysis of Nuclear Resonance Data*, JEFF Report 18, NEA/OECD (2000).

[2]. N. M. Larson, "Introduction to the Theory and Analysis of Resolved (and Unresolved) Neutron Resonances via SAMMY," in *Proceedings of the IAEA Workshop on"Nuclear Reaction Data and Nuclear Reactors: Physics, Design and Safety*, held at the International Centre for Theoretical Physics, Trieste, Italy, 23

February–27 March 1998, published by World Scientific, 1999. Also published as ORNL/M-6576, July 1998.

[3]. R. Terlizzi, et al., The ^{139}La(n, γ) cross section: Key for the onset of the *s*-process, PHYSICAL REVIEW C 75, 035807 (2007).

[4]. J. E. Lynn, *The Theory of Neutron Resonance Reactions*, Clarendon Press, Oxford (1958).

[5]. M. Lane and R. G. Thomas, R-matrix theory of nuclear reaction, *Rev. Mod. Phys.* **30**, 257 (1958).

[6]. K. Shibata, et al. "Japanese Evaluated Nuclear Data Library Version 3 Revision-3: JENDL-3.3," *J. Nucl. Sci. Technol*. 39, 1125 (2002).

Papers Published In Relation To The Project

Vương Hữu Tấn, Phạm Ngọc Sơn, Nguyễn Cảnh Hải, Trần Tuấn Anh, Nguyễn Xuân Hải, Hồ Hữu Thắng, Phù Chí Hòa; Introduction to CrossComp: a computer code for analysis of neutron resonance cross section, (to be published in the Journal of Nuclear Science and Technology; VAEC)

MICROSCOPIC STUDY OF NUCLEAR STRUCTURE AND NUCLEAR REACTION USING THE EFFECTIVE DENSITY - DEPENDENT M3Y INTERACTION

Hoang Sy Than, Dao Tien Khoa, Do Cong Cuong, Ngo Van Luyen
Nguyen Dang Chien and Nguyen Tuan Anh

Institute for Nuclear Science and Technology, VAEC

Abstract: A coupled-channel analysis of the ^{18,20,22}O(p,p') data has been performed to determine the neutron transition strengths of 2^+_1 states in Oxygen targets, using the microscopic optical potential and inelastic form factor calculated in the folding model. A complex density- and *isospin* dependent version of the CDM3Y6 interaction was constructed, based on the Brueckner-Hatree-Fock calculation of nuclear matter, for the folding model input. Given an accurate isovector density dependence of the CDM3Y6 interaction, the isoscalar δ_0 and isovector δ_1 deformation lengths of 2^+_1 states in ^{18,20,22}O have been extracted from the folding model analysis of the (p,p') data. A specific N-dependence of δ_0 and δ_1 has been established which can be linked to the neutron shell closure occurring at N approaching 16. The CDM3Y6 interaction was further used in the Hartree-Fock calculation of asymmetric nuclear matter, and a realistic estimation of the nuclear symmetry energy has been made. The nuclear pressure P was calculated in order to make the comparison with the experimental data of symmetric nuclear matter extracted from analyzing the collective flow data from relativistic heavy-ion collisions. Following is a short summary of the research results published recently by our group, under the support by Vietnam Atomic Energy Commission (Project Nr. CS/08/04-02).

In general, the isospin-dependent part of the nucleon-nucleus optical potential (OP) is proportional to the product of the projectile and target isospins, and the total OP can be written in terms of the isoscalar (IS) and isovector (IV) components [1] as

$$U(R) = U_0(R) \pm \varepsilon U_1(R), \varepsilon = (N - Z)/A \quad (1)$$

where the + sign pertains to incident neutron and - sign to incident proton. The strength of the Lane potential U_1 is known from (p,p) and (n,n) elastic scattering and (p,n) reactions studies, to be around 30-40% of the U_0 strength. In the first order of the collective model, inelastic nucleon-nucleus scattering cross section can be reasonably described, in the distorted-wave Born approximation (DWBA) or coupled channel (CC) formalism, with the inelastic form factor F given by `deforming' the optical potential (1) as

$$F(R) = \delta \frac{dU(R)}{dR} = \delta_0 \frac{dU_0(R)}{dR} \pm \varepsilon \delta_1 \frac{dU_1(R)}{dR} \quad (2)$$

The explicit knowledge of the deformation lengths δ_0 and δ_1 would give us important structure information about the IS and IV transition strengths of the nuclear excitation under study. We have recently suggested a compact folding method [2] to determine $\delta_{0(1)}$ based on the DWBA analysis of the (p,p') data only. In this approach, instead of deforming the OP, we build up the proton and neutron transition densities of a 2^λ-pole exitation ($\lambda \geq 2$) using the so-called Bohr-Mottelson (BM) prescription [3] separately for protons and neutrons.

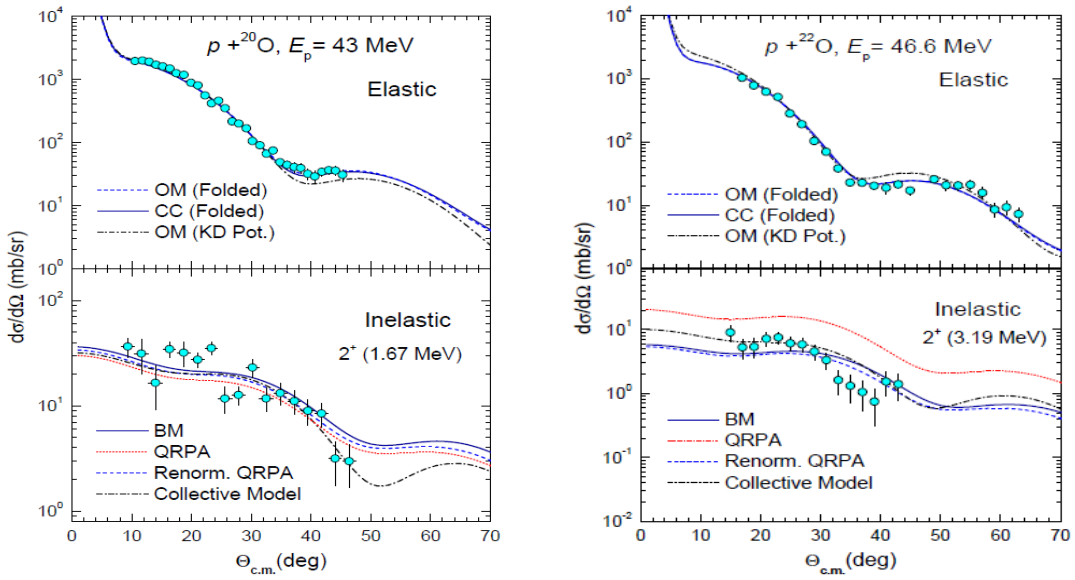

Fig. 1. Elastic and inelastic p+^{20,22}O scattering data at 43 and 46.6 MeV [4,5] in comparison with the OM and CC results given by the microscopic folded FF obtained with BM and QRPA transition densities. The collective model result is given by form factor (2) obtained with the phenomenological OP by Koning and Delaroche [6].

The folding formalism for the nucleon-nucleus OP and inelastic form factor is applied to the study of elastic and inelastic scattering of ^{18,20,22}O isotopes on proton target. The transition densities (for the low-lying 2^+ state in the oxygen isotopes) are obtained in the QRPA [4] approaches and BM prescription [3]. The elastic and inelastic ^{20,22}O+p scattering cross section data measured at E_{lab}=43 and 46.6*A* MeV are plotted in Fig. 1. In our calculations, the neutron deformation length δ_n is adjusted by the best (folding model) fit to the measured inelastic scattering data. Our folding analysis has shown quite a strong isovector mixing in the 2^+ inelastic scattering channel in the ^{20}O+p and ^{22}O+p cases.

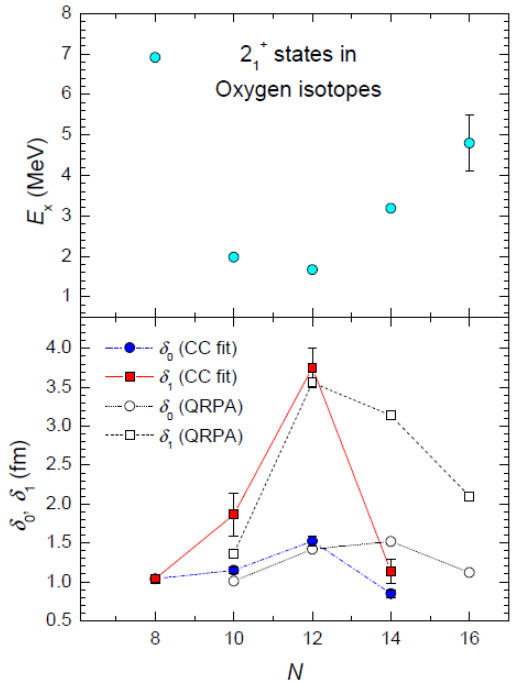

Fig. 2. Observed excitation energies (upper panel), the isoscalar (δ_0) and isovector (δ_1) deformation lengths (lower panel) of 2^+_1 states in Oxygen isotopes deduced from the folding model analyses of this work and Ref. [7] (for double-closed shell ^{16}O) and from the continuum QRPA results [4].

With a direct connection between the IV deformation and dynamic contribution by the valence neutrons to the nuclear excitation, it is natural to link the IV deformation with possible changes of the neutron shell structure. The best-fit IS and IV deformation

lengths of 2^+_1 states in Oxygen isotopes and those derived from the results of continuum QRPA calculation [4] are plotted versus the neutron number N in Fig. 2. An enhanced IV deformation (with $\delta_1>\delta_0$) resulted from the core polarization by the valence neutrons can be seen for the open-shell ^{18,20}O nuclei, with maximum of δ_1 observed for 2^+_1 state in ^{20}O or at N=12. Such a maximum of the IV deformation also corresponds to the largest M_n/M_p ratio found for 2^+_1 state in ^{20}O. With N approaching 14, the extracted δ_1 value is drastically reduced and becomes rather close to δ_0 which indicates a much weaker IV mixing in 2^+_1 excitation of ^{22}O. A similar trend has also been predicted by the continuum QRPA calculation [4], although the predicted difference between δ_1 and δ_0 still remains significant at N=14. This difference was predicted to be substantially smaller at N=16 (see open squares and circles in Fig. 2), and it is natural to suggest from the N-dependence shown in Fig. 2 that δ_1 is reaching its second minimum at N=16.

In this report we also present the results of nuclear matter calculations at various values of neutron-proton asymmetry using the CDM3Yn interactions [8]. We compare with the predictions of other types of M3Y effective interactions, namely the M3Y-P1 and M3Y-P2 interactions of Nakada [9]. Furthermore, we calculate the nuclear pressure P using these M3Y-type interactions and we compare the results with the experimental data in symmetric nuclear matter and neutron matter extracted by Danielewicz, Lacey and Lynch from analyzing the collective flow data in relativistic heavy-ion collisions [10]. For completeness, results calculated with other phenomenological interactions like the Gogny (D1S, D1N) [11,12] and Skyrme (SLy4) [13] forces are also presented.

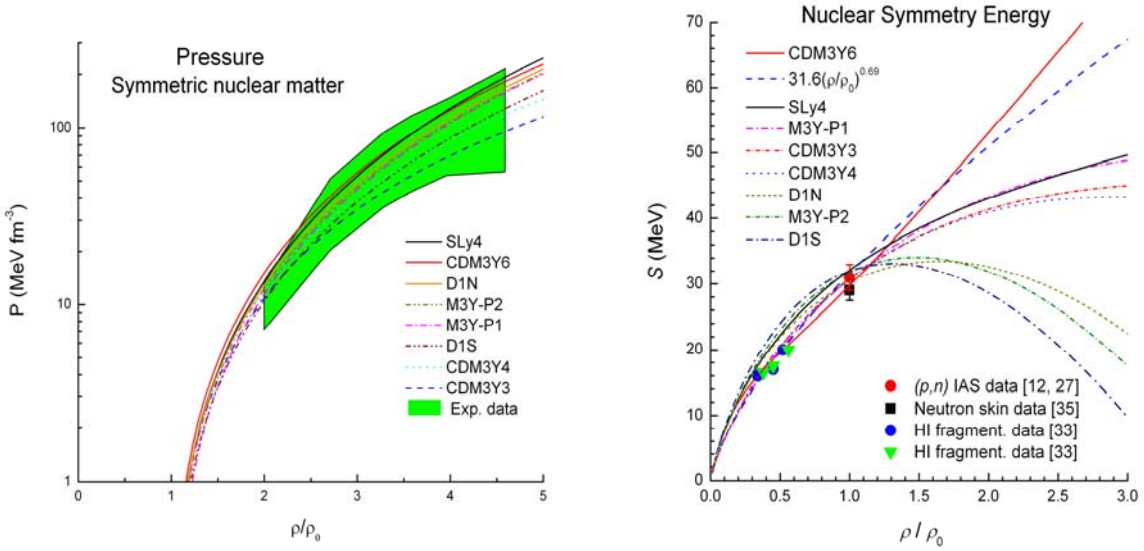

Fig. 3. Pressure as a function of density for symmetric matter (left panel). The shaded areas show the experimental constraints (from Ref. [10]) in symmetric matter. Density dependence of the nuclear symmetry energy S(ρ) (right panel). The phenomenological parametrization $S(\rho)=31.6(\rho/\rho_0)^{0.69}$ of Ref. [14] is shown for comparison. The empirical values are taken from the CC analysis of the charge exchange reactions [15}, the neutron-skin [16] and heavy ion fragmentation [14] studies.

We now discuss the predictions of pressure coming from the various models. The results are summarized in Fig. 3 where the calculated values are compared to the data [10] in the case of neutron matter and of symmetric nuclear matter in a range of density

values up to $4.5\rho_0$. In the case of symmetric matter, experimental constraints on the pressure can be extracted from the analysis of the collective flow data in relativistic heavy-ion collisions [10] in the density range of $(2\text{-}4.6)\rho_0$. In the left-panel of Fig. 3 the values of pressure P calculated with the different interactions are shown. The shaded area represents the region of experimental constraints. All models are consistent with the data at higher densities, but some predictions are at the borderline below $2.5\rho_0$.

In Fig. 3 are shown the symmetry energy curves calculated with the some interactions together with existing data extracted from charge-exchange reactions [15], neutron-skin [16] and heavy ion fragmentation studies [14]. As a general guideline is shown the parametrization $S(\rho)=31.6(\rho/\rho_0)^{0.69}$ deduced from heavy ion fragmentation data [14]. At $\rho=\rho_0$ the models predict values of $E_{sym}=S(\rho_0)$ around 29 MeV with a dispersion of about ±3 MeV. The empirical value deduced from the CC analysis of the $p(^6He,^6Li^*)n$ reaction is 31 ± 2 MeV [15]. All interactions of Fig. 3 including CDM3Y6 (E_{sym}=28.9 MeV) are within the present experimental uncertainties of E_{sym}.

In the low-density region ($\rho\sim (0.34 - 0.56)\rho_0$) there exist some empirical values extracted from heavy ion fragmentation data analysis [14]. They are represented on Fig. 3 (inverted triangles from $^{58}Fe + ^{58}Fe$ and $^{58}Ni + ^{58}Ni$ pair of reactions, solid circles from $^{58}Fe + ^{58}Ni$ and $^{58}Ni + ^{58}Ni$ pair of reactions). We should note that the analysis of heavy ion fragmentation data was based on the Antisymmetrized Molecular Dynamic (AMD) simulation [17] at finite temperatures. Thus, the comparison with predictions made for cold matter is meaningful only if temperature effects on $S(\rho)$ at low densities can be neglected.

In conclusion, a coupled channel analysis of the $^{18,20,22}O(p,p')$ scattering data has been performed, using the OP and inelastic FF calculated microscopically in a compact folding model approach, to extract the neutron transition matrixelements M_n as well as the isoscalar (δ_0) and isovector (δ_1) deformation lengths of 2^+_1 states in the Oxygen isotopes. The enhancement of the IV deformation has been confirmed again for the open-shell $^{18,20}O$ nuclei which show a strong core polarization by thevalence neutrons. Along the isotope chain, the behavior of the dynamic IVdeformation of 2^+_1 state is closely correlated with the evolution of thevalence neutron shell, and δ_1 has been found to reach its maximum at N=12. A fast decrease of the IV deformation towards N=16 should be connected with the neutron shell closure occurring at this new magic number of neutrons.

On the nuclear matter calculations , the pressure in symmetric nuclear matter, and the density dependence of the symmetry energy $S(\rho)$ are calculated. The results obtained with the CDM3Y6 interaction are consistent with the empirical bounds on pressure set by collective flow measurements in relativistic heavy ion collisions, up to $\rho\sim4.5\ \rho_0$. On the other hand, the predicted pressure curves show a wide dispersion among the different interactions considered. As for the symmetry energy $S(\rho)$, the various models span a very wide range of values beyond $\rho \geq 1.5\rho_0$ thus illustrating the difficulty of having models suitable for extrapolations.

References

[1]. A.M. Lane, Phys. Rev. Lett. **8** (1962) 171.

[2]. Dao T. Khoa, Phys. Rev. **C 68** (2003) 011601(R).

[3]. A. Bohr and B. R. Mottelson, *Nuclear Structure* (Benjamin, New York, 1975), Vol. 2.

[4]. E. Khan *et al.*, Phys. Lett. **B 490** (2000) 45.

[5]. E. Bechera *et al.*, Phys. Rev. Lett. **96** (2006) 012501.

[6]. A.J. Koning and J.P. Delaroche, Nucl. Phys. **A713** (2003) 231.

[7]. D.T. Khoa *et al.* , Nucl. Phys. **A759** (2005) 3.

[8]. D. T. Khoa, G.R. Satchler and W. von Oertzen, Phys. Rev. C **56** (1997) 954

[9]. H. Nakada, Phys. Rev. C **68** (2003) 014316.

[10]. P. Danielewicz, R. Lacey and W.G. Lynch, Science **298** (2002) 1592.

[11]. L.M. Robledo *et al.*, Phys. Lett. **B 187** (1987) 223.

[12]. F. Chappert, M. Girod, and S. Hilaire, Phys. Lett. **B 668** (2008) 420.

[13]. E. Chabanat *et al*., Nucl. Phys. **A635** (1998) 231.

[14]. D.V. Shetty, S.J. Yennello, G.A. Souliotis, Nucl. Inst. and Meth. in Phys. Res. **B261** (2007) 990.

[15]. D.T. Khoa and H.S. Than, Phys. Rev. C **71** (2005) 044601.

[16]. R.J. Furnstahl, Nucl. Phys. **A706** (2002) 85.

[17]. A. Ono, P. Danielewicz, W.A. Friedman, W.G. Lynch, and M.B. Tsang, Phys. Rev. C **68** (2003) 051601(R).

Papers Published In Relation To The Project

1. D.T. Khoa and D.C. Cuong. *Missing monopole strength of the Hoyle state in the inelastic $\alpha + {}^{12}C$ scattering*.- **Physics Letters**, 2008, **B660**, pp.331-338.
2. Nguyen Dang Chien and D.T. Khoa, *Neutron transition strengths of 2_1^+ states in the neutron rich Oxygen isotopes determined from inelastic proton scattering* . Submitted for publication in **Physical Review C**.
3. H.S. Than, D.T. Khoa and N.V. Giai, *Nuclear matter equation of state with density-dependent M3Y interactions*, ***to be submitted***.
4. Nguyễn Đăng Chiến, *Nghiên cứu vi mô tán xạ đàn hồi và phi đàn hồi của proton lên các đồng vị Oxygen*. Luận văn tốt nghiệp cao học, tháng 10/2008.

1.2 - Reactor Physics, Reactors and Nuclear Power

MONTE-CARLO DETERMINATION OF DOSE RATES IN SHPHERICAL PWR SHIELD

Le Van Ngoc, Giang Thanh Hieu and Trinh Dang Ha

Institute for Nuclear Science and Technology

Abstract: An operating nuclear reactor is a source of potentially dangerous nuclear radiation. It emits many different types of nuclear radiations. However, the neutrons and gamma rays are the main sources of radiation to give the contributions to the radiation situation in the reactor during operation, and the principal concern of reactor shielding. In current study the neutron and gamma radiation dose rates at different depths in concrete bio-shield of a PWR are calculated in spherical model by M-C simulation with using MCNP4C2. The simulation results are compared with the results obtained from similar calculations based on S_8P_3 spherical approximation with using the ANISN code.

I. Introduction

An operating nuclear reactor is a strong radiation source emitting many types of nuclear radiations. Several different types of potentially dangerous nuclear radiations created in reactor are α-particles, β-particles, recoiling fission fragments, neutrons, neutrinos, and gamma rays. The neutrons and gamma rays are produced simultaneously with the fission event, the fission fragments-highly radioactive nuclides emit α, β and γ– radiation. Neutrinos, due to small probability to interact with matter, does not play practically any role in radiation shielding problem, and is not taken into account in shielding calculations.The charged particles like α's, β's, and the heavily ionizing fission fragments, are readily stopped within, at most, a few centimeters of a dense material, so that, under normal operating conditions, most of charged particles do not penetrate beyond the fuel elements, and certainly not beyond the reactor core. Therefore, neutrons and gamma rays are the main sources of radiation to give the contributions to the radiation situation in the reactor during operation, and the principal concern of reactor shielding is to attenuate penetrative fast neutrons and energetic secondary γ-rays released in the core and shield. As the measurements of radiation levels in actual PWR shields are scarce, the calculation of these radiation levels is practically important for analyzing shield of a PWR. In this report the neutron and gamma radiation dose rates at various depths in concrete bio-shield of a PWR was calculated in spherical model by Monte-Carlo simulation based on MCNP4C2 [1].

II. Monte -carlo Calculation of Dose Rates In PWR Concrete Bio -shield

In practice of reactor shielding calculation a PWR is characterized by a spherical model [2].The assumed geometry of a PWR is specified in table 1.The neutron source distribution is given in table 2. This source distribution corresponds to the condition of operating reactor at power level of 1910 Mwatt.

The radiation field in reactor core is basically composed of neutron and gamma radiation components. Reactor gamma rays are generally divided into two categories – primary gamma rays created from fission process or the decay of fission products, and secondary gamma rays originating from the interaction of neutrons with matter, either by neutron capture or by inelastic scattering.

For Monte-Carlo calculation of neutron and gamma radiation dose rates at various depths (from the shield surface) in concrete bio-shield of a PWR in spherical model with characteristics as described in tables 1, 2 the neutron transport and the coupled transport of neutrons and photons (in a single calculation both primary neutrons and primary and secondary photons are taken into account) were simulated based on MCNP4C2 with using source biasing and Russian roulette-splitting techniques for variance reduction in calculations.

Tab 1. Spherical model for PWR shield calculation

N_0	**Region**	**Outer radius** (cm)
1	Core	154.86
2	Coolant	170.03
3	SS barrel	175.18
4	Coolant	181.15
5	SS thermal shield	187.96
6	Coolant	199.39
7	SS pressure vessel	219.39
8	Void	237.17
9	MS liner	240.98
10	Concrete	450.53

Tab 2. The neutron source distribution for PWR shield calculation

Radius (cm)	**Source** (n/cm^2-sec)	**Radius** (cm)	**Source** (n/cm^2-sec)
5	1.00E13	85	1.02E13
15	1.01E13	95	1.04E13
25	1.02E13	105	1.06E13
35	1.05E13	115	1.02E13
45	1.07E13	125	9.80E12
55	1.10E13	135	9.28E12
65	1.13E13	145	8.75E12
75	1.07E13	154.86	8.28E12

The neutrons have been simulated until their energy went down to the energy thresold of $2.5.10^{-8}$ MeV with thermalization in thermal energy range while photons have been simulated until the energy cutoff of 0.01 MeV.

The MCNP dose rate can be estimated then as

$$D_A = \frac{1}{A}\int_A F_2(r_A, E, \Omega) f(E) dE dS d\Omega$$

Here $F_2(r_A, E, \Omega)$ -surface radiation flux; *f(E)*-flux to dose rate conversion factor; *A*- surface area. The flux to dose rate conversion factors for neutrons and photons are given in [3] and used in our dose rate calculations.

The MCNP dose rates obtained by us from simulation of 2.10^9 source neutrons (for calculation of neutron dose rates with 43.5 hours of computer time on PC Pentium IV, Intel P4 2.66 GHz, Ram 256Mbx2) and 10^9 source neutrons (for caculation of gamma radiation dose rates with 114 hours of computer time on PC Pentium IV, Intel P4 2.66 GHz, Ram 256Mbx2) are given in tables 3,4 together with the results obtained from the similar calculations based on S_8P_3 spherical approximation with using the ANISN code [2] for comparision. As for total dose rates they are shown out in table 5.

We note that the relative differences between MCNP and ANISN results change from 7.1% (at depth of 9.02cm) to 339.69% (at depth of 109.02 cm) for neutron dose rates, 0.9% (at depth of 39.02 cm) to 26.18% (at depth of 89.02 cm) for gamma radiation dose rates and 5.67% (at depth of 9.02 cm) to 64.14% (at depth of 89.02 cm) for total dose rates, respectively.

Tab 3. The MCNP and ANISN neutron dose rates in concrete bio-shield of a PWR in spherical model during operation

N_0	**Depth** (cm)	**MCNP neutron dose rate** (mrem/ hr)	**ANISN neutron dose rate** (mrem/ hr)	**Relative difference** (%)
1	9.02	$(6.5250 \pm 0.0150).10^8$	$6.0930.10^8$	7.1
2	19.02	$(1.9349 \pm 0.0064).10^8$	$1.3900.10^8$	39.2
3	29.02	$(6.8794 \pm 0.0310).10^7$	$5.1700.10^7$	33.1
4	39.02	$(2.6145 \pm 0.0133).10^7$	$1.6370.10^7$	59.71
5	49.02	$(1.0374 \pm 0.0073).10^7$	$5.1700.10^6$	100.66
6	59.02	$(4.1242 \pm 0.0379).10^6$	$2.2740.10^6$	81.36
7	69.02	$(1.6533 \pm 0.0192).10^6$	$7.1809.10^5$	130.24
8	79.02	$(6.5433 \pm 0.0903).10^5$	$2.6800.10^5$	144.15
9	89.02	$(2.6589 \pm 0.0529).10^5$	10^5	165.89
10	99.02	$(1.1108 \pm 0.0296).10^5$	$3.7221.10^4$	198.3
11	109.02	$(4.3969 \pm 0.1627).10^4$	10^4	339.69
12	119.02	$(1.7001 \pm 0.0712).10^4$	$5.1700.10^3$	228.4
13	129.02	$(7.1392 \pm 0.6511).10^3$	$1.9293.10^3$	270.04
14	134.02	$(4.1411 \pm 0.4178).10^3$	10^3	314.11
15	209.55	$(8.0643 \pm 1.2822).10^{-1}$	$5.2071.10^{-1}$	54.87

Tab 4. The MCNP and ANISN gamma radiation dose rates in concrete bio-shield of a PWR in spherical model during operation

No	**Depth** (cm)	**MCNP gamma dose Rate** (mrem/ hr)	**ANISN gamma dose rate** (mrem/ hr)	**Relative difference** (%)
1	9.02	$(3.7728 \pm 0.0264).10^{7\ -2}$	$4.3867\ .10^{7}$	14
2	19.02	$(2.8081 \pm 0.0219).10^{7}$	$2.9974\ .10^{7}$	6.32
3	29.02	$(1.7773 \pm 0.0144).10^{7}$	$1.8725\ .10^{7}$	5.08
4	39.02	$(1.0090 \pm 0.0085).10^{7}$	10^{7}	0.9
5	49.02	$(5.3630 \pm 0.0526).10^{6}$	$5.1699.10^{6}$	3.74
6	59.02	$(2.7774 \pm 0.0325).10^{6}$	$2.6797.10^{6}$	3.65
7	69.02	$(1.2292 \pm 0.1018).10^{6}$	$1.1786.10^{6}$	4.29
8	79.02	$(5.8944 \pm 0.5446).10^{5}$	$5.1699.10^{5}$	14.01
9	89.02	$(3.3816 \pm 0.0680).10^{5}$	$2.6800.10^{5}$	26.18
10	99.02	$(1.6703 \pm 0.0361).10^{5}$	$1.3900.10^{5}$	20.17
11	109.02	$(7.9332 \pm 0.1960).10^{4}$	$7.1809.10^{4}$	10.48
12	119.02	$(3.9258 \pm 0.1182).10^{4}$	$3.7221.10^{4}$	5.47
13	12.02	$(1.9077 \pm 0.0700).10^{4}$	$1.6370.10^{4}$	16.54
14	134.02	$(1.3264 \pm 0.0493).10^{4}$	$1.2000.10^{4}$	10.53
15	209.55	$(7.1435 \pm 0.7458).10^{1}$	$6.1663.10^{1}$	15.85

Tab 5. The MCNP and ANISN total dose rates in concrete bio-shield of a PWR in spherical model during operation

No	**Depth** (cm)	**MCNP total dose rate** (mrem/ hr)	**ANISN total dose rate** (mrem/ hr)	**Relative difference** (%)
1	9.02	$6.9023.10^{8}$	$6.5317\ .10^{8}$	5.67
2	19.02	$2.2157.10^{8}$	$1.6897\ .10^{8}$	31.13
3	29.02	$8.6567.10^{7}$	$7.0425\ .10^{7}$	22.92
4	39.02	$3.6235.10^{7}$	$2.6370.10^{7}$	37.41
5	49.02	$1.5737.10^{7}$	$1.0340.10^{7}$	52.12
6	59.02	$6.9016.10^{6}$	$4.9537.10^{6}$	39.32
7	69.02	$2.8825.10^{6}$	$1.8967.10^{6}$	51.98
8	79.02	$1.2438.10^{6}$	$7.8499.10^{5}$	58.45
9	89.02	$6.0405.10^{5}$	$3.6800.10^{5}$	64.14
10	99.02	$2.7811.10^{5}$	$1.7622.10^{5}$	57.82
11	109.02	$1.2330.10^{5}$	$8.1810.10^{4}$	50.72

12	119.02	$5.6259.10^4$	$4.2391.10^4$	32.72
13	129.02	$2.6216.10^4$	$1.8299.10^4$	43.27
14	134.02	$1.7442.10^4$	$1.3000.10^4$	34.17
15	209.55	$7.2241.10^1$	$6.2184.10^1$	16.17

At the outermost shield surface (corresponding to the depth of 209.55 cm) the above relative difference is 54.87% for neutron dose rate and 15.85% for gamma radiation dose rate while for total dose rate this relative difference is 16.17% .

The differences between MCNP and ANISN dose rates may be explained by the fact that the different computational methods and nuclear data sources are used in MCNP4C2 and ANISN codes. Meanwile dose rate calculations with using MCNP4C2 are based on Monte-Carlo method (probabilistic method of calculation). Neutrons and gamma rays are divided into 30 and 12 different energy groups for transport calculation, respectively, similar calculations with using the ANISN code are based on discrete ordinate method (deterministic method of calculation) with approximations of 22 energy groups for neutron and 18 energy groups for gamma ray.

III. Conclusion

The neutrons and gamma rays are the main sources of radiation to give the contributions to the radiation situation in the reactor during operation. Calculation of radiation levels in PWR shield is practically important for shield analysis. In the study presented here neutron and gamma radiation dose rates at different depths in concrete bio-shield of a PWR were calculated in spherical model by Monte-Carlo simulation with using MCNP4C2.The comparision of the simulation and ANISN results has shown out that the relative differences between MCNP and ANISN dose rates vary from 7.1% to 339.69% for neutron dose rates, 0.9% to 26.18% for gamma radiation dose rates and 5.67% to 64.14% for total dose rates while at the outermost shield surface (corresponding to the depth of 209.55 cm) these are 54.87% for neutron dose rate, 15.85% for gamma radiation dose rate and 16.17% for total dose rate, respectively.

References

[1]. MCNP4C2 – Monte-Carlo N-particle transport code system, Oak Rid.ge National, Laboratory, Radiation Safety Information and Computational Center, U.S.A, 2001.

[2]. American National Standard ANSI/ANS-6.4-1997.

[3] American Natinal Standard ANSI/ANS-6.4-1977.

[4]. A.A Abagian et al. Secondary gamma-radiation in radiative shielding, Moscow, Energoatomizdat, 1984.

[5]. Maeda, S. Characterization of neutron fields using MCNP in the experimental fast reactor JOYO. Journal ASTM International (JAI), vol3, N8, 2006.

Papers Published In Relation To The Project

Le Van Ngoc, Giang Thanh Hieu, Trinh Dang Ha; Monte-Carlo determination of dose rates in shpherical PWR shield, submitted to Journal “Communication in Physics” for publication.

ROSSI-α PARAMETER MEASUREMENT OF DALAT NUCLEAR REACTOR BY ANALYSIS OF CROSS POWER SPECTRAL DENSITY OBTAINED FROM TWO ION CHAMBERS

Nguyen Minh Tuan, Tran Tri Vien, Trang Cao Su
Tran Quoc Duong and Tran Thanh Tram

Nuclear Research Institute, Dalat, Vietnam

Abstract: Analysis of reactor power level fluctuations from neutron ion chambers placed in the reactor is a powerful tool in experimental study of nuclear reactor. This method allows us to determine the important kinetic parameters such as Rossi-α parameter (prompt neutron decay constant), reactivity, square module of reactor transfer function, effective delayed neutron fractions and neutron generation time, etc.

In this report, the authors present basis on theory, system of equipment used to measure power spectral density (PSD) and cross power spectral density (CPSD) of signals obtained from 2 KHK-56 ion chambers placed in the Dalat nuclear reactor. By fitting of the theoretical curves with the measured curves, Rossi-α parameter is determined.

Keywords: Ion-chamber (I.C), Reactivity (ρ), Transfer function (H(ω)), Power spectral density (PSD), Cross-power spectral density (CPSD), Autocorrelation, Rossi-α parameter, Neutron generation time (ℓ).

I. Introduction

Noise is a general concept referring to the internal noise or interference, which superimpose on the measured signal, it is very difficult or there is no way to remove them. However, in many cases, noise reflects the nature and status of the system which we are interested in. Method of noise study is aimed at itself noise signal in order to detect and get. the necessary information.

When a nuclear reactor operating in the equilibrium status, the measured power level output from neutron detector is not always a stable value and fluctuates with very small amplitude around the average value. These fluctuations are not completely random and follow a certain distribution rules. These rules can be determined from experiments, which contain important information related to reactor kinetics parameters.

The main causes of these fission reaction fluctuations come from the random nature of the physics processes occurring in the nuclear reactor, for example fission process, slowdown, diffusion and absorption, … These processes are primarily follow Poisson distribution law. Due to these fluctuation occurred in neutron multiply medium (nuclear reactor medium) will lead to reactor power level fluctuation. When these fluctuations are small compared with the average value and the core multiply coefficient of k is approximately equal to 1, a approximate, nuclear reactor may be considered as a linear dynamics system and square transfer function module is proportion to power spectrum density (PSD). PSD can be determined by Fourier expansion of

autocorrelation of signal obtained from a compensated ion chamber which is used to measure reactor power level. Reactor kinetic parameters can be determined by analyzing autocorrelation, PSD or CPSD, experimentally.

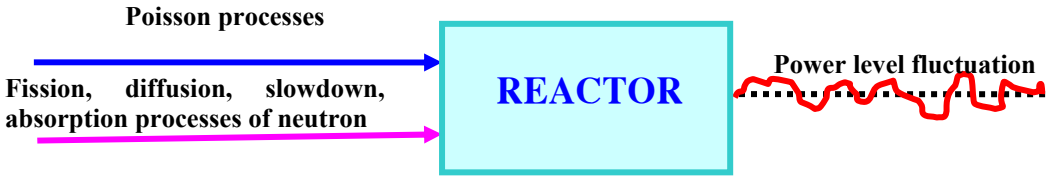

Fig. 1. Model of power level fluctuations in a nuclear reactor

In this report, the authors present basis on theory, system of equipment used to measure power spectral density (PSD) and cross power spectral density (CPSD) of signals obtained from 2 KHK-56 ion chambers placed in the Dalat nuclear reactor. By fitting of the theoretical curves with the measured curves, Rossi-α parameter is determined.

II. Summary Of Theoretical Basis

Theoretical basis of noise method using PSD and CPSD functions is presented here mainly taken from references [1].

With assumption that: k≈1 and power level fluctuation in the reactor is small in comparison with its average value, in this case the reactor can be considered as a linear kinetics system and the equation expressed the relationship between input and output signals of the system can be established as follows:

$$G_{yy}(\omega) = |H(\omega)|^2 G_{xx}(\omega) \tag{1}$$

In which:

- $\omega = 2\pi f$: angular frequency (rad/s)
- f: frequency (Hz)
- $G_{xx}(\omega)$: PSD of the input signal
- $G_{yy}(\omega)$: PSD of the output signal
- H(ω): zero power reactor transfer function

It is well known that zero-power reactor transfer function is given by [1] :

$$H(\omega) = \frac{n}{i\omega\left(\ell + \sum_i \left(\frac{\beta_i}{\lambda_i + i\omega}\right)\right)} \approx \frac{n}{i\omega/\ell + \beta}, \text{ when } \omega > \lambda_i \tag{2}$$

Due to the fluctuation of reactor input signal have random nature ($G_{xx}(\omega) \approx$ constant), from eq. 1 and 2, PSD of reactor output signal is taken the form as follows:

$$G_{yy}(\omega) = \frac{A}{\omega^2 + \alpha^2} + B \tag{3}$$

When performing more in detail calculations, the coefficient A and B are obtained:

$$A = \frac{2\varepsilon^2 q^2}{\ell n}\left(\frac{\overline{\nu^2} - \bar{\nu}}{\bar{\nu}}\right) \quad (4)$$

$$B = \frac{2q^2 \varepsilon n}{\ell} \quad (5)$$

Where:

- β_i, λ_i : abundance and decay constant of the i[th] delay neutron group
- $\alpha = \frac{\rho - \beta_{eff}}{k\ell}$: decay constant of prompt neutron
- q : average electric charge generated in the C.I.C when it absorbs one neutron
- n : total number of neutron in the reactor
- ε : C.I.C neutron efficiency
- $\bar{\nu}$: neutron number generated in one fission
- ℓ : average life-time of prompt neutron
- k: multiple coefficient

In similar way, referring to reference [1], when analysing CPSD of measured fluctuations between two different ion-chambers, the uncorrelated component in eq. 3 (B term) will become null, only the correlated component is remained. Finally, a formula similar to eq. 3 is found with term B=0 as follows:

$$G_{y1y2} = C\left|H(\omega)\right|^2 = C.\frac{A}{\omega^2 + \alpha^2} \quad (6)$$

Where:

- $G_{y1y2}(\omega)$: Cross power spectrum density of the signal from two ion-chambers
- C: proportional constant

Eq. (6) is basis of the experimental method using CPSD function. By using 2 high efficiency C.I.Cs installed near the reactor core to measure the reactor power fluctuation over time and by calculating CPSD between 2 measured C.I.C signals, the square module of zero-power transfer function can be obtained. By fitting experimental data with theoretical expression, α parameter (Rossi-α) is can be found.

III. Measurement Instrument and Experimental Configuration

To carry out the experimental measurements of CPSD, an instrumentational system, which consists of 2 channels of measurement and acquisition, was installed in Dalat nuclear reactor and connection schema as:

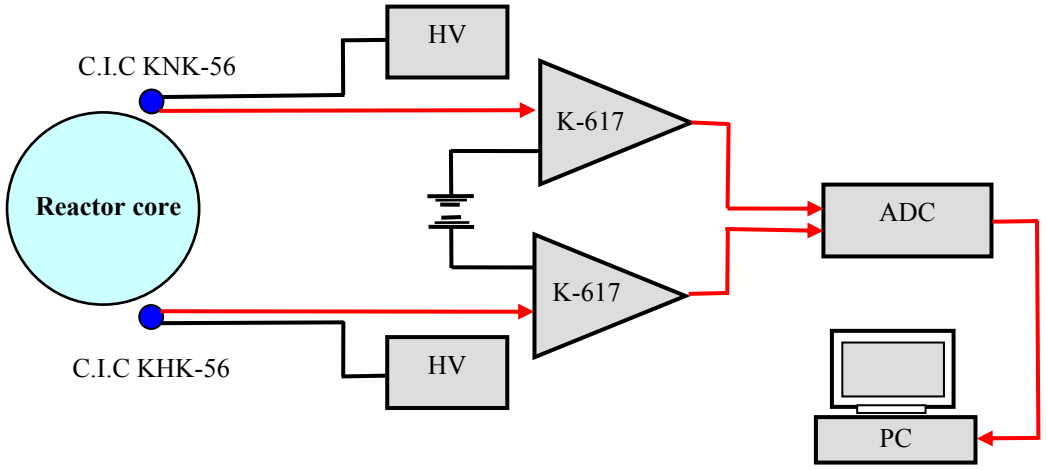

Fig. 2. Block schema of reactor noise measurement system

in which:

- C.I.C: Compensated Ion Chamber of KHK-56 with efficiency of (1.0-3.0) x 10^{-14}A/nV

- PRE-AMP: Keythley-617 meter

- ADC-12bit (50kHz sampling rate)

- PC computer and software (data acquisition, display, fast Fourier, APSD and CPSD calculation function)

Schema of installation of 2 C.I.C KHK-56 in the Dalat nuclear reactor is presented in the Fig. 3 as follows:

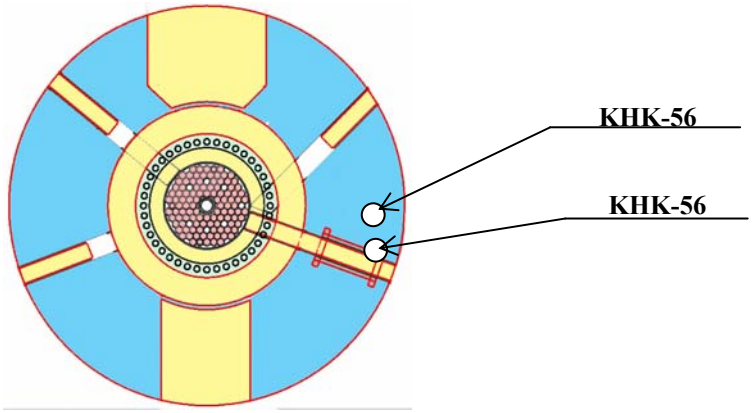

Fig. 3. Schema of installation of 2 C.I.C KHK-56 in the reactor

IV. Experiment and Result

IV.1 Dalat Nuclear Reactor

Dalat nuclear reactor is swimming pool type, 500kw thermal power, which is moderated and cooled by light water with a graphite reflector. Fuel assembly of VVR-M2 type consists of 2 kinds of enrichment, high enrichment of 36% (uranium-

aluminum alloy) and low enrichment of 19.7% (UO_2 dispersed in aluminum matrix). At present, the core are loaded 106 fuel assemblies, in which there are 6 fuel assemblies of 19.7% enrichment and 100 fuel assemblies of 36% enrichment. The reactor control system consists of 4 shim rods, safety rods, which made of Carbide boron, and one automatic rod made of stainless steel.

IV.2 Experiment and Result

The experimental conditions were selected to be ensure that the reactor completely unpoisoned and at very low power level of 10^{-5}% -10^{-3}%Pn (0.05-5W), and inlet coolant temperature was maintained from 20 to 22 ^{o}C.

During the experiments, 2 safety rods were withdrawn from the reactor core and fixed at the top position, the automatic control rod was also fixed at position of 300mm, while 4 shim rods were withdrawn step by step by manual mode. At the every subcritical status, the reactor was autostabilized in few minutes.

To monitor subcriticalities of the reactor corresponding to different experimental configurations, counter numbers, which are obtained from the 3 independent channels of neutron flux control of the ASUR-14R control system, were exploited to draw the curves of inverse count numbers in accordance with 4 shim rods position (curve of 1/N). From the curves (Fig. 4) by extrapolating 1/N value to zero, the reactor will get the criticality at 4 shim rods position of 240mm and automatic control rod position of 300mm.

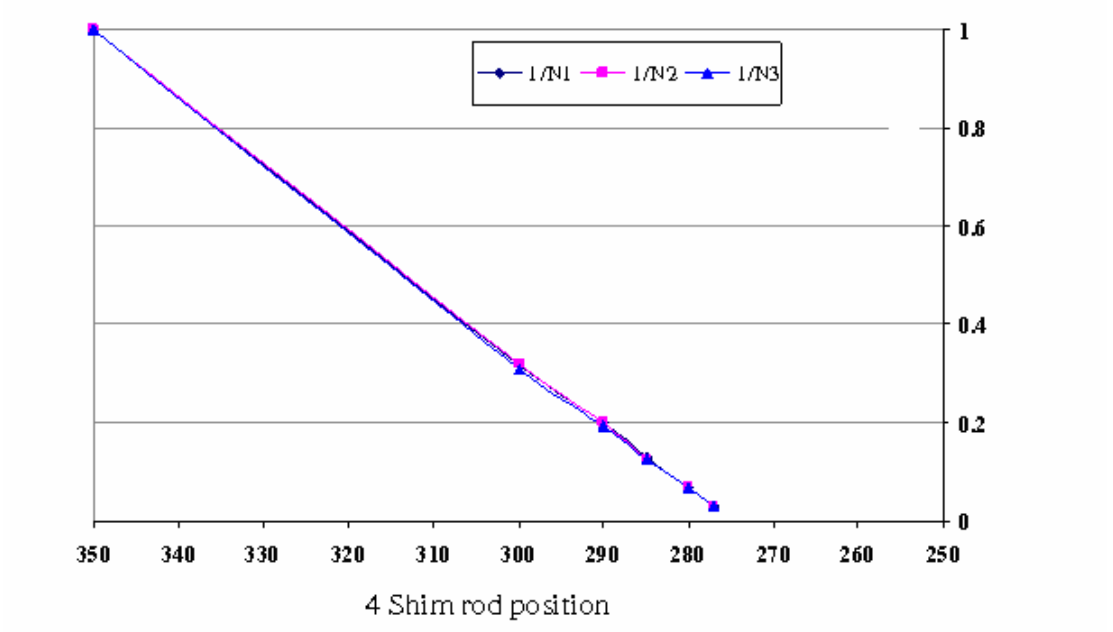

Fig. 4. Dependence of the curves of inverse-count on 4 shim rod positions

IV.3 Measurement of PSD and CPSD

In these experiments, 4 shim rods were withdrawn to the positions of 300, 280, 260, 250 and 245mm, respectively, and wait 5 minutes for stabilizing the reactor, then start acquisition system with sampling time of 0.2ms. The measurements were repeated several times with measuring time of 20 minutes.

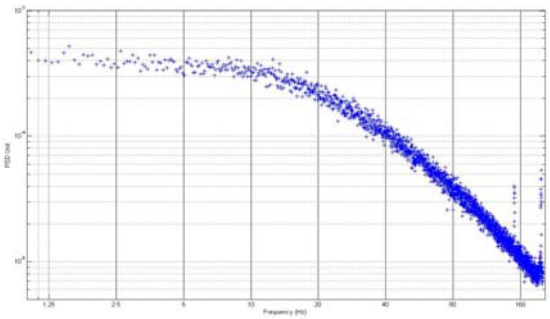

Fig. 5. PSD of the first C.I.C in the 4 shim rod shim rod configuration of 245mm

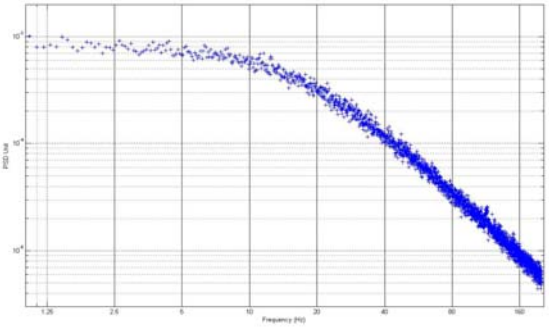

Fig. 6. PSD of the second C.I.C in the 4 configuration of 245mm

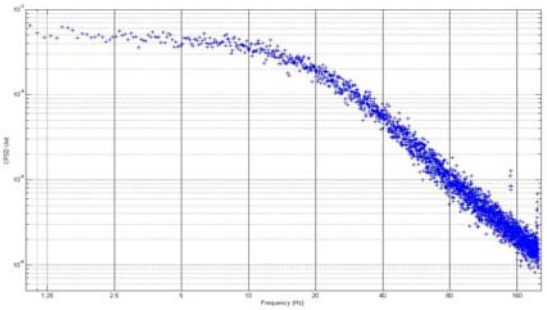

Fig. 7. **C**PSD from 2 C.I.Cs in the 4 shim rods configuration of 245mm

The experimental PSDs and CPSDs from 2 signals were determined by the software tool of Mathlab. In principal, the use of CPSD will give better results when someone uses PSD, therefore Rossi-alpha parameter ($\alpha = \frac{\rho - \beta_{eff}}{\Lambda}$) could be determined by fitting the eq. (6) with the experimental CPSDs. The table 1 summarizes the experimentally measured results corresponding to different subcritical configurations and the extrapolated value of α_c to the critical point.

Tab 1. Results of experimental measurements

4 Shim rods configuration *(mm)*	**Reactor power P** *(%)*	**Value** α^2	**Rsqr**	**Mesurement reactivity**	
				By reactor noise technique	*By double time period method*
350	$\approx 2.4 \times 10^{-5}$	252.05 ± 1.0	0.9904	1.9265	2.1132
300	$\approx 7.6 \times 10^{-5}$	136.33 ± 1.0	0.9933	0.5828	0.6915
290	$\approx 1.2 \times 10^{-4}$	120.00 ± 1.0	0.9943	0.3932	0.4116
285	$\approx 1.9 \times 10^{-4}$	109.56 ± 1.0	0.9941	0.2709	0.2732
280	$\approx 3.5 \times 10^{-4}$	96.94 ± 1.0	0.9963	0.1255	0.1359
277	$\approx 7.9 \times 10^{-4}$	91.94 ± 1.0	0.9947	0.0675	0.05436
275		- Extrapolated value: $\alpha_c \approx 86.13 \pm 1.0$ - Computer code calculation: $\alpha_c \approx 80 - 95$			

V. Conclusion

The reactor noise experiments applied PSD and CPSD technique from 2 compensated ion chambers were performed in Dalat nuclear reactor. The preliminary research results have shown that the experimental data is consistent with the data calculated results and experimental results. From this, it is concluded that PSD and CPSD technique can be applied for Dalat nuclear reactor, experimentally determined α_c value (critical Rossi-alpha value) is 86-87.

Based on the preliminary research results, the authors will continue to improve the equipment, methods and conduct more experiments in order to have enough good experimental results in comparison with theoretical calculations and expand research. The authors also hope that the method and experimental equipment could contribute to the program to restart up the reactor when implementation of core conversion project with low enrichment fuel.

Reference

[1]. ROBERT E.UHRIG, Random noise techniques in nuclear reactor systems, The Ronald press company, (1970).

[2]. CHARLES ERWIN COHN, A Simplified Theory of Pile, Nuclear Science and Engineering, 472-475, (1960).

[3]. J.MAX, Phương pháp xử lý tín hiệu và ứng dụng trong phép đo vật lý, Nhà xuất bản khoa học và kỹ thuật, (1985).

[4]. OM PAL SINGH, Lecture notes on reactor noise, IAEA training cource in Bandung, indonesia, (1987).

1.3 - Instrumentation

DEVELOPMENT OF THE SPECTROMETER SYSTEMS TO MEASURE GAMMA CASCADE, NUCLEAR DATA AND OTHER APPLICATIONS ON THE NEUTRON BEAM

Vuong Huu Tan, Pham Dinh Khang, Nguyen Xuan Hai, Pham Ngoc Son, Tran Tuan Anh Ho Huu Thang, Nguyen Canh Hai, Pham Ngoc Tuan and Nguyen Thi Thuy Nham

Vietnam Atomic Energy Commission,VAEC

Abstract: The spectrometer systems for measurement of prompt gamma and gamma cascade are developed. Manufacture of neutron filter are making new monoenergy neutron beam at Dalat nuclear reactor (DNR). Gamma two steps cascade research, nuclear data measurement, and applications research are doing at DNR.

I. Objectives

The aim of this project is support equipments for fundamental studying on the horizontal neutron channel at DNR, such as make filter neutron beams with energies of 24 keV, 59 keV and 133 keV, improve (n,2γ) spectrometer to (n,3γ), install neutron spectrometer uses recoil proton counter, and training manpower who are working in filed of neutron physics and postgraduate students.

II. Contents

The contents of this project are as follow:

- Improve qualities of thermal neutron beam, reduce gamma background for spectrometer systems at third channel and fourth channel of DNR by shielding and coincidence techniques;

- Use neutron filter techniques to make new monoenergy neutron beam with 24 keV, 59 keV and 133 keV of energy; install a neutron spectrometer uses recoil proton counter;

- Complement to TAC and improve (n,2γ) spectrometer to (n,3γ) spectrometer; use above equipments to measure average radiator capture cross section, analysis some elements such as H, B, C, N, Na, Cl, K, Ca, Cr, Mn, Fe of geological samples and analyse Hydrogen index for oil industry;

- Measure gamma cascade data that emit from non sphere nucleus after capture thermal neutron, research exited intermedia level of nucleus, analyse and evaluate the parameters of level densities.

- Help to train high-grade students with modern techniques of nuclear experiment physics.

III. Methods

For the increasing the ratio cadmium of neutron beam and designing neutron filter for monoenergy neutron beam with 24 keV, 59 keV and 133 keV, the simulation techniques and experiment techniques were used.

For calculation of average radiative cross section, the neutron and gamma measurement techniques were used.

The event-event measurement method, and the modern statistic method were used to make intermediate excited level schema of ^{172}Yb and ^{153}Sm nucleus. The level density parameters of those nucleus were evaluated by using summation of amplitude of coincident pulses (SACP).

IV. Results

- The cadmium ratio of neutron beam of horizontal channel N_0.4 was increased from 112 to 149 and of horizontal channel N_0. 3 was increased from 70 to 900.

- The gamma background of spectrometer for prompt gamma neutron activation analysis (PGNAA) was reduced significantly. In which, the 2223 keV peak of Hydrogen, it was reduced from 0,8 cps to 0,5 cps. That result was applied to analysis Hydrogen index for oil industry.

- The characteristic parameters of monoenergetic filtered neutron beams are neutron spectra, relative intensity, energy resolution, dimension of filters, and suitable composition of materials. These parameters have been calculated to create the new filtered neutron beams with monoenergies of 1.9 keV, 24.3 keV, 53.9 keV, 58.80 keV, 133 keV and 148.3 keV, at the horizontal channel No.4 of the Dalat research reactor. In which, the two available filtered neutron beams of 55 keV and 144 keV were recalculated with resulting that the beam energies should be 54 keV and 148.3 keV, respectively. The results of calculated parameters in the present work are useful for the development of new filtered neutron beams in the near future at the Dalat research reactor.

- The calculated parameters for new filters have been applied for development of three new filtered neutron beams with energies: 24 keV, 59 keV and 133 keV at the horizontal channel No. 4 of DNR. For experimental measurement of the neutron energy spectra, a proton recoil spectrometer has been installed with counter model is LND-281.

- For compliment of the SACP spectrometer, the TAC module and an interface used to FPGA technique were completed, that extended ability of SACP spectrometer for research of (n,3γ) reactions and the timing resolution of spectrometer system is about 14 nano seconds.

- Help for data analyzing of (n,3γ) reaction with timing combining, the some computer codes were written.

- The level density parameters of ^{172}Yb and ^{153}Sm according to fermi shift back model were calculated, and evaluated with help of experiment data.

- With the help of this project, three mater students were success, and two others students have been doing thesis; five of national conference reports and two of international conference reports were presented.

Tab 1. Calculated results for new filtered neutron beams at Dalat reactor.

En keV	ΔEn keV	Φ x10^5 n/cm^2/s	Purity (%)	Filter materials	Size of filter composision
1.8	1.5	24.0	95.79	^{10}B + Sc + Ti	0.2g/cm^2+200g/cm^2+1cm

24[a]	**1.8**	**2.6**	**96.72**	**^{10}B + Fe + Al + S**	**0.2g/cm^2+20cm+30cm+35 g/cm^2**
54[b]	1.5	1.7	78.05	^{10}B + Si + S	0.2g/cm^2+98cm+35g/cm^2
59[a]	**2.7**	**1.1**	**92.28**	**^{10}B + Ni +V +Al+S**	**0.2g/cm^2+10cm+15cm+5cm+100g/cm^2**
133[a]	**3.0**	**0.5**	**92.89**	**^{10}B + Cr + Ni+Si**	**0.2g/cm^2+50g/cm2 +10cm+60cm**
148[b]	14.8	7.2	95.78	^{10}B + Si + Ti	0.2g/cm^2+98cm+2cm

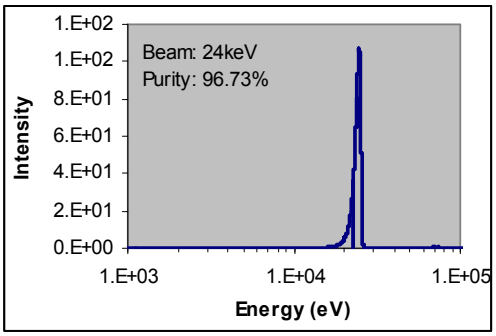

Fig. 1. Calculated energy spectrum for 24 keV filtered neutron.

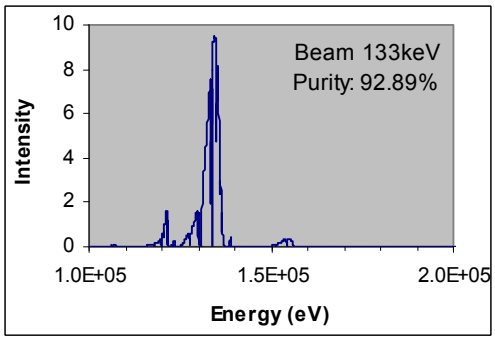

Fig. 2. Calculated energy spectrum for 133 keV filtered neutron beam.

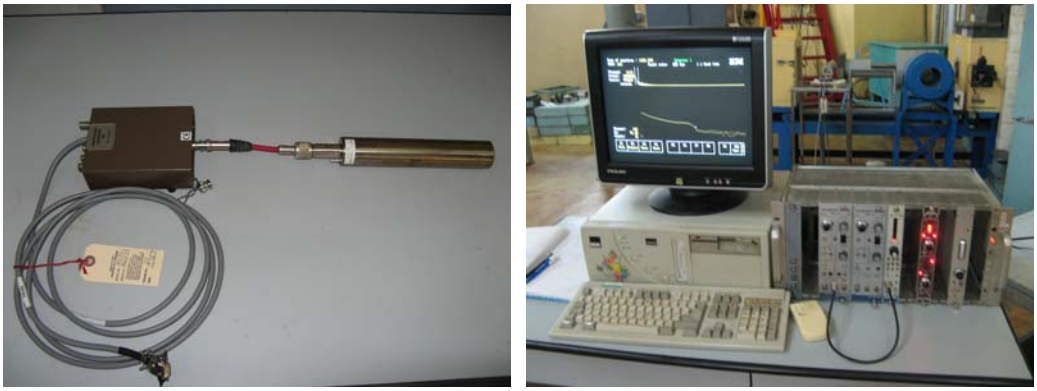

Fig. 3. The new proton recoil spectrometer installed at the Dalat Nuclear research institute.

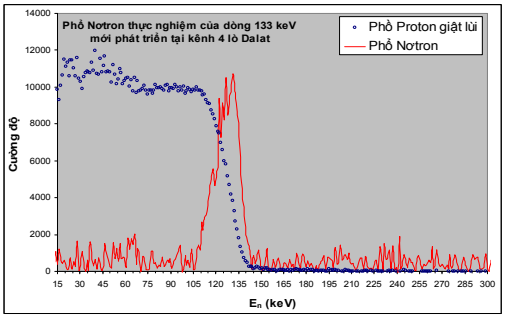

*Fig. 4***.** Pulse high proton recoil spectrum of 133 keV filtered neutron beam, developed presently in this project.

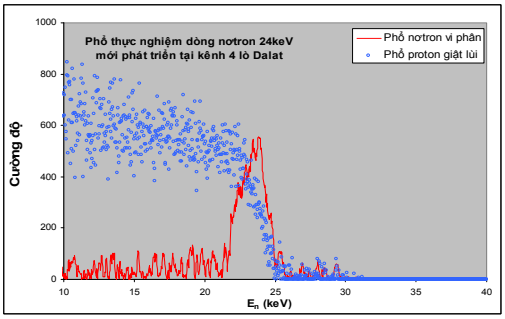

Fig. 5. Pulse high proton recoil spectrum of 24 keV filtered neutron beam, developed presently in this project.

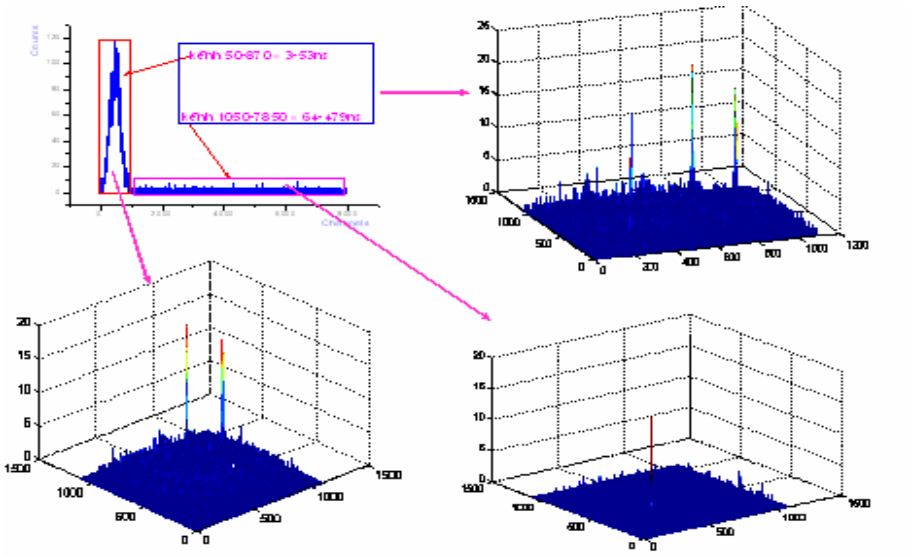

Fig. 6. The spectroscopic information of SACP spectrometer with TAC, developed presently in this project.

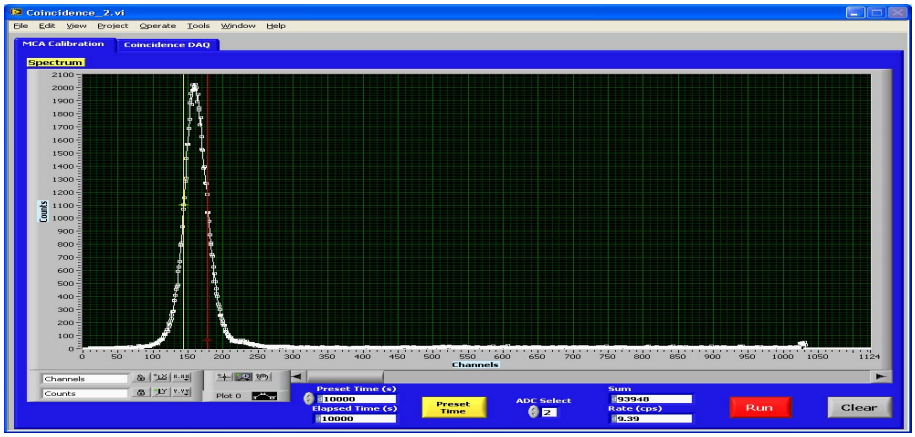

Fig. 7. The TAC spectra of ^{60}Co, measured presently in this project.

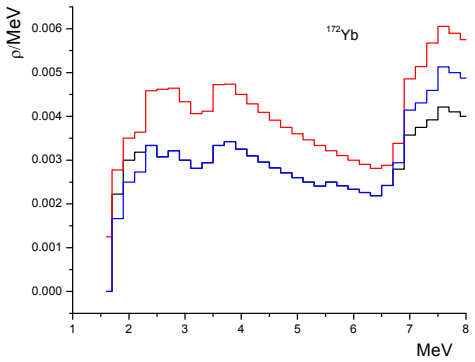

Fig. 8. The experimental excited level densities of ^{172}Yb with primary transitions of gamma, measured recently in this project.

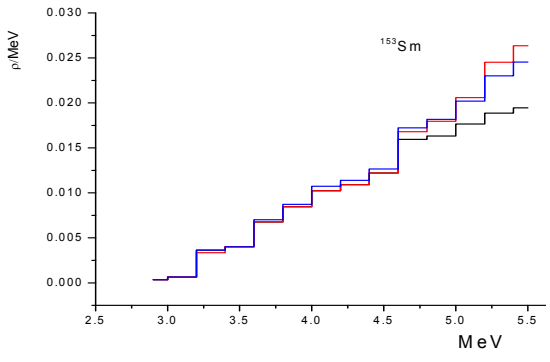

Fig. 9. The experimental excited level densities of ^{153}Sm with primary transitions of gamma, calculated recently in this project.

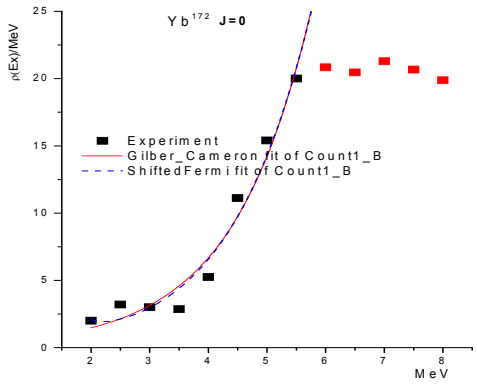

Fig. 10. The experiment and theory calculation of level densities of ^{172}Yb, the dash line is calculated according to constant of temperature model and line is calculated according to Fermi shift back model.

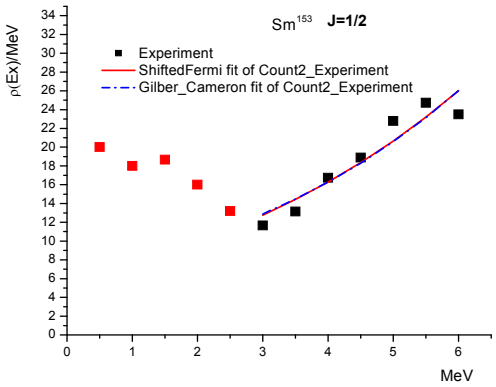

Fig. 11. The experiment and theory calculation of level densities of ^{153}Sm, the dash line is calculated according to constant of temperature model and line is calculated according to Fermi shift back model.

V. Conclusions

The project has been doing on register time, the facilities were made, it has had to complement to fundamental and application research at the DNR.

The experimental ability of participates of doing project was much more increase. They can do and explain then new experiment with high completely.

The project is the good conditions for graduate student.

The authors would like to thanks to Ministry of science, Vietnam atomic energy commission, and nuclear research.

References

[1]. Vương Hữu Tấn và cộng sự, Báo cáo tổng kết đề tài khoa học công nghệ cấp bộ năm 2005-2006, Đà Lạt tháng 12/2006.

[2]. Vương Hữu Tấn, Phạm Đình Khang, Nguyễn Xuân Hải, Nghiên cứu phổ bức xạ gamma nối tầng của ^{153}Sm và ^{172}Yb trong phản ứng bắt nơtron nhiệt, Hội nghị Khoa học và Công nghệ hạt nhân toàn quốc lần thứ VII, Đà Nẵng, 30-31/8/ 2007.

[3]. V. H. Tan, T. T. Anh, N. C. Hai, P. N. Son and T. Fukahori, "*Measurement of Neutron Capture Cross Section of ^{139}La, ^{152}Sm and ^{191,193}Ir at 55keV and 144keV",* SND2006-V.02-1, Proc. of 2006 Symposium on Nuclear Data, Jan. 25-26, 2007, RICOTTI, Tokai, Ibaraki, Japan, ISBN978-4-89047-138-6, [CD], (2007).

[4]. V. H. Tan, T. T. Anh, N. C. Hai, P. N. Son, *Measurement of Neutron Capture Cross Section of ^{191,193}Ir at 55 keV and 144 keV*, Nuclear Science and Technology, Vol. 5, No. 1, pp. 13-20, VAEC, ISSN 1810-5408, (June 2007).

[5]. V. H. Tan, P. N. Son, T. T. Anh, N. C. Hai, T. Tu Anh, M. X. Trung, *Nghiên cứu xác định các tham số hiệu chính trong phép đo tiết diện bắt bức xạ nơtron,* Hội nghị Khoa học và Công nghệ hạt nhân toàn quốc lần thứ VII, Đà Nẵng, 30-31/8/ 2007.

[6]. V. H. Tan, P. N. Son, T. T. Anh, N. C. Hai, "*Tính toán các thông số đặc trưng phục vụ phát triển các dòng nơtron phin lọc mới tại lò phản ứng Đà Lạt"*. Hội nghị Toàn Quốc về Khoa Học và Cộng nghệ hạt nhân lần VII, Đà Nẵng, 30-31/8/2007.

[7]. Hồ Hữu Thắng, Nguyễn Thị Thuý Nhâm, Nguyễn Kiên Cường, Nguyễn Xuân Hải, Ứng dụng mcnp4c2 xác định cấu hình che chắn tối ưu cho hệ phổ kế cộng biên độ các xung trùng phùng, Hội nghị Khoa học và Công nghệ hạt nhân toàn quốc lần thứ VII, Đà Nẵng, 30-31/8/ 2007.

[8]. Nguyễn Thị Thuý Nhâm, Nguyễn Xuân Hải, Hồ Hữu Thắng, Phạm Ngọc Sơn, một số vấn đề về mật độ mức hạt nhân thực nghiệm của ^{36}Cl thu được từ hệ phổ kế SACP tại NRI, Hội nghị Khoa học và Công nghệ hạt nhân toàn quốc lần thứ VII, Đà Nẵng, 30-31/8/ 2007.

[9]. V. A. Khitrov, A. M. Sukhovoj, Pham Dinh Khang, Vuong Huu Tan, Nguyen Xuan Hai, On the correctness of various approaches in the extraction of the nucleus parameters on example of analysis of the two-step gamma-cascades in ^{163}Dy compound nucleus, Proceedings of the XIV International Seminar on Interaction of Neutrons with Nuclei, May 24-27 2006, Dubna, JINR E3-2007-23, pp. 257-265.

[10]. V. A. Khitrov, A. M. Sukhovoj, Pham Dinh Khang, Vuong Huu Tan, Nguyen Xuan Hai, Possibilities to verify the level density and radiative strength functions, extracted from the two-step gamma-cascade intensities, Proceedings of the XIV International Seminar on Interaction of Neutrons with Nuclei, May 24-27 2006, Dubna, JINR E3-2007-23, pp. 266-283.

DESIGNING AND MANUFACTURING EMITTED AIR AND PARTICLE TREATMENT EQUIPMENT (CYCLONE TYPE) OF NONFERROUS METAL METALLURGY PROCESS

Tran Van Hoa, Pham Minh Tuan, Phung Quoc Khanh
Tuong Duy Nhan and Luong Manh Hung

Institute for Technology of Radioactive and Rare Elements, VAEC, Vietnam

Abstract: We have selected methods for treating emitted air and particle by studying different treatment methods of emitted air and particle in the industries, especially in nonferrous metal metallurgy process from secondary material, and by completed collecting the parameters of air emission stream from manufacturing workshops of Fero-rare-earth and Zinc oxide, a typical representation of nonferrous metal metallurgy processes from secondary material in Institute for Technology of Radioactive and Rare Elements (ITRRE). Our work includes:

- Collecting dried particle by using cyclone ЦН-15 which is suitable for the particle having the size d ≥ 10 μm. The collected particle can be reused as input material.
- Collecting wet particle by using cyclone Liot or spray tower which is suitable for the particle having the size d ≤ 10 μm and treating a portion of emitted air.
- Treating all emitted air by adding absorbed tower (packed-bed type) .

Key words: air and particle treatment, spray tower, packed-bed scrubber.

RESULTS AND DISCUSSIONS

1. Equipment Designing

1.1. Studying and Designing A Dried Cyclone For Input Material Treatment Furnace (capacity: 1500 M^3/h) and Oxidation Reverted Furnace In Zinc Oxide Manufacturing Workshop (capacity: 4500 M^3/h)

We have chosen the cyclone type ЦН-15 to design and calculate based on the characteristics of polluted air from Zinc oxide manufacturing process in input material treatment furnace and oxidation reverted furnace: particle concentration is not high (about tens g/m^3), size of particle emitted from Zinc sublimation process is small as well as on the advantages and disadvantages of different types of cyclones

We have used both general and selected methods for designing and calculating technique parameters of cyclone as following:

* The dried cyclone for input material treatment furnace (capacity: 1500 m^3/h):

▪ *Main Technique Parameters of Cyclone:*

- Cyclone type: ЦН-15
- Capacity, Q = 1500 m^3/h
- Body diameter of cyclone, D = 450 mm

- Particle collected efficiency with D≥10μm is 80÷90%; with D≤ 10μm is 40÷50%

- Producing material: Inox 304; 3 mm thickness.

▪ *Main Dimensions of Cyclone:*

- Body diameter of cyclone, D = 450 mm

- Input door height, a=300 mm

- Flange central pipe height, h_1 = 785 mm

- Cylinder height, h_2 =1020 mm

- Cone height, h_3 = 900 mm

- Outer central pipe height, h_4 = 135 mm

- Total height, H = 2050 mm

- Outer diameter of air pipe, D_1=270 mm

- Inner diameter of emitted particle door, D_2 = 160 mm

- Enter air door width, b_1 x h = 120 x 90 mm

- Enter pipe length, l = 270 mm

- Declination between cover and enter pipe, $\alpha = 150^o$

- Working volume of bunker, V = 0,4m^3

- Installed size, B x B x H = 1085 x 1085 x 3270 mm

***** Oxidation reverted furnace in Zinc oxide manufacturing workshop (capacity: 4500 m^3/h).

▪ *Main Technique Parameters of Cyclone:*

- Cyclone type: ЦН-15

- Capacity, Q = 4500 m^3/h

- Body diameter of cyclone, D = 700 mm

- Particle collected efficiency with D≥10μm is 80÷90%; with D≤ 10μm is 40÷50%

- Producing material: Inox 304; 3 mm thickness.

▪ *Main Dimensions of Cyclone:*

- Body diameter of cyclone, D = 7000 mm

- Input door height, a = 460 mm

- Flange central pipe height, h_1 = 1220 mm

- Cylinder height, h_2 =1580 mm

- Cone height, h_3 = 1400 mm

- Outer central pipe height, h_4 = 210 mm

- Total height, H = 3190 mm
- Outer diameter of air pipe, D_1=420 mm
- Inner diameter of emitted particle door, D_2 = 245 mm
- Enter air door width, b_1 x h = 182 x 140 mm
- Enter pipe length, l = 420 mm
- Declination between cover and enter pipe, $\alpha = 150^o$
- Working volume of bunker, V = 0.9m^3
- Installed size, B x B x H = 1400 x 1400 x 4840 mm

1.2. Studying and Designing A Wet Cyclone For Input Material Furnace (capacity: 1500 m^3/h)

▪ *Main Technique Parameters of EquipmentM:*

- Cyclone type: Liot
- Capacity, Q=1500 m^3/h
- Body diameter of cyclone, D = 700 mm
- Particle collected efficiency with D≥10μm is 80÷85%
- Producing material: Inox 304; 3 mm thickness.

▪ *Main Dimensions of Cyclone:*

- Body diameter of cyclone, D = 7000 mm
- Cylinder height, H_1 =1020 mm
- Cone height, H_2 = 900 mm
- Total height, H = 2050 mm
- Enter air door air size, hxb=210x100 mm
- Height from cone bottom to center of enter door, h_1 = 655 mm
- Height from cone bottom to center of enter door, h_2 = 150mm
- Installed size, B x B x H = 1400 x 1400 x 4840 mm

1.3. Studying and Designing A Spray Tower For Oxidation Reverted Furnace (capacity: 4500 m^3/h)

▪ *Main Technique Parameters of Equipment:*

- Equipment type: spray tower
- Body diameter of equipment, D = 1000 mm
- Useful height of tower, H_{ci} = 2500 mm
- Enter air door size: D_v = 320 mm
- Air velocity through tower, W_k = 1.5 m/s
- Total discharge of spray water, Q_n = 6.75 m^3/h

- Hindrance of tower, ΔP = 15-20 mm H_2O

1.4. Studying and Designing An Impingement Plate Scrubber For Oxidation Reverted Furnace (capacity: 4500 m^3/h)

- *Main Technique Parameters of Equipment:*

- Equipment type: Impingement plate scrubber

- Body diameter of equipment, D = 1000 mm

- Body height of equipment, H = 3230

- Air velocity through tower, W_k = 1.85 m/s

- Total discharge of spray water, Q_n = 2.35 m^3/h

2. Manufacturing and Installing Equipments In Oxidation Reverted Furnace - Zinc Oxide Manufacturing Workshop

We have completely produced and installed an emitted air and particle treatment system for oxidation reverted furnace - Zinc oxide manufacturing workshop with the capacity 4500 m^3/h based on the practical demanding of Zinc manufacture activities in ITRRE. The system includes (plus existed equipments):

- 01 cyclone to collect particle with size dimension: D x H = 700 x 3190 mm

- 01 spray tower wit size dimension: D x H = 1000 x 4400 mm

- 01 Impingement plate scrubber with size dimension: B x B x H = 1400 x1400 x 3700 mm

The system flowchart is showed below:

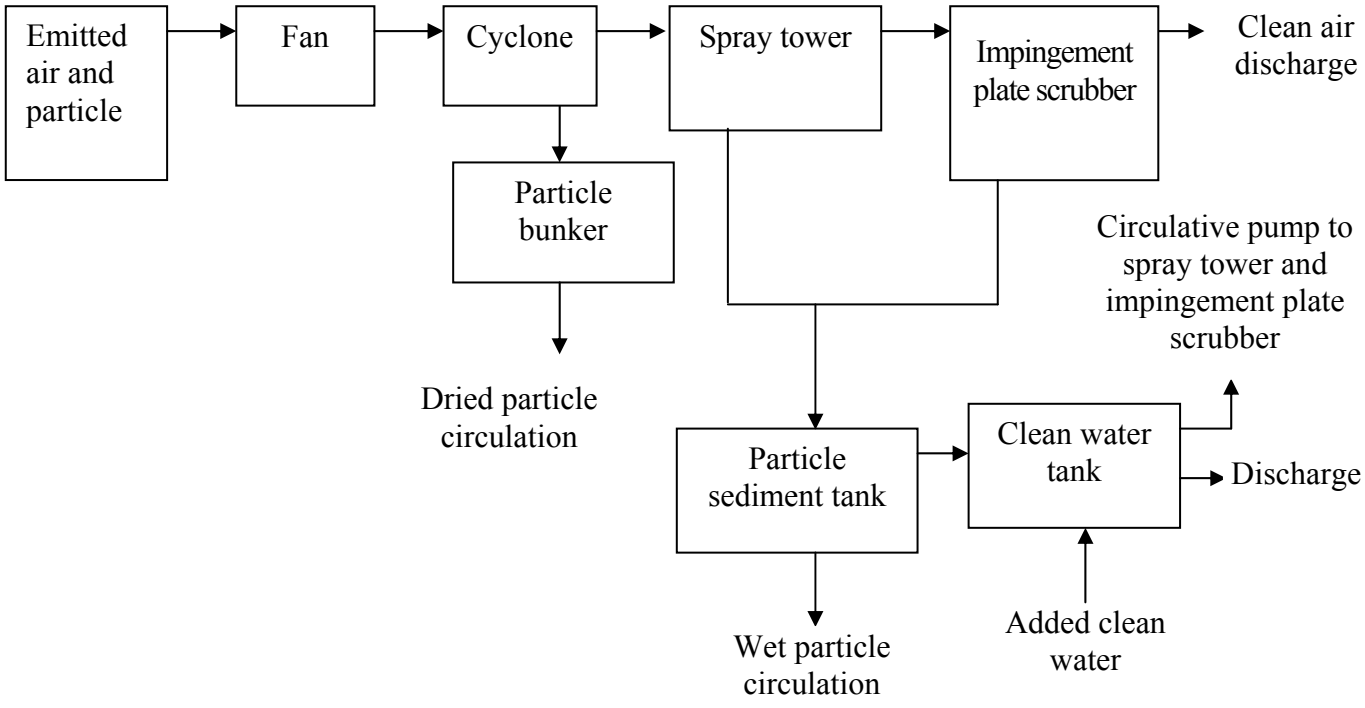

CONCLUSIONS

1. We have completely surveyed the characteristics of air emission stream from manufacturing workshops of Fero-rare-earth and Zinc oxide in ITRRE.

2. We have analyzed and selected the appropriate treatment technology from other current air treatment technologies. The flowchart of treatment system is showed bellow:

Polluted source ⟶ Fan ⟶ Dried cyclone ⟶ Treating air and particle by spray tower ⟶ Impingement plate scrubber ⟶ Discharging clean air to environment

3. We have calculated and designed a system of equipments which include:

- Dried cyclones, capacity: 1500 m^3/h and 4500 m^3/h

- Wet cyclones, capacity: 1500 m^3/h

- Spray tower, capacity: 4500 m^3/h

- Impingement plate scrubber, capacity: 4500 m^3/h

4. We have manufactured, installed and operated the air and particle treatment system for trial purpose (capacity: 4500 m^3/h) for Zinc oxide manufacturing workshops which include:

- 01 dried cyclones: D x H = 700 x 3190 mm

- 01 spray tower: D x H = 1000 x 4400 mm

- 01 impingement plate scrubber: B x B x H = 1400 x 1400 x 3700 mm

5. We have operated the air and particle treatment system for trial purpose. By using this system, we can solve 3 concern issues:

- Good sucking at the starting zone of the furnace and ensuring required technology

- Collecting particle emitted from input material

- Treating foul smell pollution

The above system is suitable for small and medium nonferrous metal metallurgy workshops, especially input material is secondary material because it can collect emitted particle from input material and partially treat air emitting from metallurgic process.

Sample Analyzing Result Table In 25/04/2009

No	Parameters	Unit	Samples									TCVN 5939: 2005
			IA	IIA	IIIA	IVA	VA	IB	IIB	IIIB	IVB	
1	TS	mg/m^3	1868.85	6276.84	4930.54	499.688	55.188	12596.4	9291.66	727.92	78.634	200
2	Coal particle	mg/m^3	1820.25	454.65	272.79	54.558	5.46	1084.14	650.48	275.24	27.52	30
3	ZnO particle	mg/m^3	41.35	5120.75	4096.6	409.79	43.03	10577.73	7938.29	396.91	45.26	5
4	$PbCl_2$ particle	mg/m^3	7.25	701.44	561.15	58.25	6.698	934.53	702.89	55.75	5.854	1000

5	CO	mg/m^3	865.75	865.75	865.75	792.5	785.25	1297.55	1297.5	1187.75	1128.35	500
6	SO_2	mg/m^3	58.75	58.75	58.75	44.06	40.75	92.25	92.08	72.15	65.135	850
7	NO_x	mg/m^3	206.25	206.25	206.25	200.25	195.2	235.75	232.5	230.76	230.25	-
8	Temperature	^oC	71.5	75	74.5	72.5	68.5	71.2	78.5	76.8	72.3	-
9	Air flow	m^3/s	4500	4500	4500	4500	4500	4800	4800	4800	4800	4800

Note:

- Sample IA: Coal loading stage in furnace 3A, before cyclone.
- Sample IIA: Material loading stage in furnace 3A, before cyclone.
- Sample IIIA: Material loading stage in furnace 3A, after cyclone.
- Sample IVA: Material loading stage in furnace 3A, after spray tower.
- Sample VA: Material loading stage in furnace 3A, after impingement scrubber.
- Sample IB: Coal loading stage in furnace 3B, before cyclone.
- Sample IIB: Material loading stage in furnace 3B, after cyclone.
- Sample IIIB: Material loading stage in furnace 3B, after spray tower.
- Sample IVB: Material loading stage in furnace 3B, after impingement scrubber.

Sample Analyzing Result Table In 15/05/2009

No	**Parameters**	**Unit**	**Samples**									**TCVN 5939: 2005**
			IA	IIA	IIIA	IVA	VA	IB	IIB	IIIB	IVB	
1	TS	mg/m^3	1557.88	5232.39	4341.1	487.24	62.15	10635.2	8204.25	726.18	66.55	200
2	Coal particle	mg/m^3	1517.37	425.85	255.51	38.33	7.66	915.35	542.91	131.23	16.61	30
3	ZnO particle	mg/m^3	34.46	4267.25	3627.16	380.85	47.61	8938.25	7016.52	526.23	42.72	5
4	$PbCl_2$ particle	mg/m^3	6.045	539.29	458.39	68.76	6.88	781.6	644.82	68.72	7.22	1000
5	CO	mg/m^3	827.39	827.39	827.39	758.38	752.43	1125.3	1125.3	1035.11	965.58	500
6	SO_2	mg/m^3	61.55	61.55	61.55	48.42	44.73	69.95	69.95	54.81	43.24	850
7	NO_x	mg/m^3	231.75	231.75	231.75	224.27	218.62	206.28	206.28	204.74	203.21	-
8	Temperature	^oC	72.5	74.2	73.8	72.1	67.8	72.5	79.8	76.9	73.2	-
9	Air flow	m^3/s	4750	4750	4750	4750	4750	4950	4950	4950	4950	4950

Note:

- Sample IA: Coal loading stage in furnace 3A, before cyclone.
- Sample IIA: Material loading stage in furnace 3A, before cyclone.

- Sample IIIA: Material loading stage in furnace 3A, after cyclone.
- Sample IVA: Material loading stage in furnace 3A, after spray tower.
- Sample VA: Material loading stage in furnace 3A, after impingement scrubber.
- Sample IB: Coal loading stage in furnace 3B, before cyclone.
- Sample IIB: Material loading stage in furnace 3B, after cyclone.
- Sample IIIB: Material loading stage in furnace 3B, after spray tower.
- Sample IVB: Material loading stage in furnace 3B, after impingement scrubber.

Sample Analyzing Result Table In 22/05/2009

No	Parameters	Unit	Samples									TCVN 5939: 2005
			IA	IIA	IIIA	IVA	VA	IB	IIB	IIIB	IVB	
1	TS	mg/m^3	1886.56	6545.15	5339.85	588.73	70.35	12875.36	9781.35	825.41	87.55	200
2	Coal particle	mg/m^3	1836.05	485.72	315.72	63.15	6.32	1108.49	665.09	99.76	12.24	30
3	ZnO particle	mg/m^3	43.075	5334.06	4425.7	450.75	54.65	10824.22	8385.72	670.86	67.09	5
4	$PbCl_2$ particle	mg/m^3	7.432	725.37	598.43	74.83	9.38	942.65	730.54	54.79	8.22	1000
5	CO	mg/m^3	925.32	925.3	925.25	848.34	778.35	1367.1	1365.7	1252.18	1185.95	500
6	SO_2	mg/m^3	64.25	64.21	64.27	50.46	39.61	96.862	95.8	75.3	58.9	850
7	NO_x	mg/m^3	215.1	215.53	214.75	213.15	198.25	245.58	247.3	245.45	243.6	-
8	Temperature	^oC	70.75	74.7	73.2	71.8	69.7	71.5	76.8	74.5	72.7	-
9	Air flow	m^3/s	4500	4500	4500	4500	4500	4875	4875	4875	4875	4875

Note:

- Sample IA: Coal loading stage in furnace 3A, before cyclone.
- Sample IIA: Material loading stage in furnace 3A, before cyclone.
- Sample IIIA: Material loading stage in furnace 3A, after cyclone.
- Sample IVA: Material loading stage in furnace 3A, after spray tower.
- Sample VA: Material loading stage in furnace 3A, after impingement scrubber.
- Sample IB: Coal loading stage in furnace 3B, before cyclone.
- Sample IIB: Material loading stage in furnace 3B, after cyclone.
- Sample IIIB: Material loading stage in furnace 3B, after spray tower.
- Sample IVB: Material loading stage in furnace 3B, after impingement scrubber.

References

1]. Hoàng Kim Cơ: Tính toán kỹ thuật, lọc bụi và làm sạch khí. Nhà xuất bản Khoa học và Kỹ thuật, Hà Nội – 2002.

2]. Đỗ Văn Đài, Trần Xoa: Sổ tay Quá trình và thiết bị công nghệ hoá học. Nhà xuất bản Khoa học và Kỹ thuật, Hà Nội – 1998.

3]. Trần Ngọc Chấn: Ô nhiễm không khí và xử lý khí thải - Tập 2&3. Nhà xuất bản Khoa học và Kỹ thuật, Hà Nội – 2001.

4]. Nguyễn Minh Tuyển: Tính toán máy và thiết bị hoá chất - Tập 1 & 2. Nhà xuất bản Khoa học và Kỹ thuật, Hà Nội – 1994.

5]. Hồ Lê Viên: Tính toán và thiết kế các chi tiết thiết bị hoá chất và dầu khí. Nhà xuất bản Khoa học và Kỹ thuật, Hà Nội – 2006.

6]. V.Straus: Làm sạch khí thải công nghiệp. Nhà xuất bản "Hoá học" Matxcova - 1981.

7]. O.C.Balabekob, L.S. Baltabaev: Làm sạch khí trong công nghiệp hoá học. Nhà xuất bản "Hoá học" Matxcova - 1991.

8]. Ydltric: Thuỷ khí động lực các thiết bị công nghệ. Nhà xuất bản "Máy và thiết bị" Matxcova - 1983.

STUDYING ON DIGITAL SIGNAL PROCESSING METHOD FOR TESTED DESIGN AND THE CONSTRUCTION OF DSP-BASED MCA 1K

Dang Lanh, Tran Tuan Anh, Vu Xuan Cach, Tuong Thi Thu Huong
Huynh Van Minh and Pham Ngoc Son

Nuclear Research Institute, Dalat, Vietnam

Nguyen Van Kien

University of Dalat, Viet nam

Abstract: DSP is one of the most useful tools for development of nuclear electronics instruments for Physics research. The method can be carried out by either a special digital signal processor or FPGA which is programmed through VHDL. In this case, Digital signal processing (DPS) is performed by VHDL. The aim of this project is to study on digital signal processing for tested design and construction of DSP-based MCA 1K.

VHDL standards for VHSIC hardware description language. Due to VHDL, memory and Central processing unit are created.

An application software for receiving data is written in LabVIEW 8.5. Spartan 3^E starter kit is used for design of the project, combining with ISE software, XilinX 9.2i.

Keywords: DSP, VHDL, LabVIEW và ISE.

1. Introduction

The world of science and engineering is filled with signals: images from remote space probes, voltages generated by the heart and brain, radar and sonar echoes, seismic vibrations, and countless other applications. Digital Signal Processing is the science of using computers to understand these types of data. This includes a wide variety of goals: filtering, speech recognition, image enhancement, data compression, neural networks, and much more. DSP is one of the most powerful technologies that will shape science and engineering in the twenty-first century. There are two main ways to perform DSP method: one is to use Digital Signal Processor (DSPs), the other is the use of FPGA through VHDL. As the above-mentioned, VHDL is used to develop DSP.

The main purpose of the project is to study on digital signal processing method for tested design and the construction of DSP-based MCA 1K.

The content includes four items:

- Studying on the hardware of Toolkit SPARTAN-3E, Xilinx with command set of VHDL,
- Performing an µP, SRAM, EEPROM inside the FPGA chip,
- Writing firmware in VHDL for control of the chip,
- Developing an application software in LabVIEW for interfacing to the firmware and linking both of them each other. The software is able to operate under Windows XP.

2. Design And The Construction Of Tested Mca 1k

The block diagram of the MCA is presented in Fig. 1. It includes:

- *Inputs*: Btn, resets memory by hand

  Clk, provides 1 second for control of operation of the unit

  ADC, gets a digital triangular signal performed by owned VHDL.

- *Outputs:* LCD, connects LCD driver for display

RS232_DTE_TXD, interfaces to a serial port for transferring data

DAC_B, provides LLD

DAC_C, provides ULD.

At first, a clock 50 MHz comes to Clk input of top entity (the boundary of an FPGA chip with VHDL components inside). The clock will be divided by a divider to give 1 sec (50 MHz divided by 50 millions is 1 Hz) which is used to reset all counters, strobe latches, and interface to PC with baudrate 38400. In the reality, the baudrate ensures that data will be transferred in a correct way! Next, a digital triangular signal will be sampled and held in

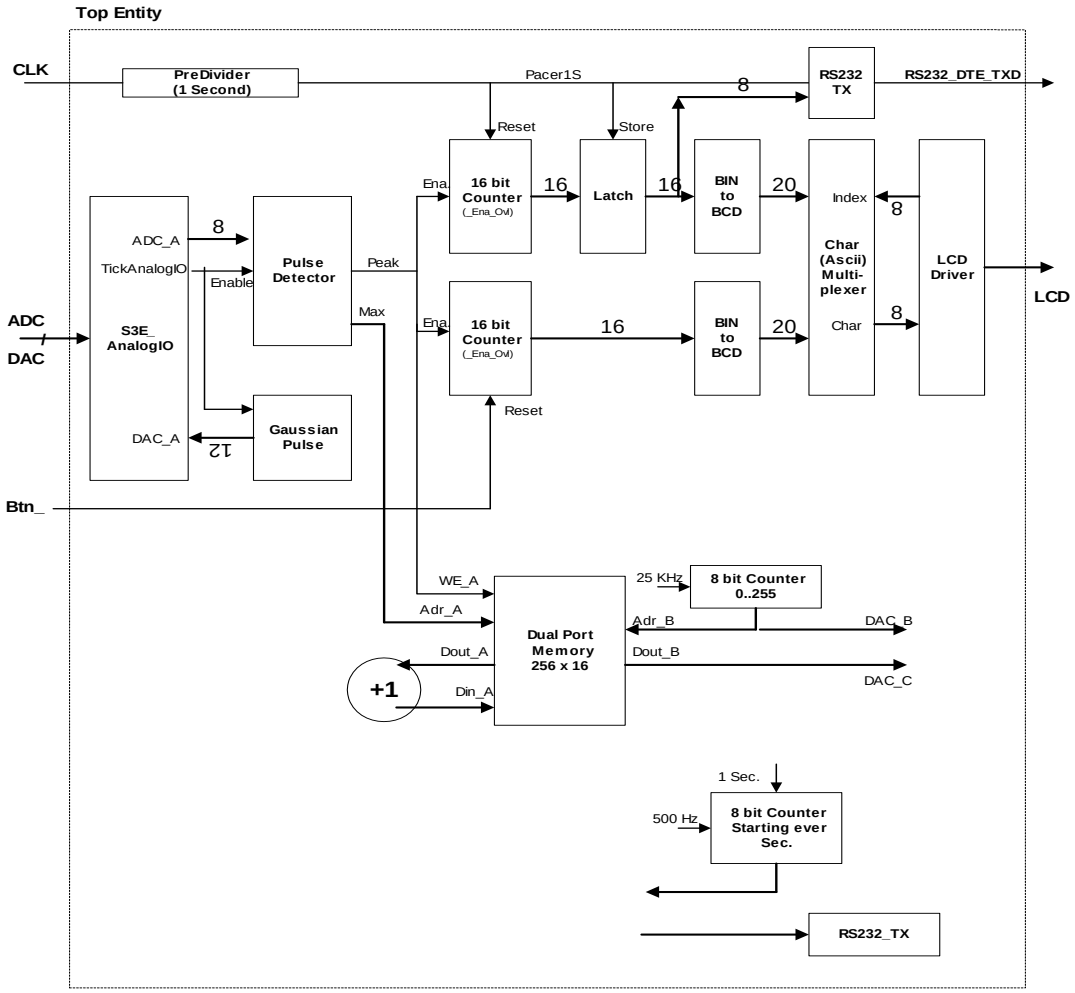

Fig. 1. Structure of the block diagram.

S3E_AnalogIO component; as a result, one data byte at ADC_A output will be detected by Pulse detector component. Owning to enable bit (from TickAanalogIO output), Peak detector component is allowed to generate a peak (one bit) and a standard logic vector Max (16 bits). Then, the peak is a positive logic that forces all latches to operate and makes two address bytes of the dual memory valid. Data from memory will be updated one byte per second via a carryout flag of the full adder. Finally, data from the MCA will be transferred to PC through the serial port. Other components (BIN to BCD, Char. ASCII, LCD driver) are also designed to display counterate, count, time and date, frequency, channel, energy of peak, etc. on the LCD.

The firmware for control of the FPGA chip is written in VHDL; it is able to link to the application software (written in LabVIEW 8.5 under Windows XP).

3. Experiments

3.1. Electronics Tests

The MCA was checked at the Nuclear Physics and Electronics, NRI, Dalat. Toolkit SPARTAN-3E is ready to use with the application software for testing. As the aforementioned presentation, there is a triangular pulser inside the FPGA chip. It was designed by DSP method through VHDL. The signal is generated from the pulser to be a digitalized one within an according frequency versus a fixed amplitude; this signal will be applied to the input of ADC. By changing its amplitude from minimum to maximum with a range from 0 to 1023, A standard spectrum of the pulser will be appeared on screen as shown in Fig. 2.

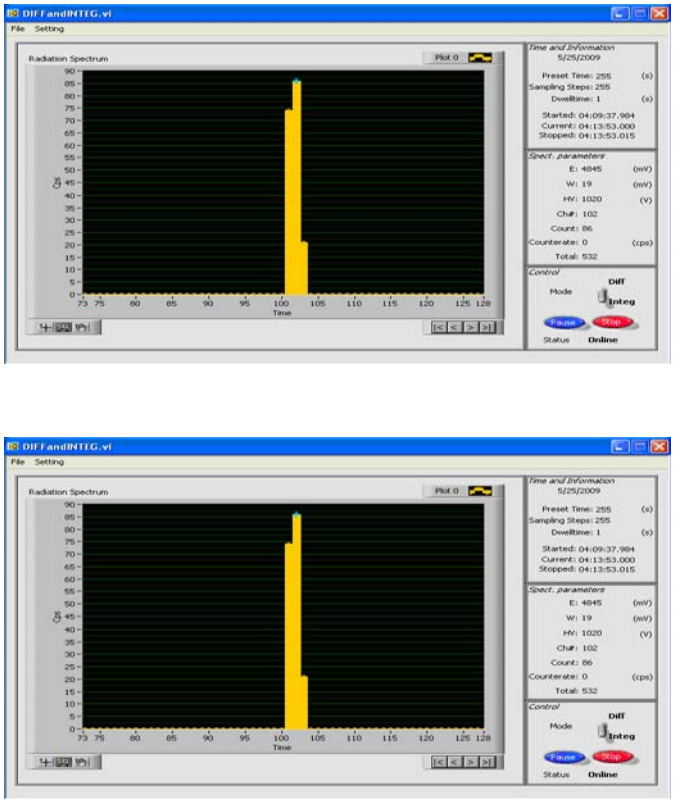

Fig. 2. Spectrum MCA is measured with the digitalised pulser under LabVIEW's application software.

3.2. Features And Parameters

- Preset time: 65535 s
- Realtime = Elapsed time + Deadtime
- Starting, current and stopping time
- Count max: 2 bytes
- Range: 1023 channels
- Drift: 1Ch after 12 hours
- SRAM: 1k
- Interfacing to PC via a serial port, Baudrate 38400.

4. Conclusion

All member staff carried the work out as follows:

1. Studying on DSP method on the basic of VHDL through FPGA chips in SPARTAN-3E Toolkit.

2. Performing the contents with the four items.

3. Applying DSP method to design the tested MCA.

4. Developing both of firmware in C and data acquisition program in LabVIEW 8.5 under Windows XP.

Through the project, we know what FPGA can used for:

+ FPGA can be used to implement almost things

+ FPGAs are currently occupying some major segments:

- **Digital Signal Processing:** since FPGAs now can contain embedded Multipliers, dedicated Arithmetic routines, large amount of On-Chip RAM, then when all these are connected together it can outperform the fastest DSPs.

- **Embedded Microcontroller:** FPGAs are becoming increasingly attractive for embedded control applications.

References

[1]. Heinz Rongen, VHDL Quick start, Julich, German.
[2]. http://www.dsptutor.freeuk.com/Introduction to DSP
[3]. Steven W. Smith, A textbook of DSP techniques, 1997.
[4]. Volnei A. Perdroni, Circuit design with VHDL, TLFeBook, 2004
[5]. Xilinx, Spartan 3^E starter kit board user guide, 2006./.

1.4 - Industrial Applications

INVESTIGATION AND DETERMINATION ON NATURAL RADIOACTIVITY IN COMMONLY BUILDING MATERIALS USED IN VIETNAM AND INITIAL ASSESSMENT ON RADIATION EXPOSURE CAUSED BY THEM

Le Nhu Sieu*, Nguyen Thanh Binh*, Truong Y*, Phan Son Hai*, Nguyen Trong Ngo*, Nguyen Van Phuc*, Nguyen Thi Linh*, Pham Hung Thai*
Mai Thi Huong and Nguyen Van Mai****

**Dalat Nuclear Research Institute*
*** Center for Nuclear Techniques at Hochiminh City*

Abstract: Naturally occurring radionuclides in building materials contribute to external and internal exposure and that is necessary to be investigated. In the research, 218 samples of 11 different kinds of commonly building materials (cement, sand, red-clay brick, gypsum, gravel aggregate, lime/limestone, glazed tile, local & imported granite, local & imported marble) were collected from housing and other building construction sites and from suppliers in Vietnam to measure the natural radioactivity of U-238, Ra-226, Th-232 and K-40. The measurements were carried out using low background gamma-ray spectrometry with HPGe detector. The specific activities of the different building materials varied from 0.89 ÷ 412.50, 0.18 ÷ 395.28, 0.10 ÷ 266.52 and 0.76 ÷ 2006.78 Bq/kg with the average values of 55.57, 52.09, 55.70 and 593.5 Bq/kg for U-238, Ra-226, Th-232 and K-40, respectively. The obtained data were compared with the corresponding reported data of other countries.

The indoor radon concentration and dose rates in 40 houses of 2 selected sites (Hochiminh and Dalat city) were measured with RAD7 equipment and portable device for gamma dose rate/thermoluminescence dosimeter, respectively. The indoor radon of observed houses in Hochiminh city varied from 0.9 ÷ 42.4 Bq/m^3 with the average value of 7.4 Bq/m^3. The indoor radon of observed houses in Dalat city varied from 1.4 ÷ 243.0 Bq/m^3 with the average value of 29.5 Bq/m^3. The dose rates of observed houses in Hochiminh city varied from 0.11 ÷ 0.16 μSv/h with the average value of 0.12 μSv/h. The dose rates of observed houses in Dalat city varied from 0.19 ÷ 0.29 μSv/h with the average value of 0.23 μSv/h.

The radon exhalation rates from 50 building materials samples were determined using solid state nuclear track detectors and/or RAD7. The average values of radon mass exhalation rates of the different building materials samples were 0.0101, 0.0400, 0.0131, 0.0072, 0.0318, 0.0028, 0.0082, and 0.0051 Bq/kg/h for sand, gravel aggregate, imported granite, marble, local granite, glazed tile, red-clay brick and cement, respectively. The average values of radon exhalation fraction (10^{-3} h) were 0.4359, 0.6843, 0.4895, 0.9011, 0.4503, 0.0323, 0.1136, and 0.1413 for the above kinds of building materials.

The activity concentration index and the annual effective dose for a model room (dimensions of 4 m × 5 m × 2.8 m; thickness of 20 cm, and density of 2.35 g/cm^3), in which the structures in a building causing the irradiation to be concerned were evaluated to assess the potential radiological hazard associated with these building materials. The results showed that the enhanced concentration values were sometimes felling into granite tiles, especially imported granite tiles; the potential of exceed the recommendation value was possible. These obtained data aimed to enlarge the database on natural radioactivity in commonly building materials used in Vietnam and to support technical aspects in hazard exposure reduction.

1. Introduction

It is always possible radiological risks to human health caused by natural and artificial radionuclides (included the external and internal exposure) with an average total effective dose of 2.96 mSv/year. Naturally occurring radioactive materials (NORMs) are the major sources which cause exposure to people by ionizing radiation of about 2.42 mSv/year (worldwide value). Materials derived from rocks and soils contain mainly natural radionuclides of the U and Th series, and K-40. These radionuclides pose exposure risks externally due to their gamma-ray emissions and internally due to radon and its progeny which emit alpha particles with the contributions of 31% and 54%, respectively to the total of annual effective dose caused by the NORMs. In the uranium series, the decay chain segment starting from radium is radiologically the most important and, therefore, reference is often made to radium instead of uranium. The worldwide average concentrations of radium, thorium and potassium in the earth's crust are about 40, 40 and 400Bq/kg, respectively (UNSCEAR, 1993 & 2000).

Building materials are commonly originated from rocks and soils and also contain the NORMs. In order to be able to assess radiological risk linking to standards and regulatories on natural radioactivity in building materials, it is important to study the levels of radiation emitted from them. Investigation levels can be derived for practical monitoring purposes. Because more than one radionuclide contribute to the dose, it is practical to present investigation levels in the form of an activity concentration index. The activity concentration index should also take into account typical ways and amounts in which the material is used in a building. The activity concentration index shall not exceed the limited value depending on the dose criterion and the way and the amount the material is used in a building.

The most important source of indoor radon is the underlying soil but in some cases the building materials may be an important source. In some cases, the main part of indoor radon on the upper floors of a building originates from building materials. Typical indoor radon concentration due to building materials is about 40 Bq/m^3, but in some zones and in rare cases it may rise up to greater than 1000 Bq/m^3. The amount of radium in building materials should be restricted at least to a level where it is unlikely that it could be a major cause for exceeding the design level of 200 Bq/m^3 for indoor radon in future constructions.

The relationship between Ra-226 specific radioactivity in building materials and indoor radon of a room is expressed by a linear parameter of radon exhalation rate. When the radon exhalation rates from all of the building materials in a house are available, the potential of indoor radon of that house can be determined.

The above mentioned subjects have been studied and developed completely in many countries and there are a lot of research works issued while the data of natural radioactivity, indoor radon or radon exhalation rate of Vietnam are rarely and confusingly. The project on "Investigation and determination on natural radioactivity in commonly building materials used in Vietnam and initial assessment on radiation exposure caused by them" has been programmed and carried out for two years in order to solve the problem; and that aims to contribute more effectively to environmental radioactivity protection affair and human health of public and to support technical aspects in hazard exposure reduction.

The objectives of the project have focused on: (1) to enlarge the database of specific radioactivites of natural radionuclides (uranium, thorium series, and radioactive potassium) in commonly building materials; (2) to evaluate primitively the indoor radiation exposures caused by natural radionuclides from building materials; (3) to support scientific and technical aspects for national project on the general investigation and assessment of public doses caused building materials in Vietnam; and (4) to support scientific and technical aspects towards to establishing design level for indoor radon concentration of new constructions.

In order to achieve the objectives, the contents of the project have been programmed and carried out as follows: (1) Standardize the method for the determination of natural radioactivities in commonly building materials by using low level gamma background spectrometry; the method for the determination of radon exhalation rate; indoor radon concentration, and dose rate; (2) design for sampling, and collect about 120 building material samples; (3) determine on specific radioactivities of natural radionuclides (U-238, Ra-226, Th-232, and K-40), and radon exhalation rates of building materials samples; (3) measure on indoor radon concentration and dose rate in some typical houses of selected sites; (4) investigate on the relationship of radiation sources and radiation exposures in some room models; and (5) apply some advanced statistics techniques for obtained data.

2. Typical Results

Summarization on the gathered information/document related to research contents of the project, included: (1) characteristic and properties of building materials; (2) building materials minerals in Vietnam; (3) natural radioactivity in building materials and indoor radon; (4) radon exhalation from building materials; (5) radiation protection principles; and (6) international and national regulatories related to this subjects.

The established methods were applied in this investigation, included: (1) the determination method of natural radioactivity in building materials samples using by low level gamma background spectrometer; (2) the indoor radon measuring method accompanied with RAD7; (3) the determination method of radon exhalation rate in building materials samples using solid state nuclear track detectors and/or RAD7; and (4) the methods of gamma dose rate measurement with portable device and thermoluminescence dosimeter.

Sample Collection and Sample Preparation:

Results of radioactivity measurement in some imported and domestic building materials, like cement, sand, red-clay brick, gypsum, gravel aggregate, lime/limestone, glazed tile, granite, marble are presented in this research. These particular materials were considered because they are dominant used in construction of dwellings in Vietnam.

The sand samples originating from major rivers of Vietnam were collected from restores of local building materials companies (30 samples). The red-clay brick samples originating from local clay mines of different provinces over the whole country were collected from brick manufactures (23 samples). The lime/limestone and gravel aggregate samples were collected from major mines being exploited (11 lime/limestone samples, 40 gravel aggregate samples). The local & imported granite, marble, and glazed tile samples were purchased from different dominant trading brands (10 of

imported granites, 9 of imported marbles, 25 of local granites, 5 of local marbles, and 35 glazed tile samples). The cement and gypsum samples were collected from some high capacity cement plants (17 cement samples, 8 gypsum samples). In addition, some of raw materials samples for cement and glazed tile produce were also collected (5 samples).

About 6kg of each sample with large grain size was ground to fine powder, except for cement, gypsum & sand samples; and then was homogenized and air dried; and was divided into two parts: one for the determination of U-238, Th-232, Ra-226 and K-40 radionuclides and the other for radon exhalation rate.

For the determination of U-238, Th-232, Ra-226 and K-40 radioactivities on low level gamma background spectrometer, building material samples were prepared as follows: An approximation of 3.5kg sample was ground to fine powder with the particle size to be less than 20μm by using Puluerisette grinder (except sand, cement, lime, and gypsum samples). About 200g of fine powder drawn out from each sample was filled into a cylinder polyethylene container (40 mm in height, 60mm in diameter) and was sealed in gas tight, impermeable radon with paraffin. An approximation of 140g fine powder drawn out from each sample was mixed carefully with ~70g polyester resin and then was cast by a cylindrical steel container (40mm height and 60mm diameter). The technique aims to approach that all of the samples get approximately a matrix density (1.224 ± 0.122 g/cm^3) and the same measuring configuration. This measuring configuration with 40mm in height and 60mm in diameter for building materials matrix has been investigated on the estimation of self-attenuation corrections over the depth of materials matrix, and it is supposed that one is the most suitable to be used in this research. The samples after casting were then stored for 25–30 days before counting in order to reach radioactive equilibrium.

For the determination of radon exhalation rates from building materials: (1) An approximation of 1000g fine powder drawn out from each sample was filled into a cylinder steel container (14cm in height, 13.5cm in diameter) accompanied with UPILON nuclear track detector inside, and was sealed in gas tight, impermeable radon. The detector was exposed for a long time at least two months; (2) about 2000g of raw sample (to keep intact condition) was sealed in Radon Box equipment (the dimensions of 57×37×16.5cm) and then determined of radon exhalation rates; and (3) about 2000g of fine powder sample (to be ground condition) was sealed in Radon Box equipment and then determined of radon exhalation rates.

Standardize The Method for The Determination of Natural Radioactivities In Commonly Building Materials By Using Low Level Gamma Background Spectrometry:

Study and investigation the optimal thickness for building material samples with cylinder polyethylene container (60mm in diameter): The soil reference materials IAEA-CU-2006-03 was applied to measure on low level gamma background spectrometer with the different thicknesses of 0.5cm sample by sample from 0.5cm to 7.0cm. The detector efficiencies were determined by different energies (peaks) and thicknesses. The curve express the decrease of detector efficiency versus increase of thickness was fitted by Disk Source Efficiency computer code (Japan). As a result, the optimal thickness for building material samples was of 4.0cm.

Investigation and correction of the self attenuation effect: The detector efficiencies were determined at any energy for the different distances from the detector to the disk source of reference materials. The experience was performed with some different distances (0.55; 0.70; 1.00; 1.50; 2.00; 2.50; 3.00; 3.50; 4.00; 4.50 and 5.00cm) from the detector to the disk source. Disk Source Efficiency computer code was applied to calculate and correct the self attenuation effect immediately.

The specific radioactivity of Ra-226 in building materials was determined through its daughters so that all of the samples were prepared to seal in gas tight & impermeable radon at least 21 days). In this study, two investigated techniques were applied: sealing by paraffin and sealing by polyester resin. The estimation of the both methods showed that the sealing technique by polyester resin was better in comparison with paraffin.

The Results of Natural Radioactivity Determination In Building Material Samples:

The radioactivity of the samples was measured on gamma spectrometry with the HpGe detector model GX3019, which has a relative efficiency of 30%, an energy resolution of 1.90keV at 1333keV and a peak-to-Compton ratio of 56:1. Computer software MAESTRO-32 was used to analyze obtained spectrums.

Detector calibration was done by soil reference materials (IAEA-CU-2006-03 containing Mn-54, Co-60, Zn-65, Cd-109, Cs-134, Cs-137, Pb-210, Am-241 radionuclides). The counting time for each measurement was around 90000s, in order to obtain good counting statistics.

To measure Ra-226, peaks from Pb-214 at energies of 295.2keV (18.53%) & 351.9keV (35.85%); and peak from Bi-214 at energy of 1764.5keV (15.36%) were used. To measure Th-232, peaks from Ac-228 at energies of 911.2keV (26.61%) and 338.3keV (11.25%) were used; and it was checked with peaks from Tl-208 at energies of 583.2keV (84.55%) and 2614.5keV (99.16%). Activity of K-40 was measured from its intensive line at 1460.8keV (10.67%).

The specific radioactivities of natural radionuclides (U-238, Ra-226, Th-232, and K-40) in 218 building material samples (divided into 11 kinds as major using in buildings which collected over the whole country) were determined by low level background spectrometer followed the established method. The means and ranges of specific radioactivities of natural radionuclides (U-238, Ra-226, Th-232 and K-40) in building material samples are shown on Table I and Fig. 1. The obtained data in this investigation reflect to the actual state and to be compared with the corresponding reported data of other countries.

Tab I. Mean and range of the specific radioactivities of Ra-226, Th-232 and K-40 in building materials used in Vietnam.

No.	Building materials	Abb.	No. of samples	Specific radioactivities, Bq/kg		
				Ra-226	Th-232	K-40
				Mean ± Std. Range	Mean ± Std. Range	Mean ± Std. Range
1	Sand	SA	30	26.74 ± 30.30	39.77 ± 61.70	506.9 ± 317.1

				2.10 ÷ 162.46	1.79 ÷ 266.52	2.5 ÷ 1096.8
2	Gravel aggregate	GA	40	47.18 ± 53.19 4.59 ÷ 224.93	51.53 ± 50.48 0.10 ÷ 196.93	720.6 ± 473.0 0.8 ÷ 1440.3
3	Imported granite	IG	10	79.15 ± 133.49 1.82 ÷ 395.28	86.19 ± 67.21 10.56 ÷ 197.26	1126.0 ± 584.8 164.1 ÷ 2006.6
4	Imported marble	IM	9	11.29 ± 14.20 0.67 ÷ 40.23	0.76 ± 0.51 0.18 ÷ 1.45	5.1 ± 5.9 1.2 ÷ 11.9
5	Local granite	LG	25	59.48 ± 43.40 0.77 ÷ 162.48	85.17 ± 55.89 0.18 ÷ 190.67	992.0 ± 443.0 162.1 ÷ 1593.0
6	Local marble	LM	5	12.37 ± 12.97 0.72 ÷ 26.40	2.30 ± 0.97 1.33 ÷ 3.64	6.6 ± 4.8 2.3 ÷ 12.5
7	Glazed tile	GT	35	95.14 ± 47.27 15.26 ÷ 270.85	74.64 ± 28.14 0.50 ÷ 147.57	658.7 ± 273.9 0.8 ÷ 1409.1
8	Lime stone	LI	11	14.32 ± 14.39 4.46 ÷ 55.64	8.79 ± 19.25 0.96 ÷ 60.04	39.0 ± 59.6 4.2 ÷ 211.5
9	Clay brick	BR	23	64.35 ± 23.78 31.34 ÷ 113.15	77.57 ± 32.49 33.29 ÷ 169.81	589.0 ± 171.8 329.0 ÷ 868.8
10	Gypsum	GY	8	8.80 ± 9.52 0.18 ÷ 28.80	6.46 ± 4.87 0.39 ÷ 16.24	74.6 ± 72.8 1.9 ÷ 195.2
11	Cement	CE	17	39.86 ± 17.43 23.54 ÷ 67.46	25.46 ± 4.69 16.27 ÷ 32.22	243.5 ± 62.2 83.7 ÷ 308.9

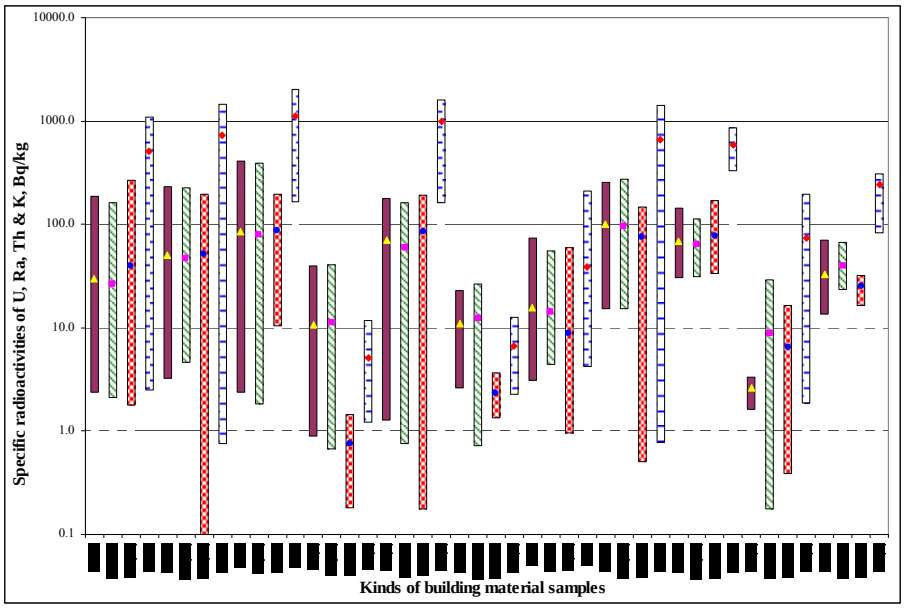

Fig. 1. Mean and range of U-238, Ra-226, Th-232 and K-40 radioactivities in 11 kinds of building materials (213 samples) used in Vietnam

The Results of The Calculation of Activity Concentration Index, Dose Rate, Annual Effective Dose Caused By Building Materials:

Activity concentration index I:

Activity concentration index, or shortly, gamma index, I is defined in the following way:

$$I = \frac{C_{Ra}}{300\,Bq.kg^{-1}} + \frac{C_{Th}}{200\,Bq.kg^{-1}} + \frac{C_K}{3000\,Bq.kg^{-1}}$$

Where C_{Ra}, C_{Th} *and* C_K are the radium, thorium and potassium activity concentrations (Bq/kg) in the building material, respectively. The activity concentration index is derived to identify whether a dose criterion is met. The gamma index should not exceed limit values depending on the dose criterion (EC 1999) and the amount material used in a building.

Investigation levels can be derived for practical monitoring purposes. Because more than one radionuclide contribute to the dose, it is practical to present investigation levels in the form of a gamma index, I. The gamma index also takes into account typical ways and quantities in which the material is used in a building. A methodology which can be used to derive such indexes is described in Annex I of Report 112.

The gamma index should be used only as a screening tool for identifying materials which might be of concern. Any actual decision on restricting the use of a material should be based on a separate dose assessment. Such assessment should be based on scenarios where the material is used in a typical way for the type of material in question. Scenarios resulting in theoretical, most unlikely maximum doses should be avoided.

The activity concentration index, I, was calculated as the above formula which was proposed by Ministry of Construction of Socialist Republic of Vietnam's Regulatory: TCXDVN 397:2007 (adopted by the European Commission 1999). The results are shown on Fig. 2. In ascending, the average gamma indexes of 11 kinds of building materials are of the sequence: local & imported marble, gypsum, lime/limestone, cement, sand, gravel aggregate, red-clay brick, glazed tile, local granite, and the highest belonging to imported granite, which is exceeds the dose criterion of 1mSv. It was found that values of I being larger than unit fell into: 2 sand samples; 8 gravel aggregate samples; 3 red-clay brick samples; 12 glazed tile samples; 14 local granites; and 5 imported granites. In particularly, the I values of some imported granites are significant to be considered in the assessment of radiological risk linking to standards and regulatories on natural radioactivity in building materials.

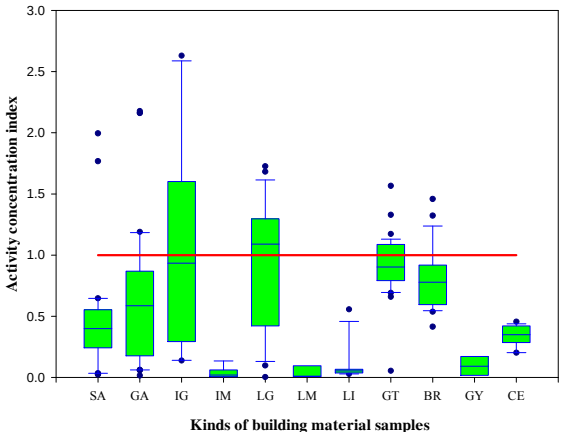

Fig. 2. Box-and-Whisker plot of activity concentration index calculated from specific radioactivities of 11 kinds of building materials over 213 samples used in Vietnam.

The activity concentration indexes were calculated over province by province (model room with the dimensions of 4m × 5m × 2.8m, thickness of 20cm, density of 2.35g/cm^3; all walls used by red-clay brick and mortar, floor and ceiling used by concrete). In this research, sand, red-clay brick, gravel aggregate were applied separately by every location; cement, gypsum were applied by the whole country mean values. The calculated activity concentration indexes are presented in Table II. The obtained data showed that the potential of exceed the recommendation value was possible in some provinces.

Tab II. The activity concentration indexes were calculated over province by province (model room with the dimensions of 4m × 5m × 2.8m, thickness of 20cm, density of 2.35g/cm^3; all walls used by red-clay brick and mortar, floor and ceiling used by concrete).

Province	**Activity concentration index, I_1**		**Note**
	Mean	***Range***	
An Giang	0.41	0.35 ÷ 0.45	Sand, red-clay brick, gravel aggregate were applied separately by every location; cement, gypsum were applied by the whole country mean values.
Ba Ria - Vung tau	0.70	0.66 ÷ 0.72	
Binh Dinh	0.75	0.72 ÷ 0.79	
Binh Duong	0.52	0.50 ÷ 0.55	
Binh Thuan	0.67	0.63 ÷ 0.70	
Lam dong	1.12	1.06 ÷ 1.20	
DakLak	0.46	0.41 ÷ 0.50	
Dong Nai	0.45	0.42 ÷ 0.48	
Dong thap	0.41	0.35 ÷ 0.45	
Gia Lai	0.62	0.53 ÷ 0.69	
Ha Noi	0.49	0.43 ÷ 0.54	
Ha Tinh	0.69	0.65 ÷ 0.72	
Thua Thien - Hue	0.78	0.75 ÷ 0.82	
Khanh Hoa	0.50	0.46 ÷ 0.53	
PQ, Kien Giang	0.60	0.56 ÷ 0.63	
Kien Giang	0.33	0.26 ÷ 0.38	
Kon Tum	1.01	0.94 ÷ 1.07	
Long Xuyen	0.40	0.34 ÷ 0.44	
Ninh Thuan	0.89	0.83 ÷ 0.95	
Phu Yen	0.52	0.48 ÷ 0.55	
Quang Binh	0.26	0.21 ÷ 0.31	
Quang Nam, Da Nang	0.61	0.54 ÷ 0.66	

Quang Ngai	0.83	0.74 ÷ 0.90	
Quang Tri	0.34	0.28 ÷ 0.38	
Song Be	0.33	0.29 ÷ 0.37	
Vinh Long	0.41	0.35 ÷ 0.45	
Vinh Phuc	0.46	0.41 ÷ 0.51	
Mean	*0.57*	*0.21 ÷ 1.20*	
The whole country mean value	**0.61**	**0.12 ÷ 1.91**	To be calculated over kind by kind of building materials

Dose Rate and Annual Effective Dose Caused By Building Materials:

The absorbed dose rates in air in a room can be calculated by using the specific dose rates given in Table III. The specific dose rates (in unit's nGy h^{-1} per Bq kg^{-1}*)* for Ra-226, Th-232 and K-40 are given for different screening tool of identifying materials which might be of concern. Indoor dose rates for a model room (the dimensions of 4m × 5m × 2.8m, thickness of 20cm, density of 2.35g/cm^3, and the background of 50nGy/h) are calculated with different structures in a building causing the irradiation as follows:

- All structures: $D^{\cdot} = 0.92\times C_{Ra} + 1.1\times C_{Th} + 0.08\times C_K$

- Floor and walls: $D^{\cdot} = 0.67\times C_{Ra} + 0.78\times C_{Th} + 0.057\times C_K$

- Floor only: $D^{\cdot} = 0.24\times C_{Ra} + 0.28\times C_{Th} + 0.02\times C_K$

- Superficial material, tile/stone on all walls: $D^{\cdot} = 0.12\times C_{Ra} + 0.14\times C_{Th} + 0.0096\times C_K$

The annual effective dose, D_E (mSv), due to gamma radiation from building materials with the annual exposure time of 7000h (EC, 1999) was calculated as follows:

$D_E = 0.7$ (Sv.Gy^{-1}) × 7000 (h) × 10^{-6} × $D^{\cdot}$ (nGy.h^{-1}),

The mean & range of dose rates and annual effective doses depending on the structures in a building causing the irradiation in 11 kinds of building material samples are also shown in Table IV. The obtained data shown that there are many building materials with annual effective doses exceeding the criterion of 1mSv in the conservative case of all structures in a building, for an example, imported granites approaches up to 3.24mSv. To reduce the hazard exposure, therefore, it is necessary to consider to using restrictively the enhanced NORMs in building construction. In this situation, for some materials where the value of *I* exceeds the recommended value, the annual effective dose can be below the upper limit. Obviously, if the above highest imported granite is used with structure of superficial material only on all walls, the annual effective dose could reduce down to 0.41mSv.

Tab III. Parameter values used in calculating the doses (EC, RP-112)

Dimensions of the model room	4 m x 5 m x 2.8 m
Thickness and density of the structures	20 cm; 2350 kg m^{-3} (concrete)
Annual exposure time	7000 h

Dose conversion	0.7 Sv Gy^{-1}		
Background	50 nGy h^{-1}		
	Specific dose rate, nGy h^{-1}/Bq kg^{-1}		
Structures in a building causing the irradiation:	***Ra-226***	***Th-232***	***K-40***
Floor, ceiling and walls (all structures)	0.92	1.1	0.080
Floor and walls (wooden ceiling)	0.67	0.78	0.057
Floor only (wooden house with concrete floor)	0.24	0.28	0.020
Superficial material: tile or stone on all walls (thickness 3 cm, density 2600 kgm^{-3})	0.12	0.14	0.0096

Table IV. Mean and range of activity concentration indexes, dose rates and annual effective doses in building materials used in Vietnam.

No.	**Building materials**	**Abb.**	**I**	**Structures in a building causing the irradiation**	$\dot{D}$ **, nSv.h^{-1}**	**D_E, mSv**
			Mean **Range**		**Mean** **Range**	**Mean** **Range**
1	Sand	SA	0.45 0.02 ÷ **1.99**	All structures	107.6 5.6 ÷ 472.6	0.53 0.03 ÷ **2.32**
2	Gravel aggregate	GA	0.64 0.02 ÷ 2.18		154.9 4.3 ÷ 530.6	0.76 0.02 ÷ **2.60**
3	Imported granite	IG	**1.07** 0.14 ÷ **2.63**	All structures	257.7 33.0 ÷ 661.4	**1.26** 0.16 ÷ **3.24**
				Floor and walls	184.4 23.6 ÷ 476.3	0.90 0.12 ÷ **2.33**
				Floor only	65.6 8.4 ÷ 170.2	0.32 0.04 ÷ 0.83
				Superficial material: material on all walls	32.4 4.1 ÷ 84.5	0.16 0.02 ÷ 0.41
4	Imported marble	IM	0.04 0.00 ÷ 0.13	All structures	9.8 0.0 ÷ 37.0	0.05 0.00 ÷ 0.18
				Floor and walls	7.1 0.0 ÷ 27.0	0.04 0.00 ÷ 0.13
				Floor only	2.6 0.0 ÷ 9.7	0.01 0.00 ÷ 0.05

				Superficial material: material on all walls	1.3 0.0 ÷ 4.8	0.01 0.00 ÷ 0.02
5	Local granite	LG	0.94 0.00 ÷ **1.73**	All structures	224.6 0.9 ÷ 409.0	**1.10** 0.00 ÷ **2.00**
				Floor and walls	160.6 0.7 ÷ 293.2	0.79 0.00 ÷ **1.44**
				Floor only	57.2 0.2 ÷ 104.6	0.28 0.00 ÷ 0.51
				Superficial material: material on all walls	28.2 0.1 ÷ 51.8	0.14 0.00 ÷ 0.25
6	Local marble	LM	0.04 0.01 ÷ 0.10	All structures	11.6 1.8 ÷ 27.3	0.06 0.01 ÷ 0.13
				Floor and walls	8.4 1.3 ÷ 19.8	0.04 0.01 ÷ 0.10
				Floor only	3.0 0.5 ÷ 7.1	0.01 0.00 ÷ 0.03
				Superficial material: material on all walls	1.5 0.2 ÷ 3.5	0.01 0.00 ÷ 0.02
7	Glazed tile	GT	0.91 0.05 ÷ **1.57**	All structures	222.3 14.7 ÷ 404.4	**1.09** 0.07 ÷ **1.98**
				Floor and walls	159.5 10.7 ÷ 291.9	0.78 0.05 ÷ **1.43**
				Floor only	56.9 3.8 ÷ 104.0	0.28 0.02 ÷ 0.51
				Superficial material: material on all walls	28.2 1.9 ÷ 51.4	0.14 0.01 ÷ 0.25
8	Lime stone	LI	0.10 0.03 ÷ 0.56	All structures	24.2 7.8 ÷ 134.2	0.12 0.04 ÷ 0.66
9	Clay brick	BR	0.80 0.41 ÷ **1.46**		191.7 100.0 ÷ 347.3	0.94 0.49 ÷ **1.70**
10	Gypsum	GY	0.09 0.00 ÷ 0.22		20.2 1.1 ÷ 48.6	0.10 0.01 ÷ 0.24
11	Cement	CE	0.34 0.20 ÷ 0.46		84.2 49.6 ÷ 114.5	0.41 0.24 ÷ 0.56

The Results of Dose Rate Measurements At Two Selected Sites (Hochiminh and Dalat City):

The measured results of indoor dose rates caused by natural radionuclides of four periods of different seasons in 40 typical houses at HCM and Dalat city are shown in Table V & VI. The results of comparison of two methods of dose rate measurement (portable device & TLD) are presented on Fig. 3. The average dose rate of observed houses in Dalat city was higher 1.92 times in comparison with Hochiminh city.

Tab V. Effective dose rates measured in some houses at Hochiminh city

Measuring site	**Effective dose rate, μSv/h**							
	Portable device			***TLD***	***Portable device***			***TLD***
	Phase 1	*Phase2*	*Mean*	*Phase 1*	*Phase 3*	*Phase 4*	*Mean*	*Phase 2*
SL-HCM-01	0.13	0.13	0.13	0.10 ± 0.01	0.13	0.13	0.13	0.14 ± 0.01
SL-HCM-02	0.14	0.14	0.14	0.08 ± 0.01	0.15	0.14	0.15	0.15 ± 0.01
SL-HCM-03	0.12	0.12	0.12	0.10 ± 0.01	0.12	0.12	0.12	0.11 ± 0.01
SL-HCM-04	0.14	0.14	0.14	0.12 ± 0.01	0.12	0.16	0.14	0.14 ± 0.01
SL-HCM-05	0.13	0.13	0.13	0.14 ± 0.01	0.13	0.14	0.14	0.16 ± 0.01
SL-HCM-06	0.13	0.13	0.13	0.10 ± 0.01	0.13	0.12	0.13	0.13 ± 0.01
SL-HCM-07	0.15	0.14	0.15	0.10 ± 0.01	0.13	0.13	0.13	0.16 ± 0.03
SL-HCM-08	0.12	0.12	0.12	0.09 ± 0.01	0.13	0.10	0.12	0.11 ± 0.01
SL-HCM-09	0.13	0.13	0.13	0.11 ± 0.01	0.14	0.13	0.14	0.14 ± 0.01
SL-HCM-10	0.14	0.13	0.13	0.12 ± 0.01	0.12	0.14	0.13	0.15 ± 0.01
SL-HCM-11	0.15	0.13	0.14	0.09 ± 0.01	0.13	0.12	0.13	0.14 ± 0.01
SL-HCM-12	0.11	0.12	0.11	0.08 ± 0.01	0.12	0.12	0.12	0.13 ± 0.01
SL-HCM-13	0.12	0.11	0.11	0.08 ± 0.01	0.11	0.11	0.11	0.12 ± 0.01

SL-HCM-14	0.13	0.13	0.13	0.08 ± 0.01	0.14	0.11	0.13	0.14 ± 0.01
SL-HCM-15	0.11	0.12	0.12	0.12 ± 0.01	0.13	0.12	0.13	0.13 ± 0.01
SL-HCM-16	0.17	0.15	0.16	0.09 ± 0.01	0.14	0.14	0.14	0.16 ± 0.01
SL-HCM-17	0.15	0.15	0.15	0.09 ± 0.01	0.16	0.15	0.16	0.16 ± 0.01
SL-HCM-18	0.14	0.13	0.14	0.12 ± 0.01	0.13	0.12	0.13	0.13 ± 0.01
SL-HCM-19	0.11	0.13	0.12	0.09 ± 0.02	0.14	0.14	0.14	0.12 ± 0.01
SL-HCM-20	0.13	0.13	0.13	0.10 ± 0.01	0.13	0.13	0.13	0.14 ± 0.01
Mean	**0.13**	**0.13**	**0.13**	**0.10**	**0.13**	**0.13**	**0.13**	**0.14**
Range	**0.11 ÷ 0.17**			**0.08 ÷ 0.14**	**0.11 ÷ 0.16**			**0.11 ÷ 0.16**

Tab VI. Effective dose rates measured in some houses at Dalat city

Measuring site	**Effective dose rate, μSv/h**							
	Portable device			***TLD***	***Portable device***			***TLD***
	Phase 1	*Phase 2*	*Mean 1&2*	*Phase 1*	*Phase 3*	*Phase 4*	*Mean 3&4*	*Phase 2*
SL-DL-01	0.19	0.19	0.19	0.17 ± 0.03	0.19	0.20	0.19	0.20 ± 0.01
SL-DL-02	0.25	0.24	0.24	0.27 ± 0.01	0.23	0.25	0.23	0.28 ± 0.03
SL-DL-03	0.22	0.23	0.23	0.19 ± 0.01	0.21	0.26	0.24	0.25 ± 0.02
SL-DL-04	0.26	0.26	0.26	0.25 ± 0.02	0.27	0.26	0.27	0.28 ± 0.01
SL-DL-05	0.23	0.23	0.23	0.23 ± 0.01	0.24	0.22	0.23	0.27 ± 0.01
SL-DL-06	0.27	0.27	0.27	0.22 ± 0.01	0.28	0.28	0.28	0.24 ± 0.02
SL-DL-07	0.25	0.25	0.25	0.24 ± 0.03	0.24	0.26	0.24	0.30 ± 0.01
SL-DL-08	0.25	0.25	0.25	0.19 ± 0.03	0.24	0.26	0.25	0.28 ± 0.02
SL-DL-09	0.27	0.27	0.27	0.25 ± 0.02	0.26	0.28	0.27	0.28 ± 0.01
SL-DL-10	0.23	0.22	0.22	0.24 ± 0.02	0.22	0.21	0.22	0.23 ± 0.02
SL-DL-11	0.20	0.21	0.21	0.18 ± 0.01	0.22	0.21	0.22	0.21 ± 0.02
SL-DL-12	0.24	0.23	0.24	0.19 ± 0.01	0.22	0.24	0.23	0.26 ± 0.02
SL-DL-13	0.20	0.26	0.23	0.21 ± 0.01	0.22	0.31	0.28	0.21 ± 0.01
SL-DL-14	0.22	0.22	0.22	0.17 ± 0.01	0.22	0.20	0.21	0.20 ± 0.01

SL-DL-15	0.20	0.23	0.22	0.21 ± 0.02	0.22	0.25	0.23	0.29 ± 0.01
SL-DL-16	0.23	0.21	0.22	0.21 ± 0.01	0.21	0.20	0.21	0.23 ± 0.01
SL-DL-17	0.21	0.22	0.21	0.20 ± 0.01	0.23	0.21	0.22	0.24 ± 0.02
SL-DL-18	0.18	0.19	0.19	0.18 ± 0.01	0.20	0.19	0.20	0.23 ± 0.01
SL-DL-19	0.19	0.21	0.20	0.22 ± 0.01	0.21	0.24	0.23	0.26 ± 0.01
SL-DL-20	0.29	0.26	0.28	0.19 ± 0.01	0.24	0.27	0.25	0.26 ± 0.01
Mean	**0.23**	**0.23**	**0.23**	**0.21**	**0.23**	**0.24**	**0.23**	**0.25**
Range	**0.18 ÷ 0.29**			**0.17 ÷ 0.27**	**0.19 ÷ 0.31**			**0.20 ÷ 0.30**

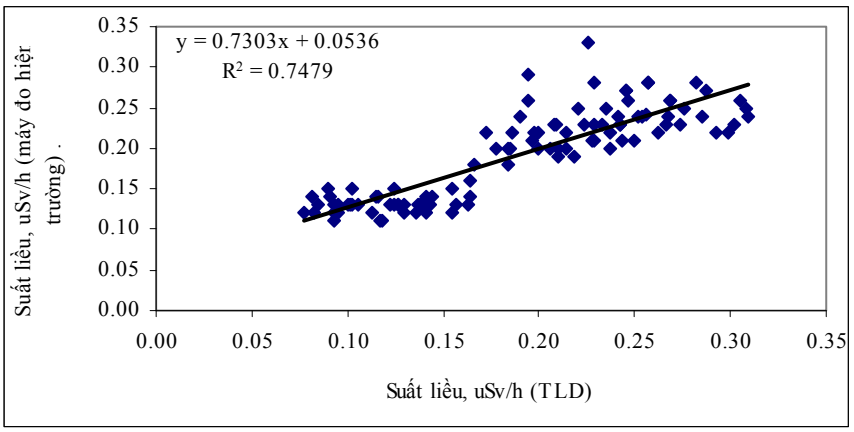

Fig. 3. Comparison of effective dose rates measured by two different methods: TLD versus portable device.

The Results of Indoor Radon Measurement In Some Houses At Two Selected Sites (Hochiminh City and Dalat city):

Hochiminh City:

The measurement of indoor radon concentration were carried out over four periods of different seasons: changing season from rainy to dry (10/2007-12/2007), dry season (1/2008-3/2008), changing season from dry to rainy (4/2008-6/2008) and rainy season (7/2008-9/2008) in 20 typical houses at HCM city. The indoor radon concentration corresponding with the above periods varied: 1.4 ÷ 39.6; 0.9 ÷ 28.3; 2.8 ÷ 42.4; and 2.8 ÷ 36.7 Bq/m^3; with the average value of 7.9; 6.2; 7.7; and 7.8 Bq/m^3, respectively. The annual mean value for the whole year was 7.4 Bq/m^3. The result shown that the average indoor radon concentration of rainy season was higher in comparison with the dry season.

The detailed information related to this experiment (type of house, kind of building materials used in observed house, room dimensions, etc.) were concerned. The selected typical houses were located widespread over districts of HCM city and were presented on Fig. 4. The means and ranges of indoor radon concentration of 20 houses in HCM city are shown on Table VII. The variations of indoor radon concentration in a day of some sites at HCM city are shown on Fig. 5. The obtained data showed that indoor radon increased towards the night and reached the peak of indoor radon at early morning time.

Tab VII. Indoor radon concentration (Bq/m^3) at HCMC

Site	**Phase 1** *(rainy→dry)*		**Phase 2** *(dry)*		**Phase 3** *(dry→rainy)*		**Phase 4** *(rainy)*	
	Mean	***Range***	***Mean***	***Range***	***Mean***	***Range***	***Mean***	***Range***
Rn-HCM-01	7.9	1.4 ÷ 17.2	5.5	0.9 ÷ 14.2	6.8	2.8 ÷ 22.9	6.4	2.8 ÷ 13.9
Rn-HCM-02	4.6	1.4 ÷ 14.3	4.9	0.9 ÷ 11.1	5.3	2.8 ÷ 11.1	8.2	2.8 ÷ 17.2
Rn-HCM-03	12.1	2.8 ÷ 21.2	15.8	4.2 ÷ 28.3	16.2	2.8 ÷ 42.4	18.1	2.8 ÷ 36.7
Rn-HCM-04	13.7	2.8 ÷ 39.6	9.1	1.4 ÷ 21.6	9.0	2.8 ÷ 22.6	10.6	2.8 ÷ 33.4
Rn-HCM-05	6.8	2.8 ÷ 14.3	4.5	0.9 ÷ 12.6	6.3	2.8 ÷ 19.5	6.3	2.8 ÷ 11.6
Rn-HCM-06	5.9	1.4 ÷ 9.9	3.9	0.9 ÷ 9.8	5.5	2.8 ÷ 11.6	5.2	2.8 ÷ 13.9
Rn-HCM-07	14.3	2.8 ÷ 30.6	11.1	5.6 ÷ 19.5	10.1	2.8 ÷ 25.0	12.6	2.8 ÷ 25.4
Rn-HCM-08	9.9	2.8 ÷ 31.1	7.1	0.9 ÷ 18.4	11.9	2.8 ÷ 39.0	5.1	2.8 ÷ 8.5
Rn-HCM-09	8.4	2.8 ÷ 22.2	6.9	2.8 ÷ 13.9	9.0	2.8 ÷ 22.9	6.9	2.8 ÷ 16.7
Rn-HCM-10	8.2	2.8 ÷ 22.2	5.4	0.9 ÷ 14.3	6.5	2.8 ÷ 17.2	7.0	2.8 ÷ 17.4
Rn-HCM-11	6.8	2.8 ÷ 17.2	4.0	0.9 ÷ 9.4	6.4	2.8 ÷ 13.9	5.4	2.8 ÷ 11.5
Rn-HCM-12	6.0	2.8 ÷ 17.0	5.8	0.9 ÷ 13.9	9.0	2.8 ÷ 25.0	5.4	2.8 ÷ 17.2
Rn-HCM-13	6.8	2.8 ÷ 19.8	3.4	0.9 ÷ 7.7	4.4	2.8 ÷ 11.6	5.3	2.8 ÷ 14.1
Rn-HCM-14	7.2	2.8 ÷ 23.2	4.6	0.9 ÷ 12.7	4.4	2.8 ÷ 13.9	8.7	2.8 ÷ 14.1
Rn-HCM-15	6.1	2.8 ÷ 17.2	6.1	0.9 ÷ 10.3	4.4	2.8 ÷ 11.6	12.4	2.8 ÷ 22.6
Rn-HCM-16	7.2	2.8 ÷ 17.0	4.3	0.9 ÷ 12.2	6.1	2.8 ÷ 17.0	5.9	2.8 ÷ 16.7
Rn-HCM-17	6.4	2.8 ÷ 13.9	4.5	0.9 ÷ 15.1	7.9	2.8 ÷ 28.7	6.0	2.8 ÷ 11.6
Rn-HCM-18	6.4	2.8 ÷ 17.0	4.7	0.9 ÷ 9.4	6.3	2.8 ÷ 19.8	6.0	2.8 ÷ 16.7

Rn-HCM-19	4.6	2.8 ÷ 8.3	5.3	1.4 ÷ 15.9	9.5	2.8 ÷ 29	5.5	2.8 ÷ 11.5
Rn-HCM-20	8.4	2.8 ÷ 22.2	6.8	0.9 ÷ 24.4	9.8	2.8 ÷ 33.9	7.8	2.8 ÷ 19.8
Mean	**7.9**	**1.4 ÷ 39.6**	**6.2**	**0.9 ÷ 28.3**	**7.7**	**2.8 ÷ 42.4**	**7.8**	**2.8 ÷ 36.7**

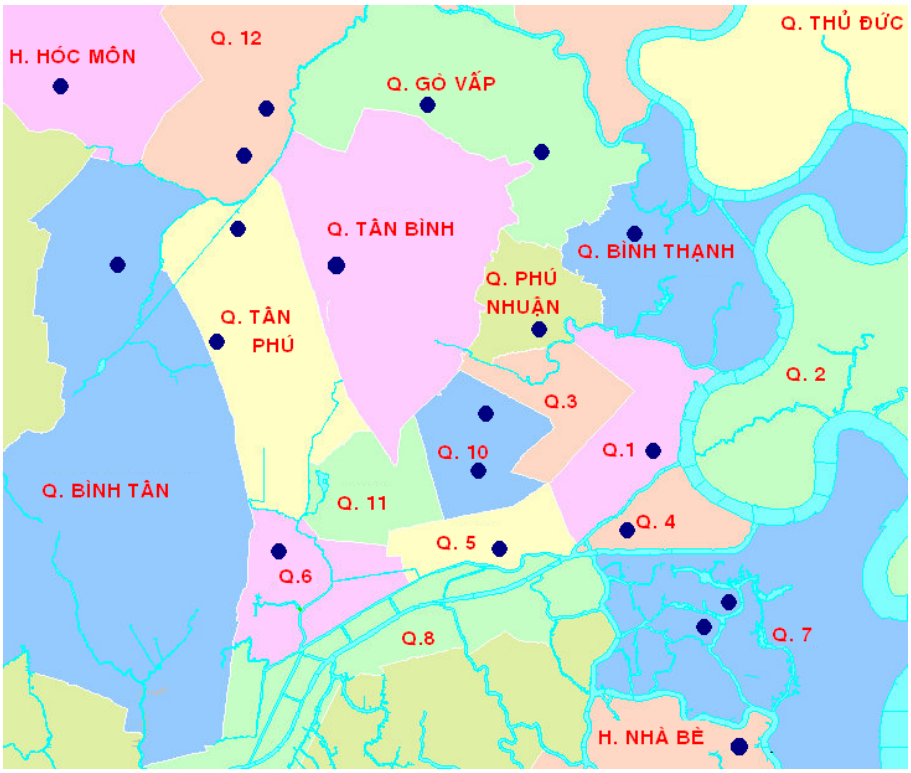

Fig. 4. The sites for indoor radon and dose rate measurement in HCMC

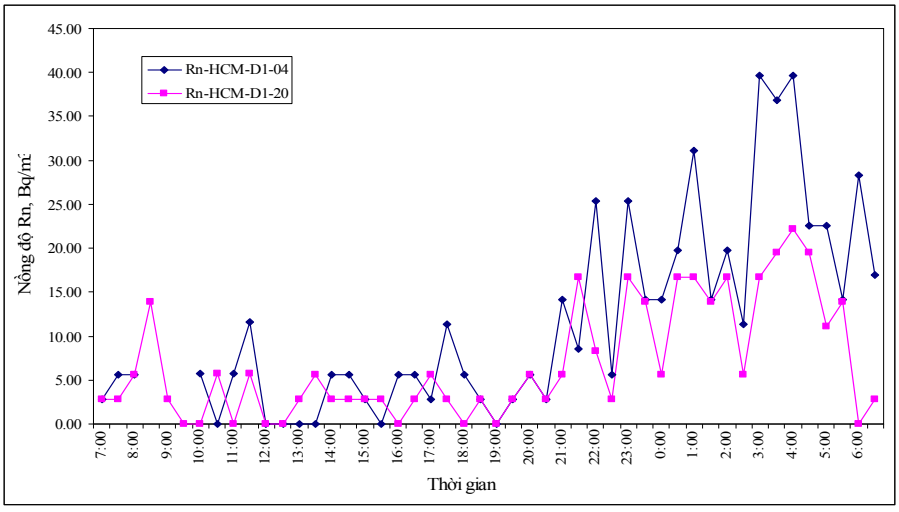

Fig. 5. Variations of indoor radon concentration by time in some sites at HCM

Dalat City:

The measurement of indoor radon concentration were carried out over four periods of different seasons: dry season (1/2008-3/2008), changing season from dry to rainy (4/2008-6/2008), rainy season (7/2008-9/2008), and changing season from rainy to dry (10/2007-12/2007) in 20 typical houses at Dalat city. The indoor radon concentration corresponding with the above periods varied: 1.4 ÷ 182.0; 2.8 ÷ 243.0; 2.8 ÷ 234.0; and 2.8 ÷ 237.0 Bq/m^3; with the average value of 28.8; 28.6; 29.1; and 31.6 Bq/m^3, respectively. The annual mean value for the whole year was 29.5 Bq/m^3. The result shown that the average indoor radon concentration of rainy season was higher in comparison with the dry season.

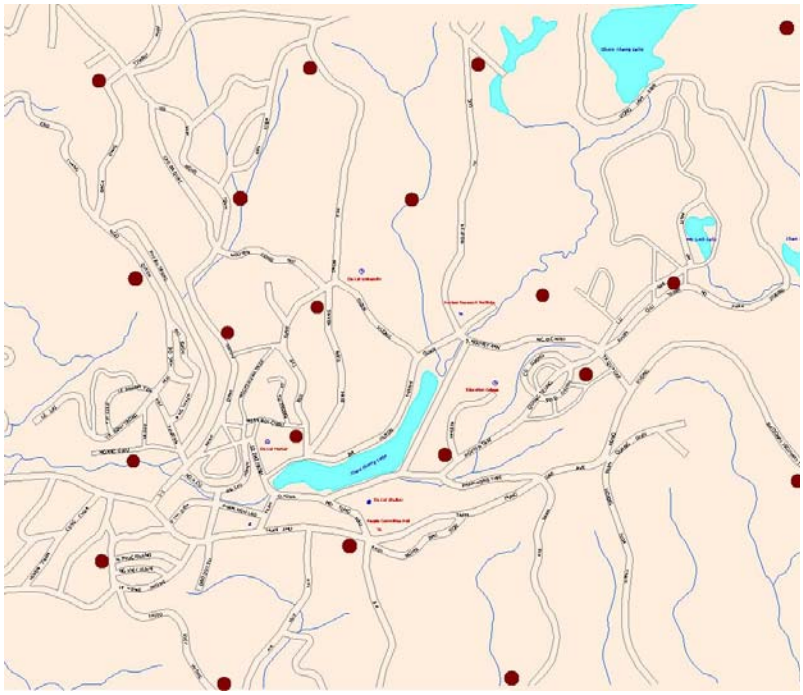

Fig. 6. The sites for indoor radon and gamma dose rate measurement at Dalat city

The detailed information related to this experiment (type of house, kind of building materials used in observed house, room dimensions, etc.) were concerned. The selected typical houses were located widespread over wards of Dalat city and were presented on Fig. 6. The means and ranges of indoor radon concentration of 20 houses in Dalat city are shown on Table VIII. The variations of indoor radon concentration in a day of some sites at Dalat city are shown on Fig. 7. The obtained data showed that indoor radon increased towards the night and reached the peak of indoor radon at early morning time. The indoor radon of some observed houses in Dalat city at peaks was exceeded in comparison with the design level (200Bq/m^3). As a result, it is high potential risk of public internal dose of local people.

Tab VIII. Indoor radon concentration (Bq/m^3) at Dalat city.

Site	Phase 1 *(dry)*		Phase 2 *(dry→rainy)*		Phase 3 *(rainy)*		Phase 4 *(rainy →dry)*	
	Mean	***Range***	***Mean***	***Range***	***Mean***	***Range***	***Mean***	***Range***
Rn-DL-01	38.4	6.5 ÷ 66.7	23.7	2.8 ÷ 55.7	36.1	2.8 ÷ 85.9	56.2	11.1÷125.0
Rn-DL-02	7.1	1.4 ÷ 16.1	7.7	2.8 ÷ 28.7	9.5	2.8 ÷ 28.7	12.1	2.8 ÷ 47.3
Rn-DL-03	26.3	10.2 ÷ 57.9	14.3	2.8 ÷ 41.7	47.0	8.3 ÷ 132.0	20.2	5.6 ÷ 44.5

Rn-DL-04	17.5	5.7 ÷ 28.8	11.0	2.8 ÷ 22.9	16.8	5.6 ÷ 36.2	27.6	5.7 ÷ 58.5
Rn-DL-05	27.5	3.7 ÷ 52.9	21.3	2.8 ÷ 58.5	29.4	5.6 ÷ 78	35.8	2.8 ÷ 103.0
Rn-DL-06	63.2	27.8÷100.2	64.5	11.5 ÷ 117	70.3	8.3 ÷ 139.0	54.8	22.3÷103.0
Rn-DL-07	14.1	5.6 ÷ 27.4	19.9	2.8 ÷ 44.5	13.0	2.8 ÷ 34.4	12.7	2.8 ÷ 25.0
Rn-DL-08	9.9	1.4 ÷ 27.5	12.2	2.8 ÷ 30.6	6.4	2.8 ÷ 22.9	16.4	2.8 ÷ 40.1
Rn-DL-09	24.8	6.7 ÷ 57.6	34.1	2.8 ÷ 78.0	11.1	2.8 ÷ 27.8	29.4	5.7 ÷ 66.9
Rn-DL-10	16.9	5.6 ÷ 28.7	16.2	2.8 ÷ 33.4	21.8	2.8 ÷ 52.9	13.8	2.8 ÷ 28.7
Rn-DL-11	38.7	11.5 ÷ 62.2	33.8	2.8 ÷ 69.6	46.4	5.6 ÷ 80.8	39.8	5.7 ÷ 66.8
Rn-DL-12	25.5	11.1 ÷ 43.6	22.1	5.6 ÷ 51.6	24.5	2.8 ÷ 53.0	32.1	11.1 ÷ 75.2
Rn-DL-13	7.1	2.8 ÷ 13.9	10.2	2.8 ÷ 25.0	7.9	2.8 ÷ 17.2	8.1	2.8 ÷ 19.5
Rn-DL-14	23.5	10.3 ÷ 43.6	23.8	2.8 ÷ 50.1	27.6	2.8 ÷ 61.2	20.7	5.6 ÷ 38.9
Rn-DL-15	12.9	1.9 ÷ 26.0	10.0	2.8 ÷ 22.9	23.8	2.8 ÷ 66.9	7.5	2.8 ÷ 19.5
Rn-DL-16	60.7	17.6÷ 133.8	36.9	5.6 ÷ 92.0	51.6	27.8 ÷ 97.6	96.5	5.6 ÷237.0
Rn-DL-17	49.2	16 ÷ 111.4	90.9	16.7÷243.0	16.9	5.6 ÷ 33.4	41.6	5.6 ÷ 89.2
Rn-DL-18	18.2	6.5 ÷ 32.4	22.9	5.7 ÷ 47.4	13.5	2.8 ÷ 35.9	20.4	2.8 ÷ 41.7
Rn-DL-19	31.2	15.9 ÷ 50.1	24.3	5.6 ÷ 50.1	35.8	11.1 ÷ 58.5	34.0	11.1 ÷ 78.0
Rn-DL-20	63.1	3.8 ÷ 182.0	72.5	5.7 ÷ 204.0	72.0	2.8 ÷ 234.0	52.2	2.8 ÷ 167.0
Mean	**28.8**	**1.4 ÷ 182.0**	**28.6**	**2.8 ÷ 243.0**	**29.1**	**2.8 ÷ 234.0**	**31.6**	**2.8 ÷ 237.0**

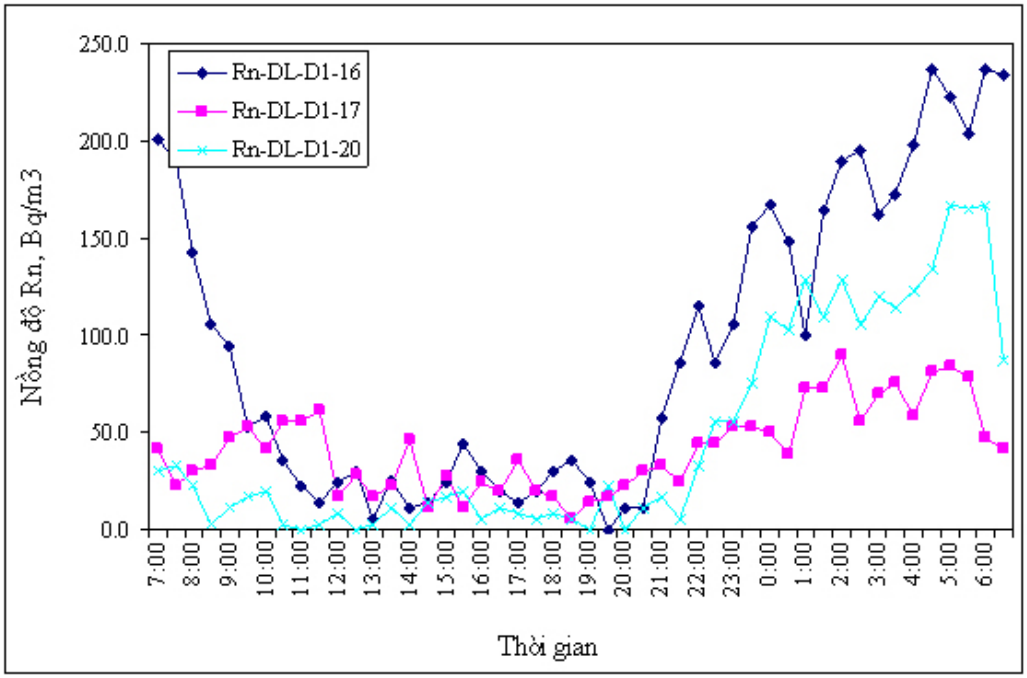

Fig. 7. Variations of indoor radon concentration by time in some sites at Dalat city

The results of radon exhalation rates from building material samples:

The radon exhalation rates from collected building material samples were determined (Fig. 8), then the radon exhalation fractions were calculated. The results are shown in Table IX and Fig. 9. In the experiment, some kinds of building materials were divided into different conditions for measuring: to keep intact condition and to be ground condition in order to compare conveniently. The results are shown in Table X.

The average values of radon mass exhalation rates of the different building materials samples were 0.0101, 0.0400, 0.0131, 0.0072, 0.0318, 0.0028, 0.0082, and 0.0051 Bq/kg/h for sand, gravel aggregate, imported granite, marble, local granite, glazed tile, red-clay brick and cement, respectively. The average values of radon exhalation fraction (10^{-3}h) were 0.4359, 0.6843, 0.4895, 0.9011, 0.4503, 0.0323, 0.1136, and 0.1413 for sand, gravel aggregate, imported granite, marble, local granite, glazed tile, red-clay brick and cement, respectively. By using the obtained data of radon mass exhalation rates, indoor radon concentration was calculated for a model room (dimensions of 4 m × 5 m × 2.8 m; thickness of 20 cm, and density of 2.35 g/cm^3), in which the structures in a building causing the irradiation to be concerned, and the results shown that the potential of exceed the recommendation value was possible.

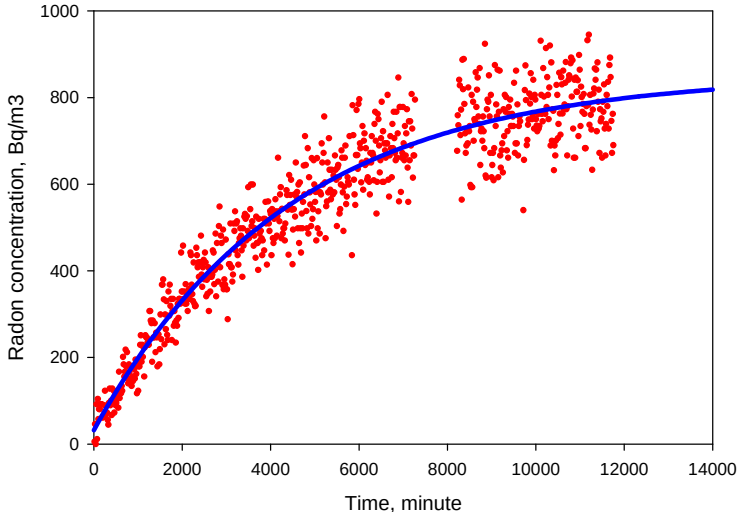

Fig. 8. Growth curves of the radon concentration in the chamber containing the samples. Solid and dashed lines show the fitting curves to a series of the measured radon concentrations for the Dalat's gravel aggregate sample

Tab IX. Radon exhalation rates and radon exhalation fractions of building material samples

Kind	**Condition**	**Origin**	**Mass radon exhalation rate,** *Bq/kg/h*	**Radon exhalation fraction,** *$10^{-3}h$*
Sand	To keep intact	Binh Dinh	0.0091 ± 0.0031	0.4442
		Ha Tinh	0.0059 ± 0.0015	0.3900
		Phu Yen	0.0037 ± 0.0013	0.2210
		Dong Nai	0.0121 ± 0.0017	0.8757
		Ha Tinh	0.0047 ± 0.0032	0.3101

		Ninh Thuan	0.0380 ± 0.0043	0.2339
		Phu Yen	0.0090 ± 0.0011	0.5434
		Quang Nam	0.0013 ± 0.0005	0.1393
		Quang Nam	0.0074 ± 0.0012	0.7653
		Mean	***0.0101***	***0.4359***
Gravel aggregate	To keep intact	Binh Dinh	0.0304 ± 0.0042	0.7024
		Ha Tinh	0.0452 ± 0.0047	0.5490
		Khanh Hoa	0.0312 ± 0.0079	0.6067
		Kon Tum	0.0111 ± 0.0042	0.7727
		Ninh Thuan	0.0394 ± 0.0054	0.7551
		Vinh Phuc	0.0157 ± 0.0037	0.6424
		Dalat, Lam Dong	0.1421 ± 0.0098	0.6778
		Quang Tri	0.0049 ± 0.0011	0.7681
		Mean	***0.0400***	***0.6843***
	To be ground	Ha Tinh	0.0559 ± 0.0217	0.6784
		Ninh Thuan	0.0436 ± 0.0089	0.8356
		Binh Thuan	0.0198 ± 0.002	0.3106
		Dalat, Lam Dong	0.1460 ± 0.0017	0.6965
		Mean	***0.0663***	***0.6303***
Imported granite	To keep intact	China (red)	0.0383 ± 0.0095	0.5186
		South Africa	0.0105 ± 0.0023	0.7856
		England (brown)	0.0109 ± 0.0043	0.4351
		India	0.0048 ± 0.0010	0.5994
		Norway	0.0009 ± 0.0001	0.1090
		Mean	***0.0131***	***0.4895***
	To be ground	India	0.0059 ± 0.0008	0.7378
		Brazil (red)	0.1247 ± 0.0061	0.5083
		Brazil	0.188 ± 0.0369	0.7666
		Norway	0.0023 ± 0.0009	0.1850
		Mean	***0.0802***	***0.5494***
Marble	To keep intact	Spain	0.0012 ± 0.0010	0.0310
		China	0.0024 ± 0.0009	1.3004
		Peru	0.0243 ± 0.0097	0.9539

	To be ground	Vietnam (Thanh Hoa)	0.0009 ± 0.0006	1.3192
		Mean	***0.0072***	***0.9011***
		Italia	0.0002 ± 0.0001	0.3338
		Italia (wood color)	0.0058 ± 0.0025	1.1086
		Italia (vokalas)	0.0032 ± 0.0012	1.2616
		China (white)	0.0023 ± 0.0008	1.2714
		Mean	***0.0029***	***0.9939***
Local granite	To keep intact	Binh Dinh (white)	0.0422 ± 0.0136	0.4108
		Binh Dinh (red)	0.0211 ± 0.0075	0.3843
		Da Nang	0.0139 ± 0.0004	0.4221
		Khanh Hoa	0.0500 ± 0.0079	0.5841
		Mean	***0.0318***	***0.4503***
	To be ground	Quang Nam	0.0574 ± 0.0096	0.8906
		Binh Dinh (red)	0.0315 ± 0.0010	0.5726
		Gia Lai (pink)	0.0109 ± 0.0033	0.5235
		Ba Ria-Vung Tau (Con Dao)	0.0023 ± 0.0004	0.5111
		Da Nang	0.0182 ± 0.0037	0.5529
		Thua Thien - Hue	0.0026 ± 0.0004	0.2386
		Khanh Hoa	0.0751 ± 0.0044	0.8773
		Phu Yen	0.0026 ± 0.0007	0.2742
		Mean	***0.0251***	***0.5551***
Glazed tile	To keep intact	Bach Ma, Binh Duong	0.0027 ± 0.0013	0.0314
		HC Milanos, Vinh Phuc	0.0020 ± 0.0006	0.0283
		Long Hau, Thai Binh	0.0031 ± 0.0009	0.0381
		Shijar, Binh Duong	0.0041 ± 0.0013	0.0320
		Ý My, Dong Nai	0.0019 ± 0.0005	0.0310
		Cosevco, Da Nang	0.0029 ± 0.0004	0.0166
		Dong Tam, Long An	0.0046 ± 0.0010	0.0651
		Macro, HCMC	0.0017 ± 0.0006	0.0251

		Vigracera, Hai Duong	0.0017 ± 0.0003	0.0230
		Mean	***0.0028***	***0.0323***
		Cosevco, Da Nang	0.0030 ± 0.0006	0.0168
		Gralico	0.0021 ± 0.0002	0.0159
		Macro, HCMC	0.0022 ± 0.0005	0.0333
	To be ground	Omega, Binh Duong	0.0016 ± 0.0004	0.0266
		Vigracera, Ha Duong	0.0028 ± 0.0021	0.0388
		Vitaly, HCMC	0.0029 ± 0.0005	0.0471
		Mean	***0.0024***	***0.0297***
Red-clay brick	To keep intact	Dalat, Lam Dong	0.0108 ± 0.0032	0.1139
		Dong Nai	0.0052 ± 0.0010	0.1021
		Binh Duong	0.0067 ± 0.0006	0.1503
		Quang Ngai	0.0099 ± 0.0011	0.0880
		Mean	***0.0082***	***0.1136***
	To be ground	Dalat, Lam Dong	0.0136 ± 0.0037	0.1433
		Dong Nai	0.0072 ± 0.0018	0.1395
		Long Xuyen	0.0037 ± 0.0004	0.0695
		Quang Ngai	0.0154 ± 0.0026	0.1371
		Vinh Long	0.0127 ± 0.0015	0.2405
		Mean	***0.0105***	***0.1460***
Gypsum		Vinh Hung factory	0.0042 ± 0.0023	
Cement		Bim Son, Thanh Hoa	0.0055 ± 0.0015	0.1903
		Holcim, Kien Giang	0.0018 ± 0.0004	0.0784
		Holcim, Kien Giang	0.0034 ± 0.0004	0.1431
		But Son, Ha Nam	0.0105 ± 0.0024	0.1551
		Hoang Mai, Nghe An	0.0080 ± 0.0023	0.1611
		Phuc Son, Hai Duong	0.0028 ± 0.0007	0.0914
		Yen Binh, Lao Cai	0.0046 ± 0.0013	0.1700
		Mean	***0.0051***	***0.1413***

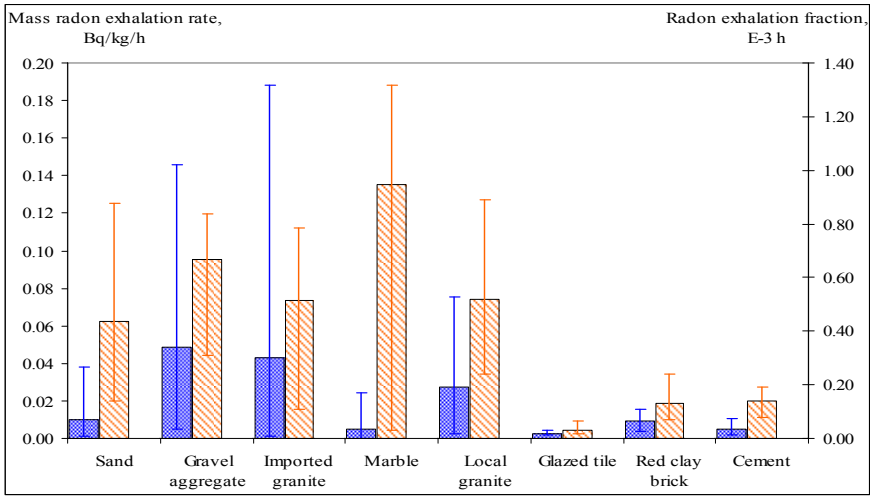

Fig. 9. Mass radon exhalation rates and radon exhalation fractions of building material samples.

Tab X. Mass radon exhalation rates J_m (Bq/kg/h) and radon exhalation fractions F_j (10^{-3}h) of some building material samples with different conditions

Kind	Origin	To keep intact		To be ground		Ratio(*)
		J_m	F_J	J_m	F_J	
Gravel aggregate	Dalat, Lam Dong	0.1421±0.0098	0.6778	0.1460±0.0017	0.6965	1.03
	Ha Tinh	0.0452±0.0047	0.5490	0.0559±0.0217	0.6784	1.24
	Ninh Thuan	0.0394±0.0054	0.7551	0.0436±0.0089	0.8356	1.11
Glazed tile	Cosevco, Da Nang	0.0029±0.0004	0.0166	0.0030±0.0006	0.0168	1.01
	Macro, HCMC	0.0017±0.0006	0.0251	0.0022±0.0005	0.0333	1.32
	Vigracera, Hai Duong	0.0017±0.0003	0.0230	0.0028±0.0021	0.0388	1.69
Red-clay brick	Dalat, Lam Dong	0.0108±0.0032	0.1139	0.0136±0.0037	0.1433	1.26
	Dong Nai	0.0052±0.0010	0.1021	0.0072±0.0018	0.1395	1.37
	Quang Ngai	0.0099±0.0011	0.0880	0.0154±0.0026	0.1371	1.56
Granite	India	0.0048±0.0010	0.5994	0.0059±0.0008	0.7378	1.23
	Binh Dinh (red)	0.0211±0.0075	0.3843	0.0315±0.0010	0.5726	1.49
	Da Nang	0.0139±0.0004	0.4221	0.0182±0.0037	0.5529	1.31
	Khanh Hoa	0.0500±0.0079	0.5841	0.0751±0.0044	0.8773	1.50
	Norway	0.0009±0.0001	0.1090	0.0023±0.0009	0.1850	2.41
Marble	China	0.0024±0.0009	1.3004	0.0023±0.0008	1.2714	0.98

(*) Ratios between the mass radon exhalation rates with to keep intact condition and with to be ground condition.

The relationship between Ra-226 specific radioactivity in building materials and indoor radon of a room is expressed by a linear parameter of radon exhalation rate. The evaluated indoor radon concentration for a model room, in which the structures in a building causing the irradiation to be concerned shown that the potential of exceed the limit was possible. The results are presented in Table XI.

TabXI. The indoor radon concentration were calculated over province by province (model room with the dimensions of 4m × 5m × 2.8m, thickness of 20cm, density of 2.35g/cm^3; all walls used by red-clay brick and mortar, floor and ceiling used by concrete)

Province	**Potential indoor radon, Bq/m^3**		**Note**
	Mean	***Range***	
An Giang	65.9	34.5 ÷ 114.5	Sand, red-clay brick, gravel aggregate were applied separately by every location; cement, gypsum were applied by the whole country mean values.
Ba Ria Vung tau	179.3	115.9 ÷ 261.4	
Bien Hoa	93.6	58.9 ÷ 140.7	
Binh Dinh	137.3	87.9 ÷ 202.3	
Binh Duong	109.0	70.7 ÷ 159.0	
Binh Thuan	190.0	124.2 ÷ 274.1	
Lam Dong	535.0	374.1 ÷ 717.7	
DakLak	61.9	32.5 ÷ 107.7	
Dong Nai	81.4	49.5 ÷ 126.3	
Dong thap	65.6	34.4 ÷ 114.0	
Gia Lai	90.2	44.4 ÷ 161.2	
Ha Noi	109.9	58.7 ÷ 187.6	
Ha Tinh	213.9	149.2 ÷ 287.7	
Thua Thien - Hue	219.4	144.9 ÷ 313.2	
Khanh Hoa	163.9	104.7 ÷ 241.5	
PQ,Kien Giang	131.9	81.3 ÷ 200.9	
Kien Giang	52.8	31.3 ÷ 85.9	
Kon Tum	169.8	70.0 ÷ 336.4	
Long Xuyen	64.0	33.4 ÷ 111.5	
Ninh Thuan	267.2	140.4 ÷ 462.4	
Phu Yen	78.4	44.7 ÷ 127.7	
Quang Binh	71.4	47.0 ÷ 104.4	
Quang Nam, Da Nang	136.1	86.8 ÷ 199.9	
Quang Ngai	156.0	97.9 ÷ 232.9	

Quang Tri	52.9	27.5 ÷ 93.6	
Song Be	53.7	26.7 ÷ 97.2	
Vinh Long	64.0	33.5 ÷ 111.6	
Vinh Phuc	108.2	57.6 ÷ 184.8	
Mean	***133.0***	***26.7 ÷ 717.7***	
The whole country mean value	**156.49**	**15.7 ÷ 1074.8**	To be calculated over kind by kind of building materials

3. Conclusions

Typical results of the project are as follows:

Summarization on the gathered information/document related to research contents of the project, included: (1) characteristic and properties of building materials; (2) building materials minerals in Vietnam; (3) natural radioactivity in building materials and indoor radon; (4) radon exhalation from building materials; (5) radiation protection principles; and (6) international and national regulatories related to this subjects.

The established methods were applied in this investigation, included: (1) the determination method of natural radioactivity in building materials samples using by low level gamma background spectrometer; (2) the indoor radon measuring method accompanied with RAD7; (3) the determination method of radon exhalation rate in building materials samples using solid state nuclear track detectors and/or RAD7; (4) the methods of gamma dose rate measurement with portable device and thermoluminescence dosimeter (TLD); and (5) the method of collection and preparation for building materials samples.

Obtaining the data of existent levels of natural radioactivity (U-238, Ra-226, Th-232 and K-40) in 218 samples over 11 kinds of building materials which are dominant used in Vietnam (cement, sand, red-clay brick, gypsum, gravel aggregate, lime/limestone, glazed tile, granite, marble); the data of indoor radon concentration and radiation doses in 40 houses (versus to climate seasons) of 2 selected sites (Hochiminh city and Dalat city); the data of radon exhalations from 50 building materials samples. The obtained data in this investigation reflect to the actual state and to be compared with the corresponding reported data of other countries.

The specific radioactivities of the different building materials samples varied from 0.89 ÷ 412.50, 0.18 ÷ 395.28, 0.10 ÷ 266.52 and 0.8 ÷ 2006.8 Bq/kg with the average values of 55.57, 52.09, 55.70 and 593.5 Bq/kg for U-238, Ra-226, Th-232 and K-40, respectively. The obtained results shown that the average specific radioactivities in investigated building materials were higher in comparison with the worldwide average concentrations of radium, thorium and potassium in the earth's crust about of 1.30, 1.39, 1.48 times, respectively; the enhanced concentration values were sometimes felling into granite tiles, especially imported granite tiles. The activity concentration index and the annual effective dose were evaluated to assess the potential radiological hazard associated with these building materials. The results shown that the activity concentration indexes of some glazed tile, granite samples were exceeded unit; the activity concentration indexes of some building materials kinds with major contribution

in buildings, for examples, sand, gravel aggregate, red-clay brick samples were exceeded the recommendation value. The evaluated annual effective doses for a model room (dimensions of 4 m × 5 m × 2.8 m; thickness of 20 cm, and density of 2.35 g/cm^3), in which the structures in a building causing the irradiation to be concerned shown that the potential of exceed the limit was possible.

The dose rates of observed houses in Hochiminh city varied from 0.11 ÷ 0.16 μSv/h with the average value of 0.12 μSv/h. The dose rates of observed houses in Dalat city varied from 0.19 ÷ 0.29 μSv/h with the average value of 0.23 μSv/h that was higher 1.92 times in comparison with Hochiminh city.

The indoor radon of observed houses in Hochiminh city varied from 0.9 ÷ 42.4 Bq/m^3 with the average value of 7.4 Bq/m^3. The indoor radon of observed houses in Dalat city varied from 1.4 ÷ 243.0 Bq/m^3 with the average value of 29.5 Bq/m^3. The obtained data shown that indoor radon increased towards the night and reached the peak of indoor radon at early morning time; the indoor radon of some observed houses in Dalat city at peaks was exceeded in comparison with the design level (200Bq/m^3). As a result, it is high potential risk of public internal dose of local people.

The average values of radon mass exhalation rates of the different building materials samples were 0.0101, 0.0400, 0.0131, 0.0072, 0.0318, 0.0028, 0.0082, and 0.0051 Bq/kg/h for sand, gravel aggregate, imported granite, marble, local granite, glazed tile, red-clay brick and cement, respectively. The average values of radon exhalation fraction were 0.4359, 0.6843, 0.4895, 0.9011, 0.4503, 0.0323, 0.1136, and 0.1413 h for sand, gravel aggregate, imported granite, marble, local granite, glazed tile, red-clay brick and cement, respectively. By using the obtained data of radon mass exhalation rates, indoor radon concentration was calculated for a model room (dimensions of 4 m × 5 m × 2.8 m; thickness of 20 cm, and density of 2.35 g/cm^3), in which the structures in a building causing the irradiation to be concerned, and the results shown that the potential of exceed the recommendation value was possible.

In conclusion, the project has been carried out for two year and all of the approval project's contents have been approached completely, and achieved to the objects. The practical, scientific significances of the objects aim to enlarge the database on natural radioactivity in commonly building materials used in Vietnam; and to estimate the relationship between sources and radiation exposures in order to support technical aspects in hazard exposure reduction.

Reference

Le Nhu Sieu et al., Finat Report of the Ministry of Science and Technology's project on Investigation and determination on natural radioactivity in commonly building materials used in Vietnam and initial assessment on radiation exposure caused by them, Viet Nam Atomic Energy Commission, Ministry of Science and Technology, Dalat, 2009.

Papers Published In Relation To The Project

Natural radioactivity in commonly building materials used in Vietnam (to be published in the Journal of Nuclear Science and Technology; VAEC).

1.5 - Applications in Ecology, Environment and Geology

APPLICATION OF REACTOR -BASED INAA AND MULTIVARIATE STATISTICAL ANALYSIS TECHNIQUE FOR MULTIELEMENTS CHARACTERIZATION AND PROVENANCE RESEARCH OF ARCHAEOLOGICAL ATERIALS COLLECTED FROM SOME ARCHAEOLOGICAL SITE, RELIC PLACES IN VIETNAM

Cao Dong Vu, Ho Manh Dung, Nguyen Van Minh, Pham Ngoc Son
Nguyen Thi Sy and Le Thi Ngoc Trinh

Nuclear Research Institute, VAEC, Vietnam

Trinh Thi Tu Anh

Dalat University, Dalat, Vietnam

Nguyen Kim Dung

Vietnam Institute of Archaeology, Hanoi, Vietnam

Pham Thi Hai

Lamdong Museum, Dalat, Vietnam

Abstract: Collection of provenance information from the multi-elemental characterization and their interrelations is the goal of the authors. The obtained results from this study are the first foundation for setting up a database of raw-clay material in some places in Vietnam; take part in the provenance research on pottery and the restoration of highly culture remains and ruins which are being naturally devastated. In this research, 03 archaeological sites were chosen for investigation, as follow: (1) Cat Tien archaeological site (Lamdong), (2) My Son Holy land (Quangnam), and (3) Emperor's rampart relic (Binhdinh).

The aims of our research includes: (i) Investigation and collection more than 250 samples (raw clay materials, ancient brick and ceramic) at 03 archaeological sites; (ii) Setting up the multi-element analyzing procedure by the reactor-based k_0-NAA method; and (iii) Designing of 01 computer program in order to statistically treat the data by Principle Components Analysis (PCA) and Clusters Analysis (CA).

The main results of this study can be summarized as follow: (1) The analyzing procedure for 29 elements (Al, As, Ba, Ce, Co, Cr, Cs, Dy, Eu, Fe, Ga, Hf, K, La, Lu, Mn, Na, Nd, Rb, Sb, Sc, Sm, Ta, Tb, Ti, Th, U, V and Yb) by k_0-NAA method was set up, (2) Analyzed data with 8062 analyses for 29 elements, as mentioned above, in 278 archaeological samples and raw clay materials collected in this study were achieved, and (3) A computer program for statistical multivariate- analysis PCA and CA was designed and developed. Initial information about the provenance of collected samples was suggested.

1. The Aim of Theme

Application of chemical composition determination of archaeological sample as a support tool for provenance research has quickly developed in the recently decades, particularly in the Latin American countries. Many analyzing methods such as, XRFA, NAA, ICP-MS, AAS, etc., have been used for this purpose. The most effective and

successful method, however, is Neutron Activation Analysis - NAA which has been carried out by some groups all over the world.

In Vietnam, problem of determining the provenance of archeological samples by scientific tools has not been employed. Some previous researches were not completely done and can not thoroughly solve the provenance question.

Twenty five years since Dalat nuclear research reactor was renewed and re-operated, along with other trends of research, Instrumental Neutron Activation Analysis - INAA has being invested and successfully applied in different disciplines such as: geology, environment, petroleum, agriculture, biology, etc.

Besides, there are some highly culture remains and ruins of archaeology which need to be researched, preserved, maintained and restored in Vietnam. From that fact, along with the success of some studies on the world in the recently decades, in combine with the domestic archaeologist, we carried out a theme named *"Application of reactor-based INAA and multivariate statistical analysis technique for multielements characterization and provenance research of archaeological materials collected from some archaeological site, relic places in Vietnam"*

Provenance research on earthen archaeological materials by determination of multielement composition and their correlation.

2. Processes and Techniques Were Employed

- Processes

+ Establishment of three multielement analytical processes by using k0-NAA for earthen archaeological materials.

Tab 1. Brief of three multielement analytical processes by k0-NAA

Irradiation time, *Mass)*	**Irradiation site *(ϕ_{th}, α, f)***	**Decay time, T_d**	**Counting time, T_c**	**Measured isotope**
90s *(~30mg)*	7-1 Channel *($4,2\times10^{12}$ $n.cm^2.s^{-1}$, 0,017, 9,8)*	15-20m	120s	^{28}Al, ^{49}Ca, ^{165}Dy, ^{56}Mn, ^{51}Ti and ^{52}V.
1h *(~70mg)*	Rotary rack *($3,7\times10^{12}$ $n.cm^2.s^{-1}$, 0,073, 40)*	2-3d	900s	^{76}As, ^{82}Br, ^{72}Ga, ^{42}K, ^{140}La, ^{24}Na, ^{153}Sm and ^{239}Np (U)
6h *(~100mg)*	Rotary rack *($3,7\times10^{12}$ $n.cm^2.s^{-1}$, 0,073, 40)*	5-7d	1800s	^{131}Ba, ^{177}Lu, ^{147}Nd, và ^{86}Rb
		> 30d	10800s	^{141}Ce, ^{51}Cr, ^{152}Eu, ^{59}Fe, ^{181}Hf, ^{124}Sb, ^{46}Sc, ^{182}Ta, ^{160}Tb, ^{233}Pa (Th), and ^{169}Yb.

+ Design a program for multivariate statistical analysis on analytical data set by using PCA and CA methods named MSAP. It is written by Visual C^{++}, and is internal validated before using.

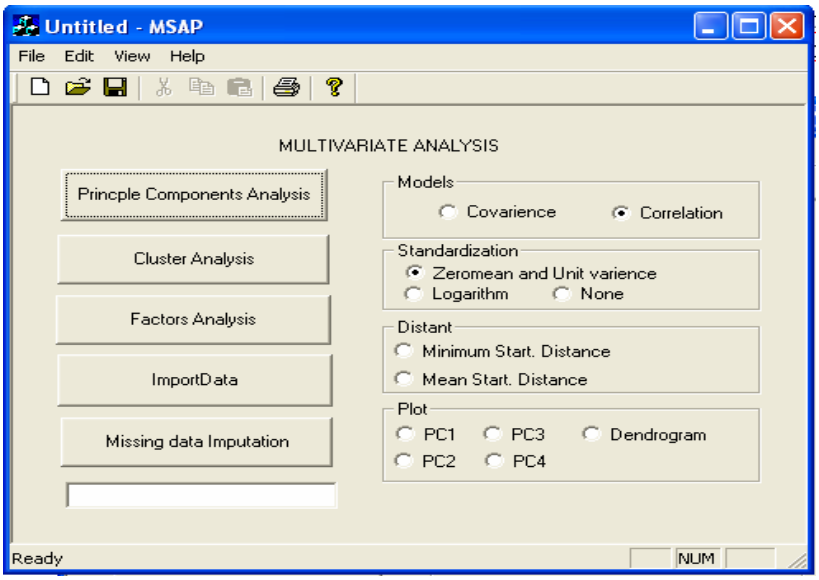

Fig. 1. Interface of MSAP program Ver.1.0

- Techniques

+ Using of k_{zero} method of neutron activation analysis for multielement examination in earthen archaeological sample.

+ Using of multivariate analysis methods of PCA and CA to analyze chemical composition data, from which we can find out their correlation in order to support for provenance research.

3. Results and Comments

- Investigation and collection of 256 samples, including: 73 clay samples, 102 antique brick samples, 69 pottery samples, 12 tile samples and 6 model brick samples from three relics, My Son (Quangnam), Emperor's rampart (Binhdinh) and Cattien archaeological site to serve for the project.

- Establishment the set of three multielement analytical processes by using k0-NAA on reactor for earthen archaeological materials and apply them to determine 29 elements in 256 samples collected by project.

- Some typical results of statistical analysis by MSAP

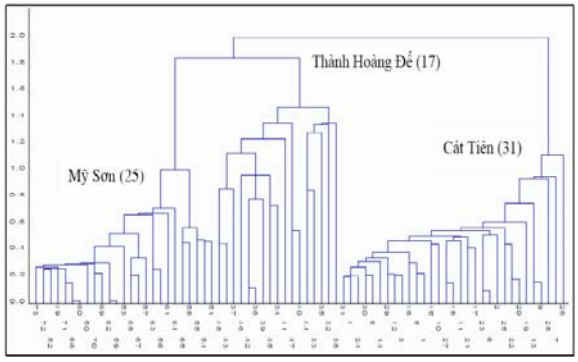

Fig. 2. Result of CA analysis for 73 clay samples at three sites: Cattien (31), Myson (25) and Emperor's rampart (17)

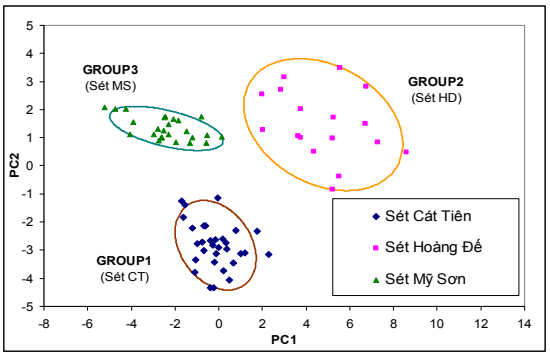

Fig. 3. Result of PCA analysis with 95% confident level for 3 clay groups from Cattien, Myson and Emperor's rampart.

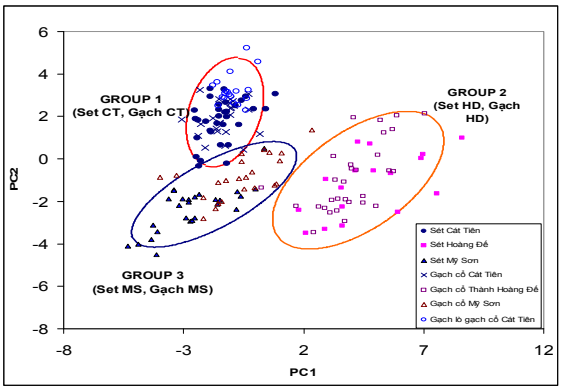

Fig. 4. Result of PCA analysis with 95% confident level for 101 brick samples and 73 clay samples from three investigative sites.

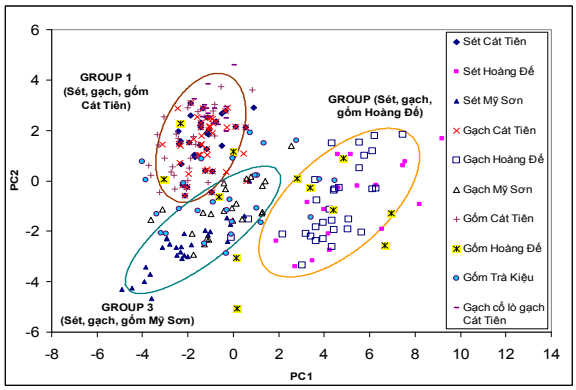

Fig. 5. Result of PCA analysis with 95% confident level for 250 samples of clay, brick and pottery from three investigative sites

- *For Cattien archaeological site:* Bay Mau field could be a main providing center of raw meal for antique people public in Cattien in the past. This result also show that their ability about producing pottery for themselves. Also, we can conclude that the ancient community in Cattien existed individually and the exchange of goods to the other groups was rarely carried out, at least for the earthen archaeological objects.

- *For the site at My Son:* The brick in temples in this site had origin from many sources and Ao Vuong was one of them. For the raw material of ceramic collected at Tra Kieu town, however, there was no evident show that they were produced from the Ao Vuong's clay source.

- *For the Emperor's rampart:* Bau Sen and the field of Nhan Hau might be defined as the origin of the main source of clay for producing brick from Champa dynasty (Do Ban rampart) to Tay Son dynasty (Emperor's rampart). For the pottery, only a few has provenance from Bau Sen and Nhan Hau field's clay, most of them were produced at another places.

4. Conclusions and Recommendations

- Provenace study of the earthen archaeology materials by combining the Neutron Activation Analysis and the multivariante analysis was successfully applied for the first time in Vietnam.

- The initial results shows that NAA, espesially k0-NAA, has much possibility in the origin investiagation problem with high acuracy and feasibility.

- On methodology, the realization and the logic of the provenace study were clarified through the results of this project.

- At archaeology aspect, from the obtained results, we can judge that: (i) the raw material for producing brick, tile in the temples and towers were collected at local site and quite concentrated; (ii) for the ceramic, the origin distribution was complex and dispersed on a wide area. To understand the origin of ceramic object, therefore it is needed to investigate the clay source on a large area. From that study, we can establish the data for material versus area, ceramic type and so on, accumulate by time which can be used for the provenance study in the future.

References

[1]. *Glascock M D and Neff H* 2003 Neutron activation analysis and provenance research in archaeology Meas. Sci. Technol. 14 1516–1526.

[2]. *IAEA* 2003 Technical Report series N^0. 416.

[3]. *T. B. Việt* 2007 Đền tháp Chămpa bí ẩn xây dựng.

[4]. *Neff H* 2002 Quantitative techniques for analyzing ceramic compositional data Ceramic Production and Circulation in the Greater southwest: Source Determination by INAA and Complementary Mineralogical Investigations ed D M Glowacki and H Neff (Los Angeles, CA: Costen Institute of Archaeology, University of California) Monograph 44.

[5]. *Bailey S W* 1980 American Mineralogist, summary of recommendations of AIPEA nomenclature committee on clay minerals, vol 65, P.1-7

[6]. http://vi.wikipedia.org/wiki/%C4%90%E1%BA%A5t_s%C3%A9t

[7]. *Glascock M D* 1992 Characterization of archaeological ceramics at MURR by neutron activation analysis and multivariate statistics Chemical Characterization of Ceramic Pastes in Archaeology ed H Neff (Madison: Prehistory Press).

[8]. http://en.wikipedia.org/wiki/Pottery#Background

[9]. *Weigand P C, Harbottle G and Sayre E V* 1977 Turquoise sources and source analysis: Mesoamerica and the Southwestern USA Exchange Systems in Prehistory ed T K Earle and J E Eriscon (New York: Academic).

[10]. *Neff H* 2000 Neutron activation analysis for provenance determination in archaeology Modern Analytical Methods in Art and Archaeology (Chemical Analysis Series*)* vol 135, ed E Ciliberto and G Spoto (New York: Wiley).

[11]. *B. C. Hoàng, N. K. T. Kiên, N. Q. Mạnh, B. X. Long* 2007 Báo cáo điều tra – thám sát – khai quật các di tích khảo cổ học trên địa bàn huyện Cát Tiên.

[12]. *Sở Văn hoá thông tin tỉnh Lâm Đồng* 2001 Kỷ yếu hội thảo khoa học di tích khảo cổ học Cát Tiên.

[13]. *N. T. Đông* 2002 Luận án tiến sĩ lịch sử "Khu di tích Cát Tiên ở Lâm Đồng".

[14]. *Viện khảo cổ học* 1998 Báo cáo khai quật khu di tích Cát Tiên.

[15]. http://vi.wikipedia.org/wiki/Th%C3%A1nh_%C4%91%E1%BB%8Ba_M%E1%BB%B9_S%C6%A1n

[16]. *N. V. Doanh* 2005 Mỹ Sơn Relics, Thế giới Publishers.

[17]. *L. Đ. Phụng* 2007 Thành Hoàng Đế Kinh đô Vương triều Tây Sơn, nhà xuất bản Khoa học Xã hội.

[18]. *Hồ Mạnh Dũng* 2003, Nghiên cứu và phát triển phương pháp K–Zero trong phân tích kích hoạt neutron lò phản ứng hạt nhân cho việc xác định đa nguyên tố, Luận án Tiến sĩ Vật lý, Trường ĐHKHTN Tp.HCM.

[19]. *Alvin Rencher C* 2002 Methods of Multivariate Analysis, 2 End, WILEY-INTERSCIENCE, A JOHN WILEY & SONS, INC. PUBLICATION, ISBN 0-471-41889-7.

[20]. *Wolfgang Hardle and Leopold Simar* 2003 Applied Multivariate Statistical Analysis, version 29th, MD-TECH.

[21]. *Thangavel K, Qiang Shen and Pethalakshmi A* 2006 Application of Clustering for Feature Selection Based on Rough Set Theory Approach, AIML Journal, Volume (6), Issue (1).

[22]. *Anton Buhagiar* 2002 Exploration and reduction of data using principal

component analysis, Malta Medical Journal Volume 14 Issue 01.

[23]. *Mục 5.4*, 'Yêu cầu chung về năng lực của phòng thử nghiệm và hiệu chuẩn', TCVN ISO/IEC 17025:2001

[24]. *Thompson M, Ellison S L R, Wood R* 2002 Harmonized guidelines for single laboratory validation of methods of analysis", Pure Appl. Chem. 74(5), 835-855.

[25]. "*EURACHEM Guide* 1998 'The fitness for purpose of analytical methods. A laboratory Guide to method validation and related topics'. EURACHEM Website.

Papers Published In Relation To The Project

1. *C. Đ. Vũ, P. N. Sơn, L. T. N. Trinh, P. T. Nhựt, N. T. Sỹ, N. V. Minh, H. M. Dũng, P. T. Hải và N. K. Dung*, **"Phân tích kích hoạt nơtrôn và nghiên cứu nguồn gốc trong khảo cổ"**, kỷ yếu kỷ niệm 25 năm khánh thành và vận hành an toàn – Khai thác hiệu quả Lò phản ứng hạt nhân Đà Lạt (20/3/1984-20/3/2009).
2. *C. Đ. Vũ, P. N. Sơn, L. T. N. Trinh, P. T. Nhựt, N. T. Sỹ, N. V. Minh, H. M. Dũng, P. T. Hải và N. K. Dung*, "**Ứng dụng phương pháp phân tích kích hoạt nơtrôn lò phản ứng trong nghiên cứu nguồn gốc vật liệu khảo cổ đất nung"**, Tạp chí phân tích Hóa, Lý và Sinh học. (đã gửi bài)
3. *C. Đ. Vũ, P. N. Sơn, L. T. N. Trinh, P. T. Nhựt, N. T. Sỹ, N. V. Minh, H. M. Dũng, P. T. Hải, N. K. Dung và V. H. Tấn,* "**Một số kết quả nghiên cứu nguồn gốc vật liệu khảo cổ đất nung tại khu di tích Cát Tiên bằng phương pháp phân tích kích hoạt nơtrôn và thống kê đa biến"**, Tạp chí Khảo cổ học (đã gửi bài).
4. *C. Đ. Vũ, P. N. Sơn, L. T. N. Trinh, P. T. Nhựt, N. T. Sỹ, N. V. Minh, H. M. Dũng, P. T. Hải, N. K. Dung và V. H. Tấn*, **"Những kết quả ban đầu và tiềm năng ứng dụng phương pháp phân tích kích hoạt nơtrôn trong nghiên cứu nguồn gốc vật liệu khảo cổ đất nung ở Việt Nam"**, hội nghị Khoa học và Công nghệ Hạt nhân toàn quốc lần thứ VIII, 20-22/8/2009, Nha Trang, Khánh Hòa.
5. *C. Đ. Vũ, P. N. Sơn, L. T. N. Trinh, P. T. Nhựt, N. T. Sỹ, N. V. Minh, H. M. Dũng, P. T. Hải, N. K. Dung và V. H. Tấn,* "**Một số kết quả ban đầu về nghiên cứu nguồn gốc vật liệu khảo cổ đất nung tại khu di tích Mỹ Sơn (Quảng Nam) và khu di tích Thành Hoàng Đế (Bình Định) bằng phân tích kích hoạt nơtrôn và thống kê đa biến"**, tạp chí Khảo cổ học.
6. *P. N. Son, C. D. Vu and V. H. Tan,* **"MSAP: A computer program for multivariate statistical analysis",** hội nghị Khoa học và Công nghệ Hạt nhân toàn quốc lần thứ VIII, 20-22/8/2009, Nha Trang, Khánh Hòa.
7. *L. T. N. Trinh, C. Đ. Vũ, N. T. Sỹ, P. T. Nhựt,* **"Xác định hiệu lực của phương pháp phân tích kích hoạt nơtrôn dụng cụ đối với mẫu đất và vật liệu khảo cổ bằng đất nung"** hội nghị Khoa học và Công nghệ Hạt nhân toàn quốc lần thứ VIII, 20-22/8/2009, Nha Trang, Khánh Hòa.

USING ENVIRONMENTAL ISOTOPES TO IDENTIFY AND ESTIMATE RECHARGE OF PRECIPITATION INTO HOLOCENE AQUIFER

Vo Thi Anh, Pham Quy Nhan, Trieu Duc Huy, Pham Quoc Ky

Vo Tuong Hanh and Nguyen Van Hoan

Institute for Nuclear Science and Technology, VAEC

Abstract: Groundwater recharge estimation has become a priority issue in the investigation of the interaction between surface water, rain water and groundwater as well as to research into the sources of contamination. This study will present the results of the recharge estimation of precipitation and Red river into the Holocene aquifer in the Dan Phuong area. Environmental isotopes of precipitation as well as of water from main stream of the Red River and it's channels and groundwater were analyzed. The results obtained show that there is a sound interaction between Northern channel of Red River, precipitation and groundwater in the Holocene aquifer. In the dry season, the Northern channel is received 67% (method of ^{18}O isotope) or 70% (method of ^{2}H isotope) of its resource from Holocene aquifer. On contrary, in the rainy season, the Holocene aquifer is recharged with 86% of its resource from the Red river and 14% from the precipitation (method of ^{18}O isotope) or with 88% of its resource from the Red river and 12% from the precipitation (method of ^{2}H isotope).

Groundwater is a vital to human health, and its importance as a drinking water will grow because of population increases. There is therefore, a need to improve estimates of groundwater recharge (renewal) is very important and necessary for groundwater resources management. However, quantifying groundwater recharge is difficult. Environmental isotopes such as ^{18}O and D are powerful tools for recharge estimation. This study aims to apply environmental isotope tracer methods to initially estimate the recharge rate of rain water into Holocene aquifer.

Dan Phuong wellfield is collected to set up experiment and collect groundwater samples of Holocene aquifer monthly. That is an area of De Tu young sediments with a typical wellfield of fluvial delta plain. It has not still impacted by human activities and remains natural hydrogeology and geochemical characteristics. There are 3 boreholes collected to take groundwater samples monthly (from April to November of 2008). These boreholes are pumpted from Holocene aquifer with defferent depth. In addition, samples of Red river water is also collected monthly with the same time as groundwater. Apart from samples of rain water is collected daily. Taking these samples is subject the strict regulations of IAEA's guideline and sent to Lab of Isotope Hydrology, Institute of Nuclear Science and technology for analyse of ^{18}O and D delta.

The results obtained show that there is a sound change of composition of ^{18}O and D of groundwater of Holocene aquifer following time between season (dry season and rainy season). It seems that the composition of both of ^{18}O and D changes following season with the enrichment in the dry season and the contrary in the rainy season. (Figures 1, 2).

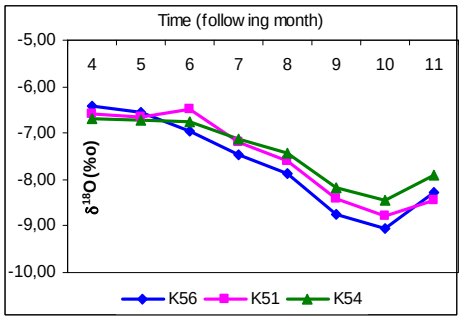

Fig. 1. The change of $\delta^{18}O$ composition of groundwater in the Holocene aquifer following monthly in 2008

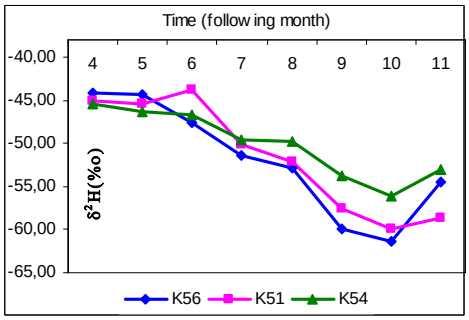

Fig. 2. The change of δD composition following of groundwater in the Holocene aquifer monthly in 2008

Figures 1 and 2 reveal that the composition of both ^{18}O and D is the lowest in October. That may be suitable for the change of the stable isotope composition of precipitation and Red river water in the rainy season. Because the stable isotope composition of both precipitation and Red river water is lower in the rainy season.

Besides, there is also a sound change of composition of ^{18}O and D of groundwater of Holocene aquifer following the depth of boreholes. Setting up the relationship between the the stable isotope composition with the depth of 4 boreholes including K56 (9,2m); K51 (10,8m); K54 (13,6m) and T1A (33m), it reveals that, the stable isotope composition of both ^{18}O and D is higher than in the rainy season following the depth of boreholes (Figure 3 and 4). On the contrary, they is lower than in the dry season following those of (Figure 5 and 6). The reason explained is that, in the rainy season, the groundwater of Holocene aquifer is recharged by precipitation and Red river water with lower composition of both ^{18}O and D. Following the depth of these boreholes, the dilution of precipitation and Red river water recharged into the groundwater of Holocene aquifer with its groundwater is reduced and as a result of, . However, in the dry season, the groundwater of Holocene aquifer is mainly recharged by precipitation vertically. The vertical percolation of precipitation with characteristic of higher composition of both ^{18}O and D in the dry season makes the stable isotope composition of groundwater of Holocene aquifer lower than following the depth.

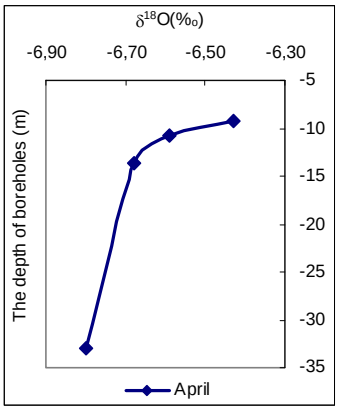

Fig. 3. The change of $\delta^{18}O$ composition of groundwater in the Holocene aquifer in April, 2008

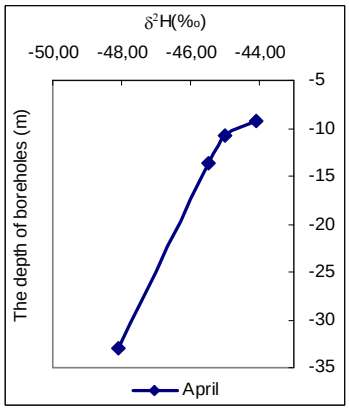

Fig. 4. The change of δD composition of groundwater in the Holocene aquifer in April, 2008

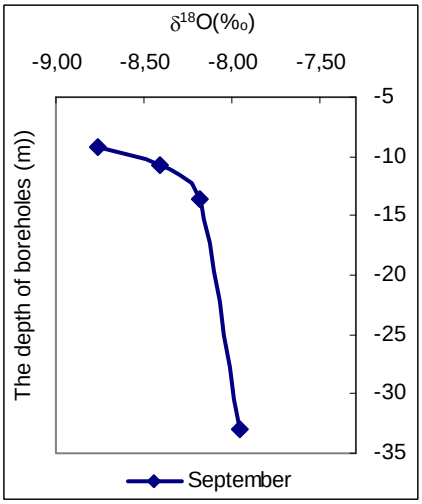

Fig. 5. The change of $\delta^{18}O$ composition of groundwater in the Holocene aquifer in September, 2008

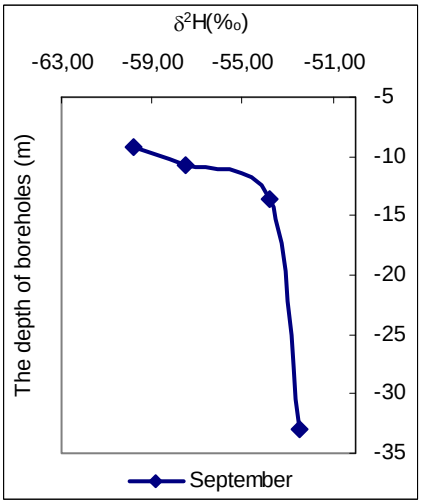

Fig. 6. The change of δD composition of groundwater in the Holocene aquifer in September, 2008

The analyses results show that there is a sound interaction between Northern channel of Red River, precipitation and groundwater in the Holocene aquifer. And that, groundwater in the Holocene aquifer is originated by the mixture of Red River water and precipitation. In the rainy season, groundwater in the Holocene aquifer is recharged from Red River water. On contrary, the Northern channel of Red River is received water from Holocene aquifer in the dry season (Figure 7). The conclusion is suitable for the study result of Hydraulic heads between Red River water and groundwater in the Holocene aquifer following season.

The result of estimating the recharge rate is that, in the dry season, the Northern channel is received 67% (method of ^{18}O isotope) or 70% (method of ^{2}H isotope) of its resource from Holocene aquifer. On contrary, in the rainy season, the Holocene aquifer is recharged with 86% of its resource from the Red river and 14% from the precipitation (method of ^{18}O isotope) or with 88% of its resource from the Red river and 12% from the precipitation (method of ^{2}H isotope).

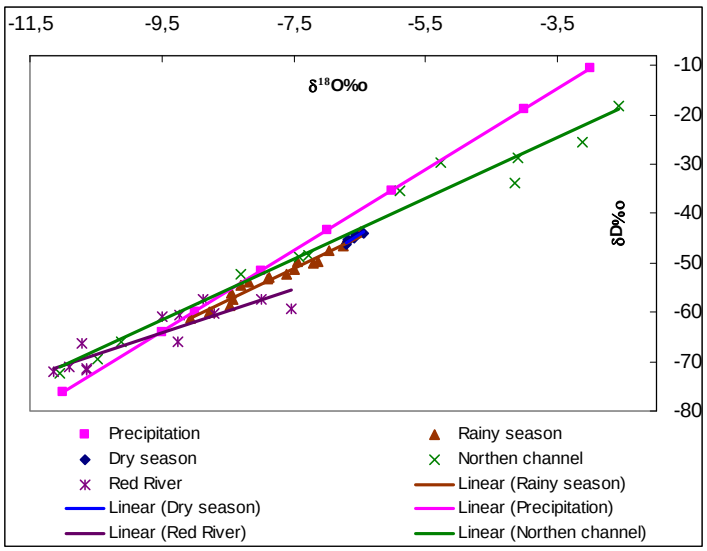

Fig. 7. The relationship between δD and $\delta^{18}O$ of precipitation, Red river water,Northen channel water and groundwater in the Holocene aquifer in 2008

References

[1]. Basmaci Y, Al-Kabir MA (1988), "Recharge characteristics of aquifers of Jeddah-Makkah-Taif region", In: *Simmers I (ed) Estimation of natural groundwater recharge, NATO ASI Series C222, Reidel*, pp 367-375.

[2]. Bazuhair A. S., Wood WW (1996), "Chloride-mass balance method for estimating groundwater recharge in arid areas: example from western Saudi Arabia", *J Hydrol 186*: 153-159.

[3]. Brunke M., Gonser T. (1997), "Special Review: The ecological significance of exchange processes between river and groundwater", *Freshwater Biology, 37*, pp: 1-33.

[4]. Clark, I., and Fritz, P.(1997), *Environmental Isotopes in Hydrogeology*. Lewis Publishers, 328 pp.

[5]. Coplen, T.B. (1996), "New guidelines for reporting stable hydrogen, carbon, and oxygen isotope ratio data", *Geochimica et Cosmochimica* Acta 60, 17, 3359-3360.

[6]. Eriksson, E., and V. Khunakasem. 1969. Chloride concentration in groundwater, recharge rate and rate of deposition of chloride in Israel Coastal Plain. J Hydro., 7, 178-197.

[7]. Flemming L., P.Q.Nhan, D.D.Nhan, N.V.Hoan, H.V.Hoan, N.B.Thao, T.D.Huy (2008), "Geological and Hydrogeological Control on the distribution of Arsenic in a Holocene Aquifer, Red River Plain, Vietnam" *Submitted to Appl. Geochem. 2008*.

[8]. Gholma. Kzemip et al (2006), *Groundwater age* ISBN-13;978-0-471-71819-2.

[9]. Ian D. Clark and Peter Fritz, (1999), *Environmental Isotopes in Hydrogeology*-ISBN - L56670-249-6.

[10]. IAEA (2002), *Water and Environment Newsletter of the Isotope Hydrology Section, International Atomic Energy Agency*. Issue No. 16, Nov 2002: 5.

[11]. Jenny N., Sparrenbom C. J., Berg M., Dang Duc Nhan, Pham Quy Nhan, Sigvardsson E., Baric D., Moreskog J., Harms-Ringdahl P., Nguyen Van Hoan, Rosqvist H., Jacks G. (2008), "Arsenic mobilisation in a new well-field for drinking water production along the Red River, Nam Du, Hanoi", *Submitted to Appl. Geochem 2008*.

[12]. Judson W. Harvey, Jungyill Choi, and Robert H. Mooney (2005), "Hydrologic Interactions Between Surface Water and Ground Water in Taylor Slough, Everglades National Park", *Water Resour. Res. 56*, 212–231

[13]. Nielsen, L. H., Mathiesen, A., Bidstrup, T., Vejbæk, O.V., Dien, P.T., Tiem, (1999), "Modelling of hydrocarbon generation in the Cenozoic Song Hong Basin, Vietnam: a high prospective basin", *Journal of Earth Sciences 17*, pp269-294.

[14]. Nguyen Van Hoan, Đang Duc Nhan, Flemming L., Pham Quy Nhan, Trinh Van Giap, Đang Anh Minh, Vo Thi Anh, Ha Lan Anh (2008), "Identification and evaluation of groundwater recharge into the Holocene aquifer Using chloride - mass balance and environmental isotopes - A case study for the Đan Phượng wellfield in Ha Tay", Proceeding National Workshop: *Arsenic Cotamination in Groundwater in Red River Plain*, the second, Ha Noi, University of Mining and Geology, pp 62-71.

[15]. Subyani A. M**.** (2004), "Use of chloride-mass balance and environmental isotopes for evaluation of groundwater recharge in the alluvial aquifer, Wadi Tharad, western Saudi Arabia", *Environ Geol 46*:pp741-749.

[16]. Wood, W. (1999), "Use and misuse of the chloride mass balance method in

estimating ground water recharge", *Technical Commmentary. Ground Water*, 37:1, pp64-76.

Papers Published In Relation To The Project

1. Nguyễn Văn Hoàn, "Nghiên cứu quá trình bổ cấp của nước mưa cho nước ngầm tầng chứa nước Holocene vùng Đan Phượng – Hà Tây bằng kỹ thuật đồng vị và kỹ thuật liên quan". Luận văn thạc sĩ , 31/8/2008.
2. Nguyễn Văn Hoàn, Đặng Đức Nhận, Flemming Larsen, Phạm Quý Nhân, Đặng Anh Minh, Võ Tường Hạnh, Bùi Học, Triệu Đức Huy, (2009) " Xác định lượng bổ cấp của nước mưa, nước sông cho nước ngầm tầng Holocene vùng Đan Phượng Hà Tây bằng kỹ thuật đồng vị", đã được chấp nhận đăng tại Tạp chí Địa chất, quý 3 năm 2009.
3. Nguyễn Văn Hoàn, Đặng Đức Nhận, Flemming Larsen, Phạm Quý Nhân, Trịnh Văn Giáp, Đặng Anh Minh, Võ Thị Anh, Hà Lan Anh, "Identification and evaluation of groundwater recharge into the Holocene aquifer Using chloride - mass balance and environmental isotopes - A case study for the Đan Phượng wellfield in Hà Tây", *Hội thảo QG về ô nhiễm As* (2008), Hà Nội, tr 62-71.

DETERMINATION OF OCCURRING CONCENTRATION OF NATURAL RADIOISOTOPES AND TOXIC HEAVY METALS (AS, CD, HG, NI, PB, PO, SB, TH, U,…) IN MARINE MATTERS BY NUCLEAR AND RELATIVE METHODS IN BA RIA -VUNG TAU COAST

Nguyen Dao, Nguyen Giang, Nguyen Thanh Tam, Nguyen Thi Mui, Tran Dinh Khoa, Tran Van Hoa and Truong Phuong Mai

Nuclear Research Institute, VAEC, Vietnam

Abstract: Marine environment is a complicated ecology system. Research, evaluate environmental impact for coastal areas is a new term and a necessary duty.

The methods INAA, RNAA, AAS, natural gamma spectrometry, alpha spectrometry were applied to analyze collected samples of marine matters such as surface water, sediment and some kinds of biota (pompano, herring, squid, barnacle, shellfish, seaweed, and alga) along the coast of Ba Ria - Vung Tau. Investigated concentration of elements in the surface water samples, such as As (0.16 – 0.24 ppm), Cd (0.23 – 0.74 ppm), Cu (0.78 – 1.33 ppm), Hg (0.039 – 0.062 ppm), Pb (0.45 – 1.59 ppm), Zn (10.8 – 15.00 ppm) ... are extremely lower than their limited amount in the index of TCVN 5942-1995 - Water quality - Criteria for surface water quality, TCVN 5943-1995 - Water quality - Criteria for surface seawater quality of coastal, and QCVN10-2008/BTNMT - The National standardization technology for seawater quality of coastal.

1. Experiment

1.1. Applied Methodologies

- AAS
- INAA, RNAA,
- Natural gamma spectrometry, alpha spectrometry

1.2. Kind of Samples

Surface water (10), sediment (11), and some kinds of marine matters (pompano, herring, squid, barnacle, shellfish, seaweed, and alga).

2. Result

Tab 1. Concentration of elements in the samples of sediment

TT	Element	VT -1	VT -2	VT -3	VT -4	VT -5
1	Al (%)	2.71±0.13	3.32±0.14	4.12±0.33	2.87±0.21	3.45±0.34
2	As (mg/kg)	8.0±0.6	7.7±0.9	10.1±1.1	8.2±0.9	9.0±1.0
3	Ba (mg/kg)	272±14	146±16	193±12	243±19	146±12
4	Ca (mg/kg)	2594±120	501±36	760±36	5157±258	1170±92
5	Cd (mg/kg)	1.4±0.2	1.2±0.2	2.2±0.2	1.1±0.2	1.0±0.1
6	Co (mg/kg)	11.8±1.1	9.2±0.5	11.5±1.5	15.1±1.2	8.5±0.8

7	Cr (mg/kg)	67.0±5.1	39.7±3.2	52.8±4.2	74.4±6.3	46.3±3.3
8	Cu (mg/kg)	13.8±1.4	15.3±1.4	12.9±1.3	14.3±1.9	9.7±1.0
9	Eu (mg/kg)	1.18±0.22	0.8±0.1	0.9±0.1	1.4±0.3	0.68±0.08
10	Fe (%)	4.4±0.5	3.6±0.4	5.1±0.5	3.7±0.4	4.5±0.5
11	Hf (mg/kg)	7.7±0.7	10.2±1.2	9.4±1.2	1.7±0.2	15.4±1.3
12	Hg (mg/kg)	1.22±0.2	1.08±1.1	2.11±0.22	0.97±0.10	1.74±0.24
13	La (mg/kg)	28.1±2.2	25.7±2.8	26.8±1.9	37.8±2.7	21.9±1.8
14	Mg (mg/kg)	2209±334	2517±182	3671±184	4298±245	3002±154
15	Mn (mg/kg)	227±16	224±12	292±16	319±19	225±24
16	Na (%)	0.51±0.06	0.42 ±0.05	0.52±0.06	0.46 ±0.06	0.39 ±0.04
17	Ni (mg/kg)	13. 3±1.0	11.2±1.3	15.9±1.3	17.1±1.2	8.1±0.9
18	Pb (mg/kg)	15.7±1.7	15.6±1.2	14.8±1.7	17.8±1.8	14.4±1.4
19	Rb (mg/kg)	122±10	73.3±6.2	97.9±9.2	171.5±14.2	96.8±7.5
20	Sb (mg/kg)	2.11±0.20	0.54±0.06	1.12±0.21	1.37±0.22	1.91±0.24
21	Sc (mg/kg)	9.8±0.8	7.1±0.7	8.5±0.9	10.8±1.0	6.2±0.6
22	Se (mg/kg)	2.2±0.3	1.6±0.2	0.87±0.09	1.7±0.2	1.5±0.2
23	Sm (mg/kg)	6.03±0.51	3.70±0.27	5.12±0.42	7.68±0.57	4.34±0.32
24	Sr (mg/kg)	1136±63	849±44	1027±53	1022±74	818. ±93
25	V (mg/kg)	41.1±4.2	55.2±2.3	46.3±3.7	97.4±4.9	65.7±6.7
26	Zn (mg/kg)	68.2±5.3	60.3±5.0	55.9±5.3	64.0±6.4	30.3±3.1

Tab 2. Radioactivity of elements in the samples of sediment (*Bq/Kg)*

Element	**VT - 1**	**VT - 2**	**VT - 3**	**VT - 4**	**VT - 5**
Be-7	0.21	2.40	-	-	0.54
Cs-137	0.73	0.48	0.61	0.47	0.48
K-40	374.66	436.80	354.61	415.28	345.91
Pb-210	41.95	49.75	37.20	51.11	38.05
Ra-226	21.70	32.55	24.41	32.23	27.97
Ra-228	22.43	30.65	27.20	29.88	24.34
U-238	30.68	40.59	32.26	39.12	29.78
Th-228	37.01	40.85	39.47	-	-
Th-230	27.25	26.80	28.57	-	-
Th-232	44.86	47.98	42.42	-	-

Tab 3. Concentration of elements in the samples of surface water

TT	**Element**	**Water 1**	**Water 2**	**Water 3**	**Water 4**	**Water 5**
1	As (µg/L)	0.21±0.02	0.17	0.24	0.23	0.16
2	Ca(mg/L)	570±33	640±35	550±27	660±42	620±46
3	Cd(µg/L)	0.23±0.03	0.71±0.06	0.24±0.03	0.23±0.03	0.29±0.03
4	Co(µg/L)	0.33±0.04	0.27±0.03	0.19±0.02	0.24±0.03	0.31±0.03
5	Cr(µg/L)	2.14±0.18	1.68±0.21	3.21±0.33	1.89±0.24	1.63±0.22
6	Cu(µg/L)	1.05±0.14	0.78±0.09	1.05±0.09	1.33±0.12	1.33±0.12
7	Fe(µg/L)	15.7±1.6	11.1±1.2	12.1±1.2	14.6±1.3	16.6±1.3
8	Hg(µg/L)	0.041±0.005	0.039±0.004	0.054±0.006	0.043±0.004	0.062±0.006
9	K(mg/L)	446±33	596±41	483±28	499±42	479±47
10	Mg (mg/L)	785±55	782±63	792±71	824±72	769±66
11	Mn(µg/L)	1.5±0.2	0.75±0.08	1.25±0.11	0.75±0.04	1.0±0.10
12	Sb(µg/L)	1.2±0.2	2.8±0.3	0.8±0.08	1.1±0.1	0.9±0.1
13	Sr(µg/L)	66.5±6.5	53.4±5.0	61.7±6.1	45.7±4.1	62.7±5.5
14	Pb(µg/L)	0.99±0.09	0.45±0.05	1.22±0.11	0.63±0.06	1.59±0.16
15	V(µg/L)	1.11±0.12	0.87±0.08	1.63±0.09	1.54±0.11	0.99±0.10
16	Zn(µg/L)	15.0±1.1	11.8±1.5	14.0±1.3	10.8±1.2	12.3±1.3

Tab 4. Concentration of elements in the samples of biota

TT	Element	Pompano	Herring	Squid	Barnacle	Shellfish	Seaweed	Alga
1	As (mg/kg)	0.25±0.03	0.69±0.07	0.05±0.01	0.04±0.01	0.03±0.01	15.7±1.6	1.09±0.11
2	Ba(mg/kg)	9.9±1.1	6.0±0.7	16.7±1.5	33.7±3.2	16.6±1.2	128±13	17.5±1.6
3	Ca(g/kg)	2.59±0.11	3.57±0.24	0.89±0.09	2.54±0.18	2.85±0.14	34.7±0.15	4.05±0.22
4	Cd(mg/kg)	0.12±0.05	0.14±0.05	0.21±0.02	0.39±0.04	1.38±0.13	0.76±0.07	0.28±0.06
5	Co(mg/kg)	0.45±0.05	0.48±0.05	0.42±0.04	7.96±0.71	7.34±0.72	3.28±0.33	5.95±0.61
6	Cr(mg/kg)	0.67±0.07	0.25±0.03	0.21±0.02	0.67±0.07	0.91±0.09	1.27±0.13	2.34±0.22
7	Cu(mg/kg)	4.30±0.41	7.50±0.72	5.10±0.52	6.50±0.62	7.40±0.77	5.00±0.63	3.70±0.28
8	Eu(mg/kg)	0.10±0.01	0.09±0.01	0.05±0.01	0.16±0.14	1.18±0.12	0.14±0.02	0.13±0.02
9	Fe(mg/kg)	147±12	112±10	51.2±8.2	53.0±4.8	247±18	1241±111	997±86
10	Hf(mg/kg)	0.10±0.01	0.26±0.03	0.22±0.02	0.27±0.03	0.26±0.03	0.53±0.05	0.29±0.03
11	Hg(mg/kg)	0.14±0.02	0.16±0.02	0.04±0.01	0.14±0.02	0.45±0.05	1.07±0.11	0.30±0.03
12	K(g/kg)	13.3±1.2	9.8±1.0	1.6±0.2	3.4±0.3	4.8±0.4	30.7±2.8	39.8±4.1

13	La(mg/kg)	0.11±0.01	0.14±0.01	0.15±0.01	0.49±0.04	0.83±0.04	1.13±0.06	0.20±0.02
14	Mg(g/kg)	1.42±0.11	1.52±0.15	1.64±0.12	1.13±0.12	0.82±0.08	11.9±1.2	4.09±0.50
15	Mn(mg/kg)	1.10±0.11	2.81±0.24	2.33±0.18	14.2±1.2	1.95±0.16	28.6±2.3	23.5±1.8
16	Pb(mg/kg)	0.16±0.02	0.49±0.05	1.07±0.08	0.34±0.04	0.14±0.02	2.09±0.14	0.16±0.02
17	Rb(mg/kg)	35.4±3.3	21.1±1.8	11.8±1.2	33.8±3.1	65.8±5.2	122.4±6.7	177.4±5.8
18	Sc(mg/kg)	0.07±0.01	0.06±0.01	0.05±0.01	0.71±0.07	0.28±0.03	0.82±0.08	0.30±0.03
19	Se(mg/kg)	1.33±0.12	1.89±0.21	1.21±0.14	0.40±0.04	0.91±0.08	0.28±0.03	0.05±0.01
20	Sm(mg/kg)	0.26±0.03	0.11±0.01	0.10±0.01	0.13±0.02	0.59±0.06	0.21±0.02	0.16±0.02
21	Sr(mg/kg)	22.5±2.4	44.3±3.7	63.6±4.2	75.8±6.1	171±11	1174±114	885±45
22	Zn(mg/kg)	24.8±2.3	41.8±4.2	54.1±5.3	48.3±4.2	49.4±4.3	8.3±0.8	20.1±2.1

3. Discussion and conclusion:

Tab 5. Concentration of elements in samples of surface water compared with the samples of Gành Rái[5]

No.	**Elements**	**VT** (µg/L)	**GR** (µg/L)
1	As	0.20	1.21
2	Cd	0.34	0.49
3	Co	0.27	0.24
4	Cr	2.11	1.82
5	Cu	1.11	12.53
6	Fe	14.02	10.83
7	Hg	0.05	0.06
8	Mn	1.05	3.30
9	Sb	1.36	2.17
11	Pb	0.98	0.05
12	V	1.23	1.25
13	Zn	12.78	12.80

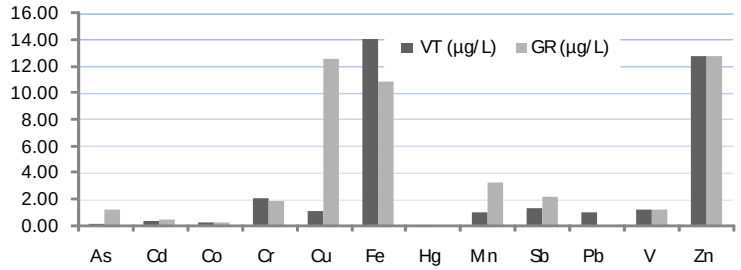

Fig. 1. Concentration of elements in surface waters

Most of concentration of the elements (As, Cd, Cu, Mn, Sb) in the analyzed samples are smaller than amount of the corresponding elements in the samples of Gành Rái. However, some others are approximately (Hg, V, Zn) or higher (Co, Cr, Fe, Pb) than the corresponding elements in the samples of Gành Rái. This can tell that: (1) The level of industrial development in the survey area is increased so that the amount of waste that contains elements of industrials (Co, Cr, Fe, Hg, Pb, V, Zn) are increased, too. (2) There is a significant amount of pollutants of heavy elements may have other derivatives, such as corrosion of transportation facilities on the sea or pollution of other activities on the sea. It explains why there are more many elements with higher content in the analyzed samples than the others of Gành Rái.

Tab 6. Concentration of elements in samples of sediment compared with the samples of Gành Rái[5]

No.	Elements	VT (ppm)	GR (ppm)
1	As	8.60	8.20
2	Cd	1.38	1.00
3	Co	11.22	5.38
4	Cr	56.04	30.40
5	Cu	13.20	12.73
6	Eu	0.99	0.63
7	Hg	1.42	1.17
8	La	28.06	19.40
9	Pb	15.66	32.78
10	Sb	1.41	1.38
11	Sc	8.48	6.02
12	Se	1.57	1.55
13	Sm	5.37	5.08
14	Zn	55.74	68.83

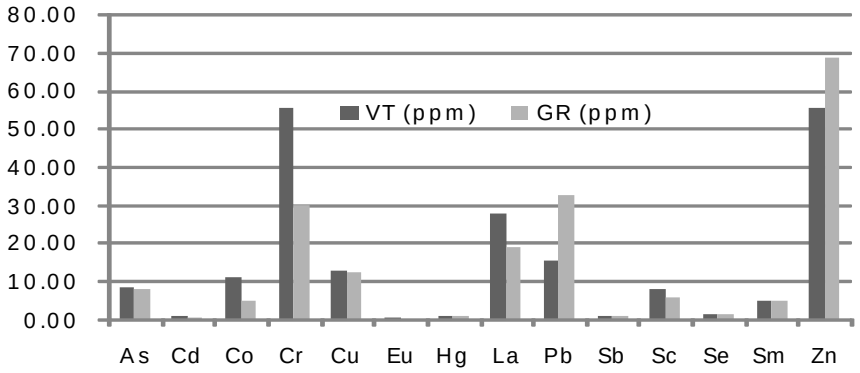

Fig. 2. Concentration of elements in sediments

Tab 7. Concentration of elements in samples of biota compared with the samples of Gành Rái[5]

No.	Elements	Seaweed, VT (ppm)	Seaweed, GR (ppm)	Shellfish, VT (ppm)	Shellfish, GR (ppm)
1	As	15.70	48.40	0.03	7.10
2	Cd	0.76	1.35	1.38	1.54
3	Co	3.28	1.36	7.34	0.42
4	Cr	1.27	11.40	0.91	1.20
5	Cu	5.00	5.38	7.40	7.46
6	Eu	0.14	0.01	1.18	0.05
7	Hg	1.07	1.42	0.45	1.99
8	La	1.13	1.11	0.83	5.96
9	Mn	28.60	82.85	1.95	12.80
10	Pb	2.09	5.53	0.14	2.01
11	Sc	0.82	0.11	0.28	0.12
12	Se	0.28	0.18	0.91	1.60
13	Sm	0.21	0.22	0.59	0.71
14	Zn	8.30	16.20	49.40	49.80

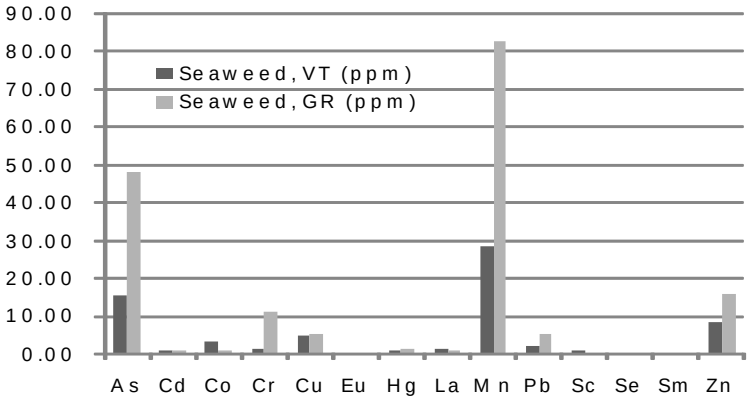

Fig. 3. Concentration of elements in seaweeds

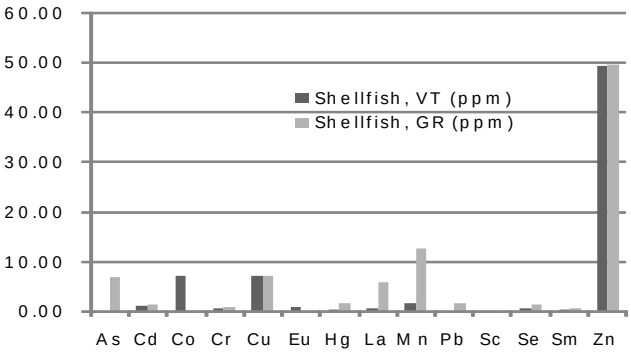

Fig. 4. Concentration of elements in shellfishes

- The contents of Hg, Pb, Sb, V, Zn,... in sediment, surface water and biota samples are increasing. It may cause to accumulate of them to the compartments in marine environment. Hamful to human life when they become to diet of human.
- The result of accumulation of heavy, toxic elements (As, Cd, Hg, Pb, Zn ...) is certainly of the interaction of the living to the compartments of the environment... Food quality such that may cause infections.
- Zinc is the benefit element for health, especially in the biological forms, but we have to take care when it is accompany with the others such as As, Cd, Cu, Hg, Pb, Se ... in foods.
- The need what we have a routine plane to monitor the processing waste of resources to environment in order to reduce the impact.

References

[1]. Ba, Le Huy. Environmental toxicology. National Press, Ho Chi Minh City, 2005

[2]. Hai, P.S. et al. (2003). Final report, 2003. Nuclear Research Institute, Dalat, 2/2004.

[3]. Giang, Nguyen et al. Final report, 2003 - *"Determination of concentration of volatile elements Hg, As, Se and Sb by hydride generator technique – AAS*". Nuclear Research Institute, 2004.

[4]. Ngo, Nguyen Trong et al. Final report, 2004 – 2005 - *"Status of the radiation and toxic elements in some kinds of foods in primary diet of Vietnam."* Nuclear Research Institute, 6/2006.

[5]. Tuan, Nguyen Ngoc et al. Final report, 2006 - "*Application of nuclear analytical techniques and other methods to investigate the contents of some heavy-toxic metal elements in marine environmental samples in some spacial areas at the South of Vietnam"*. Nuclear Research Institute, Dalat 2/2007.

[6]. TCVN. The National standard of Vietnam of Environment. Volume 1. Water quality. Hanoi 1995, p. 52.

[7]. Caitcheon, G. et al. (1991). The snowy River sediment study: Sourcing sediment using environmental tracers. Division of water Resources Report No. 80, Australia**.**

[8]. Gascoyne, M., 1992. Geochemistry of the Actinides and their daughters. Uranium – Series Disequilibrium: Application to Earth, Marine and Environmental Sciences, Second edition, pp. 34 – 59.

COMBINED USE OF ^{137}Cs AND ^{7}Be TO ASSESS THE EFFECTIVENESS OF SOIL CONSERVATION FOR GREEN-MANURE HEDGEROWS IN SHORT-DAY CROP LANDS IN BAN ME THUOT

Phan Son Hai, Nguyen Dao, Tran Van Hoa, Tran Dinh Khoa and Nguyen Thi Mui

Nuclear Research Institute, Dalat, Vietnam

Trinh Cong Tu

National Institute for Soil and Fertilizert, Vietnam

Abstract: The fallout radionuclide ^{7}Be was applied for assessment of short-term soil erosion rates at conventional runoff plots in the Central Highlands. In comparison with data from runoff plot method, following remarks can be drawn: (i) In the case of low erosion rates (less than 4.5 t ha^{-1} mo^{-1}), soil erosion rates estimated by ^{7}Be technique using the Profile-Distribution Model were consistent with net soil erosion rates when particle size correction factor P is taken into account; (ii) In the case of high erosion rates (greater than 4.5 t ha^{-1} mo^{-1}), the conversion model overestimated soil erosion rates when P was not allowed for, and underestimated erosion rate when P factor was taken into account.

The combined use of ^{137}Cs and ^{7}Be for assessment of medium- and short-term soil erosion rates for corn fields using Tephrosia hedgerows as a soil conservation technology has been carried out. The average medium-term erosion rate of 50 years assessed by ^{137}Cs technique is 4.61 t ha^{-1} mo^{-1} and short-term soil erosion rate of 5 months assessed by ^{7}Be technique is 1.40 t ha^{-1} mo^{-1}. By using Tephrosia hedgerows as the soil conservation technology, soil erosion rate was considerably controlled and it reduced from 4.61 t ha^{-1} mo^{-1} to 1.40 t ha^{-1} mo^{-1}. By using ^{7}Be technique, the affectiveness of soil conservation technologies applying in sloping lands can be quickly assessed. Therefore, parametres of soil conservation measures such as the width of hedgerows, the kind of crops, the distance between rows, etc. can be modified so that the efficiency in retaining eroding soil should be improved.

I. Introduction

In the period of 1990-1997, the project "Sustainable Farming on Sloping lands in Vietnam" was carried out by the National Institute for Soils and Fertilizers in cooperation with: the International Board for Soil Research and Management (IBSRAM); the Australian Center for International Agricultural Research (ACIAR); and the Agricultural Institute of Canada (AIC). In this project, experimental runoff plots with the area ranging between 180 m^2 and 300 m^2 were built at 12 sites in the North and Central Vietnam. Data obtained from runoff plots showed that: (i) Soil loss for cultivated land without soil conservation techniques ranged between 5 t ha^{-1} y^{-1} and 105 t ha^{-1} y^{-1} depending on gradient slope, rainfall, crops and tillage way; (ii) Soil erosion resulted in loss of 60-80 kg N, 25-35 kg P_2O_5 and 20-30 kg K_2O per hectare every year; (iii) By using contour hedgerows made of shrubby green manure crops, soil loss and nutrient loss were reduced by 30-90% and by 40-50%, respectively in comparison with controls (Thai Phien et al., 1998).

Owing to the small area, limitted slope length and it's isolation, surface water flow in runoff plot is much different from that in whole hillside. Therefore, data from runoff plots usually is not close to net erosion rates. The assessment of the efficiency in retaining eroding soil for soil conservation measures appling in fields is necessary for improvement of technical factors such as the width of hedgerows, the kind of crops, the distance between rows, etc.

During the last three decades, fallout radionuclides in particular ^{137}Cs have successfully been used in studies of soil erosion and redistribution (Ritchie, 1974; Longmore, 1983; McHenry, 1985; Loughran, 1990; Sutherland, 1992; Hai P.S., 2000). In recent years radionuclide ^{7}Be has also been used for studying short-term soil erosion rate (Wallbrink P.J., 1996; Walling, 1999; Zapata, 2003).

In Vietnam, Cs-137 has been used for assessment of soil erosion rates during last ten years (Phan S. Hai, et al., 2000, 2003, 2004; Trinh Công Tư và nnk., 2005; Phan Sơn Hải và nnk., 2006; Nguyễn Hào Quang, 2000; Nguyễn Quang Long, 2004; Bùi Đắc Dũng, nnk., 2005). Fallout radionuclide ^{7}Be has also been utilized in soil erosion studies in last several years (Phan S. Hai, et al., 2006, 2007; Phan Sơn Hải và nnk., 2007). In this study, ^{137}Cs and ^{7}Be were applied for assessment of soil redistribution patterns and rates of soil loss on sloping land cultivated with short-day crops such as corn, soil bean, etc. in the Central Highlands.

II. Results and Discussion

2.1. Validation of Conversion Models

Conversion Models were tested using 5 runoff plots at Dalat which have the same area of 128 m^2 and the slope of about 25%. Soil erosion rates estimated by ^{7}Be technique were compared with data obtained from runoff plot method. In the period of 5 years 11 campaigns were carried out using ^{7}Be for assessment of soil erosion rates at 5 plots. Results showed that:

- In the case of low erosion rates (less than 4.5 t ha^{-1} mo^{-1}), soil erosion rates estimated by ^{7}Be technique using the Profile-Distribution Model were consistent with net soil erosion rates obtained by runoff plots when particle size correction factor P is taken into account.

- In the case of high erosion rates (greater than 4.5 t ha^{-1} mo^{-1}), the conversion model overestimated soil erosion rates when P was not allowed for, and underestimated erosion rate when P factor was taken into account.

- Shallow penetration of ^{7}Be in soil and high soil erosion rate account for the big difference between the net soil loss and the result given by the Profile-Distribution Model. This conversion model will give results not close to real values when it is applied for estimation of soil erosion at high sloping areas in the Central Highlands.

2.2. Assessment of The Effectiveness of Soil Conservation for Green -manure Hedgerows In Short-day Crops Lands

2.2.1. Study Area

The study was carried out at a 0.34 ha corn field (70m x 49m) in Daklak province ($12^{0}38.33$'N; $108^{0}07.82$'E), which is located in the west of the Central Highland of Vietnam. The study site has the elevation of 570 m above sea level and the mean slope

of about 20%. In order to reduce soil erosion rates, seven *Tephrosia* hedgerows were planted 7 metres apart along contour lines in 1995. There are two distinct seasons for the region. The dry season lasts about 5 months, from December of the last year to April and the rainy season lasts from May to November. The mean annual rainfall over 20 years is 1850 mm.

2.2.2. Results

2.2.2.1. Assessment of Medium -term Soil Erosion Rates Using ^{137}Cs

a) Inventory of ^{137}Cs at Reference Sites

The depth distribution of ^{137}Cs at the reference sites was shown in Figure 2.1. The mean reference inventories of ^{137}Cs was 320 ± 24 Bq.m^{-2}. By using the Regression Model (P.D. Hien et al., 2002) described the relationship between the ^{137}Cs inventory at virgin sites I (Bq m^{-2}) and latitude L (degree) and annual rainfall AR (m), ^{137}Cs inventories ranged between 222 and 404 Bq m^{-2} (the mean value: 300 Bq m^{-2}). The predicted values are consistent with experimental values in the range of uncertainties.

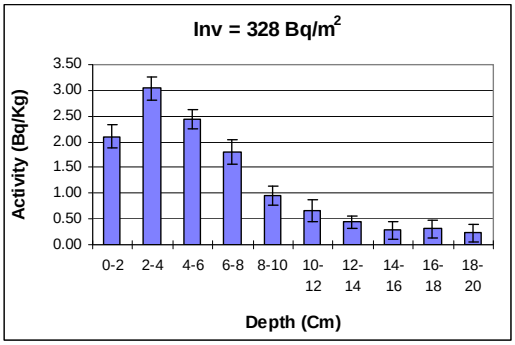

Fig 2.1. The depth distribution of ^{137}Cs in undisturbed soils

b) Medium-term Soil Erosion Rates Assessed by ^{137}Cs

^{137}Cs inventories for 42 sampling points along 3 downslope transects were determined with analytical uncertainties ranging between 5% and 10% at the 95% level of confidence. In order to convert ^{137}Cs loss or gain data to soil loss or gain, two conversion models were used, namely the Proportional Model and NRI empirical Model. Results obtained from two models have the difference of about 3% - 12%. The mean soil erosion rate for a period of about 50 years is 32,3 t ha^{-1} y^{-1}.

The Pattern of Medium -term Soil Redistribution:

The pattern of soil redistribution rates within the corn field was showed on Figure 2.2. Study results showed that:

- About 95% of the study area sufferred from erosion; the erosion rate varied from 5.9 t ha^{-1} y^{-1} to 41.7 t ha^{-1} y^{-1} (mean: 34.7 t ha^{-1} y^{-1});

- About 5% of the study area was deposited with the average rate of 1.47 t ha^{-1} y^{-1};

- The role of Tephrosia hedgerows planted in 1995 was not clearly showed in the 50 year medium-term pattern of soil redistribution.

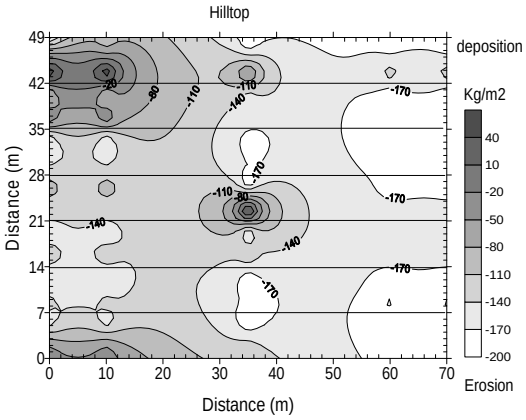

Fig. 2.2. The pattern of soil erosion rates obtained from ^{137}Cs data

2.2.2.2. Estimation of Erosion Rates Using ^{7}Be

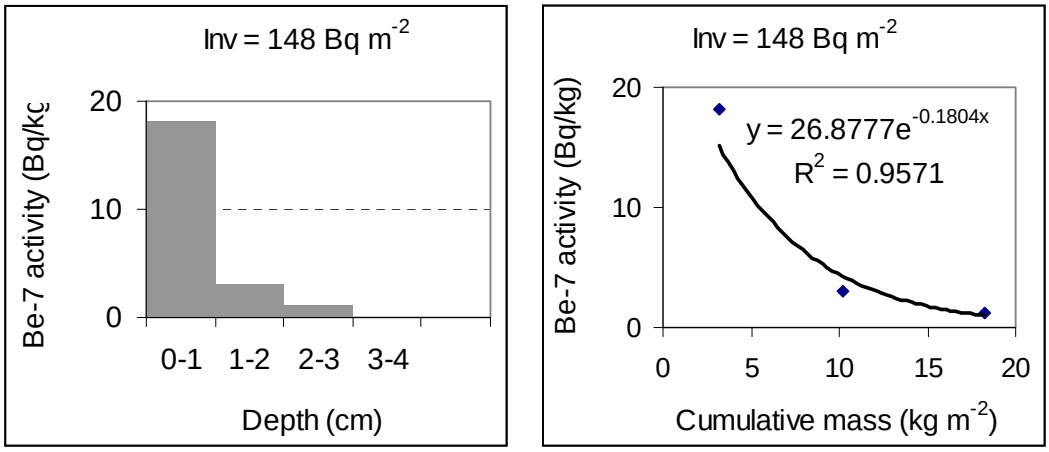

Fig. 2.3. The depth distribution of ^{7}Be in undisturbed soil at reference site

a) Inventory of ^{7}Be at reference site

The depth distribution of ^{7}Be at reference site was shown in Figure 2.3. The ^{7}Be activity exhibits an exponential decline with depth with high correlation coefficients (r^2 = 0.96). The relaxation mass depth h_0 estimated from the distribution was 8.1 $kg.m^{-2}$. The mean reference inventory of ^{7}Be obtained from bulk soil samples at reference site was 140 $Bq.m^{-2}$ at the time of sampling.

b) Inventory of ^{7}Be at study site immediately after cultivation

Inventories of ^{7}Be at 10 sampling points within study area immediately after cultivation are very low - the same magnitude as LOD of spectrometers (~ 20 Bq m^{-2}). This mean that, after cultivation the inventory of ^{7}Be in surface soil can be considered to be equal zero. For this reason, "natural reference sites" are not suitable for determination of referent inventories. Instead of this, "artificial reference sites" can be created and they must be cultivated in the same way and at the same time as those for study sites.

c) Assessment of short-term soil erosion rates by ^{7}Be

^{7}Be inventories for 28 sampling points along 2 downslope transects were determined and then soil erosion rates at sampling points were assessed using Profile-Distribution Model. Short-term soil erosion rate for the whole field was 1.4 t ha^{-1} mo^{-1}. With the 12 year presence of seven Tephrosia hedgerows, short-term erosion rate is 3.3 times as low as medium-term erosion rate.

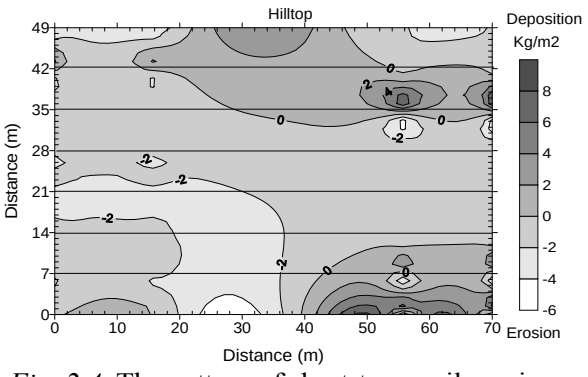

Fig. 2.4. The pattern of short-term soil erosion rates obtained from ^{7}Be data

d) The pattern of soil redistribution

Short-term soil redistribution within the field was presented in Fig. 2.4. Study results showed that:

- Seven Tephrosia hedgerows have the role in retaining eroding soil. Therefore, short-term soil erosion rate was decreased considerably in comparison with medium-term soil erosion rate.

- About 82% of the whole area suffered from erosion with the rates ranging between 2.0 t ha^{-1} y^{-1} to 45.6 t ha^{-1} y^{-1}; and 18% of the area was deposited with the rates varing from 8 t ha^{-1} y^{-1} to 72 t ha^{-1} y^{-1}.

III. Conclusion

Fallout radionuclide ^{7}Be is an effective tool for assessment of short-term soil erosion rates in sloping cultivated lands. The Profile-Distribution Model usually overestimated soil erosion rates when the particle size correction factor P was not allowed for. When factor P was taken into account, the Conversion Model gave the results consistent with net soil loss in the range of uncertainty in the case of low erosion rates (less than 4.5 t ha^{-1} mo^{-1}) and underestimated soil erosion rate in the case of high erosion rates (greater than 4.5 t ha^{-1} mo^{-1}). The Profile-Distribution Model ia not suitable for regions having high gradient slope, high rainfall and poor vegetation.

When ^{7}Be is applied for assessment of soil erosion rate within short-day crops lands, artificial reference sites should be created instead of using natural reference sites. If natural reference sites are used, the ^{7}Be method can overestimate soil erosion rates.

The average of 50 year medium-term erosion rate assessed by ^{137}Cs technique is 4.61 t ha^{-1} mo^{-1} and 5 month short-term soil erosion rate assessed by ^{7}Be technique is 1.40 t ha^{-1} mo^{-1}. By using Tephrosia hedgerows as the soil conservation technology, soil erosion rate was reduced from 4.61 t ha^{-1} mo^{-1} to 1.40 t ha^{-1} mo^{-1}. ^{7}Be technique can be utilized to quickly assesse the affectiveness of soil conservation technologies applying in sloping lands . Therefore, parametres of soil conservation measures such as the width of hedgerows, the kind of crops, the distance between rows, etc. can be modified so that the efficiency in retaining eroding soil should be improved.

References

[1]. Hien, P.D. et al., 2002. Derivation of Cs-137 deposition density from measurements of Cs-137 inventories in undisturbed soils. *Journal of Environmental Radioactivity, 62 295 - 303.*

[2]. Loughran, R.J. et al., 1990. Determination of Rate of Sheet Erosion on Grazing Land Using Cs-137. J. *Applied Geography, 10, pp. 125-133.*

[3]. P.S. Hai, et al. (2000). Assessment of erosion and accretion in catchment areas based on Pb-210 and Cs-137 concentrations in soil and sediment. *In Proc. 3ICI, World Scientific Publishing Co. Pte. Ltd, 2000, p. 415-418.*

[4]. Phan Sơn Hải và nnk., (2006). Xác định tương quan giữa mất Cs -137 và tốc độ xói mòn đất bề mặt vùng Tây Nguyên. *Tạp chí Khoa học đất, No. 26, 2006. Hội Khoa học đất Việt Nam, ISSN 0868-3743. pp. 92–94.*

[5]. S. Hai Phan, et al. (2006). Assessment of soil erosion rates and the effectiveness of soil conservation measures using fallout radionuclides and plots. *Proc. of the*

third RCM of the FAO/IAEA CRP, Vienna, Austria, 27-30 March 2006, pp. 115–122.

[6]. Phan S. Hai, et al., 2007. Application of Cs-137 and Be-7 to assess the effectiveness of soil conservation technologies in the Central Highlands of Vietnam. *The final RCM of the FAO/IAEA CRP, Vienna, Austria, 15-19 Oct. 2007.*

[7]. Phan Sơn Hải và nnk. (2007). Đánh giá tốc độ xói mòn và hiệu quả các giải pháp bảo vệ đất bằng phương pháp đồng vị phóng xạ và ô thí nghiệm. *Tạp chí Khoa học đất, No. 27, pp. 154-159.*

[8]. Ritchie, J.C., et al. (1974). Fallout Cs-137 in the Soils and Sediments of Three Small Watersheds. *Ecology, Vol. 55, No. 4, pp. 887-890.*

[9]. Sutherland, R.A. (1992). Cs-137 Estimates of Erosion in Agricultural Areas. *Hydrological Processes, Vol. 6, pp. 215-225.*

[10]. Thái Phiên & Nguyễn Tử Siêm (Ed.), 1998. Canh tác bền vững trên đất dốc ở Việt Nam - Kết quả nghiên cứu giai đoạn 1990-1997. *NXB Nông Nghiệp.*

Papers Published In Relation To The Project

1. PHAN S. HAI, T. D. KHOA, N. DAO, N. T. MUI, T. V. HOA, T. C. TU. Application of Cs-137 and Be-7 to assess the effectiveness of soil conservation technologies in the Central Highlands of Vietnam(to be published in the Journal of Nuclear Science and Technology; VAEC)
2. Phan Sơn Hải, Trần Văn Hòa, Trần Đình Khoa, Nguyễn Đào, Nguyễn Thị Mùi, Trình Công Tư. So sánh kết quả đánh giá tốc độ xói mòn đất bằng kỹ thuật Be-7 với kết quả đo trực tiếp trên các ô thí nghiệm truyền thống. *Hội nghị Khoa học và Công nghệ hạt nhân toàn quốc lần thứ VIII, Nha Trang, 20 - 22/8/2009.*

1.6 - Applications in Biology, Agriculture and Medicine

STUDY ON THE APPLICATION OF PZC ADSORBENT FOR ^{99m}Tc-GENERATOR PREPARATION

Duong Van Dong, Pham Ngoc Dien, Bui Van Cuong, Mai Phuoc Tho
Nguyen Thi Thu, Vo Thi Cam Hoa, Nguyen Giang and Pham Ngoc Tuan

Centre for Research and Production of Radioisotope, Nuclear Research Institute

Abstract: Tc-99m is a main radioisotope for nuclear medicine application, accounting for more than 80% of all diagnostic nuclear medicine procedures expecially in organs function imaging techniques. The chemical synthesis for the preparation of adsorbent (PZC) and the investigation on loading procedure for preparation generator of PZC based chromatographic Tc-99m was described in detail . In-process production was described by schemes of process, especially, designs PZC-Tc-99m generator were in detail reported . The column loading process for production and results of quality control Tc-99m was highly evaluated as a competent technology for the preparation of PZC-Tc-99m based chromatographic generator of high performance using ^{98}Mo(n,γ)^{99}Mo of low specific radioactivity produced on low power research reactors.

I. Introduction

Tc-99m is a mainstay radioisotope for nuclear medicine application. This radioisotope now-a-day is eluted routinely from a radionuclide chromatographic generator using a parent Mo-99 radionuclide produced by (n,γ) or (n , fission) nuclear reaction and a chromatographic column on which Mo-99 parent nuclide is adsorbed. The chromatographic column packing material can be Alumina adsorbent, zirconium-molybdate or titanium–molybdate gel powder and a newly developed Polymer Zirconium Compound (PZC). Each column packing is specified for a particular case of Tc-99m generator type. The Tc-99m generator technology using a recently developed PZC column packing adsorbent is noted as a new alternative one.

In this publication the procedures for the preparation of PZC based Tc-99m generator are reported.

The column loading procedure for the preparation of PZC based chromatographic Tc-99m generator production was recently developed by FNCA members. This procedure seems to be safe and more comfortable in the operation .

This procedure is intended to be applied for the production of a generator of radioactivity ranging from 200 mCi to 1000 mCi Tc-99m which can be satisfactorily used in the clinical nuclear medicine application.

II. Materials and Methods

A. Materials

- Chemicals: Isopropyl alcohol (iPrOH), $ZrCl_4$; HCl, NaOH, THF, N_2, NaCl, Al_2O_3, MoO_3, MoO_3 enriched,

- Tools: 1000ml Round flask (3 neck); Hot plate; Beaker; Melting point measuring instrument; Syringe (Glass); Stirring bar; Stopper; Septum; Needle; Spatula. Ice bath, electric stirrer, filtering funnel, extracting funnel, rotary evaporator. Dose calibrator, Peristaltic…

B. Preparation

1. PZC Synthesis

PZC adsorbent was synthesized from isopropyl alcohol (iPrOH) and $ZrCl_4$ under strickly controlled conditions of reaction. $ZrCl_4$ were carefully added to iPrOH.The temperature of reaction mixture will immediately reached at 90 ^{o}C. By keeping temperature of solution at 90 ^{o}C ,stir this solution gently by magnetic stirrer in N_2 gas until this solution become viscous. As the reaction temperature is increased, a water-soluble gel PZC (an intermediate precursor) will be formed at 140 ^{o}C. The water-insoluble, solid PZC particles of mesh size around 50 are splitted out by keeping the reaction temperature at 160 ^{o}C for 30 minutes. This finished product of PZC adsorbent is light brown in colour.

$$ZrCl_4 + \text{iso-PrOH} \xrightarrow[24h]{\text{THF}} ZrCl_x(OPr)_y(OH)_z \xrightarrow[160^oC]{\text{heat 30'}} \text{PZC}$$

2. ^{99}Mo adsorption on PZC column

- PZC column preparation

Mix 90ml of distilled water with 5ml 0.1M NaOH solution and 5ml 1.5% NaOCl solution to get a solution for PZC column preparation.Add 4g PZC to the above prepared solution and shake mixture gently for 2 hours at room temperature then let it stand for one minute and remove the fine PZC powder from solution mixture by the decantation of the supernatant solution. Wash PZC powder and decant supernatant twice with 100 ml bi-distilled water. Check-up the acidity of solution. pH around pH = 2 should be chosen. Pack gently PZC powder into a glass column of 12 mm in diameter and 80mm in length with G3 fritted glass filter on one of its ends. Place a small piece of fine glass wool on the surface of PZC bed and apply the column stopper on the column ends.

- ^{99}Mo adsorption solution preparation

+ Reagents

- MoO_3 (pre-purified, sufficiently dried natural MoO_3) is used as a target: 2 grams.
- (^{99}Mo) Molybdate solution (optional item, commercially available ^{99}Mo solution);
- PZC adsorbent : 1-4 grams;
- 6 M NaOH solution : 5 ml;

- 1 M NaOH and 1 M HCl solutions for pH adjustment;
- 0.9% saline solution containing 0.05% NaOCl oxidizing agent for column conditioning;
- 0.9% saline solution for generator elution;
- Al_2O_3 (Alumina);
- Bi-distilled water is used for all steps of experiments.

+ Preparation of ^{99}Mo solution

Activate 2 g MoO_3 by thermal neutron in a nuclear reactor, then dissolve the irradiated MoO_3 in 5 ml 6M NaOH solution. Adjust pH of the solution to pH =7 with 1N HCl (or with 1N NaOH if necessary). Dilute the solution with Bi-distilled water to 25 ml to get a ^{99}Mo solution of concentration of C_{Mo} = 53.4 mg Mo/ml. This resulting solution is called the Original ^{99}Mo Solution**.**

Pipette out 5 ml of original ^{99}Mo solution and put into a penicillin type vial of 10 ml volume for ^{99}Mo radioactivity measurement. Measure the ^{99}Mo radioactivity of this solution (noted as $\mathbf{a_o}$)using a radioisotope dose calibrator and calculate the ^{99}Mo radioactivity of 20 ml original ^{99}Mo solution (noted as $\mathbf{A_o}$) which will be used for the Molybdenum adsorption on PZC adsorbent in the following steps.

- ^{99}Mo radioactivity of 20 ml original ^{99}Mo solution (calibrated at time of radioactivity measurement of the original ^{99}Mo solution)

$$\mathbf{A_o} = 20 \text{ x } \mathbf{a_o} : 5$$

- Specific radioactivity of original ^{99}Mo solution (noted as S_o)

$$S_o\left(\frac{mCi\ ^{99}Mo}{mg\,Mo}\right)=\frac{A_o}{20\,x\,53.4}$$

+ Alumina column preparation

This preparation batch is used for loading 5 Alumina column (each column contained 2g Alumina). Pour 10g Alumina into 100ml 0.1N HCl solution while stirring. After mixing check-up the pH of the aqueous phase several times during the first hour; the solution should remain acidic. Add more hydrochloric acid solution when pH rise to neutral values and stir well. Then allow the mixture to stand overnight. Next stir the suspension and allow it to settle and decant off the supernatant. Repeat the stirring-decanting steps with 100 ml distilled water to get clear supernatant of acidity between pH = 4 and pH = 5. Pack the alumina into 5 glass columns of 9 mm in diameter and 50 mm in length with G3 fritted filter disk on one of its ends. Sterilize the prepared alumina column by autoclaving at 121^{0}C for 20 minutes.

+ Calculation of ^{99}Mo radioactivity of ^{99}Mo -PZC column

- Non-adsorbed ^{99}Mo content (at reference time t=0)

$$A_1\,(mCi\ ^{99}\mathrm{Mo}) = \frac{a_1}{5}\,x\,500$$

- Calculated ^{99}Mo radioactivity of ^{99}Mo -PZC column (noted as A_{cc}) at the reference time t=0

$$A_{cc}\,(mCi^{99}Mo) = (A_0 \times f_0) - A_1$$

(f_o : ^{99}Mo decay factor for the time period from ^{99}Mo radioactivity measurement of the ^{99}Mo original solution to the reference time t=0)

- ^{99}Mo -PZC column radioactivity deviation between measured and calculated values (noted as δ

$$\delta(\%) = \left[100\, x \frac{(A_{mc} - A_{cc})}{A_{cc}} \right]$$

- ^{99}Mo adsorption percentage (noted as *p*)

$$p(\%) = \frac{A_{cc}}{A_o . f_o} x 100$$

- Specific radioactivity of PZC (noted as S) at the time of radioactivity measurement of original Mo-99 solution.

$$S\left(\frac{mCi\,^{99}Mo}{g\,PZC} \right) = \frac{A_{cc}\, x100}{4(100-\sigma).f_o}$$

- Molybdenum adsorption capacity of PZC (noted as $K_{c(Mo)}$)

$$K_{c(Mo)}\,(\frac{mg\,Mo}{g\,PZC}) = \frac{A_{cc}}{A_o . f_o} x \frac{20\, x\, 53.4\, x 100}{4(100-\sigma)}$$

- Factor of the effective adsorption capacity of PZC column:

$$Fc = K_{c(Mo)}/K_{Mo}$$

3. Elution process

After 24 hours of standing from the reference time t=0 (from the end of loading and conditioning step) , elute the build- up Tc-99m from above assembled ^{99}Mo – PZC – Alumina based ^{99m}Tc generator system with 20 ml sterilized 0.9% saline by sucking Tc-99m eluate completely into an evacuated sterilized bottle of 30 ml volume or by passing exhaustively with gravity force and collecting Tc-99m eluate in a 30 ml bottle. Pipette 5 ml Tc-99m eluate into 10 ml penicillin type vial under aseptic conditions and measure the Tc-99m radioactivity and the Mo-99 radioactivity of this portion of Tc-99m eluate with a radioisotope dose calibrator (using a lead pot of 5 mm thickness to attenuate 140 KeV gamma ray of Tc-99m for Mo-99 radioactivity measurement. Repeat this elution process every twenty-four hours and collect all measured data for calculation.

4. Generator design

The ^{99m}Tc generator system must be designed correctly to fulfill QA & GMP requirements for the production of radiopharmaceuticals.These ^{99}Mo – PZC – Alumina based ^{99m}Tc generator systems were successfully designed.

5. Quality control

The radionuclidic purity , radiochemical purity , pH , sterility , the pyrogenity of Tc-99m Pertechnetate solution were investigated in accordance with 21st US Pharmacopoeia.

- The radionuclidic purity: The amount of ^{99}Mo in $Na^{99m}TcO_4$ obtained from the elution of PZC-based genegator was not greater than 0.15 kBq per MBq (0.15 mCi/mCi) of Tc-99m as determined by either dose calibrator and HPGe detector connected to a multichannel analyzer. Rapid determination of ^{99}Mo by dose calibrator is measured by two reading. Mo-99 is measured with 5mm thick lead canister and Tc-99m is measured without lead shieldin

- Radiochemical purity: Chromatoggraphic method imployed to determine radiochemical purity

- Chemical purity: Aluminium content, Molybdenum content

- pH: The pH must be 4.0 to 7.0 as measured by a standardized pH meter or appropriate pH paper

- Sterility test: Aseptically tranfer the proper volume of sodium pertecnetate solution to the vessels containning culture mediums. Two culture mediums are used. Fluid thioglycollate medium is incubated with sample solution at 30^{o}C to 35^{o}C for 14 days to test for most common aerobic, facultative and anaerobic microorganisms. And incubat sample solution in soybeancasein digest medium at 25^{o}C for 14 days to test for aerobic bacteria and fungi. Anu microbial growth must not be observed in both medium to meet the requirement of the test for sterility.

- Pyrogen test: Bacteril endotoxins test is a test for apyrogenicity which Limulus Amebocyte Lysate (LAL) prepared from the blood of Limulus polyphemus, is used as a gel-clot formation reagent. In the presence of minute concentrations of bacterial endotoxin, the LAL forms an opaque gel under optimm condition of temperature (37^{o}C) and pH (6.0-7.5). After incubation of the mixture for one hour, completely undistuebed, the formation of the firm gel represents a position test endpoint reaction.

- Biodisbution: Radiopharmaceuticals kits are labeled with ^{99m}Tc obtained from PZC-based generator. After the radiochemical purity of 99mTc-complex is confirmed, the biodistribution study in animal is also performed. The biodistribution study involes the administration of radiopharmaceuticals into animals such as rat or rabbit.

III. Results and Discussion

1. The Result of PZC Synthesis

PZC could be easily synthesised by the reaction using isopropyl alcohol (iPrOH) and $ZrCl_4$ in the present of THF at 160^{o}C during 30' The product was found to be pure as characterized of Crystal picture, ^{99}Mo adsorption capacity, IR spectrum, labeling effiency, element and metal trace and impurity tracer analysis.

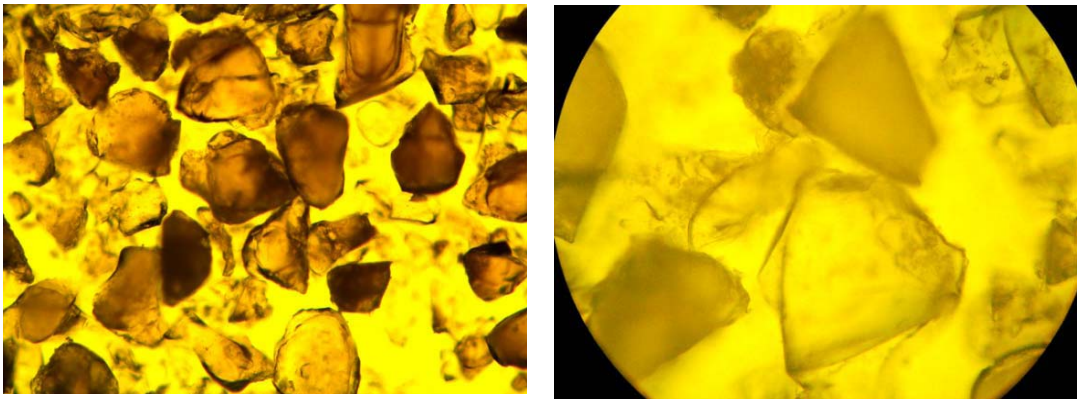

Fig. 1. Crystal picture size: 0.5-0.01mm Before and after Mo-adsorption

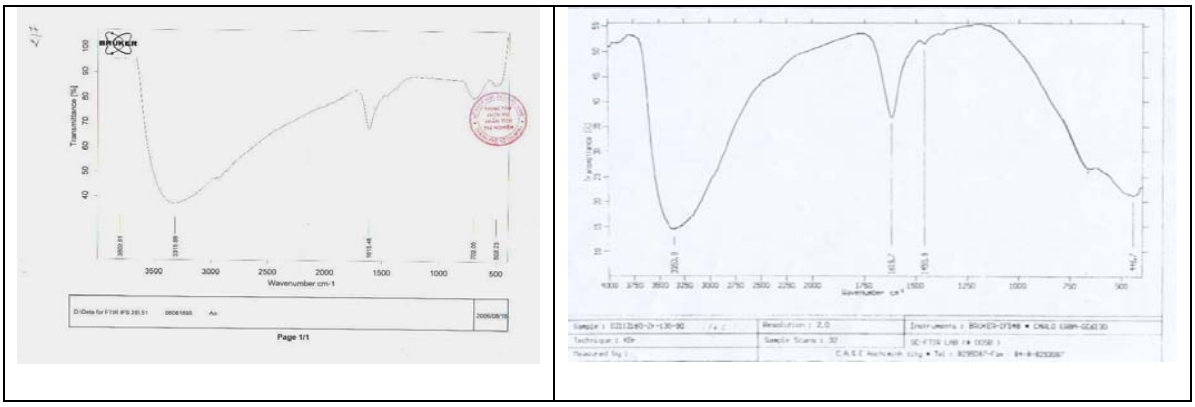

Fig. 2. Infrared spectra of synthesized PZC and control sample

Tab 1. Infrared absortion of PZC sornents

Wave numbers, cm^{-1}	Intensity	Chemical bond characteristics	Specified function groups
3500-3000	Very strong (broad)	ν (OH) ν (OH_3^+)	OH in Zr-OH and -CH_2-CH(OH)-CH_3
2900	Very strong	ν (CH)	-CH_2-CH_2-
2900	Weak	ν (H_3O^3)	
1700-1500	Medium	δ (H_2O)	
700-600	Medium	ν (Zr-O)	

The obtained results to infrared absorption data of ZrO_2xH_2O samples a good agreement was found. The organic trace amount retained in the PZC samples were detected at 2900cm^{-1} (very strong) is assigned by-product of chemical synthesis reaction, but not to the reactant isopropyl alcohol (-CH_2-CH_2-)

2. The result of generaor ^{99m}Tc

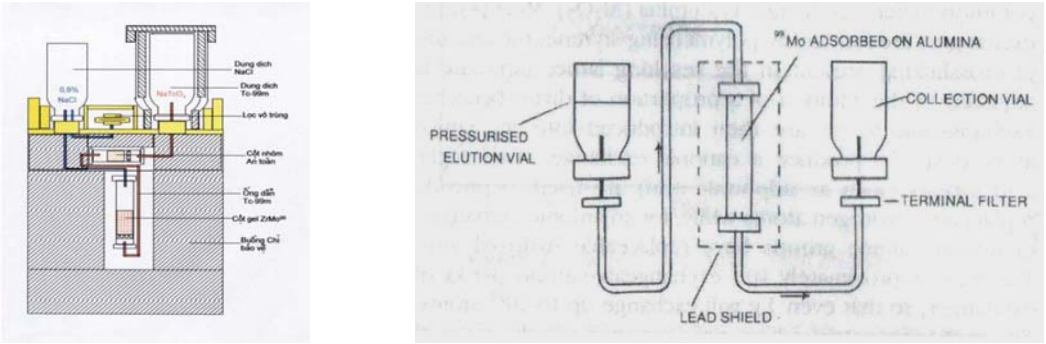

Fig. 3. Model of generator Tc-99m

Fig. 4. To assemble of generator spare-part

3. The result of elution process Tc-99m

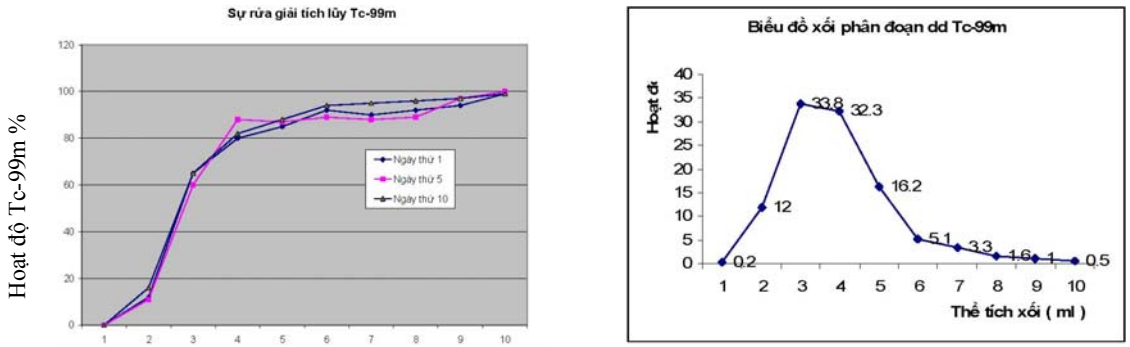

Fig. 5. Tc-99m elution characteristics (The elution is performed with 0.9% NaCl)

4. The result of quality control Tc-99m generator

Tab 2. The result of 99mTc generator

Elution rate of Tc-99m	>80%
Radionuclidic impurity - ^{99}Mo	<0.15 µCi/$_{mCi}{}^{99m}_{Tc}$

- I-131	<0.05 µCi/$_{mCi}^{99m}$Tc
Radiochemical purity	>99%
pH	4.5-7.0
Sterility	cleared
Pyrogenicity	cleared
Heavy metals - Aluminium - Molybdenum - Zirconium	 <0.2µg/ml <0.5µg/ml <0.5µg/ml

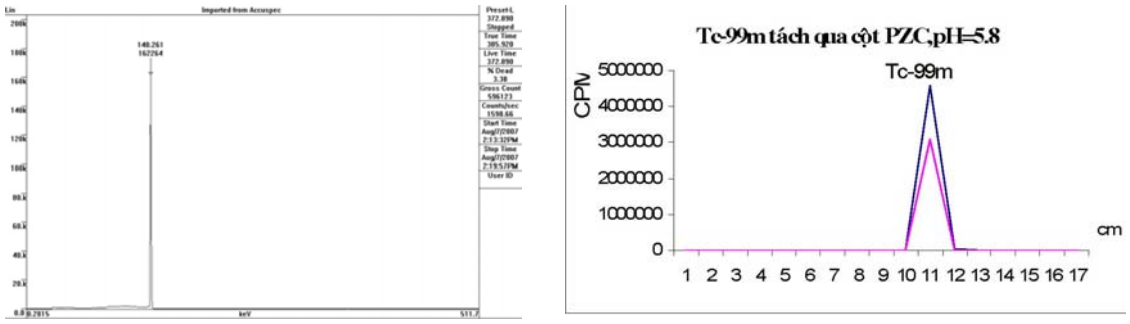

Fig. 6. Radionuclidic purity and radiochemical purity of Tc-99m

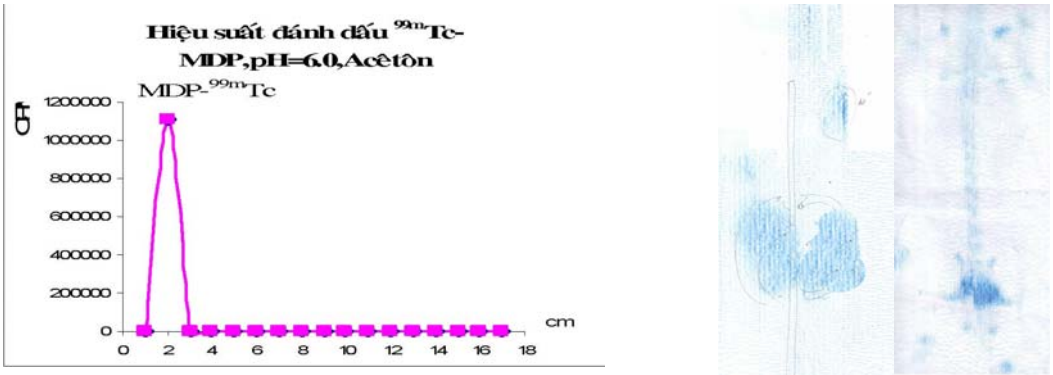

Fig.7. Labeling ^{99m}Tc–MDP kit (labeling yeild > 99%) and biodistribution of DMSA-^{99m}Tc in rabbit

Conclusion

PZC adsorbent of high performance for Mo-99 adsorption easy to synthesize and Tc-99m elution was successfully synthesized from isopropyl alcohol (iPrOH) and $ZrCl_4$.

The procedures and relevant Tc-99m generator designs for the preparation of PZC based Tc-99m generators were successfully set up.The columns of from 1.0 gram to 4.0

gram weight of PZC and from 100 mCi to 1500 mCi Mo-99 can be used to produce portable , chromatographic type Tc-99m generators which have a good performance for application in clinical investigations. Among the established procedures the column loading procedure was highly evaluated, because it proved to be prominent figures for easy and safe operation , for low cost of technology facilities and equipment and for the capability to match the traditional technology of the fission Mo-99 based Tc-99m generator production.

In conclusion, it is strongly believed that PZC based generator would play an importance role as alternative technology for production of $^{99}Mo/^{99m}Tc$ generator from (n,γ) ^{99}Mo. However this method isn't very appropriate for low power research reactor.

References

[1]. Masakazu Tanase, Katsuyoshi Tatenuma, et al., ^{99m}Tc Generator using New Inorganic Polymer adsorbent for (n, gamma) ^{99}Mo.
Appl. Radiat . Isot. Vol. 48, No. 5, pp. 607-611, 1997.

[2]. Le Van So , Investigation on the performance of polymer Zirconium compound (PZC) for chromatographic Tc-99m generator preparation.
JAERI- conf. 200..., Proceedings of the 2002 Workshop on the Utilization of Research Reactors, January 13 – 17 , 2003 , Serpong, Indonesia

[3]. **A**. Mutalib , et al, A performance evaluation of (n, gamma) ^{99} Mo / ^{99m}Tc Generators produced by using PZC Materials and Irradiated Natural Molybdenum.
JAERI- conf. 2003-004, Proceedings of the 2001 Workshop on the Utilization of Rsearch Reactors .1.33 ,P. 202 - 210. November 5- 9, 2001, Beijing, China

[4]. Tatenuma K., Ishikawa K., Nishino M., Hasegawa Y., Kurosawa K., Sekine T., Tanase M., A practical ^{99m}Tc generator using (n,γ) ^{99}Mo, Proceedings of 1999 Workshop on the Utilization of Research Reactors, JAERI, Japan, Dec 2 (1999)

Papers Published In Relation To The Project

Accession number; 07A0225945

Title;STATUS OF THE STUDY ON PZC BASED Tc-99m GENERATOR AND POTENTIAL OF ITS COMMERCIAL
PRODUCTION IN VIETNAM

Author;DONG DUONG VAN (Nuclear Res. Inst., Dalat, Vnm)

Journal Title;Nihon Genshiryoku Kenkyu Kaihatsu Kiko JAEA-Conf

Journal Code: L2150A

ISSN:

VOL.;**NO.**;**PAGE.**25-29(2007)

Figure &Table&Reference;

Pub. Country; Japan

Language;English.

STUDY ON THE LABELING OF ANTI CD20 MONOCLONAL ANTIBODY WITH I-131 FOR BLOOD CANCER THERAPY

Nguyen Thi Thu[1], Duong Van Dong[1], Vo Thi Cam Hoa[1], Chu Van Khoa[1], Bui Van Cuong[1]
Pham Ngoc Dien[1], Mai Phuoc Tho[1], Nguyen Thanh Binh[1], Dang Ho Hong Quang[1]
Lê Quang Huan[2] and Mai Trong Khoa[3]

1. Nuclear Research Institute, VAEC, Vietnam
2. Biotechnology Hanoi, Vietnam
3. Bachmai Hospital, Hanoi, Vietnam

Abstract: In recent years, radio immunotherapy (RIT) has become a highly promising oncologic therapeutic modality with established clinically efficacy, particularly in the therapy of hematological malignancies. Rituximab, a chimerical monoclonal antibody targeted against the cluster designation (CD20) antigen was labeled with ^{131}I used in the treatment of B cell non Hodgkin's Lymphoma (NHL), B cell leukemia. In this study, the Rituximab and single chain variable fragment (scfv) CD20 monoclonal antibody were labeled with ^{131}I using chloramines T method (ChT). The optimized ChT concentration for the oxidation of 740MBq of Na^{131}I solution and 1500µg of Rituximab was 40µg/40µl. The latter antibody was labeled with 37MBq of Na^{131}I, 50µg of antibody and 10µg of ChT. The reaction time was 3 minutes at room temperature. The labeling reaction has stopped using sodiummetabisulphite (SMB). Labelling efficacy was controlled by ITLC. The reaction mixtures were purified through the sephadex G-25 PD10 Pharmacia column. The collected ^{131}I-antibodies were filtered through a 0.20µm milipore sterile filter. The radiochemical labeling yields was more than 95%. Radiochemical purity (RCP) of the radiopharmaceutical after purification was more than 99%. The product has been passed the test for sterility, bacterial endotoxins, to be sufficiency in vivo and in vitro stable after labeling, labelled antibody ready for clinical use.

Keywords: Anti CD-20 monoclonal antibody, ^{131}I-Rituximab, Radioiodination, Radiopharmaceuticals.

I. Introduction

In recent years, the radioactive labeled monoclonal antibodies have been widely used in diagnosis and clinical therapy. Method of therapy using monoclonal antibodies antibody is called the method of targeted therapy. This method of therapy is also called radio immunotherapy (RIT). The blood cancer non-Hodgkin Lymphoma (NHL) is cancer of lympho B cells in blood, when cancer appears, on the surface of the B lympho cells strange agents are expressed, by the help of advanced molecule-biological techniques, scientists in the world has determined that they were CD20 antigen and their molecule structure were well defined. The molecule of antibody perform the function for targeting by attaching the special resources of resistance to target CD20, destroy the tumor by the mechanisms actions such as Antibody Dependent Cellular Cytotoxicity (ADCC), Complement-Dependent Cytotoxicity (CDC), apoptosis and ionizing radiation. With the average energy particle of 192keV, gamma rays of 364 keV, half life of 8.04 days, ^{131}I can be used for imaging studies to monitor therapy and long enough radiation to the tumor, ^{131}I is an ideal radioisotope for target therapy when conjugate with antibodies, especially suitable for the treatment of hematological malignant cells.

II. Materials and Methods

II.1 Antibodies and Reagents: Iodine-131 ($Na^{131}I$) 200mCi/ml concentration at calibration time, more than 99.9% radionuclide purity, in carbonate buffer was from the Centre for Research and Production of radioisotopes of our Nuclear Research Institute, Dalat, Vietnam. Rituximab (CD20 monoclonal antibody) 500mg/50ml, was purchased from ROCHE, Lot No. MF 0072005B2074 and EU/1/98/067/002 B5057. Scfv CD20 antibody and CD20 antigen were provided from Biotechnology Institute, Hanoi. Sephadex G25, PD10 was purchased from Amersham Bioscences, Lot No. 170851-01. 0.9% NaCl solution was from B. Braun Medical AG, Chloramines T (ChT), Sodium-metabisulphite (SMB) and other chemicals were p.a. grade and purchased from Sigma.

II.2. Methods of Radiolabelling: Monoclonal antibody anti CD20 was labelled with ^{131}I using chloramin T method. The experiments were performed on the ^{131}I-labeled CD20 antibody. The 50µl of $Na^{131}I$ (740MBq) was added to the reaction vial containing 50µl phosphate buffer and 150µl (1500µg) of Rituximab (10mg/ml) and then 40µl ChT (1mg/ml). The reaction mixture was lightly mixed and incubated for 3 minutes at room temperature. To stop the reaction, the 40µl of SMB (2mg/ml) was added and mixed it for 30 seconds. The labeling solution was purified and quality control. The scfv CD20 antibody were added into the reaction vials with 50µl of phosphate buffer, 50µl (50µg) of antibody, 5µl of $Na^{131}I$ (37MBq), 10µl (10µg) of ChT and then 20µl (20µg) of SMB (fig. 1, 2).

II.3 Gel Chromatography: The reaction mixture was applied to the top of a column of sephadex G25, PD10 and then eluted with saline 0.9% with 30cm^3/h flow. The ^{131}I-CD20 antibody was separated from free ^{131}I. Sequential fractions of the eluate are collected by means of 1ml fraction and the radioactivity is measured in each fraction. The amount of product is expressed as ratio (as a percentage) of its radioactivity to the total radioactivity placed on the column (fig. 3, 5).

II.4 Fast Protein Liquid Chromatography (FPLC): Quality was controlled by FPLC using 6850A system, Perkin Elmer, Agilentb Zorbax GF-250 column, 0.1mol/L PBS buffer, pH7, injected 4µl sample (Rituximab, ^{131}I - Rituximab and ^{131}I), 0.6mL/min flow, 280nm ultraviolet detector and radioactivity monitor (fig. 9).

II.5 Instant thin Layer Chromatography (ITLC): A small aliquot (5µl) of the samples are spotted on an ITLC strip (ITLC strip are made of glass fiber impregnated with silicagel (SG) size 1 x 10cm). Chromatography is carried out by dipping the spotted strip into a solvent of MeOH and Saline at a ratio of 85:15 contained in a chamber. Chromatography time is 5 minutes. Unbound ^{131}I-iodide is move to the solvent line (R_f = 0.9-1) and the complex ^{131}I-antibodies are at the origin (R_f = 0) (fig. 4, 6, 7, 8).

II.6 Stability Studies: The stabilities of the labeled antibody were carried out at the storage 4^0C and -20^0C with and without acid ascorbic (AA). After the interval time of 1, 2, 3, 4, 6, 8, 10, 12, 13, 15 days, the products were analysis by ITLC method. The labeled antibody was also incubation in human serum at 37^0C, after 0, 4, 6, 24, 48, 96, 120, 144, 168 hours, it has been performed using TCA method to determination the free of ^{131}I in the product. The final product could remain stability until 15 days storage and 168h stable in human serum. RCP determination both was more than 98% (fig. 10, 11).

II.7 Sterility and Bacterial Endotoxin Testing: According to the USP XXII, sterility tests are performed by incubating the labeled antibody in fluid thioglicollate at 30 to 35^{0}C for 7-14 days. Another test uses soybean-casein digest medium for incubation at 20-25^{0}C for 7-14 days. Bacterial endotoxin was tested using limulus amebocytes lysate (LAL) kit. The test is base on the formation of an opaque gel by pyrogen.

II.8 Biodistribution and Blood Clearance: Load syringe with 100µl of ^{131}I-Rituximab (100µCi) and inject into tail vein of mice, group 5 mice, at the end of post injection period of 1, 4, 16, 24, 72, 96, 120, 168 hours, dissect each group and collect tissue samples blood, heard, liver, kidneys, intestinal, lung, bladder, spleen, thyroid and tail. Weigh and count the radioactivity and calculate the percent injected dose per gram (ID%/g) (table 1). Inject into ear vein 1ml (2mCi of ^{131}I-Rituximab), collect the blood at the end of post injection period of 20, 28, 48,72, 120, 144 hours, count the total activity, calculate the percent blood clearance with time (fig. 12, 13).

III. Results and Discussion

III.1 Optimization: We present the results of a comparative labeling study starting with 2 different specific antibodies anti CD20 of Rituximab and scfv antibody, with one of the labeling being performed in the framework of a clinical study. Preparative work had been done to optimize the chemical labeling conditions using chloramine T. The radio labeling yields were determined at the concentration of chloramines T (ChT) range 0.1-1000µg (at constant pH 7.5 and 1mCi ^{131}I/mg antibody). The optimized concentration of ChT in the reaction was 10µg. The influence of incubation time 1, 3, 10, 20 minutes on the radiochemical yields of the anti-CD20 antibody labeled with iodine-131 was observed. Time optimization was 3 minutes (fig. 1). In order to determine the optimized pH, phosphate buffer 0.5M, pH range 5 - 9.5 was used for the reaction of 1mCi of ^{131}I, 100µg of antibody and 10µg of ChT. The optimized pH for the best labeling yield was around 7.5-8.5 (fig. 2).

III.2 Labeling: Rituximab and scfv antibody were labeled with ^{131}I at the optimum ChT and pH condition. The different specific activity 10mCi per 1.5mg of antibody Rituximab and 1mCi per 0.05mg of svfv antibody were carried out. The radio labeling yields in both were 95-97%. The residual free iodine-131 is eliminated by gel filtration through a Sephadex G25 column. For both labeling, radiochemical yields as determined by ITLC and gel chromatography before purification (fig. 3, 4 and fig. 5, 6).

In the reaction mixtures, iodine binds firmly and irreversibly to aromatic compounds, beside that it is also binding to amino and sulfhydryl groups. The chloramines T is a mild oxidizing agent and the labeling procedure could not alter the immunoreactivity of the antibody. The iodination of scfv-antibody could give very high yields its mean iodine is easy incorporation into the antibody.

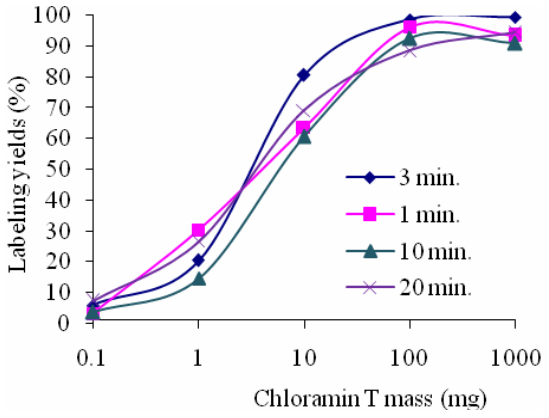

Fig. 1. Influence of incubation time, ChT mass on the radiolchemical yields

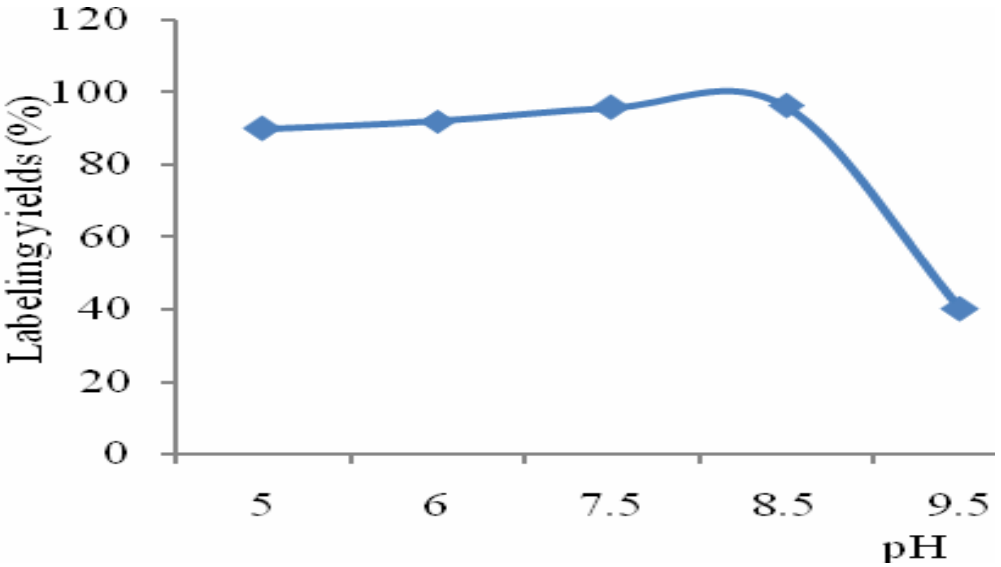

Fig. 2. pH optimization of the labeling ^{131}I with Rituximab

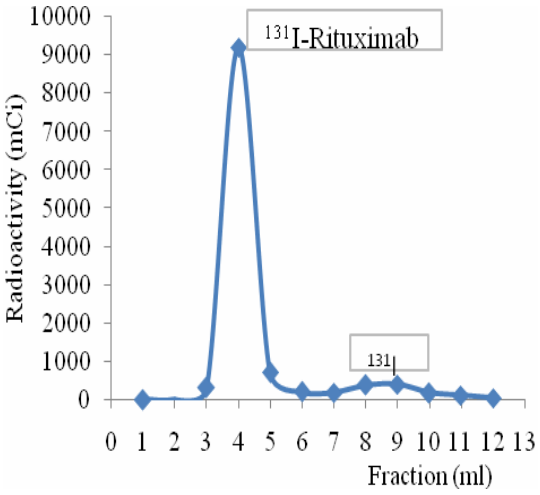

Fig. 3. Purification of ^{131}I-Rituximab (using Sephadex G-25 column)

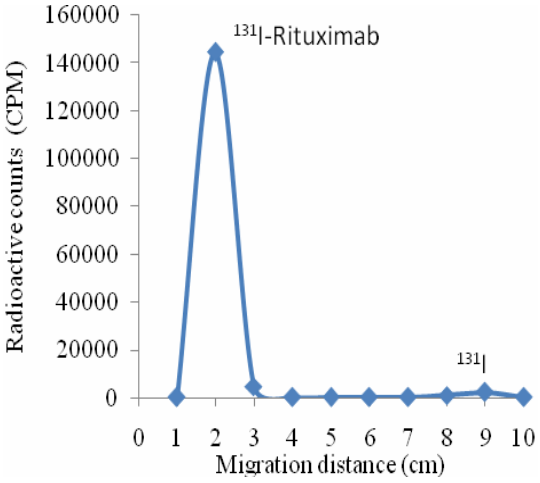

Fig. 4. Labeling yields ^{131}I-Rituximab (ITLC)

The reducing agent of SMB was added to stop the oxidation reaction:

$$Na_2S_2O_5 + NaOH + I_2 \longrightarrow Na_2SO_4 + H_2O + NaI$$

Labelling of whole antibody or fraction antibody is similar procedure. Fig 5 and 6 show that the purification of the reaction mixture was needed more eluents.

Quality control: The radiochemical purity of ^{131}I for labelling was more than 99,9% (fig. 7). The labelled antibodies after purification by gel chromatography as assessed by ITLC was more than 99.9% (fig. 8).

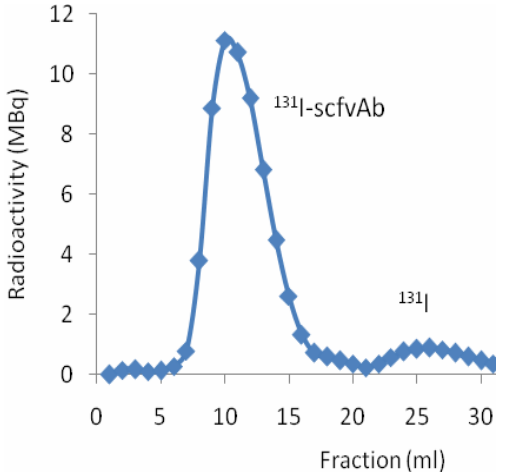

Fig. 5. Purification of ^{131}I-scfvAb (ScFv) using Sephadex G25

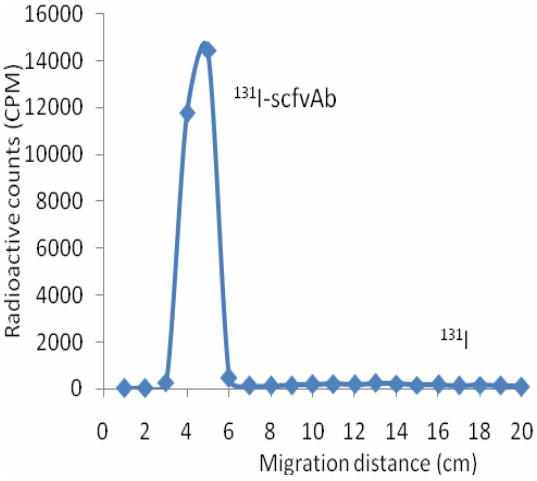

Fig. 6. Radiochemical purity of ^{131}I-scfvAb

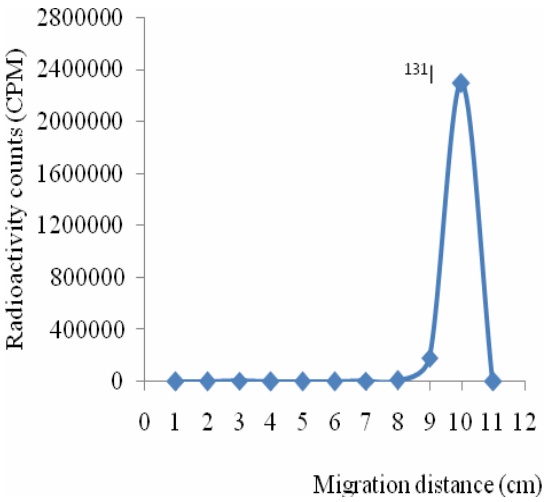

Fig. 7. Radiochemical purity of ^{131}I

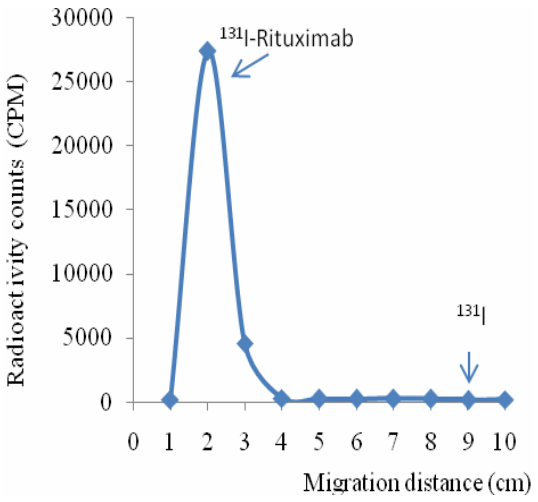

Fig. 8. Radiochemical purity of ^{131}I-Rituximab

The results of RCP of the products were confirmed by FPLC, which found a RCP of more than 99% and the radio labeled aggregates as determined by FPLC was not much different from the unlabeled antibody (fig. 9a, 9b, 9c). The retention time of 12.5 min for aggregates, 14.0 min for ^{131}I-Rituximab and 22.2 min for free ^{131}I. Radiochemical purity was more than 99%. ^{131}I-Rituximab prepared in this way, resulted in more than 99% radiochemical purity with some aggregate formation or degradation products. It is the convention method for the preparation of iodination antibodies for medical use. No significant increase in aggregation could be observed.

^{131}I-Rituximab of high radiochemical purity was obtained after Sephadex G-25 PD10 gel purification and stability studies were carried out. The product could be store at -20^{0}C or +4^{0}C until 15 days (fig. 10). The labeled antibody was stable in human serum around 7 days (fig. 11). Other degradation products of the antibody were not observed even after storage.

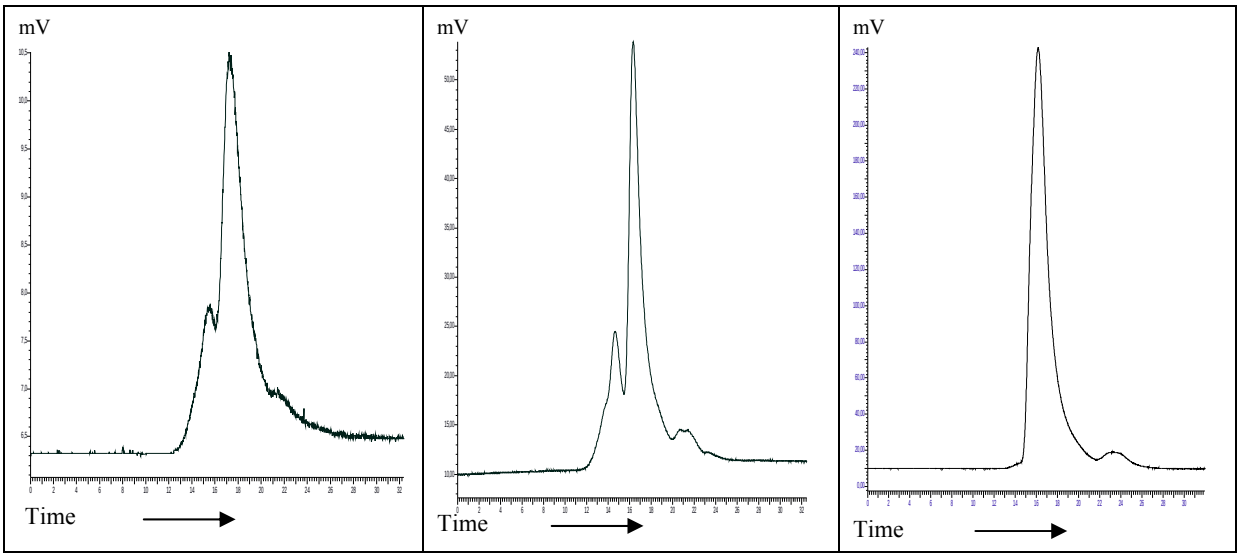

Fig. 9a. ^{131}I-Rituximab (FPLC UV detector, 280nm)

Fig. 9b. ^{131}I-Rituximab (FPLC radio detector)

Fig. 9c. Rituximab (FPLC UV detector, 280nm)

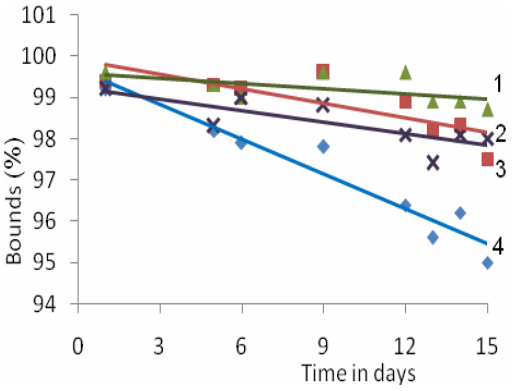

Fig. 10. Stability of ^{131}I-Rituximab with time
1: Store at -20^{0}C with acid ascorbic
2: Store at +4^{0}C with acid ascorbic
3: Store at -20^{0}C without acid ascorbic
4: Store at +4^{0}C without acid ascorbic

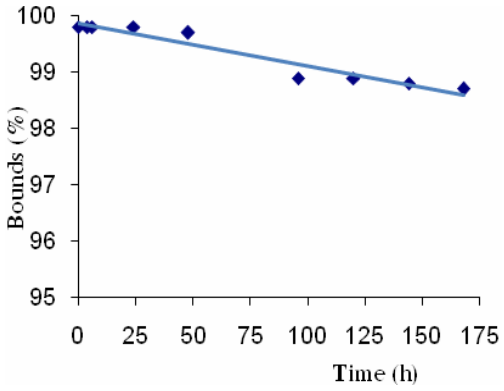

Fig. 11. Stability of ^{131}I-Rituximab in human serum at 37^{0}C

The labeled antibody have passed test for sterility and bacterial endotoxin.

Biodistribution and clearance studies: Table 1 shows the results of biodistribution in normal mice. In this biodistribution study, total blood, liver and kidneys uptake was high comparable with the antibody distribution, about 30% ID%/g in blood, 10% in liver and kidneys. Blood clearance was fast, and the compound was excreted by both renal and intestine routes, thyroid uptake was not high, showing the in vivo stability of the radioiodinated antibody.

Tab 1. Biodistribution of ^{131}I-Rituximab on mice (% dose/gram, n = 5)

Organ	**1 h**	**4 h**	**16 h**	**48 h**	**72 h**	**120 h**	**168 h**
Liver	9.6 ± 10.82	8.75 ± 10.79	7.77 ±3.54	5.52 ± 0.78	4.09 ± 10.21	2.67 ± 12.29	0.79 ± 10.79

spleen	0.63 ± 0.52	0.57 ± 1.04	0.46 ±0.10	0.36 ± 0.08	0.26 ± 0.40	0.17 ± 0.85	0.05 ± 0.67
Kidneys	9.43 ± 1.78	8.96 ± 1.52	7.33 ±2.81	5.43 ± 0.80	3.98 ± 6.35	2.51 ± 2.46	0.73 ± 2.69
Lung	3.29 ± 2.18	2.94 ± 7.18	2.51 ±0.21	1.87 ± 0.89	1.37 ± 0.83	0.98 ± 1.84	0.35 ± 5.25
heard	4.32 ± 0.09	3.40 ± 0.41	3.33 ± 0.27	2.57 ± 0.04	1.89 ± 0.33	1.18 ± 2.46	0.35 ± 1.48
Blood	26.87 ± 4.82	24.36 ± 7.44	20.74 ± 5.46	15.50 ± 4.37	11.53 ± 7.45	7.34 ± 9.24	2.43 ± 9.76
Intestinal	5.73 ± 9.50	5.16 ± 3.02	4.43 ± 4.38	3.32 ± 0.86	2.41 ± 7.95	1.56 ± 3.92	0.43 ± 3.71
Stomach	4.54 ± 5.17	4.17 ± 6.32	3.48 ± 5.32	2.68 ± 4.66	1.97 ± 6.66	1.22 ± 0.26	0.37 ± 2.17
Thyroid	0.14 ± 0.1	0.26 ± 0.06	0.12 ± 0.06	0.08 ± 0.05	0.05 ± 0.06	0.04 ± 0.19	0.016 ± 0.19

The labeled antibody was complete clearance after 7 days injection. ^{131}I-Rituximab was also blood clearance after 120 hours when we injected into vein ear in 2 rabbits (fig.12).

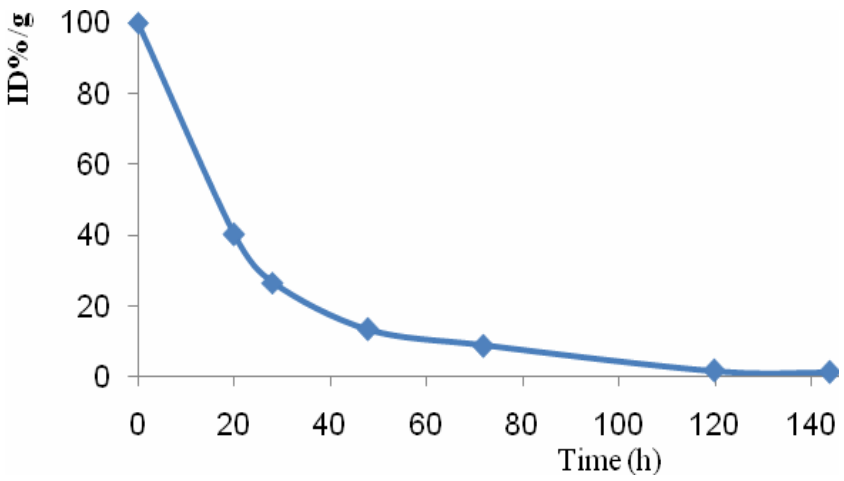

Fig. 12. Blood clearance of ^{131}I-Rituximab (perform on rabbits)

^{131}I-Rituximab was approved for biodistribution in patients in refractory NHL and positive CD20. The radioimmunoscintigraphy was taken using ECAM SPECT after dose 5mCi. Dosimetry for ^{131}I-Rituximab regimen has shown that tumor targeting is specific and significantly higher than that for the total body (fig. 13).

Fig. 13. Radioimmunoscintigraphy for the ^{131}I-Rituximab (5mCi)

IV. Conclusions

The labeled antibody ^{131}I-Rituximab specific to the malignance lymphoma B have been studied and prepared. In our laboratory, we could prepare the radioimmunoconjugate with the high radiolabel led yields, radiochemical purity and in vivo and in vitro stability, ^{131}I-scfv antibody have prepared with the high purity., nevertheless. It will be carried out the preclinical evaluations. These are the radiopharmaceuticals used in cancer therapy with RIT. This study have the goal of research and develop and clinical testing. It has the potential to be a new method of treatment for RIT domestically.

Reference

[1]. Mark S. Karminski. Kenneth R. Zasadny. Isaac R. Francis. Adam W. Milik et al. (1993). Radioimmunotherapy of B-Cell Lymphoma with [^{131}] Anti B1 (anti-CD20) Antibody. The New England Journal of Medicine Volume 329:459-465

[2]. Fisher. R. I. (2003). Overview of non-Hodgkin's lymphoma: biology. staging. and treatment. *Seminars in oncology.* 30:3-9

[3]. Maeda. T.. Yamada. Y. Tawara. M.. Yamasaki. R.. Yakata. Y.. *et al*. (2001). Successful treatment with a chimerical anti-CD20 monoclonal antibody (IDEC-C2B8. rituximab) for a patient with relapsed mantle cell lymphoma who developed a human anti-chimerical antibody. *International journal of hematology.* 74:70-75

[4]. Anti-Human CD Clustered (CD) Antibodies. (2003). Table of Human CD Antigens with antibody Links from Research Diagnostics Inc.

[5]. Pescovitz. M. D. (2006). Rituximab. an anti-CD20 monoclonal antibody: history and mechanism of action. *Am J Transplant.* 6:859-866

INVESTIGATION INTO THE CONCENTRATION OF RADIONUCLIDES IN MAJOR IMPORTED AND EXPORTED FOODS & FOODSTUFFS TO DERIVE DATA BASE ON THE RADIOACTIVITY IN VIETNAMESE FOOD & FOODSTUFFS

Nguyen Quang Long, Tran Tuyet Mai, Ngo Tien Phan, Nguyen Thu Ha
Dinh Thi Bich Lieu, Vuong Thu Bac, Doan Thuy Hau and Duong Van Thang

Institute for Nuclear Science and Technology, VAEC
179 Hoang Quoc Viet, Nghia Do, Ha Noi

Abstract: Investigation into radionuclides concentration in foods and foodstuffs and establishment of database on the radioactivity of the goods is important for the internal dose assessment for every country. Therefore, in the 2007-2008 the Ministry of Science and Technology Vietnam sponsored a Project encoded 11/09/NLNT with the aims of to identify and quantify the radioactivity of radionuclides in imported to and exported from Vietnam products. About 130 foods and foodstuffs samples were collected and analyzed for the radioactivity in it. The radionuclides analyzed in this work are natural occurring isotopes such as Bi-214, Ac-228 and that originated from the U and Th series and K-40. The artificial gamma emitter Cs-137 was subjected to the quantification also. Additionally, total alpha, beta and gamma in the samples were analyzed as well. Data obtained showed that the radioactivity of K-40, Ac-228, Bi-214, total beta, total alpha, and total gamma activity in Vietnamese foods and foodstuffs ranging from 10.4 Bq/kg to 856.6 Bq/kg with an average of 255.3 Bq/kg, from 0.3 Bq/kg to 9.0 Bq/kg (average 1.3 Bq/kg), from 0.3 Bq/kg to 3.1 Bq/kg (average 1.1 Bq/kg), from 2.1 Bq/kg to 519.3 Bq/kg (average 110.9 Bq/kg), and from less than the limit of detection (0.02 Bq/kg) to 306.7 Bq/kg (average 31.9 Bq/kg), respectively. The radioactivity range of both NORM and artificial radioisotopes in Vietnamese food and foodstuffs was comparable and low with those recommended by the ICRP. A preliminary estimate for the effective internal dose from food consumption among Vietnamese adults has been presented also.

1. Introduction

The investigation into radionuclides concentration in foods and foodstuffs and establishment of database on the radioactivity of the goods is important for the internal dose assessment for every country. Therefore, in 2007-2008 the Ministry of Science and Technology, Vietnam sponsored a Project encoded 11/09/NLNT with the aims of to identify and quantify the radioactivity of radionuclides in imported to and exported from Vietnam products.

The aim of this study is to survey the level of radioactivity of natural occurring radioisotopes (NORM) and K-40 and Cs-137 in major Vietnamese food and foodstuffs.

2. Materials and Methods

2.1 Sample Collection and Preparation

Food samples collected from the local farmers were carefully washed to remove external contamination from soil and atmospheric depositions. Those samples in tuber form were cut into small pieces with a knife and were allowed to dry to a constant

weight at room temperature. The cereal samples were also kept at room temperature and other samples prone to biodegradation were oven dried at a temperature of 100 ^{0}C until a constant weight was achieved. The samples were carefully enclosed in polyethylene bags ready for grinding to powdered form. Thereafter, each of the samples was weighted (300 g and 1000 g ± 10mg) then transferred into a polyethylene beaker. The sample was ready for gamma analysis.

2.2 Analysis

Gamma Spectrometry

The gamma-spectrometry measurements for the samples were carried out at the Radiation Protection and Environment Center of INST using a high-purity germanium detector (HPGe). Counting time was long enough to get a satisfied uncertainty. The time is usually 24 hours. Obtained spectra were analyzed using specific software ORTEC MAESTRO (GAMMAVISION 5.1). Bi-214 was quantified using the gamma line at 609 keV, Ac-228: at 910 keV and K-40: at 1460 keV. Standard samples from IAEA were used for the quanlity assurance and Quality control (QA/QC) of the measurement. Additionally, the QA/QC of the laboratory is guaranteed by its regular participation in national and international inter comparison exercises.

Total alpha and beta activity measurements for the samples were carried out using a counting system of ultra low background (*ca*. 2 counts per 10000 seconds for alpha and 2 counts per minutes for beta).

3. Results and Discussion

3. 1 Statistics of The Analytical Data

Results of the measurement for 130 foods and foodstuff samples collected were treated statistically to derive as mathematic average, geologic average, standard error, standard deviation, range, max and min values. The obtained data for K-40, Ac- 228, Bi-214, total alpha, total beta and total gamma were shown in Table 1.

Tab 1. The statistical data on the activity measurement for the foods and foodstuffs samples

	K-40 (Bq/kg)	**Ac-228** (Bq/kg)	**Bi -214** (Bq/kg)	**Total beta** (Bq/kg)	**Total alpha** (Bq/kg)	**Total gamma** (Bq/kg)
Mathematic Average	255.3	1.3	1.1	110.9	31.9	369.6
Standard Error	25.6	0.2	0.1	14.1	6.9	37.3
Geologic Avevage	198.6	0.8	0.8	60.8	14.9	281.0
Standard Deviation	226.0	1.6	0.7	124.4	60.8	329.8
Range	846.3	8.7	2.8	517.2	384.9	2003.4
Min values	10.4	0.3	0.3	2.1	ND*	25.7
Max values	856.6	9.0	3.1	519.3	306.7	2029.1

** less than detection limit*

The data were in good agreement with the range of natural occurring radioisotopes concentration in food as reported early with a range of 40-600 Bq/kg. For example, the activity of potassium in liquid milk usually found to be 50 Bq/kg but that for powder milk, potatoes and beef was, respectively 420 Bq/kg, 165 Bq/kg and 125 Bq/kg. Ramachandran and Mishra reported that the K-40 level in different kind of food was ranging from 45.9 to 649.0 Bq/kg while that of Ra-226 was 0.01-1.16 Bq/kg and Th-228 was 0.02-1.26 Bq/kg. [1]

3.2 A Correlation Between Radioactivity and The Total Alpha, Beta and Gamma of The Samples

The **gamma vision** software offered by the gamma spectrometer supplier allows one to investigate the correlation between the radioactivity of individual isotope and the values of the total gamma, total alpha and total beta.

In practice the value of total gamma could be served as a good indicator about the radioactivity in the samples. Based on the radioactivity derived for K-40, Ac-228, Bi-214 and the values of the total gamma, alpha and beta one can ensure that the results obtained in this research were believeable as there a good correlation between the values of the analysis was revealed. These results are shown in Table 2.

Tab 2. The correlation between analytical results for a sample

	K - 40	**Ac - 228**	**Bi - 214**	**Total beta** (Bq/kg)	**Total alpha** (Bq/kg)	**Total gamma** (Bq/kg)
K - 40	1.000					
Ac - 228	0.312	1.000				
Bi - 214	0.494	0.720	1.000			
Total beta (Bq/kg)	0.163	0.431	0.292	1.000		
Total alpha (Bq/kg)	0.197	0.246	0.133	0.494	1.000	
Total gamma Bq/kg	0.678	0.362	0.631	0.343	0.164	1.000

As can see from Table 2 a close correlation between total gamma and activity of K-40 (R^2=0.678, Table 2). This is because K-40 emits a gamma line of 1460 keV that caused high total gamma in samples when the concentration of K in samples is high. Similarly it was revealed a good correlation between the total gamma and activity of Bi-214 (R^2=0.631, Table 2). It seems that the main contribution of the total gamma in the sample is from K-40 and Bi-214. It is interestingly to note that the activity of Bi-214 and Ac-228 is well correlated between each other (R^2=0.720, Table 2). It is understood because Bi-214 and Ac-228 is natural occurring isotopes that originated from the U and Th series meaning that comparable activity of U and Th series in the samples. This argument is also known in early publications [2], [3], [4], [5].

3.3 Radioactivity In Foods and Foodstuff and Evaluation of The Intake

The average of radioactivity in sub-group of foods and foodstuffs was given in Table 3

Tab 3. Average radioactivity of major gamma emitters in food sub-group

Food	**Cs-137** (Bq/kg)	**K-40** (Bq/kg)	**Pb-214** (Bq/kg)	**Bi-214** (Bq/kg)	**Ac-228** (Bq/kg)	**Pb-212** (Bq/kg)
Rice	0.09	44.00	0.65	0.65	0.44	0.44
Vegetable	0.30	636.46	1.35	1.35	1.49	1.49
Beans, tubers and fruits	0.17	387.42	1.12	1.12	0.81	0.81
Milk	0.23	175.48	0.61	0.61	0.60	0.60
Meat	0.15	86.95	0.88	0.88	0.63	0.63
Fish	0.22	297.41	1.51	1.51	2.36	2.36

Knowing the average activity in different food one can estimate the daily/ annual intake of radioactivity by a human body based on the data of daily food consumption with a common menu. The results of the estimation is shown in Tabe 3.

Tab 3. Annual average radioactivity in took by a human body through the food chain

Food	**Cs-137** Bq/year	**K-40** Bq/year	**Pb-214** Bq/year	**Bi-214** Bq/year	**Ac-228** Bq/year	**Pb-212** Bq/year
Rice	12.19	9038.44	127.24	127.24	118.36	118.36
Vegetable	25.51	52374.57	141.12	141.12	148.10	148.10
Bean, tuber, fruit	9.88	31591.90	98.45	98.45	89.45	89.45
Milk	0.38	333.71	1.36	1.36	1.41	1.41
Meat	2.21	1304.22	13.24	13.24	9.49	9.49
Fish	1.94	2646.95	13.40	13.40	21.03	21.03

It is clear a fact that the internal dose (mSv) for a human body caused by a (i) nuclide present in (j) food is dependent upon the concentration of the (i) nuclide in the (j) food and the amount (m) of (j) food consumed daily or annually by the individual. And the dose is dependent on the effective transfer coefficient (K) implying the effectiveness of the individual in digestion of the food. Logistically, the activity of (i) radioisotope retained in human body through the food chain could be estimated by a formula:

$$A_{j,i} = C_{m,i} \times M_m \times F_{mm} \times F_{dm} \times T_m$$

Where:

$A_{j,i}$: activity of “i” isotope in took in a human body through consumption of food “j”, Bq

$C_{j,i}$: activity of “i” siotope found in “j” food at the moment of sampling, Bq/kg

Tj : the time interval since the 'J' food has been in took, days

Mm : the daily intake of "j" food, kg/day

Fmm: a dilution factor of the "j" food

Fdm : a lost factor of radioactivity during cooking "j" food

For long live isotopes, like K-40 one can omit the correction for the physical decay of radionuclides within the time period from sampling to measurement.

So, the internal dose (H) caused by the intake could be estimated as

$$H = \sum_j \sum_i K_i . A_{j,i} \text{ [6]}$$

Where H is effective internal dose caused by the intake, mSv

K_i is a converting factor for the intake of radioisotope "i", mSv/Bq

The factor K_i is used to convert activity (Bq) into dose unit (mSv) and it could be referred to the UNSCEAR 2000 recommendation. Table 4 shows the recommended K_i values.

Tab 4. Converting factor K_i of some typical isotopes usually found in food and foodstuffs

K_i	**K-Cs-137**	**K-K40**	**K-Pb-214**	**K-Bi-214**	**K-Ac-228**	**K-Pb-212**
Unit	mSv/Bq.10^{-6}	mSv/Bq.10^{-6}	mSv/Bq.10^{-6}	mSv/Bq.10^{-6}	mSv/Bq.10^{-6}	mSv/Bq.10^{-6}
	13.00	6.20	0.14	0.11	0.43	6.00

Based on the data of Table 3 and Table 4 the effective dose caused from consumption food among Vietnamese people could be estimated as high as values in table 5.

Tab 5. Estimate of annual internal dose caused by consumption of food among Vietnamese adult

H from	**Cs-137** (μSv/year)	**K-40** (μSv/year)	**Pb-214** (μSv/year)	**Bi-214** (μSv/year)	**Ac-228** (μSv/year)	**Pb-212** (μv/year)
Rice	0.1585	56.0383	0.0178	0.0140	0.0509	0.7102
Vegetable	0.3316	324.7223	0.0198	0.0155	0.0637	0.8886
Bean, tuber, fruit	0.1285	195.8698	0.0138	0.0108	0.0385	0.5367
Milk	0.0050	2.0690	0.0002	0.0001	0.0006	0.0085
H from	Cs-137 (μSv/ year)	K-40 (μSv/year)	Pb-214 (μSv/year)	Bi-214 (μSv/year)	Ac-228 (μSv/year)	Pb-212 (μv/year)
Meat	0.0287	8.0862	0.0019	0.0015	0.0041	0.0570
Fish	0.0252	16.4111	0.0019	0.0015	0.0090	0.1262
Sum	0.6774	603.1967	0.0553	0.0434	0.1668	2.3271

The total effective internal dose caused by all the isotopes in a Vietnamese adult through food consumption is the sum of the dose comes from each isotope, and its is:

H = 0.6774+ 603.1967+0.0553+0.0434+0.1668+2.3271 = 606.4667 μSv/year or 0.607 mSv/year.

It revealed that the major contribution in the total internal dose through the food consumption is from K-14. The value H estimated above is still very rough as its was not yet corrected for the food dilution, the lost of isotopes during its cooking as well as the ratio of the isotope retained in human body but not excretion. All the factors mentioned are less than unique, so one could expect that the effective internal dose caused by food consumption among Vietnamese adults would be <0.607 mSv/year. UNSCEAR 2000 took in account all the corrected factors and recommended that the value of effective internal dose from food consumtion among adults should be around 0.29 mSv/year. [6]

4. Conclusion

The analytical data derived from the research possesses good accuracy because it was done with a certain QA/QC procedure. The results showed that the activity of all the interested radioisotopes in Vietnamese food and foodstuffs is low and safe in term of radiological safety. An estimate of the effective internal dose caused by the food consumption among Vietnamese adults showed in the range recommended by UNSCEAR 2000.

References

[1]. Natural and Induced Radioactivity in Food, IAEA-TECDOC-1287.

[2]. Stahlhopen, Assessment of Radioactivityin man, Vol 2, pp 505-519, IAEA, Vienna (1964).

[3]. Turner, Heathphisics. 1, 262 (1958).

[4]. H.G. Tetrow, New York Univ. Annual Report, NYO-3086-1, (1965)

[5]. UNSCEAR, 1966, pp 24-26.

[6]. UNSCEAR, 2000.

NUCLEAR TECHNIQUES APPLIED FOR OPTIMIZING IRRIGATION IN VEGETABLE CULTIVATION

Dang Duc Nhan[1], Nghiem Hoang Anh[2], Bui Dac Dung[1], Dinh Thi Bich Lieu[1], Dang Anh Minh[1], Vo Tuong Hanh[1], Nguyen Thi Thai[1], and Nguyen Thi Hong Thinh[1]

1) Institute for Nuclear Sciences and Technologies, VAEC
2) Institute for Vegetables and Fruits Researches, Vietnam Academy of Agricultural Sciences; Gia Lam, Ha Noi

Abstract: Optimizing irrigation in vegetable cultivation has been carried out based on the water use efficiency (WUE) parameter. The experiment has been conducted with Chinese cabbage planted on alluvial soil using traditional furrow, and drip irrigation technique with scheduling and limitation of the amount of irrigated water estimated based on the water balance to compare to each other. Soil moisture and Evapotranspiration (*ET*) of the crop were controlled, respectively, using a neutron probe (NP, model PB 205, FielTech, Japan) and a meteorological station installed in the field. Calibration for the NP has been performed directly in the field based on the measurement of the count ratio (R_n) and the soil moisture determined gravimetrically. Productivity of the crop in each experiment was determined as the total biological (Y_{bio}) and the edible yield (Y_E) harvested and the WUE was estimated as a ratio of the productivity and the amount of irrigated water in unit of kg m^{-3}.

Experimental results showed that the drip irrigation could save up to 10-19% of water as compared to the furrow irrigation depending on the cultivation seasons. Thus, WUE was improved up to 1.4 times, as estimated either by Y_E or by Y_{bio} productivities.

The drip irrigation with scheduling technique could be transferred to semiarid areas in Vietnam for not only vegetable but also fruit, e.g. grape in the southern central part of the country.

Key words: drip irrigation, water use efficiency, neutron probe, water balance

Introduction

Water is one of the important components for crops to produce biomass and yield. In irrigation, a quantity expressed by the ratio of crop productivity to the amount of irrigated water is called water use efficiency, WUE [*Keller, A. and Keller, J., 1995; Robinson, B., et al., 2000*]. The unit of the WUE is *kg* or m^3 per m^3 or *mm*. In the tropical areas WUE is dependent upon the rain and irrigated water, so to gain a better benefit it is necessary to optimize the irrigation. Irrigation optimization, in practical term, is understood that with a reasonable investment in irrigation practice to increase the useful water irrigated to crops could rise up an achievable high yield, i.e. the WUE is maximal. The optimization could be achieved by the improvement of the irrigation practice, e.g. changing from the furrow to drip or sprinkle technology and combination with water scheduling and limitation of the amount of irrigated water to those just satisfied the demand of the crops. The irrigated water in this case would be estimated based on the water balance [*www.ext.colostate.edu/pubs/ crops/04707.html*].

$$\Delta S = P + I - ET - R - D \quad (1)$$

Where ΔS is the change of water storage in a certain soil depth; P is the precipitation (mm); I is the amount of irrigated water; ET is the evapotranspiration of a

vegetation; R is the amount of run off water; and D is the amount of water drained into deeper soil layer by the capillary forces.

If irrigation could be controlled by such a way that run off (R) and drainage (D) could be neglected then the equation (1) would be converted to:

$$\Delta S = P + I - ET \quad (2)$$

In the dry season, the precipitation in most cases is very small as compared to the irrigation, so it could also be neglected, and

$$\Delta S = I - ET \quad (3)$$

or

$$I = \Delta S + ET \quad (4)$$

Thus, in the controlled case, the amount of irrigated water is equal to the sum of soil moisture expressed as water storage in a certain soil depth and the evapotranspiration of crops. Agronomists proposed that when ΔS in the rooting zone is reduced down to the Refill Point (RP) that is equal to the half of the Available Soil Water Content (ASWC) one has to irrigate to crops. This means that:

$$\Delta S = RP = 0.5\ ASWC \quad (5)$$

And ASWC of a certain soil could be estimated as:

$$ASWC = FC - WP \quad (6)$$

Where FC is the filed capacity that is defined as the water depth in a soil that equal to the gravimetrical force and all the extra water has to be drained, and WP is the wilting point that is defined as the lowest water depth in soil below which crops would be permanently wilted. The FC and WP values could be found in [*USDA, 1960*].

Combined equations (4), (5) and (6) one can get:

$$I = 0.5ASWC + ET = 0.5(FC-WP) + ET \quad (7)$$

So, to achieve the highest value of WUE one has to estimate the amount of irrigated water just to be equal to the sum of the refill point and to meet the demand of the crops for its evapotranspiration (Eq. 7). The scheduling in irrigation is understood as to determine the time when crop needs to water. It is clear from the Eq. 5 that the time when crop needs to be watered is the moment when the soil moisture was down to the half of the ASWC.

A procedure for the irrigation optimization thus could be developed as follows. The first step is to determine the soil type by its texture in order to know the FC and WP. The second step is to estimate the ASWC (Eq. 6) and then RP (Eq.5). The third step is to determine the ET of the crop in order to estimate the necessary amount of I (Eq.7).

The value of ET for a certain crop could be estimated as:

$$ET = K_c * ET_0 \quad (8)$$

Where K_c is crop coefficient and it is dependent on the stage of crop development. ET_0 is the potential evapotranspiration. The ET_0 and K_c values could be derived from

the meteorological data for the region based on the Penman-Monteith [*Allen, 2000, MAFF, 2001*], respectively.

The aim of this study is to experimentally develop a practical procedure for optimizing the irrigation to cabbage planted on alluvial soil. Cabbage was chosen for the experiment because it is a broad leave vegetable needed more water than any other. The study is expected to get an appropriate guide for the local farmers in their vegetable cultivation.

I. Materials and Method

The experiment was conducted in the Nam Hong commune, Dong Anh district, Hanoi in the 2006 and 2007. Cabbage of *X species* from the US Petoseed Company was chosen for the study. The root zone of the vegetable was proposed to be 450 mm [*Simonne et al., 2007*]. Soil for the experiment was identified as silt-clay-loam by the USDA classification [*Ammis, 1996*]. For that soil the FC and WP is 22% and 5%, respectively. The experiment was conducted in two plots, to one of which traditional furrow irrigation but for another drip irrigation was applied.

The soil moisture in the two plots was controlled by using a neutron probe (NP) of PB-205 model (FielTech, Japan) that operates on the measurement of back scattering neutrons emitted from ^{252}Cf source [*TCS No.16, 2003*]. Calibration for the probe was conducted on the field with 27 aluminum source guide tubes (ϕ43 and L1.300) inserted and distributed evenly within the experimental field.

The potential ET_0 in the region was derived from a meteorological station (Davis Instruments, California, USA) installed in the field. The K_c values (Eq. 8) for cabbage are 0.7, 1.05 and 0.95, respectively, for the initial stage (0 day till 10% of the land was covered by its canopy), head formation (from 10% to 80% canopy coverage) and harvesting stage.

The type and rate of fertilizer and pesticides to control pest insect was followed by the local farmer practice. 10 tons per hectare of chicken muck was initially put into the soil before cabbage planting then 360 kg/ha of urea, 510 kg/ha super phosphate and 270 kg/ha of potassium sulphate was split into 4 times for fertilizing the vegetable. The 1st time was the basal fertilizing (20%), the 2nd time (25%) was at the time of rooting, the 3rd time (33%) was leave spreading and the last time (22%) was the head formation. Pesticides, most of the pyrethroid group that quickly decomposed in the environment were applied to the vegetable to control flea, head borer, green insects, and fungi. The impact of the irrigation practice on the pest insect damage to the vegetable was evaluated following the guideline of the Asian Vegetable Research and Development Center [*AVRDC, 2000*].

The water scheduling in the experiment was conducted based on the value of soil moisture measured by the NP. The time when it needs to water to the crop was a moment when the soil moisture in the rooting zone (45 cm from the surface) was down to the refill point defined by the equation (5), or when ΔS = 0.5*ASWC= 0.5*(FC-WP) = 0.5*(22-5) = 8.5% = 450*0.085 = 38,25 mm. The amount of water needed to water to the crop was estimated by the Eq. 7. For different stages of vegetable development and meteorological conditions of each watering event the amount of irrigated water was:

$$I\ (mm) = 38{,}25 + K_c * ET_0 \quad (9)$$

The irrigation (I, mm) could be converted into the unit of cubic meter by simply multiply I (mm) with the area of the plots.

The principle of the scheduling (eq. 5) and water limitation (eq.7) is as follows.

When moisture probe shows the soil moisture down to 8.0-8.5%, the valve from a water tank located at the elevation of 2.5 m above the ground was open. The soil moisture at that time corresponded to the half of the available soil water content (eq.5). When the water amount supplied to the field was reached the value estimated by the eq.7 the valve was close. The irrigation was commonly dependent upon the meteorological conditions (ET_0) and the time period of the vegetable development (K_c) (eq.7).

Productivity of the vegetable was estimated by both biological and edible yield (Y_{bio} and Y_E). The former yield represented as total weight of the crop but the later one is the weight of cabbage head only. The WUE in each irrigation practice was calculated based on the total amount of irrigated water for the whole cultivation season and the amount of irrigated water of the irrigation practice.

The data presented in the table were obtained for the 2 autumn-winter and 2 winter-spring seasons of the 2006-2007. The data were statistically processed with the Fisher test to identify whether the data of two different groups were significant differentiated.

II. Results and Discussion

Fig 1 depicted the calibration curve of the neutron probe (NP) model PB-205 (FieldTech, Japan).

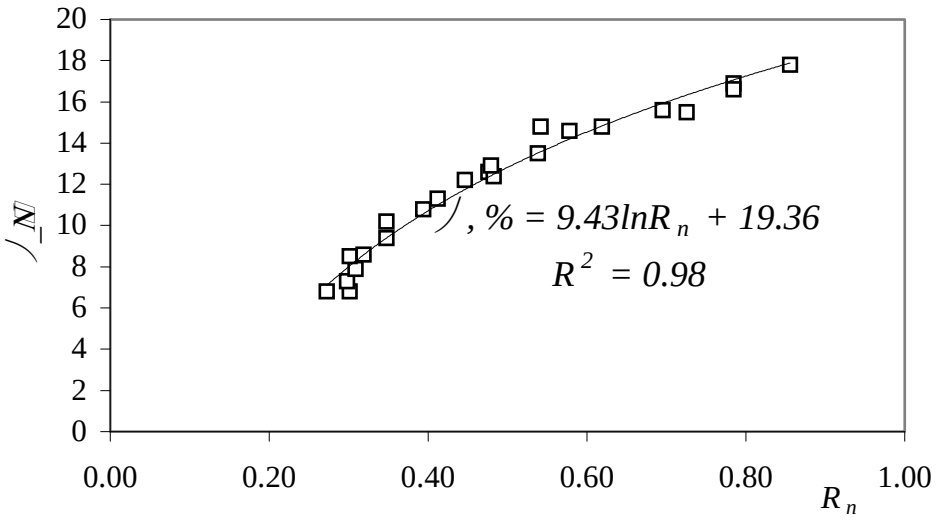

Fig. 3. Calibration curve in the soil moisture range of 6-18% for the NP model FIELDTECH PB-205, Japan

The calibration curve for the NP after correction for the soil organic matter of the field followed a trend:

$$\varphi\,(\%) = 9{,}43 \ln R_n + 19{,}36 \qquad (10)$$

Where φ *(%)* is the soil moisture in %, R_n is the count ratio representing the ratio of the count number of back scattered neutrons when the source is located in the shielding block (N_{Std}) and that in a certain soil depth (N_n) with a certain moisture. The use of the R_n instead of absolute values of N_n makes the uncertainty in the calibration to be much improved as the error caused by the disintegration of the source in neutron flow counting of N_{Std} and N_n could be compensated each other [*Annuziatta, 1998*].

Table 1 showed the influence of the irrigation techniques on the duration of the cabbage development in the autumn-winter (Oct-Dec) and winter-spring (Jan-Mar) seasons.

Tab 1. Development of cabbage (*X sp*.) planted on alluvial soil in autumn-winter (AW) and winter-spring (WS) seasons of 2006-2007

	Time period of cabbage development							
	Rooting time		*Leave development*		*Head formation*		*Harvesting day*	
	AW	WS	AW	WS	AW	WS	AW	WS
Drip	6-8	8-12	25-36	36-42	42-51	50-54	75-80	88-95
Furrow	6-8	8-12	27-35	38-42	43-51	50-54	78-80	92-95
F test	*ns*	*ns*	*ns*	*ns*	*ns*	*ns*	*ns*	*ns*

ns: no significance

Table 2 presented the influence of the irrigation techniques on the pest-insect damage to cabbage during the two cultivated seasons.

Table 3 summarized the yield and WUE of cabbage (*X-sp*., Petoseed, USA) from the two plots with furrow and drip irrigation. The data in the Table 4 was calculated based on the yields harvested from each plot and the total amount of water irrigated that recorded for each season. The plot with furrow irrigation has an area of 230 m^2 but the plot with drip irrigation has 85 m^2.

Tab 2. Scale of pest insect damage on cabbage in the experiment conducted with drip and furrow irrigation

	Pest insect				**Fungus**	
	Caterpillar	*Flea*	*Green pest*	*Head borer*	*Leave rottenness*	*Leave burn*
	In the autumn-winter season (2006-2007)					
Drip	1	2	1	1	1	1
Furrow	1	2	1	1	1	1
	In the winter-spring season (2006-2007)					
Drip	2	2	1	2	1	1
Furrow	2	2	1	2	2	1

Tab 3. The water use efficiency (WUE) of cabbage (*X sp*.) planted on alluvial soil in the 2006-2007 with different irrigation techniques

	WUE*, kg/m^3 (water)			
	Autumn-winter seasons		*Winter-spring season*	
	By Y_E	*By Y_{bio}*	*By Y_E*	*By Y_{bio}*
Drip	2,11 (±13%)	3,42 (±14%)	2,20 (±11%)	3,40 (±11%)
Furrow	1,61 (±12%)	2,61 (±15%)	1,48 (±10%)	2,37 (±15%)

It could be said that neutron probe (NP) is the most suited facility offering the ability to measure direct soil moisture. By this reason at many meeting organized by IAEA the equipment has been strongly recommended for the use in the water, soil and nutrition management [*APW, 2005, IAEA, 1st CRP D1.20.09 Meeting, 2007*]. NP could be calibrated on the fields, however sometime it could make a large uncertainty because of unknown channels made by earthworms in rooting zone that deviated the neutron back scattering flow. On the other hand, it must be noted that to get suited calibration curve for a neutron probe like that shown in Fig 3 one has to have data of the soil organic matter to correct for soil moisture. Another disadvantage of NP is its cost is still rather high, from 10 to more than 30 thousand USD excluded the cost for source guide tubes usually made from aluminum of 1 mm thickness and around 1.5 m length, so it is not so popular among farmers from developing countries.

It appeared that irrigation techniques did not, but cultivation seasons did in some extent affect on the development of the vegetable. In the autumn-winter season, period of rooting was 6-8 days after planting, and leave development was 25-36 days, head formation was 42-51 days and from the day of 75-90 the vegetable could give to harvest. However, in the winter-spring the respective time was 8-12, 36-42, 50-54 and 88-95 days (Table 1) implying latter as compared to those in the autumn-winter season. It is likely due to the temperature during the winter-spring is usually lower than that in the autumn-winter season, particularly in January-February.

As can see from Table 2 the severity in damage of the vegetable by pest insect was related to the cultivation seasons only. In the winter-spring season the damage severity was usually higher than that in the autumn-winter seasons (Table 2). The damage severity of the vegetable by pest insect was score in 5 scales [*AVRDC, 2000*]. Scale 1 attributed to the case when on vegetable was not or less than 5% in an area of 100 m^2 affected by pest insect. Scale 2 attributed to the case of 5-20% of vegetable in 100 m^2 area was affected, scale 3: 20-40%, scale 4: 40-60% and scale 5: more than 60% of vegetable in 100 m^2 land area was affected. It was found that the irrigation techniques did not cause additional damage to the vegetable. On the other hand, it should note that the two plots were in an open area so it could not too much tell about the impact of the irrigation techniques on the insect pest development because it was obvious that pest insect from other places could migrate to the study area.

As seen from Table 3 the water use efficiency (WUE) of cabbage in the plot of drip irrigation in both autumn-winter and winter-spring seasons of the 2006-2007 is higher (2.1-2.2 kg/m^3 and 3.4 kg/m^3, respectively, by Y_E and Y_{bio}) than that for the plot

of traditional furrow irrigation (1.48-1.61 kg/m^3 and 2.37-2.61, respectively by Y_E and Y_{bio}). The WUE of the vegetable with drip irrigation technique is in a range of 1.3-1.4 times higher as compared to that with furrow one (Table 3).

The total amount of water recorded for the drip and furrow irrigation in the autumn-winter season was (1.793±49) mm and (1,967±91) mm and that in the winter-spring season was (1,680±11) and (2,007±48) mm, respectively. These data imply that in the autumn-winter season drip irrigation could save around 10% but in the winter-spring season the figure was around 20% of irrigated water as compared to traditional furrow irrigation. The deviation in the water save for the two seasons could be attributed to a fact that in the winter-spring season water source for the vegetable was the only irrigated water but in the autumn-winter season there were two sources: irrigated and rain water.

Conclusion

It is obvious that neutron probe PB 205 (FieldTech, Japan) in combination with a meteorological station (Davis Instruments, USA) could be used to monitor continuously for soil moisture and potential evapotranspiration serving the basic for the optimizing irrigation in agronomy with the water use efficiency (WUE) parameter. The WUE of cabbage planted in alluvial soil of the Red River could be improved up to 1.4 times if drip irrigation technique were applied instead of the traditional furrow irrigation. Thus, one could save up to 10-20% water in irrigation practice. The irrigation technique could be transferred to semiarid areas in the southern central part of Viet Nam for not only vegetable but also fruit like grape production.

Acknowledgement

The study was financial supported by the Research Contract BO/06/04-02 of the Ministry of Science and Technology, MOST, Viet Nam for the period of 2007-2008. The authors wish to thank Mr. Pham Van Ngu, Chief of the Tang My Cooperative, Nam Hong Commune for his fruitful help in the rent of a land for the experiment. The family of Mr. Nguyen Van Truong and Mrs. Nguyen Thi Mai is acknowledged for their high responsibility in planting and looking after the vegetable during the two years experiment.

References

[1]. Allen R. G., 2000. Using the FAO-56 dual crop coefficient method over an irrigated region as part of an evapotranspiration intercomparison study. J. Hydrol. 229(1-2):27-41.

[2]. Annunziatta M. F., 1998. Handbook of radioactivity analysis. Academic Press. London, 1998. 771 pp.

[3]. APW, 2005. Asia Pacific workshop on:"Use of nuclear techniques to improve water management for sustainable agriculture", IAEA/CAS, Nanjing 21-23 Nov, 2005.

[4]. AVRDC, 2000. A guideline for estimate of pest-insects on vegetables, Asian Vegetable Research and Development Center, BangKok, Thailand, 2000.

[5]. IAEA 1st CRP meeting. 2007."Managing irrigation water to enhance crop productivity under water-limited conditions using nuclear techniques (D1.20.09).

Vienna, Austria, Nov 26-30, 2007.

[6]. IAEA Training Course Series No.30, 2008. Field estimation of soil water content. A practical guide to methods, instrumentation and sensor technology. IAEA, Vienna, Austria, 2008. 132 pp.

[7]. Keller A. A., Keller J., 1995. Effective efficiency: A water use efficiency concept for allocating freshwater resources. Discussion papers No.22. Center for Economic and Policy Studies. Winrock Int'l, 1995. 19 pp.

[8]. Neutron and gamma probes: Their use in agronomy. TCS No.16, 2003. IAEA, Vienna, 2003, 73 pp.

[9]. Robinson D. H., Freebairn D., Wockner G., 2000. Managing drought is about optimizing water capture and use. Managing climate makes money. Dalby RSL, 11-12 July 2000, 5 pp.

[10]. Sammis T., 1996. Soil texture analysis. New Mexico University.

[11]. Simonne E. H., Duke M. D., Haman D. Z., 2007. Principles and practices of irrigation management for vegetables. Factsheet No EA260 http://edis.ifas.ufl.edu/ pdffiles/ CV/CV10700.pdf

[12]. USDA. 1960. Soil water holding capacity. The US Dept. of Agriculture Bulletin No.462, 1960.

APPLICATION OF MOLECULAR MARKER (ISSR AND IRAP) TO DETECT CHANGES IN DNA OF RICE MUTANTS

Hoang Thi My Linh, Phan Dinh Thai Son, Nguyen Thi Vang and Nguyen Thi Nu

Center for Nuclear Techniques, VAEC

Abstract: Project: "Application of molecular marker (ISSR and IRAP) to detect changes in DNA of rice mutants" was carried out in 2008 with the purpose of consideration for using the two simple and inexpensive molecular markers to estimate changes in DNA of rice mutant after gamma irradiation.

Changes in DNA of the mutants BĐS; TĐS and VNĐ95-20, induced by gamma irradiation, in comparison to their parents: Basmati 370; Tam Thơm and IR64 were successfully assessed using two PCR based markers known as ISSR (Inter Simple Sequence Repeat) and IRAP (Inter-Retrotransposon Amplified Polymorphism). Statistics was carried out using Population Genetics software. Results showed that, both ISSR and IRAP could detect changes in DNA of rice mutants after gamma irradiation compared to their parents. Percentage of DNA changes determined by ISSR-PCR (Inter Simple Sequence Repeat – Polymerase Chain Reaction) in Basmati 370 -BĐS; Tam Thơm - TĐS and IR64- VNĐ95-20 were 12.69%; 9.74% and 5.02%. These numbers recorded by IRAP-PCR (Inter-Retrotransposon Amplified Polymorphism -Polymerase Chain Reaction) were 6.81%; 5.88% and 6.25% respectively.

Optimum protocols for employing ISSR and IRAP markers to detect changes in DNA of rice mutants after gamma irradiation have been selected for use in the molecular lab at Center for Nuclear Techniques, Ho Chi Minh city.

1. Introduction

Spontaneous and induced mutations are the ultimate source of all existing genetic variation in plants, and are commonly used in plant breeding. However the occurrence of spontaneous mutations in nature is relatively rare and difficult to identify because they are mainly recessive, or are deleterious and quickly eliminated [1]. Therefore, increasing the rate of mutation (ie induced mutations) can provide additional sources of variant genotypes important in plant breeding.

Mutation is random and unpredictable, selected mutant lines, therefore, may possess real genotypic changes or sometimes merely a phenotypic adaptation. Detecting genomic changes at the DNA level could provide evidence as to whether these mutations are genotypic or phenotypic in origin, and therefore whether the observed changes are heritable or merely a response to the environment. Project: "Application of molecular marker (ISSR and IRAP) to detect changes in DNA of rice mutants" was carried out with the purpose of consideration for using the two simple and inexpensive molecular markers (ISSR and IRAP) to detect changes in DNA of rice mutants in order to assist mutation breeding.

ISSR (Inter Simple Sequence Repeat) and IRAP (Inter-Retrotransposon Amplified Polymorphism) are the two simple and inexpensive markers that have been used successfully by many researchers to study biodiversity in many species such as Citrus [2,3], Larch [4] Wheat and Rice [5,6,7,8,9].

ISSR and IRAP are PCR based dominant markers. They were used via PCR (polymerase chain reaction). ISSR-PCR and IRAP-PCR were conducted using short primers (15 to 25 bases). PCR products were analyzed by electrophoresis on agarose gel. The presence or absence of bands was determined by examining each gel photograph.

2. Materials and Methods

2.1. Plant Material: Tissue culture leaves of varieties Tam Thom (TT1) and its mutants TDS, Basmati 370 - its mutants BDS, and IR 64 - its mutants VND 95-20 (induced by gamma irradiation) were used.

2.2. Extraction of genomic DNA: Genomic DNA from leaf of rice mutants, varieties Tam Thom (TT1) TDS, Basmati 370 BDS IR 64 and VND 95-20 were extracted using CTAB (Cetyltrimethylammonium bromide) method [10,11].

2.3. PCR optimization: To obtain reproducible results from a PCR reaction, it was necessary to determine the optimum reaction conditions for each primer. In this project, different amounts of genomic DNA (20, 30, 40 50 and 60 ng), three different concentrations of Mg^{2+} (1.0 mM, 1.5 mM and 2.0 mM) and 1.0, 1.25 and 1.5 unit tag DNA polymerase were tested, along with the three different PCR program temperature profiles described below

2.4. ISSR –PCR: ISSR-PCR was carried out on DNA samples using 50 ISSR primers in an Eppendorf Master Cycler Gradient. Each reaction was performed in a final volume of 20 µl containing 2.5 µl of 10 X *Taq* Polymerase Reaction Buffer [67 mmol/L Tris-HCl - pH 8.8, 16.6 mmol/L $[NH_4]_2SO_4$, 0.45% (w/v) Triton X-100, 0.2 mg/ml gelatin] (Biotech), 0.8 µl of each of dATP, dTTP, dCTP, dGTP (mix dNTP-Biotech), varying amounts of genomic DNA (30, 40, 50 and 60 ng), $MgCl_2$ (1.0 mM, 1.5 mM and 2.0 mM), and *Taq* DNA polymerase (1.0, 1.25 and 1.5 units) (Biotech), with 2.5 µl of each primer and varying amounts of sterile distilled water to make the final volume up to 20µl. Three annealing temperatures 45^0C; 50^0C and 55^0C were tested with following profile: Denaturation at 94°C for 5 minutes, followed by 32 cycles of denaturation at 94°C for 30 seconds, annealing at 45^0C or 50^0C or 55^0C for 45 seconds and extension at 72^0C for 2 minutes, with a final round of extension at 72^0C for 7 minutes.

2.5. IRAP –PCR: Each IRAP-PCR reaction was performed in a final volume of 25µl containing 2.5 µl of 10 X *Taq* Polymerase Reaction Buffer (67 mmol/L Tris-HCl - pH 8.8, 16.6 mmol/L $[NH_4]_2SO_4$, 0.45% (w/v) Triton X-100, 0.2 mg/ml gelatin) (Biotech); 0.8 µl of mix 10mM dNTPs; 20, 30, 40 or 50 ng DNA; 1.0, 1.25 or 1.5 Unit *Taq* DNA polymerase; 1 µl of 10 nmol/µl of each forward and reverse primers and varying amounts of sterile distilled water to make the final volume up to 25µl. Reactions were carried out in a PCR cycler (Eppendorf Master Cycler Gradient). Three annealing temperatures 52^0C, 56^0C and 60^0C were tested with following profile: Denaturation at 94°C for 5 minutes, followed by 35 cycles of denaturation at 94°C for 1 minute, annealing at 52^0C, 56^0C or 60^0C for 1 minute and extension at 72^0C for 2 minutes, with a final round of extension at 72^0C for 8 minutes.

PCR products were separated on 1,5% agarose gel containing 25% of fine agarose and 75% of routine agarose.

2.6. Data analysis: Data was analysed with Population Genetics software.

3. Results And Disscusion

3.1. PCR Optimization: The optimum amount of $MgCl_2$ required in each PCR reaction varied according to the particular primer combinations. Optimum concentration of MgCl2 was determined based on the brightness, sharp and the consistency of bands [12]. In this experiment, 1.5mM of $MgCl_2$ was found suitable and produced strong and consistent banding patterns for both ISSR and IRAP primers. At a concentration of $MgCl_2$ lower than these amounts (about 1.0 mM) bands were faint and difficult to record. Higher concentrations of $MgCl_2$ (2.0 mM) showed no further improvement on the pattern and strength of the bands obtained, or on their reproducibility.

Of the five genomic DNA concentrations tested (20, 30, 40, 50 and 60 ng), 40 ng of genomic DNA produced the strongest and most consistent bands in both ISSR-PCR and IRAP-PCR. The optimum amount of tag polymerase for ISSR-PCR and IRAP-PCR was determined at 1.25 unit.

The most suitable thermal profile for ISSR-PCR in this study was: denaturation at 94^0C for 5 minutes, followed by 32 cycles of denaturation at 94^0C for 30 seconds, annealing at 55^0C for 45 seconds and extension at 72^0C for 2 minutes, with a final round of extension at 72^0C for 7 minutes. Optimum thermal profile for IRAP-PCR in this study was: denaturation at 94^0C for 5 minutes, followed by 35 cycles of denaturation at 94^0C for 1 minute, annealing at 56^0C for 1 minute and extension at 72^0C for 2 minutes, with a final round of extension at 72^0C for 8 minutes.

ISSR-PCR and IRAP-PCR products with all components being optimized on 1.5% agarose gel were showed in figure 3.1.

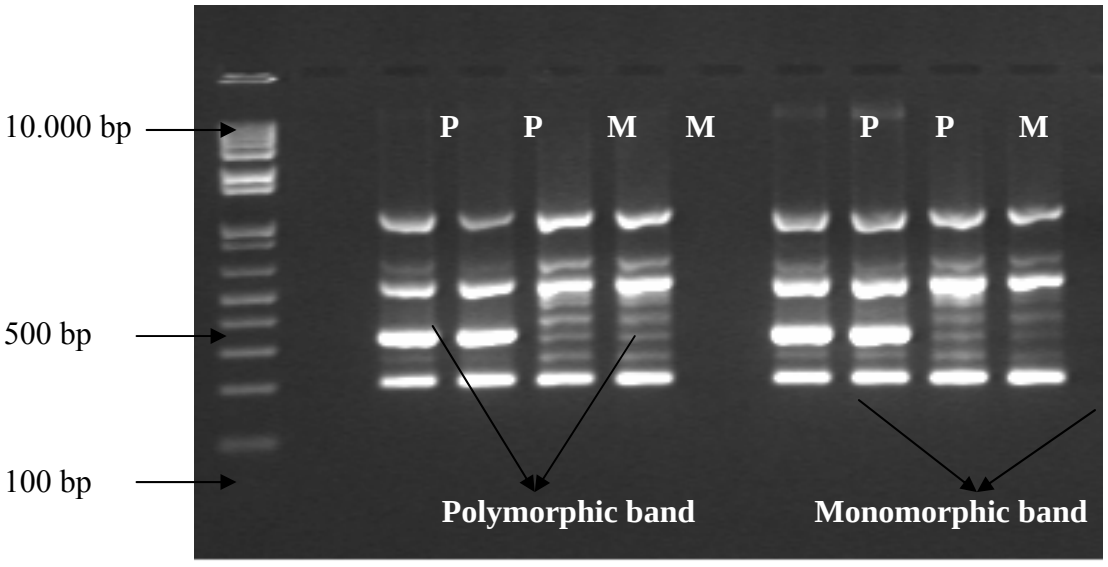

(a)

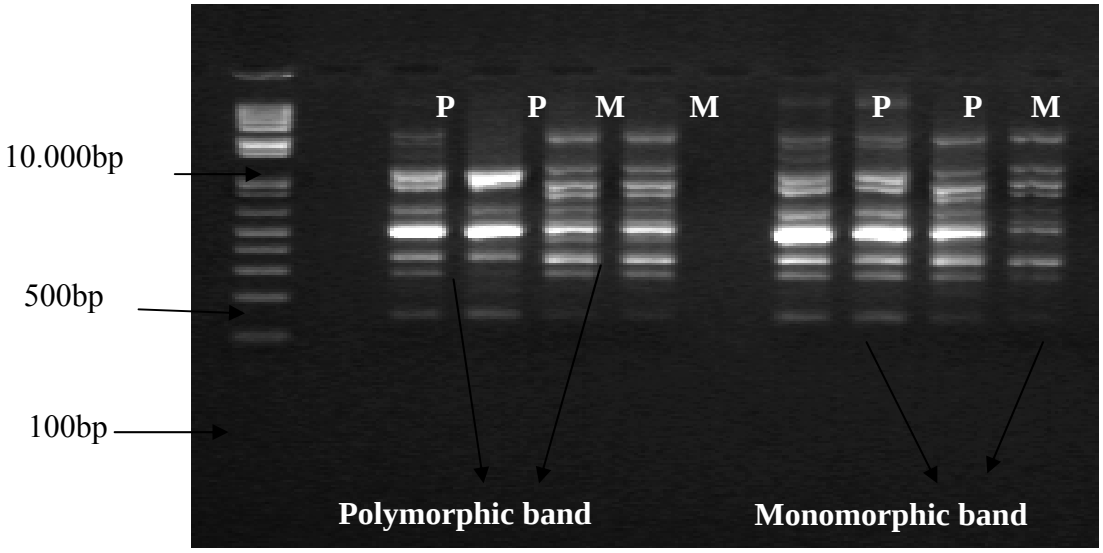

Fig. 3. 1. PCR products of Basmati 370 and Basmati mutant in ISSR-PCR (a) và IRAP-PCR (b) with all components being optimized.

Note: P: Parents; M: Mutant

3.2. Estimation of Changes In Dna Of Rice Mutants Using ISSR Markers: The total number and number of polymorphic bands generated by ISSR primers in Basmati 370 – BDS; Tam Thom (TT1) –TDS; and IR 64 - VND 95-20 is given in Table 3.1.

Tab 3.1. DNA Polymorphism between Basmati 370 – BDS; Tam Thom (TT1) – TDS; and IR 64 - VND 95-20 as detected by ISSR-PCR. Results are for triplicate PCR and only consistent bands were recorded.

	Total bands scored	**Number of polymorphic bands**	**% Polymorphism**
Basmati 370 & BĐS	252	32	12.69%
TT1 & TĐS	154	15	9.74%
IR64 & VNĐ 95-20	179	9	5.02%

Of the 50 ISSR primers tested, 21 primers could produce shape, bright and consistent bands in all cultivars and mutants examined. Some primers worked on one or two varieties but others and 10 primers were recorded not working well for all cultivars. Percentage of polymorphism between parent and its mutant varies from 5.02% in IR 64 - VND 95-20 to 9.74% in Tam Thom (TT1) –TDS and 12.69% in Basmati 370 and BDS.

Procedure of Using ISSR Marker To Detect DNA Changes In Rice Mutant

- Extract DNA following CTAB (Cetyltrimethylammonium bromide) method.

- Conduct ISSR-PCR with each reaction in a final volume of 20 µl containing 2.5 µl of 10 X *Taq* Polymerase Reaction Buffer [67 mmol/L Tris-HCl - pH 8.8, 16.6 mmol/L $[NH_4]_2SO_4$, 0.45% (w/v) Triton X-100, 0.2 mg/ml gelatin] (Biotech), 0.8 µl of each of dATP, dTTP, dCTP, dGTP (mix dNTP- Biotech), 40 ng genomic DNA, 1.5 mM

$MgCl_2$, 1.25 units *Taq* DNA polymerase, 2.5 µl of each primer and varying amounts of sterile distilled water to make the final volume up to 20µl. The optimum profile was: Denaturation at 94°C for 5 minutes, followed by 32 cycles of denaturation at 94°C for 30 seconds, annealing at 55^0C for 45 seconds and extension at 72^0C for 2 minutes, with a final round of extension at 72^0C for 7 minutes.

- Analyze data with Population Genetics software.

3.3. Estimation of Changes In DNA Of Rice Mutants Using IRAP Markers

The total number and number of polymorphic bands generated by IRAP primers in Basmati 370 – BDS; Tam Thom (TT1) –TDS; and IR 64 - VND 95-20 is given in Table 3.2.

Tab 3.2. DNA Polymorphism between Basmati 370 – BDS; Tam Thom (TT1) – TDS; and IR 64 - VND 95-20 as detected by IRAP-PCR. Results are for triplicate PCR and only consistent bands were recorded.

	Total bands scored	**Number of polymorphic bands**	**% Polymorphism**
Basmati 370 & BĐS	88	6	6.81%
TT1 & TĐS	85	5	5.88%
IR64 & VNĐ 95-20	96	6	6.25%

Percentage of polymorphism between parent and its mutant detected by IRAP primers as Basmati 370-BĐS: 6.81%; Tam thơm – TĐ: 5.88% and IR64-VNĐ95-20: 6.25%.

Procedure of Using IRAP Marker To Detect DNA Changes In Rice Mutant

- Extract DNA following CTAB (Cetyltrimethylammonium bromide) method.

- Conduct ISSR-PCR with each reaction in a final volume of 25 µl containing 2.5 µl of 10 X *Taq* Polymerase Reaction Buffer [67 mmol/L Tris-HCl - pH 8.8, 16.6 mmol/L $[NH_4]_2SO_4$, 0.45% (w/v) Triton X-100, 0.2 mg/ml gelatin] (Biotech), 0.8 µl of mix dATP, 40 ng genomic DNA, 1.5 mM $MgCl_2$, 1.25 units *Taq* DNA polymerase, 1 µl of forward primer, 1µl reverse primer and varying amounts of sterile distilled water to make the final volume up to 25µl. The optimum profile was: Denaturation at 94°C for 5 minutes, followed by 35 cycles of denaturation at 94°C for 1 minute, annealing at 56^0C for 1 minute and extension at 72^0C for 2 minutes, with a final round of extension at 72^0C for 8 minutes.

- Analyze data with Population Genetics software.

4. Conclutions

- The success or failure of a PCR reaction depends upon the optimization of conditions for the PCR. Especially the amount of $MgCl_2$, DNA and annealing temperatures had a significant effect on the success of a PCR.

- Percentages polymorphism in DNA between Basmati370 - BDS, TT1 - TDS, and IR64 - VND 95 -20 detected by ISSR-PCR were 12.69%; 9.74% và 5.02% respectively; This figures were recorded by IRAP-PCR as Basmati 370- BDS: 6.81%; Tam thơm – TDS: 5.88% và IR64-VND95-20: 6.25%.

- Both ISSR and IRAP can detect changes in DNA of parents and mutants. However, PCR with ISSR primer was more stable and easier to conduct than that with IRAP primer. Moreover, ISSR primers are quite available to get, therefore the expenditure for analyzing DNA changes with ISSR primers is lower than that with IRAP primers. This makes ISSR marker more competitive than IRAP marker in practice. Generally speaking, ISSR marker should be given priority to detect changes in DNA of rice mutants.

Acknowledgments

We thank Vietnam Atomic Energy Institute for supporting this research.

References

[1]. H. Wada, T. Koshiba, T. Matsui, M. Sato, Involment of peroxidase in differential sensitivity to γ-radiation in seedlings of two *Nicotiana* species, Plant Sci. 132 (1998) 109-119.

[2]. D.Q.Fang, R.R. Krueger, and M. L. Roose. Phylogenetic relationships among selected citrus germplasm accessions revealed by inter-simple sequence repeat (ISSR) markers. J Am Soc Hort Sci., 123(1998) 612-617.

[3]. D.Q. Fang and M. L. Roose, Inheritance of intersimple sequence repeat markers in citrus. J. Heredity, 90(1999) 247-249.

[4]. A.F Arcade, A.P. Faivre Rampant, M. C. Lesage, L. E. Pouques, and D. Prat, Application of AFLP, RAPD and ISSR markers to genetic mapping of European and Japanese larch. Theor Appl Genet., 100 **(**2000) 299 - 307.

[5]. M. W. Blair, O. Panaud, and S. R. McCouch, Inter-simple sequence repeat (ISSR) amplification for analysis of microsatellite motif frequency and fingerprinting in rice (Oryza sativa L.). Theor Appl Genet, 98 **(**1999)780-792.

[6]. A. Baumel, A. Malika, R. Kalendar and A.H. Schulman, Retrotrasnposons and genomic stability in populations of the young Allopolyploid species anglica C.E. hubbard (Poaceae), Mol.Biol.Evol., 19 (8) (2002): 1218-1227.

[7]. L.Gao, E.M.McCarthy, E.W.Ganko and J.F.McDonald, Evolutionary history of *Oryza sativa* LTR retrotraspsons: a preliminary survey of the rice genome sequences. BMC Genomics, 5 (2004) 18

[8]. R.A.Queen, B.M. Gribbon, C. James, P.Jack, and A.J. Flawell, Retrotransposon-based molecular markers for linkage and genetic diversity analysis in wheat. Mol. Gen. Genomics, 271 (2004) 91-97**.**

[9]. D.Guo, H. Zhang, and Z. Luo, Genetic relationships of *Diospyros kaki* Thunb. and related species revealed by IRAP and REMAP analysis. Plant Science, 170 (2006) 528-533.

[10]. E. Magel, S. Hauch, L.F. De Filippis, Random amplification of polymorphic DNA and reverse transcription polymerase chain reaction of RNA in studies of sapwood and heartwood, in: N. Chaffey (Ed.), Wood Formation in Trees, Harwood Academic, Malaysia, 2000, pp. 317-335.

[11]. L. De Filippis, E. Hoffmann, R. Hampp, Identification of somatic hybrids of tobacco generated by electrofusion and culture of protoplasts using RAPD-PCR, Plant Sci. 121 (1996) 39-46.

[12]. Y.H. Park and R.J. Kohel, Effect of concentration of $MgCl_2$ on random amplified DNA polymorphism, Bio Techniques, 16 (1994) 652- 653.

1.7 - Radiation Protection and Radioactive Waste Management

PREPARATION OF A HIGHLY SENSITIVE ETHANOL CHLOROBENZEN (ECB) DOSIMETER FOR THE LOW DOSE RANGE OF 1-7 kGy

Pham Thi Thu Hong*, Doan Binh*, Le Quang Thanh* and Le Huu Tu**

** Research and Development Center for Radiation Technology, HCM City*
*** Nuclear Research Institute, Dalat City*

Abstract: A highly sensitive modified ECB dosimetry system for the low dose range of 1-7 kGy has been prepared from mixture of chlorobezene and some sensibilizers (S) as dichlorobenzene (DCB), trichloroethylene (TCE) and chloroform (CF). Total concentration of the CB/S in dosimetry solutions is 24 % (v/v). Irradiated dosimetry solutions were analysed to determine the HCl concentration by mercurimetric titration with diphenylcarbazone indicator. The radiation chemical yield in terms of G(HCl) values of CB/CF (50:50) and CB/CF (25:75) systems were approximately 2,30 and 3,42 μM/J, respectively. Sensitivity of the modified ECB dosimeters is higher than 2 to 4 times compared with the ECB dosimeter. Absorbed dose of the dosimetry systems are measured by an oscillometer. In the 3 months of stored duration, the stability of modified ECB dosimetry systems has been tracked before and after ^{60}Co gamma irradiation. Standard curve of the modified ECB dosimetry system is based on the system of the silver dichromate dosimeter to use for measurement of absorbed dose with an accuracy of 5%.

I. General Introduction

Ethanol chlorobenzene dosimetry system has been approved by ASTM in 2004 as a routine dosimetry system in a dose range from 1 300 kGy both for gamma and electron irradiations. However, in actual applications of ECB dosimeter have a weakness of grave error in low dose range of 1-7 kGy because of a low sensitivity and the radiation chemical yield G(HCl) values was approximately only 0.5 0.6 μM/J. Up to now, it was not yet found any project related to research on improving of the sensetivity of ECB dosimeter for the low dose range of 1-7 kGy when the absorbed dose are measured by an oscillometer. The aim of this study is insreasing of the radiation chemical yield G(HCl) value through increasing of formed HCl concentration. Standard curve of the modified ECB dosimetry system is based on the system of the silver dichromate dosimeter to use for measurement of absorbed dose with an accuracy of 5%.

II. Experimental Procedures

1. Raw Materals

Clorobenzen, ethanol, distilled water, $Ag_2Cr_2O_7$,.. (Merck) were used for experiments.

2. The Gamma Irradiation

Of the dosimeters were performed with gamma cell source (GC-5000, India) of Nuclear Research Institute, Dalat City and the ^{60}Co gamma irradiation source of Research and Development Center for Radiation Technology.

3. Preparation of Standard Dosimester

In this study, dicromate dosimesters were prepared following the ASTM 51401-2003(E) [12] for the low range of 1- 12 kGy, measurement wavelenght 350 nm by using an UV-spectrophotometer (Shimazu-2401PC). The dicromate solution was pre-irradiated to a dose about 1 kGy. Each dosimeter contained 2.5 ml of dosimetic solution

4. Preparation of Modified ECB Dosimeters

All the solutions of modified ECB dosimeter were prepared by following the ASTM 51401-2003(E) [12]. Total concentration of the CB/S in dosimetry solutions was 24 % (v/v). The percentage of CB/S includes 0/100, 25/75, 50/50, 75/25. Each dosimeter contained 2.5 ml of dosimetic solution. The absorbed dose of irradiated ECB and modified ECB dosimeters were determined by using an oscillometer (D-001)

5. Determination of The Radiation Chemical Yeild (G_{HCl}) Values

Irradiated dosimetry solutions were analysed to determine the formed HCl concentration in each dosimeter by mercurimetric titration with diphenylcarbazone indicator by following the ASTM 51401-2003(E) [12]. The G_{HCl} value of dosimeter solutions was calculated at each absorbed dose applied and it can be calculated according to the following formula:

$$G_{HCl} = [Cl^-]/ D * \rho$$

Where $[Cl^-]$: concentration of formed HCl (mol/dm^3); D: dose absorbed by the dosimeter solution (kGy); ρ: density of the dosimetry solution (kg/m^3)

III. Results

1. Calculation of Standard Dosimester

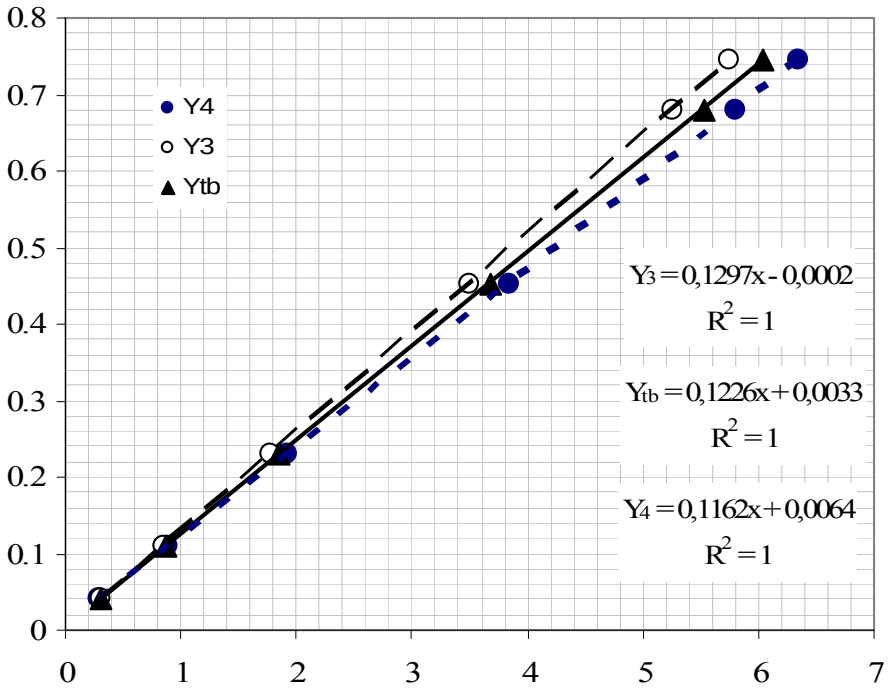

Fig. 1. Standard curves of dicromate dosimeters, irradiated at dose rate 3.22 kGy/h and temperature 40 °C, dose range of 1-7 kGy

After γ-ray irradiated, the absorbed dose of silver dicromate dosimesters were determined by using the average standard curve Ytb of Y1 (following the ISO/ASTM 51401-2003(E) [12]) and Y2 (following [5]).

2. Properties of Modified ECB Dosimeter

2.1 The Influence of Sensibilizers

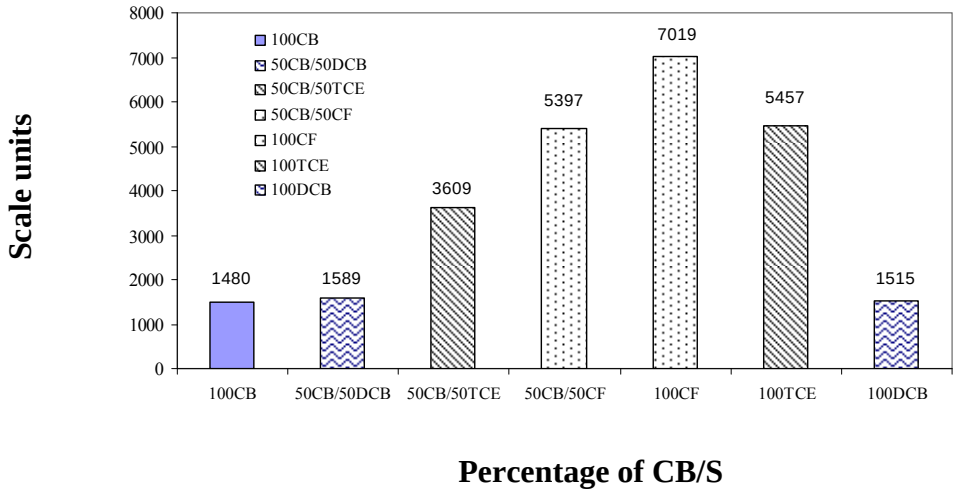

Fig. 2. Dependence of the oscillotitrator reading on the various formulation of modified ECB systems, absorbed dose 4.3 kGy, dose rate 1.4 kGy/h, temperature ~ 10°C

The results of oscillometric measurement (fig.2) is shown that the sentivity of modified ECB system formulated from composition of CB/CF is higher than the others.

2.2 The Influence of Absorbed Dose

The results of oscillometric measurement (fig.3) is shown that dependence of the oscillotitrator reading on the absorbed dose of modified ECB dosimeters was linear in the dose range of 1-7 kGy

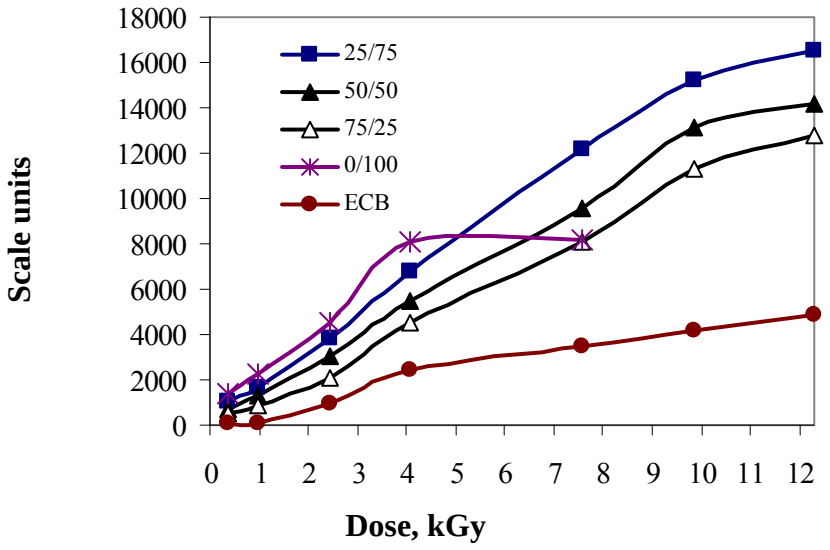

Fig. 3. Changes in the oscillotitrator reading on the absorbed dose of modified ECB dosimeter at the different percentages of CB/CF, dose rate1.4 kGy/h, temperature 10°C

2.3 The Radiation Chemical Yield of G_{HCl} Values

The G_{HCl} value of ECB and modified ECB dosimetry systems are given in table 1. The results were shown that the sensitivity of the modified ECB dosimeters is higher than 2 to 4 times compared with the ECB dosimeter.

Tab 1. G_{HCl} values for some ECB and modified ECB dosimetry systems at the dose range of 0.7 - 12.3 kGy, dose rate 1.4kGy/h, irradiated temperature 10°C

Dosimeters	Absorbed dose, kGy	G_{HCl}, μmol/j
50CB/50CF	0.9	2.58
	2.2	2.01
	4.0	2.44
	7.7	2.47
	11.4	2.56
25CB/75CF	0.7	3.10
	3.9	2.85
	6.2	3.98
	8.2	3.62
	123	3.24
ECB	4.0	0.86

2.4 The Influence of Dose Rate and Irradiation Temperature

The small difference in the oscillotitrator reading coefficients was found in irradiation temperature range 10 - 30°C, as shown in fig. 4.

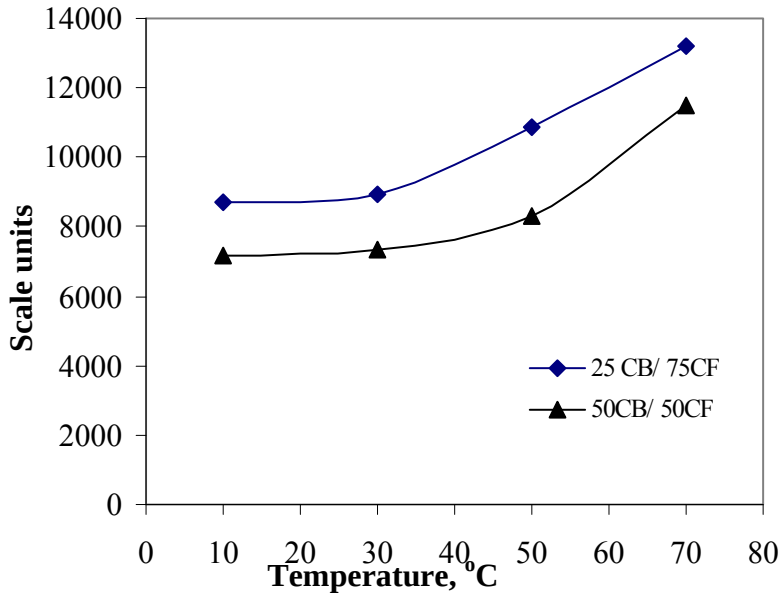

Fig. 4. Dependence of the oscillotitrator reading on temperature of modified ECB systems at absoebed dose 5 kGy and dose rate 1.4 kGy/h

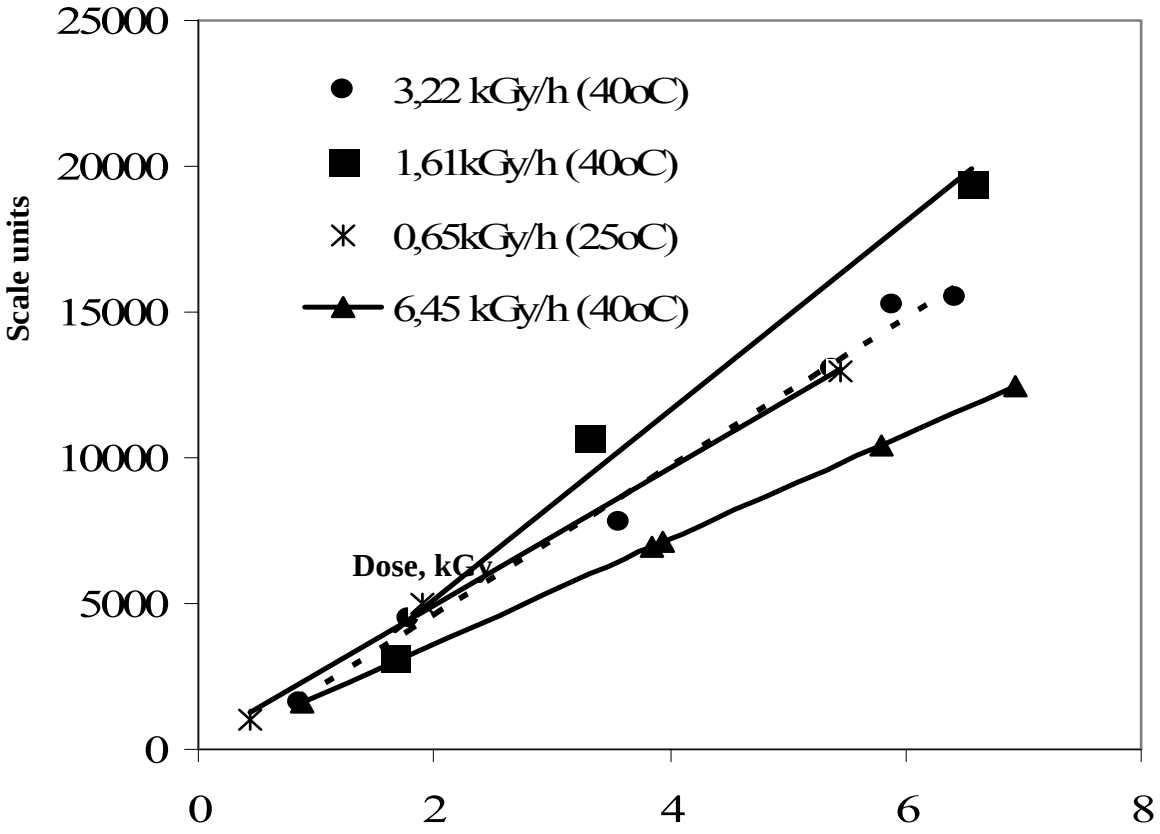

Fig. 5. The oscillotitrator reading of irradiated modified ECB system (25CB/75CF) at different temperature and dose rate

The results in fig.5 were shown that at the high irradiation temperature 40 ^{o}C the oscillotitrator reading of modified ECB system has been influenced by irradiation temperature in different dose rates.

2.5 The Influence of Storage Time of Modified ECB and Standard Systems

Tab 2. Change in the oscillotitrator reading of modified ECB system as a function of time under storage at 25 ^{o}C, dose rate 1.4 kGy/h, absorbed dose 5.3 kGy

Storage time(months)	Scale units	
	Non-irradiated	Irradiated
0	453 ± 95	12,720 ± 76
1	434 ± 77	12,350 ± 49
3	472 ± 45	12,629 ± 77

In the 3 months of stored duration, the stability of modified ECB dosimetry systems has been tracked before and after ^{60}Co gamma irradiation (Table 2). The oscillotitrator reading of modified ECB standard system was stabilized in the storage time for the low dose range.

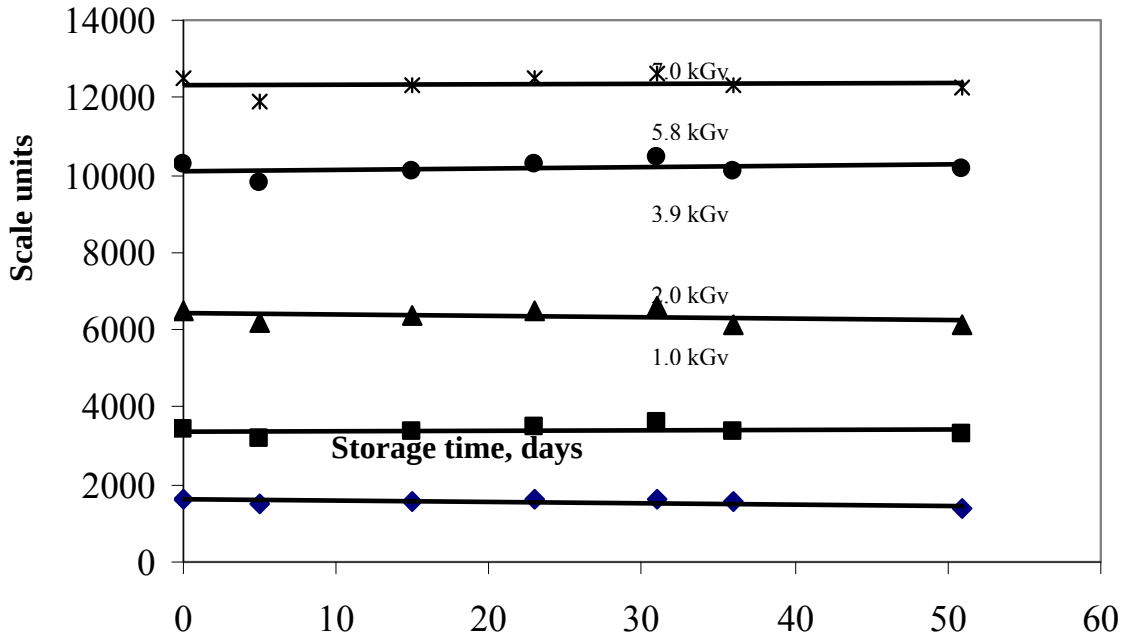

Fig. 6. The oscillotitrator reading stability of modified ECB standard system in the low dose range of 1-7 kGy, temperature storage 25 ^{o}C

IV. Conclusions

A highly sensitive modified ECB dosimetry system for the low dose range of 1-7 kGy has been prepared from the composition of CB and CF by using an osillometer to measure the absorbed dose. The charateristics of modified ECB dosimetry system are the following:

- The concentration of CF in dosimetry solutions: 50-75 % (v/v);
- Each dosimeter contained 2.5 ml of dosimetic solution;
- Application for ^{60}Co γ-ray irradiation; dose range 1-6 kGy; dose rate 1.4 kGy/h;
- Irradiation temperature 10-30^{o}C;
- The sensitivity is higher than 2-4 times compared with ECB system;
- With an accuracy of ± 5%;
- Sealed dosimeters were kept in the dark at the temperature 23-25 ^{o}C.

Future investigations should combined effects of oxygen, temperature at each dose applied on the G_{HCl} values and started to test out the modified ECB dosimetry system for frozen foods and fruits radiation processing at the low range of 0.5-6 kGy at Research and Development Center for Radiation Technology.

References

[1]. Application of the ethanol-chlorobenzene dosimeter to electron beam and gamma radiation dosimetry: II. Colbalt-60 gamma rays, D. Razem, I. Dvornik, *Proc. IAEA Symp. on Dosimetry in Agriculture, Industry, Biology and Medicine*, IAEA, Vienna, 1973, pp. 405-419.

[2]. Consistency of the ethanol- monochlorobenzene dosimetry, D. Razem, et. al, *Proc. IAEA Symp. on High Dose Dosimetry,* IAEA, Vienna, 1985, pp. 143-156.

[3]. Ethanol-Chlorobenzene dosimetry for absorbed dose below 1 kGy, D. Razem, et. al., *Appl. Radiat. Isot.* 1987, Vol. 38, No. 12, pp. 1019-1025.

[4]. Effects of temperature during irradiation and spectrophotometry analysis on the response of aqueous dichromate dosimeters, H.H.Mai., H. Tachibana., T. Kojima, *Radiat. Phys. Chem*. 1998, 53, pp. 85-91.

[5]. Nghiên cứu ứng dụng dung dịch $K_2Cr_2O_7$ để đo liều bức xạ gamma Co -60 trong khoảng liều từ 0,1-1,0 Mrad, Nguyễn Quốc Hiến, Nguyễn Mộng Sinh, Lê Hải, Nguyễn Tấn Mân, *Tạp chí Hóa học*, T. 31, số 2, tr. 12-13, 1993.

[6]. Neutron response of the chlorobenzene - ethanol - trimethylpentane dosimetry ststem, S. Miljaníc and D. Razem, *Radiation Protection Dosimetry,* 2007, Vol. 126, No. 1-4, pp. 198-205.

[7]. Radiolysis of aqueous chloroform solutions, B. J. Rezansoff, et. al., *Canadian Journal of Chemistry.* 1969, 48, 271.

[8]. Radialysis of aqueous solutions of dihalobenzenes: studies on the formation of halide ions by ion chromatography, D.B. Naik, Hari Mohan, *Radiat. Phys. Chem.* 2005, Vol. 73, pp. 218-223.

[9]. Radiation induced reaction in the ethanol-monochlorobenzene dosimeter solution, A. Kvács, et. al., *Radiat. Phys. Chem.* 1993, Vol. 41, No. 3, pp. 521-526.

[10]. Response of the chlorobenzene-based dosimetry systems to protons in the energy range 3.0-5.5 MeV, S. Miljaníc, et. al., *Radiat. Phys. Chem*. 1998, Vol. 51, No. 2, pp. 185-189.

[11]. Simple optical readout for ethanol-chlorobenzen dosimetry system, B. Ilijas, et. al., *Journal of Radioanalytical ang Nuclear Chemistry*. 1999, Vol. 242, No. 2, pp. 445-449.

[12]. Standards practice for use of the ethanol- chlorobenzene dosimetry system, *Standards on dosimetry for radiation processing, ASTM (2nd edition*), September 2004, pp. 87-97.

[13]. Standards practice for use of a dicromate dosimetry system, *Standards on dosimetry for radiation processing, ASTM (2nd edition*), September 2004, pp. 69-74.

[14]. The radiation-induced oxidation of trichloroethylene, Armen R. Kazannjian, et. Al., *The Journal of Physical Chemistry,* 1971, Vol. 75, No. 5.

[15]. Temperature effects on the ethanol-chlorobenzene dosimeter (Dvornik dosimeter), H.H.Mai, et. al., *Appl. Radiat. Isot.* 1991, Vol. 42, No. 7, pp. 637-641.

Papers Published In Relation To The Project

Chế tạo liều kế etanol clobenzen (ECB) có độ nhạy cao dùng đo trong dải liều thấp từ 1-7kGy, Tuyển tập báo cáo Hội nghị KH &CN Hạt nhân Toàn quốc lần thứ VIII năm 2009

MEASUREMENT METHOD AND MEASURING CONFIGURATION DATA OF PHOTON BEAM ON MEDICAL LINEAR ACCELERATOR

Nguyen Ngoc Huynh, Nguyen Huu Quyet, Nguyen Van Sy
Vu Van Tien and Nguyen Thi Thuy Mai

Institute for Nuclear Science and Technology, VAEC

Abstract: The Medical linear accelerator have been using at Vietnam in 2001, recently of a few years, The medical linear accelerator are coming popular and now there are about near tens of the linear accelerator in all of Vietnam, However, the number of Medical Physicist, Radiotherapy Technologist are very lacking and don't have any university educate this field

The aim of this study is to measure some of photon beam data as percent depth dose, beam profile, output factor…. for all of open fields and wedge fields. On other hand, this study to help our group research to improve the measurement capacity of photon beam data on medical linear accelerator and to afford commissioning, QA, QC and absolute dose calibration for linear accelerator

1. Introduction

For commissioning a linear accelerator for clinical use, medical physicists are faced with many challenges including the need for precision, a variety of testing methods, data validation, the lack of standards, and time constraints. Since commissioning beam data are treated as a reference and ultimately used by treatment planning systems, it is vitally important that the collected data are of the highest quality to avoid dosimetric and patient treatment errors that may subsequently lead to a poor radiation outcome

Advances in computer technology have led to the availability of sophisticated three-dimensional (3D) treatment planning systems (TPS) for use in many radiotherapy centers at Vietnam. One aim of introducing such sophisticated 3D TPSs is to improve the accuracy of dose calculations in radiotherapy planning. The accuracy in radiation therapy have been discussed in protocol TRS 398 that errors in dose delivery should not exceed 5%

2. Methods

All of these measurements were performed for both open and wedge fields. All measured depth dose curves and beam profiles were scanned using Welhofer WP600 radiation field analyzer using 0.1 cc, IC10 Welhofer ionization camber. relative output factors were measured using Farmer dosimeter with 0.6 cc graphite guarded stem ionization chamber type 2571 from Nuclear Enterprise.

Linear accelerators were used in this study at Ho Chi Minh City Oncology Center proviced by Varian Manufacturer and the energy used is 6MeV

1- Central-axis depth doses at field sizes 3x3, 4x4, 6x6, 8x8, 10x10, 12x12,

15x15, 20x20, 25x25, 30x30, 35x35 and 40x40 cm2 at 100 cm source-surface-distance (SSD) in both of open fields and wedge fileds. These depth dose data are used in determination of energy spectrum and modelling of contaminating electrons.

2- Tranverse dose profiles in water at 5 depths of $d_{max(10x\ 10)}$, 5, 10, 20 and 30 cm with SSD=100 cm for the same field sizes as above in both of open fields and wedge fields with angle of wedge 15, 30 and 45 degree. On other hand data of diagonal profile dose for the largest open field are also measured and all of these beam profiles data are used for penumbra modeling and to calculate the beam flatness factor , the beam symmetry factor

3- Tranmistion factor for blocks and trays must be measured to difinte dose on patient, these factor are measured with small field size as 3x3 or 4x4

4- Output factors in water for open and open fields at the reference SSD and depth using different field sizes. These factors are used to monitor unitcalculations.

3. Results

1-This test compared calculated depth dose lines measured depth dose lines at SSD =100 cm for 10 x 10 cm2 field sizes. It showed a general agreement between them for different SSDs at depths larger than depth of the maximum dose with difference less than 1%. As found for SSD = 100 cm, the difference in the build-up region varies between 2-3%. Fig. (1):

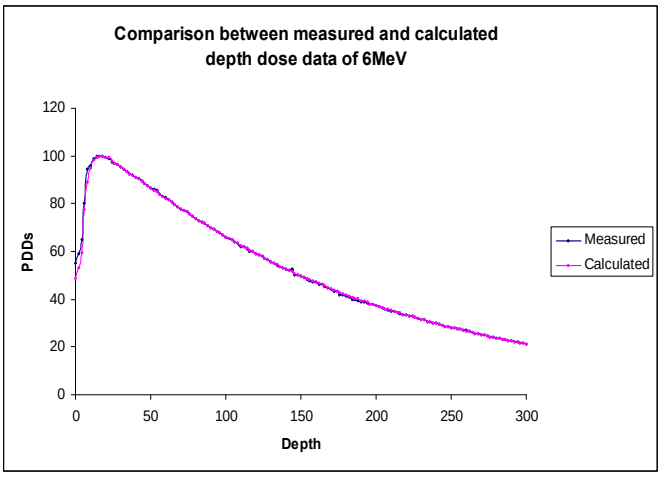

Fig. 1. measured and caculated depth dose curves

2-

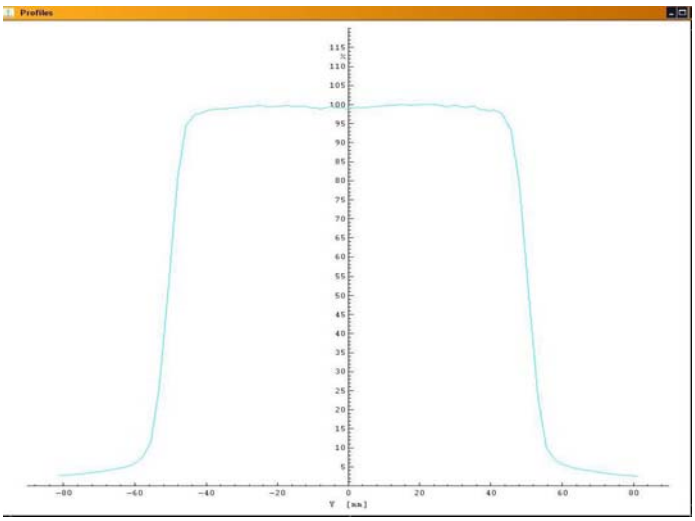

Fig. 2. Measured profile dose with field size 10x10cm^2

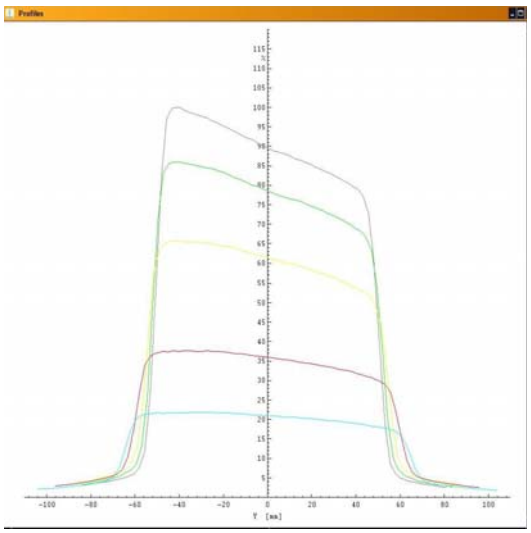

Profiles with 5 depths for wedge 15 degree

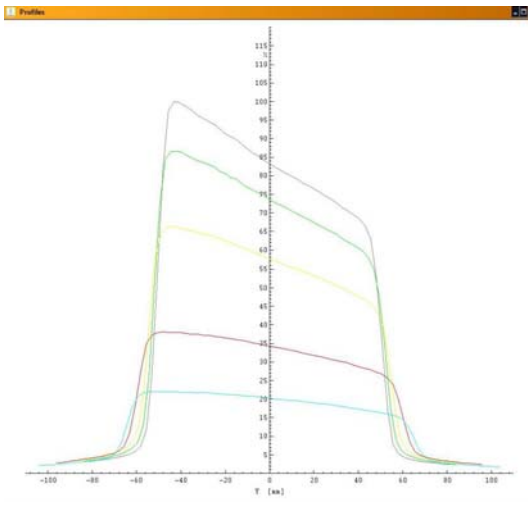

Profiles with 5 depths for wedge 30 degree

Fig. 3. 4- An example of comparison between measured and calculated depth dose data of 6 MV photons generated by Varian linear accelerator at 100 cm SSD whith 12 different field sizes (3x3, 4x4, 6x6, 8x8, 10x10, 12x12, 15x15, 20x20, 25 x25, 30x30, 35x35 and 40x4cm2). The depth doses divided by monitor unit is normalized at 10x10 cm2 field.

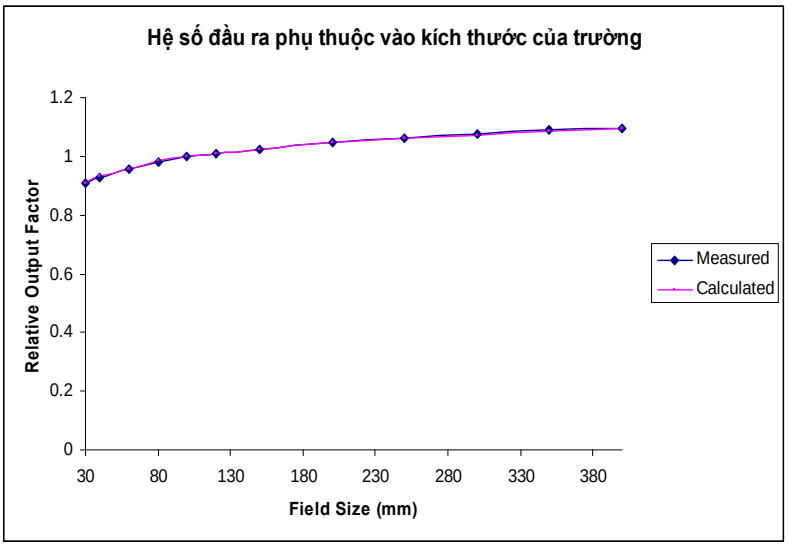

Fig. 4. Measured and caculated relative ouput factor (output factor divided by output factor of 10 x 10 cm2 field)

4. Discussion

Comparison of calculated depth dose with measured data for both of the open fields and wedged fields showed excellent agreement for energy of 6MeV. In both the useful beam and penumbra regions, the difference was < 1% in both directions.

The calculated output factors are showing good agreement with the measured values for open fields using energy of 6MeV from the linear accelerators at the Ho Chi Minh City of Onconoly Center. Fig. 1. shows an example of this result for open fields of 6 Mev photon from Varian.

References

[1]. Radiation Oncology Physics. A handbook For Teachers and Students E.P.Podgorsak, technical editor.

[2]. Eclipse Beam Data Collection Guide, Varian Medical System.

[3]. Technical Reports Serial No 398. Absorbed Dose Ditermination in External Bean Radiotherapy.

[4]. Medical Electron Accelerators. C.J. Karzmark.

[5]. BJR Supplement 25, Central Axis Depth Dose Data for Use in Radiotherapy 1996

[6]. Medical Physics Department, Radiation Oncology Physics Group manual. Feb, 2000.

[7]. Quanlity Control and Absolate dose calibraton for medical linear accelerator, Project of Ministry Grade, Nguyen Huu Quyet, 2007.

STUDY ON THE ESTABLISHMENT OF THE TECHNICAL PROCEDURE FOR TREATMENT AND CONDITIONING OF SPENT ION EXCHANGE RESINS IN THE PRIMARY COOLING SYSTEM AT THE DALAT NUCLEAR RESEARCH REACTOR

Pham Hoai Phuong, Ong Van Ngoc, Nguyen Thi Thu, Phan Cong Thuyet, Nguyen Thi Thu Phuong, Nguyen Thi Kim Tuyen, Tran Tuan Anh and Nguyen Thanh Tam

Nuclear Research Institute, VAEC

Abstract: Ion exchange resins are used for removing radioactive contaminants of the primary cooling water at Dalat Nuclear Research Reactor as well as minimizing corrosion or degradation of system components. After being used a period of time, the ion exchange resins get degraded and lose their physical and chemical properties considerably. They are no longer useful because of its reduced ion exchange capacity and they represent one of the most important solid wastes. Due to the large amount of radioactivity contained inside these spent ion exchange resins, they have to be stored as such. For safe disposal of spent ion exchange resins, the report shows the technique to remove the fissile element as well as fission product radionuclides entrapped in the resins and the method to solidify this waste by cementization techniques. The studies were carried out to optimize a suitable procedure for treatment and conditioning the spent ion exchange resins from the reactor.

Key words: treatment, conditioning, ion exchange resin, solidification.

I. Experimental and Results

I.1 Optimizing The Conditions To Remove Radionuclides From Spent Ion Exchange Resins

I.1.1 Apparatus and Reagents

- Chemicals: HCl, HNO_3, NaOH, NaCl, $(NH_4)_2SO_4$;

- A coaxial high pure Ge detector coupled with a multichannel pulse height analyzer has some parameters as listed below:

- Detector volume: 256 cm^3
- Resolution (at 1332 keV): 2 keV
- Relative Efficiency: 60%
- Peak/Compton ratio: 60
- Shield: 10cm Pb
- Background (from (100keV to 2000keV): 7 pulse/second

- Glass column: inner diameter ID = 3cm, height h = 30cm; glass and beaker.

- Spent ion exchange resins including Lewatit Monoplus S100 và Lewatit Monoplus M500.

I.1.2 The Effect of Elutants

- Preparation of column: diameter ID = 3cm, height h = 30cm;

- Weigh out 90g of wet resins into the column (ID = 3cm, h = 30cm)

- The flow rate was set at 0.6ml/min

- The volume for each solution was 200 ml

- The elution solutions were counted by the coaxial high pure Ge detector coupled with a multichannel pulse height analyzer, counted time: 6h

Tab 1. Influence of elution agent concentration to release radionuclides

Elutants	**Conc.**	**Radionuclides, K_d^A**								
		Cs-134	Cs-137	Co-60	Eu-152	Eu-154	Co-58	Mn-54	Zn-65	Sb-125
HCl	1%	0	0	0	0	0	0	0	0	0
	2.5%	4.6	4.6	0.5	0	0	0.4	0.5	0.6	17.3
	5%	11.7	10.9	2.9	2.4	0	2.6	3	3.5	12.3
	15%	37	41.7	50.6	44	45.7	40.1	48.5	1.3	11.8
HNO_3	0.3M	2.7	1.1	0.7	2.2	0	0.6	3.4	2.7	1.9
	0.5M	17	17.2	5	2.2	0	4	4.4	5.6	16
	1.5M	21.6	23.3	26.5	8.6	0	26.5	23.7	5.6	11.3
NaOH	0.5%	0	0	0	0	0	0	0	0	0
	2%	14.7	13.7	0.4	0	0	0.2	0.5	17.7	29.8
	5%	57.6	51.9	3.6	3.4	0	3.2	11.1	46.7	28.5
	10%	0	0	5.7	0	0	4.5	4.6	5.2	0
NaCl	5%	19.5	14.3	0.6	1.9	0	0.5	0.5	1.7	31.5
$(NH_4)_2SO_4$	0.1M	0.3	3.8	4.4	0	0	0.4	0.2	0	15.1
	0.5M	53.3	59.5	71.4	42.8	33.8	22.2	54.2	44.7	35.2
	1.5M	70.2	69.6	67.5	71.7	52.7	68.7	70.3	69.9	32
	2M	67.1	73	75.6	85.7	82.4	73.5	71.6	74.7	23.6
	3M	98.6	59.5	71.4	81.3	92.6	94.5	45.2	98.2	45.7

K_d^A: elution efficiency (%)

I.1.3. Effect of The Volume of The Elutant 2M $(NH_4)_2SO_4$

- Preparation of column: diameter ID = 3cm, height h = 30cm;

- Weigh out 90g of wet resins into the column (ID = 3cm, h = 30cm)

- The flow rate was set at 0.6ml/min

- The volume for each solution was 50 ml

- $(NH_4)_2SO_4$ solution with vary volume: 50ml, 100ml, 150ml, 200ml, 250ml, 300ml, 350ml, 400ml.

- The elution solutions were counted by the coaxial high pure Ge detector coupled with a multichannel pulse height analyzer, counted time: 6h

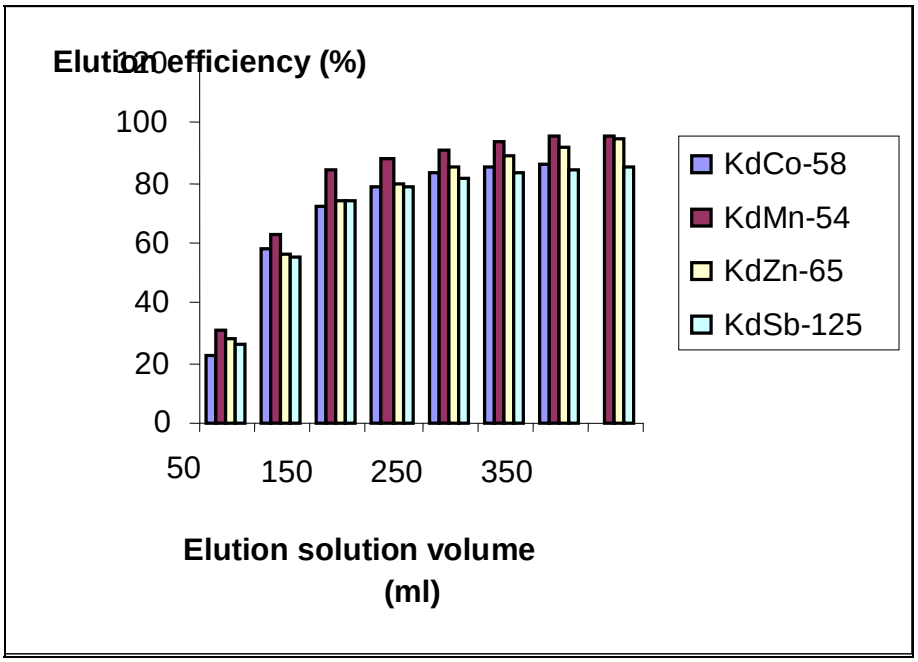

Fig. 1. Diagram express relationship between volume of elution solution and elution efficiency to releasing group 1 radionuclide

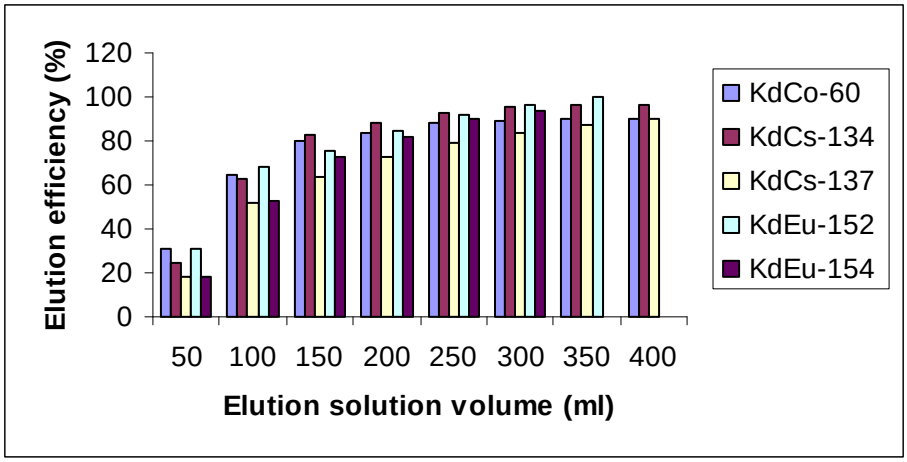

Fig. 2. Diagram express relationship between volume of elution solution and elution efficiency to releasing group 2 radionuclides

Radionuclides of group 1: Co-60, Cs-134, Cs-137, Eu-152, Eu-154;

Radionuclides of group 2: Co-58, Mn-54, Zn-65, Sb-125.

I.1.4. Effect of The Flow Rate of The Elutant 2M $(NH_4)_2SO_4$

- Preparation of column: diameter ID = 3cm, height h = 30cm;

- Weigh out 90g of wet resins into the column (ID = 3cm, h = 30cm)

- The flow rate of solution was set for each elution at 20ml/min, 5ml/min, 1.6ml/min and 0.7ml/min

- The volume for each solution was 100 ml

- The elution solutions were counted by the coaxial high pure Ge detector coupled with a multichannel pulse height analyzer, counted time: 6h

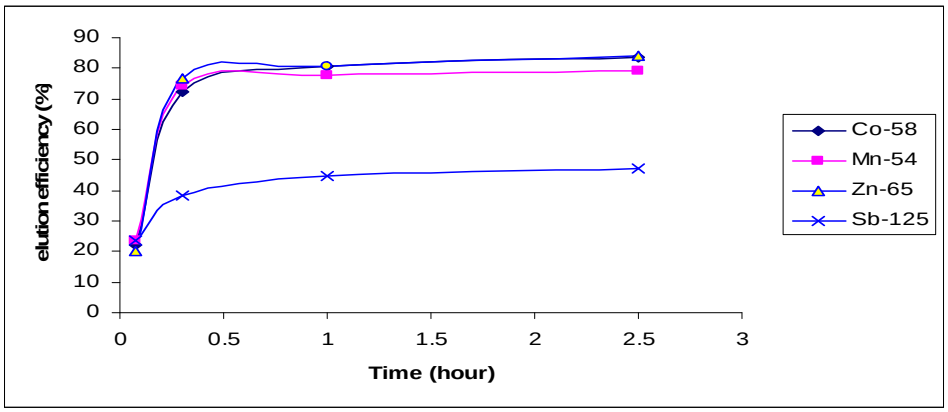

Fig. 3. Diagram express relationship between time for each elution of solution and elution efficiency to releasing group 1 radionuclides.

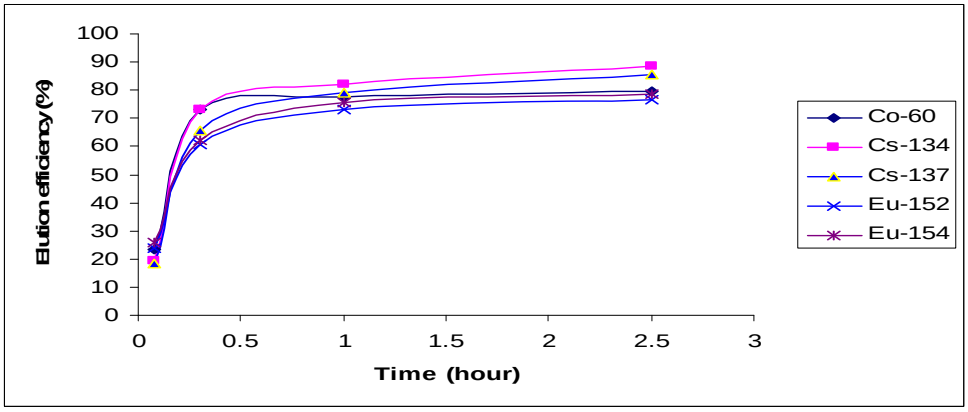

Fig. 4. Diagram express relationship between time for each elution of solution and elution efficiency to releasing group 2 radionuclides

I.2 Direct Immobilization of The Spent Ion Exchange Resin In Cement

I.2.1. Material, Equipment and Chemical

- Spent mixed ion exchange resin: including Lewatit Monoplus S100 và Lewatit Monoplus M500

- Porland cement: Bim Son, PCB40;

- Prism tray: 40mm x 40mm and 40x160mm length;

- Chemical: $Ca(OH)_2$

- Equipment for test of compressive strength: TYA – 2000; Test method: TCVN 6016:1995

I.2.2 Pretreatment for Spent Mixed Ion Exchange Resin

A process for cement solidification treatment of spent ion exchange resins, which comprises dehydrating the wet resin particles to remove free water therefore; Applying a small amount of cement powder thereon under stirring as pre-treatment to coat the surface of the resin particles with the cement powder; then, adding cement powder and water to the pre-treated resin particles and kneading to form a uniform mixture of cement past ; and finally casting the cement paste into a vessel to solidify it therein. The cast product contains much more resin particles.

Pre-treatment: Cement/ wet resin ratio (wt): 0.05; 0.11; 0.14; 0.16; and 0.27

Tab 2. Effect of cement/wet resin ratio for pre-treatment on the compressive strength

Sample No.	**Sample date**	**Test date**	**Sample dimension** (mm)	**Average compressive strength** (kG/cm^2)	**Sample age** (day)
A1-40g	17/03/2009	21/04/2009	40 x 40 x 80	253.51	>28
A2–20g	17/03/2009	21/04/2009	40 x 40 x 80	231.47	>28
A3–100g	19/03/2009	21/04/2009	40 x 40 x 80	210.79	>28
A4–50g	23/03/2009	21/04/2009	40 x 40 x 80	226.62	>28
A5–60g	23/03/2009	21/04/2009	40 x 40 x 80	215.68	>28

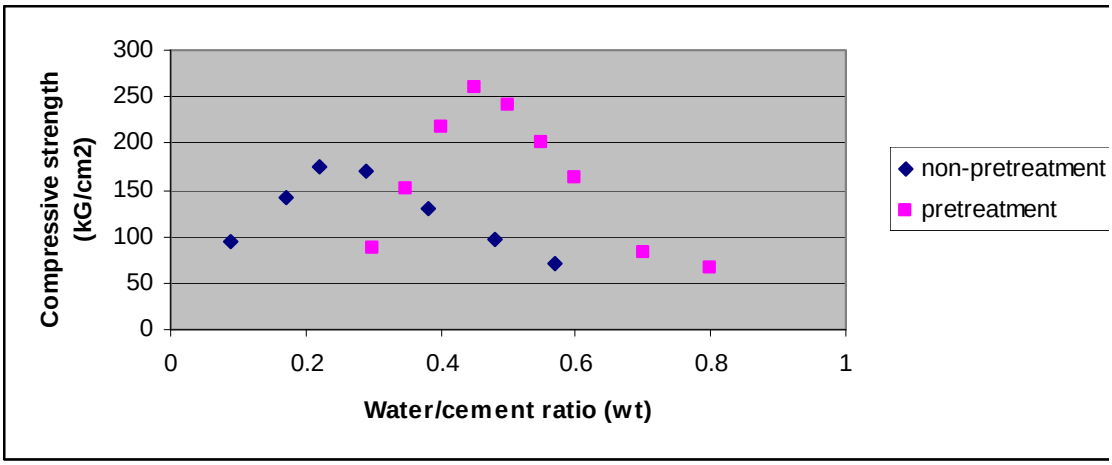

Fig. 5. Comparing the compressive strength between pretreatment resins and non-pretreatment resins.

As can be seen in Fig. 5, the wet resins/cement for the solidification of spent ion exchange resin is the same on both pretreatment resins and non-pretreatment resins, but

the result of the compressive strength was different. The optimum compressive strength was achieved at 259.6Kg/cm2 in case the spent ion exchange resins was pretreated. On the other hand, resins without pretreatment just obtained the optimum compressive strength 174.7Kg/cm2. That is to say, there was a strength increasing in pretreatment resins. So it can be allowed to add amount of resins into a solidification product.

I.2.3 Effect of waste and water/cement ratio

A considerable amount of research has been carried out to determine the limits for the composition of an acceptable resin – cement mixture. The process for immobilizing wastes consists of mixing the cement with the waste and allowing the mixture to harden. Obtaining a free standing product, in which there is no free standing water, is the basic criterion.

The composition of a waste form is often expressed by the terms “waste content” and “water/cement ratio”. The amount of waste in the final waste form is one of the important properties that influence to the strength of the cement matrix

Survey three cases of vary between terms “waste content” and “water/cement ratio”.

- Wet resin: 220 gram
- Pretreatment: cement/wet resin ratio (wt): 0.11

Solidification:

1. Wet resin/cement ratio (wt) = 0.2 ; Water/cement ratio (wt): 0.2; 0.25; 0.3; 0.35; 0.45; 0.5; 0.6; 0.7; 0.8;

2. Wet resin/cement ratio (wt) = 0.5 ; Water/cement ratio (wt): 0.3; 0.35; 0.4; 0.45; 0.5; 0.55; 0.6; 0.7; 0.8

3. Wet resin/cement ratio (wt) = 0.8 ; Water/cement ratio (wt): 0.35; 0.4; 0.5; 0.65; 0.8; 0.9; 1.0; 1.1; 1.2

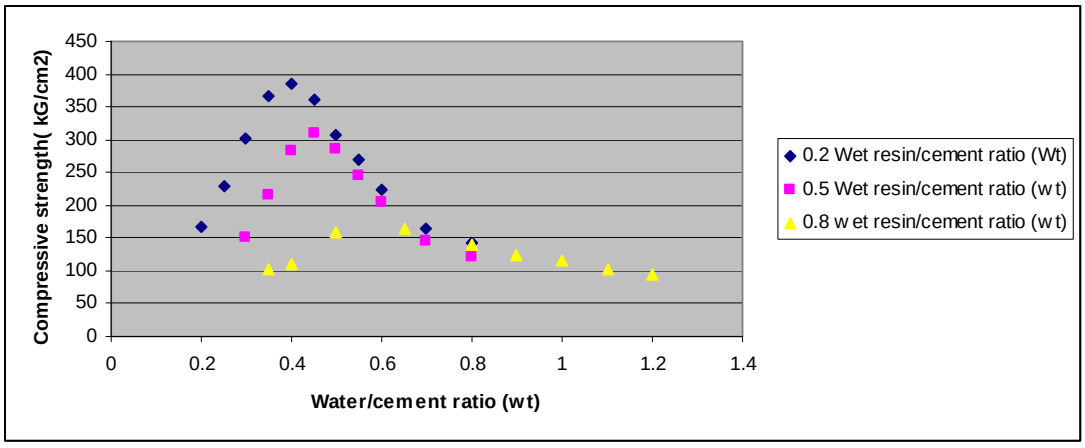

Fig. 6. Effect of water/cement ratio and waste/cement ratio on the compressive strength.

As can be seen in Fig. 6, wet resins/cement ratio and water/cement ratio considerably effect on the compressive strength.

II. General Assessment, Discussion

As can be seen on the whole of the experimental results, treatment of the spent ion exchange resins by directly cementization has some advantages, such as requiring simple equipment, easy scaling-up, low cost, good physical, chemical and mechanical properties, high stability, good radioactive shield, moderate leaching rate, etc. This method has a disadvantage that is not reducing the volume of solidified product. However, the pretreatment method had improved the solidification of spent ion exchange resins by cement. With elution method, this technique also meet a few disadvantages, such as the secondary liquid radioactive waste made during elution folds from 3 to 4 times of resins volume, and the apparatus for the elution is complex and expensive. However, elution of spent ion exchange resin have some advantages, such as isolation long-live isotopes that they have special demand for treatment and management, and elution efficiency is achievable over 85% for radionuclides.

Reference

[1]. IAEA, Treatment of Spent Ion Exchange Resins for Storage and Disposal, 1985

[2]. Cement Solidification Treatment of Spent Ion Exchange resins (Document Type and Number: United States Patent 4904416), 1990.

[3]. IAEA, Improved Cement Solidification of Low and Intermediate Level Radioactive Wastes, 1993.

[4]. IAEA, Application of Ion Exchange Process for the Treatment of Radioactive Waste and Management of Spent Ion Exchanger, 2002.

[5]. IAEA, Predisposal Management of Radioactive Waste, 2004.

[6]. IAEA, Characterization of Radioactive Waste Forms and Packages, 1997.

[7]. IAEA, Conditioning of low – and intermediate – level radioactive wastes, 1983.

QUALITY ASSURANCE STATUS ON RADIOTHERAPY IN VIETNAM

Nguyen Huu Quyet[a], Le Ngoc Thiem[a] , Chu Vu Long[a]
Nguyen Trung Hieu[b] and Nguyen Xuan Ku[c],

[a] *Institute for Nuclear Science and Technology, VAEC*
[b] *Ho Chi Minh Cancer Center*
[c] *K Hospital*

I. Introduction

Vietnam was one of the first countries, which early applied ionizing radiation in medicine. Dr. Marie Curie herself certificated supplying radium sources to Hanoi Cancer Hospital (today name is the K Hospital) for cancer treatment since 1923.

In spite of early application of radiation in medicine, Vietnam is now facing to problem of deficiency of radiotherapy facilities. 13 cobalt units and 7 Linear Accelerators (linac) per 84 millions population are working in the whole country, meanwhile about 100,000 patients suffered by cancer and tumor disease per year and only 10 percent of these are treated by radiation. The deficiency of the facilities leads to an ugly overloading with patients in the cancer centers and hospitals. The problem could be resolved by increasing the number of Cobalt therapy units and introducing of more effective tools for treatment as linear electron accelerators and other related equipment and by close cooperation and effort of physicists and physicians in the field of application of ionizing radiation in medicine to effectively use of facilities and ensure QA&QC in radiotherapy.

II. Radiotherapy Situation In Vietnam

In Vietnam, which has a population of about 84 millions, more than 100,000 new patients suffered from tumor and cancers each year. Cancer is the nation's second rank of diseases causing to death in Vietnam. (For information, the 1st rank diseases causing to death is cardiovascular disease) According to formal statistics, in the city of Hanoi, Ho Chi Minx, Hue and Danang, the most common cancers among male are lung, stomach, liver, nasopharynx, colorectal cancer and those among female are breast, cervix uterus, stomach, nasopharynx, lung, liver and colorectal cancer.

In Vietnam, surgical treatment, chemotherapy, immunotherapy, radiation therapy and combinations of these therapies have been used for cancer therapy. However, the facilities and equipment available for treatment - providing these therapies are old and deficient. As for actual therapy recipient figures, only 20 % of patients in Hanoi and its environments are being treated at the following two hospital that are located in urban areas of Hanoi city: the National Cancer Center (K hospital) and the Hanoi Cancer Hospital .

At present, except the tow first linear accelerators (linac) which has been installed in K hospital since 2001, 2 linacs in Ho Chi Minh Cancer Center, 2 linacs in Cho Ray Hospital and 1 in French- Vietnam hospital, in Vietnam only old fashion cobalt therapy is being performed. To improve treatment track records, the introduction of effective

treatment facilities and the significant improvement of equipment and measurements including dosimetry are required, although it is also necessary to upgrade/renew the facilities of the above- mentioned hospitals. .Radiation facilities are also in poor conditions. In the nationwide, there are total 13 cobalt units (most of them are second-hand and too old), 9 brachytherapy machines (only four of these are new, the remain ones are second-hand and LDR type, using the Cs-137 sources); 8 simulators (two of them are second-hand) located in 11 radiotherapy departments. Distribution of radiation facilities in Vietnam is presented in Table 1.

In Vietnam, except some very short training courses, there is no university, no school to train the professional medical physicists and radiation therapists. The nuclear physicists usually have to study by themselves to become medical physicists of radiotherapy centers. So the human resources of medical physicists & radiation therapists are shortage in Vietnam at present time. The staffs are involved in Radiotherapy at different oncology centers are given in Table 2.

Tab 1. Present radiotherapy facilities in Vietnam

Location	Cobalt units	Linear Accelerator	Brachytherapy units	Simulators
Oncology Dept. (Thai nguyen Central Hospital)	1		0	0
National Cancer Institute (K Hospital)	3	2	3	2
Hanoi Cancer Hospital (Hanoi City)	1		1	1
Oncology Dept. (103 Army Hospital)	1		1	0
Oncology Dept. (Headphone Hospital)	2		0	0
Oncology Dept. (Hue Central Hospital)	1		1	1
Oncology Dept. (Danang Hospital)	1		0	0
Oncology Dept. (Khan Hoa Hospital)	1			1
Ho Chi Minh Cancer Center (HCM city)	3	2	4	2
Oncology Dept. (Cho Ray Hospital)		2		1
Oncology Dept. (Vietnam- French Hospital)		1		1

Tab 2. The staffs are involved in Radiotherapy at different oncology centers

Institutions	Radiation Oncologists	Medical Physicists	Technicians
Oncology Dept. (Thai nguyen Central Hospital)	3	1	3
National Cancer Institute (K Hospital)	18	9	9
Hanoi Cancer Hospital (Hanoi City)	6	2	6
Oncology Dept. (103 Army Hospital)	5	1	3
Oncology Dept. (Haiphong Hospital)	5	1	6
Oncology Dept. (Hue Central Hospital)	4	1	3
Oncology Dept. (Danang Hospital)	3	0	3
Oncology Dept. (Khanh Hoa Hospital)	3	1	4
Ho Chi Minh Cancer Hospital (HCM city)	20	9	12
Oncology Dept. (Cho Ray Hospital)	10	5	6
Oncology Dept. (Vietnam- French Hospital	3	1	3

III. Role of the secondary standard dosimetry laboratory

Since late eighties , application of ionizing radiation into medicine , industry have increased rapidly. High accuracy in the dosimetry of ionizing radiation is essential in order to assure the quality of radiotherapy throughout the world and in order to compare successfully clinical results on an international basis. This accuracy can only be achieved if calibrated radiation dosimeters are available and checked regularly to maintain accep table measurement performance. Various kinds of survey meters, area monitors, environmental personal dosimeters have been using at Nuclear Research Institutes, Hospitals, Factories,... to measure and observe radiation level. These radiation monitoring instruments must be excellent in reliability. That's reason of an establishment of National Dosimetry Calibration Laboratory (NDCL) and in 1990, the NDCL was established. This calibration laboratory has been equipped with the following facilities :

- Reference gamma collimated sources Cs-137 (20Ci/ 1990) OB6/ Buchler traceable to SSDL - IAEA.

- Secondary standard dosimetry systems FARMER including standard electrometers 2570A, 2570B , PTW , and ionization chambers NE 2571 , 2581 , PTW (0.6cc) , 417 (600cc) calibrated against secondary standard of SSDL - IAEA.
- Calibrated well - type chamber and electrometer used for brachytherapy.
- Some water cubic phantoms.
- Barometers, thermometers.
- QC test tool for diagnostic radiology.

The maximum possible calibration distance from the source is 7m. By adding additional attenuates (Pb : 2cm, 4cm thickness) to decrease dose rate of radiation beam so that the radiation dosimeters working at lower level are able to be calibrated with this source. Since 1997, calibration setting up for X-ray reference machine was completed at the NDCL. Some kinds of X-ray beam qualities were carried out at radiation protection level with narrow spectrum series, low air kerma rate, wide spectrum series. Besides of these , three X-ray beam qualities were generated for radiotherapy level. The measured HVL are quite close to ISO 4037 with uncertainties less than ± 5 %. Absolute air kerma rates were determined for all established X-ray beam qualities.

The NDCL is able to calibrate radiation dosimeters, radiation survey meters, to carry out QC for diagnostic radiology and radiotherapy unit.

In the end of 1999 , the NDCL has been accredited as member of IAEA/WHO Secondary Standard Dosimetry Laboratory (SSDL) network . Since 2000, annually SSDL-Vietnam has participated in the TLD based dose intercomparison program of IAEA for both radiation protection level and radiotherapy level. Usually our stated doses and IAEA measured doses are agreed within ±5% for radiation protection level and ±2% for radiotherapy level.

Due to the lack of qualified medical physicists and the radiation instruments in the radiotherapy centers, SSDL-Vietnam has played the special role in dosimetry and QA for radiotherapy in whole country. For long time, SSDL was sole organization responsible for measuring output of any radiotherapy equipment in Vietnam. Normally every 2 years, SSDL staffs come to every radiotherapy center to check on site and carry out QC for Cobalt unit.

IV. Carrying out quality control for radiotherapy equipment

In Vietnam , up to now there are 11 radiotherapy centers with 4 Linacs,13 radiotherapy cobalt- 60 sources and several therapeutic X-ray machines and afterloading machines being used. Measurement of radiation output of radiotherapy equipment in air and a water phantom under standard conditions at the treatment distance was performed by staff of NDCL. Generally, measurements have done every two years with standard dosimetry system traceable to SSDL of IAEA. After setting up , commissioning , repairing radiotherapy units and changing the new source, Ministry of Health asked NDCL doing acceptance tests for radiotherapy equipment. On - site visit , apart from measurement of radiation output , various parameters of equipment were controlled as follows :

- Verification of mechanical parameters including correspondence between the mechanical axis of the collimator and the light beam axis , isocenter position , optical distance meter, symmetry of the collimator jaws, geometrical field size indication

- Verification of photon beam characteristics including correspondence between the light field and the radiation field at reference depth, flatness and symmetry of radiation field ...

Sometimes IAEA experts come to radiotherapy departments to measure beam output of equipment by both expert's and local secondary standard dosimetry systems.

Recently, Vietnam Directorate of Standard and Quality has issued the protocol named "Cobalt-60 teletherapy equipment: Methods and means of verification" to enhance the quality of radiotherapy equipment [1].

With 15 years -experience of performing QC for X-ray machines, Cobalt-60 units, ISNT is likely able to satisfy the requirement of physics problems for radiotherapy. However it is very difficult for us to solve the mechanical problems of radiotherapy units found from QC of these equipment.

V. Establishment of External Audit Group and the TLD postal programme for radiotherapy departments

The External Audit Group (EAG) was established on the base of staff and facilities of SSDL, Medical Physics group of radiotherapy departments and officers of Vietnam Radiation Protection & Nuclear Safety Agency (VARANSAC) and Ministry of Health. The flowchart of EAG was shown in Figure 1. Since 2001 EAG has organized the TLD based quality audit in dosimetry for radiotherapy departments annually.

The EAG has prepared some forms and documents for the audits following IAEA guidelines such as :

- instruction sheets describing the geometrical set up for TLD irradiations and the irradiation procedures,

- data sheets for the clinical beams, where details concerning beam calibration and the TLD irradiations are reported by the participating departments, including the date of irradiation of TL-dosimeters, the dose delivered to the dosimeters, the quality index for photon beams, the ion chamber calibration factor and its traceability, information on the dosimetry protocol used and date of the last external audit in which the center has been involved.

TL-dosimeters have been prepared in SSDL – Vietnam which belongs to Center of Radiation Protection & Environment Monitoring. Usually we try to run this programme simultaneously with IAEA TLD audits for radiotherapy departments in Vietnam. So at the same time every radiation beam to be participated in the TLD audits is provided with the above-mentioned instruction sheets and data sheets, a holder for irradiation of the TLD samples and two sets of TLDs for the irradiations, together with control capsules to monitor the background, undesirable accidental irradiation…(one from SSDL-Vietnam, another from IAEA). After TLDs were irradiated, they will have been returned to SSDl- Vietnam together with calculated, reported sheets and data sheets. One set of TLD will be sent to IAEA for reading and another will be read out in SSDL-Vietnam by Harshaw reader 4000. After that EAG & IAEA will inform every

participating radiotherapy department the results of doses related to their radiation beam including the ratio of the dose D_{TLD} measured with the TLD method to the dose D_{stat} stated by the participating center ($CF = D_{TLD}/ D_{stat}$). The percentage relative deviation between the stated and the measured dose (defined as $Dev= 100\% \times (D_{stat}- D_{TLD})/ D_{TLD}$) should also be informed by EAG and IAEA. A relative deviation with negative (positive) sign will indicate that the user estimates lower (higher) dose than what is measured, a patient would therefore receive higher (lower) dose than what is intended, as expressed by the factor given in the last column.

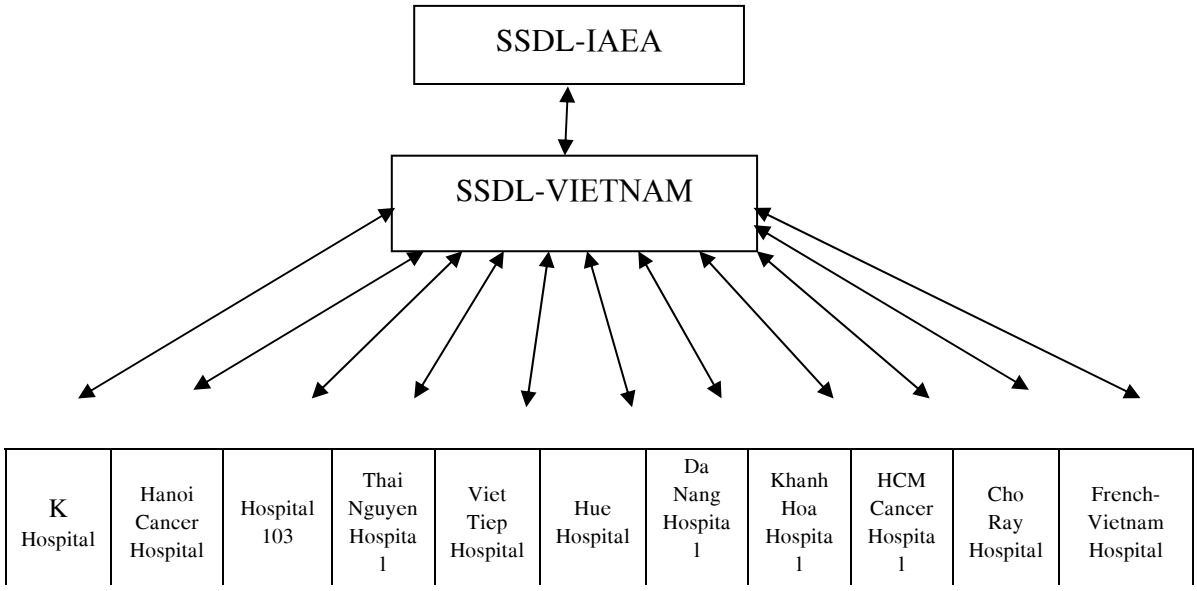

Fig. 1. Flowchart of the External Audit System

In order to organize the national audit programme for radiotherapy successfully we have to set up and improve the measuring systems and related procedures [2,3,4].

1. Measuring system

a) Farmer Dosimeter system 2570/1A, NE 2571 0.6cc chamber

b) Harshaw Reader 4000 with the reading regime : PT 160°C, RT 260°C, 20s, 16°C/s.

c) TLD-700 powder

d) Co-60 Source Theratron T780E, , 6000Ci.

e) LINAC Primus (Siemens), E = 6 MV, 15MV.

f) IAEA's water phantom 30x30x30 cm^3 and standard insert.

g) Annealing oven.

2. Checking of the repeatability of TLD readings

For setting up the measuring procedures it is necessary to improve the skill of measuring and treating TLD powders and to check the repeatability of readings for the technicians. Two TLD powder dispensers were investigated. One was purchased from IAEA, another was made in Vietnam. The standard deviations of mass were less than 1% for both of two dispensers. The masses of TLD powder of dispensers were shown in Table 3.

Tab 3. The masses of TLD powder of dispensers

Dispensers	25mg	30mg/33mg	50mg
IAEA		X	
Vietnam	X	X	X

The results of measurements showed that the home made dispenser has more stick effect than that of IAEA's dispenser. The high humidity (more than 90%) effected randomly on the readings. It is difficult to control this effect and the air conditioner and humidifier were used for reducing the humidity in the laboratory. Although our staffs have experiences and skills to measure and treat TLD for achieving a good repeatability of TL readings less than 2%, it is necessary to retrain the staffs. Therefore more than 100 TLD capsules were irradiated with dose of 2 Gy. It was found that at right beginning, the technician can make the measurements with the standard deviations up to 7% but after long measuring time they can reduce the these of measurements to 1%.

3. *Checking of the stability of TLD readings.*

The good repeatability can not show the stability of readout and irradiation of TLD capsules. So the comparison of mean values of readings were done for Harshaw readings.

It is found that discrepancy of mean values-Mean(i)/Average of TL readings laid out in the interval from 0.985 to 1.015 :

$$0.985 \leq (\text{Mean(i)}/\text{Average}) \leq 1.015,$$

Where Mean(i) is the average of TL readings of i^{th} capsule and Average is that of all capsules irradiated with the same dose of 2Gy.

4. Determination of absorbed dose in water

In order to calibrate the TLD powder with Cobalt source the absorbed dose to water at depth of 5 cm with field size 10x10 cm^2 at SSD of 80 cm should be known. This value were determined by the secondary standard ionization chamber NE 2571 following IAEA TRS 277.

Similarly the absorbed dose to water at depth of 5 cm or 10cm with field size 10x10 cm^2 at SSD of 100 cm for 6 MV or 15 MV respectively were determined by the secondary standard ionization chamber NE 2571 following IAEA TRS 277. That value is necessary for calibrating the TLD powder with Linac.

5. Calibration of TLD

The calibration has been done at 5 points : 1.5 Gy, 1.75 Gy, 2Gy, 2.25 Gy and 2.5 Gy with Co-60, Theratron T780E 6000 Ci and LINAC Primus (Siemens). For Co-60, the exposure time were corrected with the transit time of the radiation source. Figure 2 showed the calibration curve with Co-60.

The absorbed dose can be determined by :

$$D = 1E\text{-}04 * TL + 0.0352 \quad (Gy),$$

Where TL are readings in nC, D are the absorbed doses in Gy. with correlation coefficient R^2= 0.9941. Similarly Figure 3 showed the calibration curve with Linac. The absorbed dose for Linac can be determined by :

$$D = 1E\text{-}04^* TL + 0.0206 \quad (Gy),$$

Where TL are readings in nC, D are the absorbed doses in Gy. with correlation coefficient R^2= 0.9909.

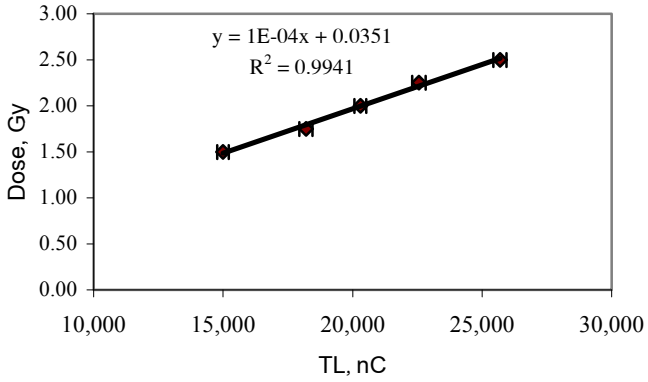

Fig. 2. Calibration curve of TLD with Co-60 Theratron T780E

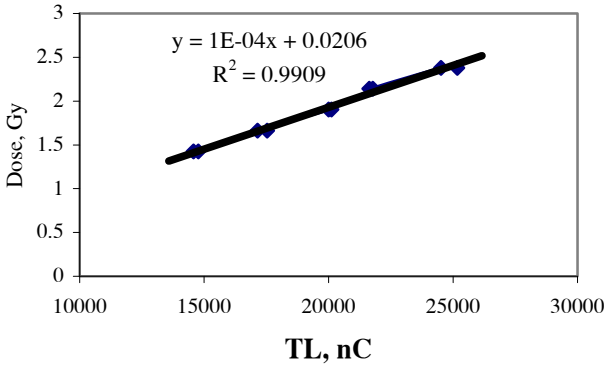

Fig. 3. Calibration curve of TLD with Linac Primus T780E

6. *The results and discussions*

a. Comparison the measured doses by TLD s between SSDL-Vietnam and SSDL-IAEA

The ratio of $CF_{SSDL\text{-}VN}/CF_{SSDL\text{-}IAEA}$ should be considered as a referent indicator to evaluate the SSDL-Vietnam's competency as well as the skill of irradiating TLDs at radiotherapy departments. Figures 4 and 5 show the ratios of $CF_{SSDL\text{-}VN}/CF_{SSDL\text{-}IAEA}$ for cobalt units and linacs respectively. It is assumed that the IAEA's measured data are accurate.

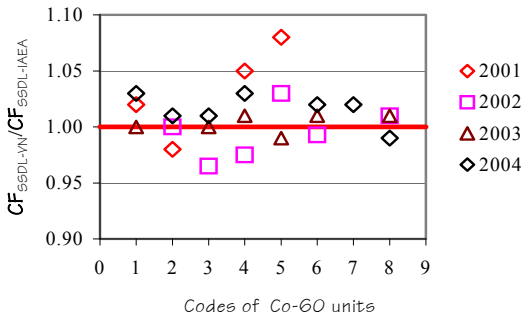

Fig. 4. $CF_{SSDL\text{-}VN}/CF_{SSDL\text{-}IAEA}$ for cobalt units

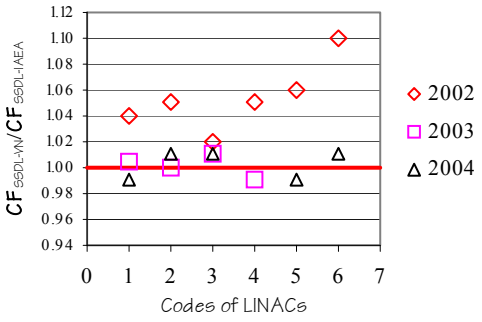

Fig. 5. $CF_{SSDL\text{-}VN}/CF_{SSDL\text{-}IAEA}$ for Linacs

From Fig. 4 and Fig. 5 it is found that at starting time the ratios of $CF_{SSDL\text{-}VN}/CF_{SSDL\text{-}IAEA}$ are rather large. The differences between $CF_{SSDL\text{-}VN}$ and $CF_{SSDL\text{-}IAEA}$ for Cobalt units are up to 8% and for Linac 15 MV up to 10%. In fact in 2002, all

$CF_{SSDL-VN}$ are more than $CF_{SSDL-IAEA}$ systematically at least 2%. It was due to the lack of SSDL-VN's experiences at beginning stage of dosimetry for Linac. However since 2003 the agreement between $CF_{SSDL-VN}$ and $CF_{SSDL-IAEA}$ have been within ± 2% and accep table.

b. Results of the TLD audits for teletherapy equipment in Vietnam

Kinds of radiotherapy equipment in Vietnam and their stated & measured output doses are summarized in Table 4.

It is easy found that not all equipment audited every year because of overloading patients in 2 biggest radiotherapy centers in Hanoi and Ho Chi Minh city and the Cobalt sources become too weak after more than 2 its half lives in other departments. Figures 6 and 7 illustrated the audit results of radiotherapy equipment and permissible tolerances according to the recommendation of WHO/IAEA (also DLVN-40) for radiotherapy department and SSDL. The results in Table 4 and Figures 6 & 7 show that except Cobalt unit No. 5, all deviations of all radiotherapy equipment operating in Vietnam now are less than ± 5%. In 2004, 64% (9/14) of checked equipment's deviations are within 3.5 % (permissible tolerance for SSDL). This proved that after 4 years running TLD audits, the status of QA in radiotherapy dosimetry becomes better. However the accuracy of output of equipment is still not consistent, for example Cobalt unit No.8 had the deviation only 1.3 % in 2003 but it increased to 4.3 % in 2004; and Linac beam No.5 had the deviation only 0.5 % in 2002 but it increased to 4.8 % in 2004.

Tab 4. Results of TLD audit for teletherapy equipment in Vietnam carried out by IAEA in period of 2001-2004

T/T	Equipment	2001		2002		2003		2004	
		σ, %	CF	σ, %	CF	σ, %	CF	σ, %	CF
Co-60 Units									
1	Picker C-9	–2.0	1.02			0.2	1.00	–2.7	1.03
2	Chisobalt	0.2	1.00	–0.2	1.00			–0.8	1.01
3	Theratron T780E			3.6	0.965	–0.5	1.00	–1.2	1.01
4	Theratron 80	–2.0	1.02	2.6	0.975	–0.6	1.01	–3.1	1.03
5	Chisobalt	–10.0	1.08			1.3	0.99		
6	Picker C-9	–0.2	1.01	–3.6	1.04	–0.9	1.01		
7	Elite 80							–1.9	1.02
8	Theratron T780E			–4.8	1.05	–1.4	1.01	–4.3	1.05
LINACs									
1	Primus, 6MV			–0.5	1.01			1.3	0.99
2	Primus 3544, 6MV			1.9	0.98	0.1	1.00	–1.9	1.02

3	Primus 3525, 6MV			–1.5	1.02	–0.7	1.01	–0.6	1.01
4	Primus 3544, 15MV			4.0	0.96	1.7	0.98		
5	Presice 5847, 6MV			–0.5	1.01			–4.8	1.05
6	Presice 5847, 15MV			–0.5	1.01			–1.3	1.01

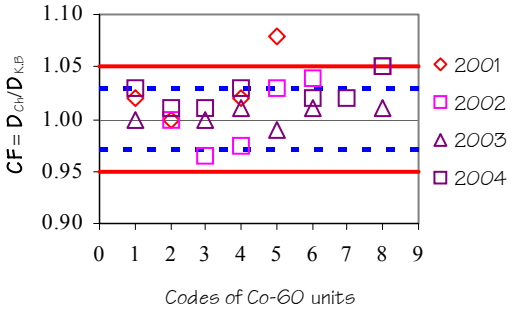

Fig. 6. Accuracy of Co-60 units' output compared with IAEA standard by TLD measurement

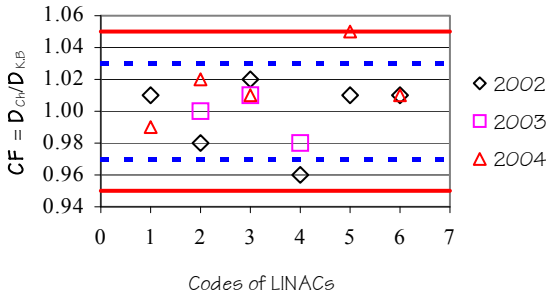

Fig. 7. Accuracy of Linacs' output compared with IAEA standard by TLD measurement

VI. Conclusion

The radiotherapy departments become familiar with external TLD based audit programme of radiotherapy equipment's output and understand more clearly the protocol for delivering the accurate doses to patients.

1. The significance for a hospital to participate regularly in external audits to reach and maintain an adequate level of dosimetry has been observed. Nowadays, all radiotherapy equipment participating in this programme have the deviations less than ± 5%.

2. Physicists', physicians' and technicians' Knowledge and skill on radiation treatment already have improved through this external audit programme. However the quality assurance of radiotherapy in Vietnam is still at first stage (level 1).

3. Close Coordination of Ministry of Science & Technology, Ministry of Health, Radiation Protection & Nuclear Safety Agency, Vietnam Atomic Energy Commission and IAEA is very necessary to improve the quality of radiotherapy in Vietnam.

Acknowledgements

The authors wish to thank Ministry of Science & Technology, Ministry of Health, Radiation Protection & Nuclear Safety Agency, Vietnam Atomic Energy Commission for their strong supports during 5 past years. We also want to express our gratitude to

IAEA and other international organizations for improving QA of radiotherapy in Vietnam through many technical cooperation activities in this field. The active participation of the radiotherapy departments in the QA programme is appreciated greatly.

References

[1]. DLVN 40 - 1999, Cobalt-60 teletherapy equipment- Methods and means of verification, Vietnam Directorate of Standard and Quality.

[2]. Guidelines for the Preparation of a Quality Manual for External Audit Groups on Dosimetry in Radiotherapy, IAEA, Draft 1997.

[3]. Absorbed Dose Determination in Photon and Electron Beams, IAEA TRS 277.

[4]. TLD Postal Dose Quality Audit Service for External Radiotherapy, DOLP.009, Draft 1998.

THE DISTRIBUTION OF DOSE -EFFECT OF DICENTRIC ABERRATIONS INDUCED IN LYMPHOCYTES EXPOSED TO LOW DOSE RATE OF GAMMA RAYS

Tran Que, Nguyen Thi Kim Anh, Hoang Hung Tien, Ha Thi Ngoc Lien
Pham Ngoc Duy and Nguyen Van Kinh

Nuclear Research Institute, Dalat, Vietnam

Explanation of Some Specific Terms

ADN: axit deoxiribonucleic
Chromosome: Nhiễm sắc thể, tồn tại 2 trạng thái: Thể 1 và thể đôi.
Chromatid: Một nửa của nhiễm sắc thể đôi, là phiên bản của nửa kia của nhiễm sắc thể
Chromosome aberration (CA): Sai hình nhiễm sắc thể
Chromosome finger: Phần mềm phân tích sai hình nhiễm sắc thể tự động
Chromatid break: Đứt gãy nhiễm sắc tử
Mitose: Phân bào nguyên nhiễm
Mitotic index (MI): Chỉ số phân bào nguyên nhiễm
PCC (Premature Chromosome Condensation): Kỹ thuật ngưng kết chromosome
RBE (Relative Biological Efficiency): Hiệu suất sinh học tương đối
Chromosome finder: Phần mềm phân tích sai hình nhiễm sắc thể tự động.
BAT (Biological Assessment Tool): Chương trình quản lý y tế các sự cố phóng xạ.

Abstract: In common with affirmation on the optimal properties of lymphocyte's chromosome aberrations in biodosimetry, the limit of the technique of chromosome aberration's analysis such as numbers of metaphase and time of cell culture are overcome by the automatic analysis system and PCC cell culture technique. Biodosimetric technique was used to estimate the aspects of radiation risks on the World. The low dose rate and low doses are specific characteristic of radiation sources used in industry and hospitals, biodose assessment in these cases depended on the calibration curves of dose-effect relationships at low dose of low dose rate source. The calibration of dose-effect distribution curve is an important mission of biodosimetry recommended by IAEA.

Gamma rays with dose rate 125 mGy/h were used to investigate. Five combinations of blood samples consisted 6 points per combination were exposed to doses 0; 0.1; 0.2, 0.3, 0.4 and 0.5Gy. Thermal Light Dosimeters were contacted to everyone blood sample for dosimetry. The data presented the frequencies of Dicentric aberration and Fragment aberrations detected in 30 samples of five combinations in the range of 0Gy; 0.1Gy; 0.2Gy; 0.3Gy; 0.4Gy and 0.5Gy. The distribution curve of response dose-effect related to general square equation $y = \alpha D + \beta D^2 + C$ with relative coefficiency $r(y,z) = 0,985 \pm 0,005$. The experimental coefficiencies of genaral equantion were $\alpha = (0,492 \pm 0,151).10^{-2}$. Gy^{-1}; $\beta = (3,054 \pm 0,417).10^{-2}$. Gy^{-2}. The special equation of distribution curver was $Y = 0,492D + 3,054D^2 + C$.

Introduce

The Co-ordinate Research Program on the Use of chromosome aberration analysis in radiation protection was initiated by the IAEA in 1982 with the aim of encouraging

and expanding the use of chromosome aberration analysis for dose assessment as a complement to routine physical dosimetry. Along with affirmation on the role of chromosome aberration analysis in biodosimetry, the ranges of metaphase amount and time of data reading were rub out by FISH technique (basic of automatic analysis) and PCC technique (to shorten the cell culture time). The application of Biodosimetry and Radiation Casualty Management Software (BAT) and Chromosome Finder Software was the new progress on technique and the role of biodosimetry. We can acknowledge the great distribution of biodosimetry such as an important role to settle the problems on health safety, radiation protection and the bad public opinions. A request on medical management after radiation risks was enforced at Vietnam, but some mistakes on using the clinical criterions lead to alarming of victims and to disturbance of public opinion. Along with the developing of radiation sources in industry and medicine, the solutions to make sure the public safety are the head mission of the radiation sources. Biodosimetry was considered the most effective solution to estimate the source risks in any case. The calibration curves of dose-effect relationships at low dose of low dose rate sources were the tools of biodosimetry and medicinal management of the low radiation sources. There were some radiation risks at Vietnam, the biodosimetric results at Biodosimetric Laboratory of Nuclear Research Institute were presented and contributed in the evaluation of radiation protection at there. The objective of this investigation was obtained more experimental data for biodosimetry in future. The calibration curve of dose-effect relationships at low dose in the range 0-0.5Gy of low dose rate sources in 125 mGy/h were a mission of biodosimetry and radiation protection at Vietnam Atomic Energy Commission also Nuclear Research Institute.

Object and Method

1. OBJECTS

- Five blood samples (5 combinations) from healthy donors who were not yet contact to radiations and passed chromosome test with dicentric frequency 0/1000 metaphases. The blood samples with heparin were stored in 4oC before exposing.

- The Cobal (Co^{60}) source with activity 592 Ci (9/1985), dose rate 125 mGy/h at Department of Radiation Protection, Nuclear Research Institute was used to expose.

2. METHODS

2.1. Exposing and Dose Assessments

Six small blood bottles (1 ml blood) contact to TLD dosimeter per combination were used to expose. The range of doses was 0, 0.1, 0.2, 0.3, 0.4 and 0.5Gy. The absorbed doses of every point were presented by TLD measurements contacted in bottles. Thirty points (6 points per combination) were presented.

2.2. Lymphocytes Culture

The exposed blood samples were cultured in standard medium with F_{10} (Diffco), fetal calf serum (Diffco), Phytohemaglutinine (Sigma), kanamicine and L-glutamine. IAEA protocol for biodosimetry was used to culture.

2.3. Microscope Slide

- *Fixing lymphocytes:* After 46 hours in incubator, the cultures were added 60 µl colchicine (160 µg/ml)/bottle, the cultures had to fixed at 48 hours. Centrifuge at 1500

rpm/15 minutes, take out liquid, put KCl (5.6 g/l), mix well and keep in water batch 37oC/20 minutes. Centrifuge at 1500 rpm/15 minutes. Take out liquid, put cacnoa (3 methanol : 1 acid acetic), mix lightly and centrifuge again. Repeat 3 times with cacnoa. Keep the cell in 2 ml cacnoa, mix softly and store in 4oC for sliding.

- *Sliding*: Take the fixing cell in cacnoa by pasteur pipette, drop on clean slide covered by cacnoa, put it in space of slide machine 65oC/100s. Write marks and immersed it in ethylic 70%/10 minutes. Change slides to standard gemmsa solution/20 minute, take out and clean through system water and dry. Test and cover slides by UKITT mounting and lament.

2.4. Chromosome Aberrations Analysis

- Using Savage theory for classifications and analyzing chromosome aberrations in all series.

- Using Nikon microscope eclipse 80i and digital photograph for chromosome aberration analyze.

- The data presented all classification and frequencies of chromosome aberrations of all 30 points (five combinations).

2.5. The Experimental Distribution Dose -effect Curve

- Fixing the equation of general experimental distribution curve of dose-effect: The equation of general experimental distribution curve of dose-effect depended on the value of line relative coefficiencies or square relative coefficiency.

- Fixing the calibration equation of experimental distribution dose-effect curve: The experimental recurrent coefficiencies were determined by solving the general distribution equation with the experimental data dose (Gy) – effect (frequencies of dicentric aberrations).

Results and Discussion

1. Effect of Gamma Rays To Mitotic Index (MI)

MI = % mitose (ΣM)/cell (ΣTB). The mitotic index was analyzed in all thirty samples (five combinations) in the range of doses 0-0.5Gy. The correlation between MI (%) and dose (Gy) presented follow: 4.312%±0.085% at 0Gy; 4.344%±0.064% at 0.1Gy; 4.256%±0.178% at 0.2Gy; 4.335%±0.096% at 0.3Gy; 4.187%±0.133% at 0.4Gy and 4.113%±0.111% at 0.5Gy, these results showed that the doses in the range 0 to 0.5 Gy were not influenced to mitotic index. Gamma ray in dose rate 125 mGy in range 0.1 Gy to 0.5 Gy were not decreased lymphocyte's division.

2. The Creating of Chromosome Aberrations In Lymphocytes Exposed To Gamma Rays In Low Dose Rate

- *Types of Chromosome Aberrations:* There were no dicentric aberrations in control samples. Dicentric aberrations and fragments were detected in all samples exposed to doses from 0.1 Gy to 0.5 Gy.

- *Frequencies of Chromosome Aberrations:* The data presented the difference on frequencies of dicentric aberrations and fragments among doses in the range 0 to 0.5 Gy. The frequencies of dicentric aberrations increased with doses.

- *Relative Biological Efficiency:* RBE can be considered in terms of effect per unit dose, I,e. the ratio of the effect produced by a particular dose of the test radiation to the effect produced by the same dose of the reference radiation. RBE = f_x/f_γ with f_x: frequency of dicentric detected by D Gy of investigator source and f_γ: frequency of dicetric produced by D Gy of 150 mGy/h gamma rays. The correlative values of dose – RBE were 0.1 Gy –0.703; 0.2 Gy – 0.664; 0.3 Gy – 0.644; 0.4 Gy – 0.632 and 0.5 Gy – 0.624. The difference of RBE values in range 0.1 Gy to 0.5 Gy had the evidence above, these results proved that dicentric aberrations can produced in all doses in the range 0.1 Gy to 0.5 Gy of gamma rays 125 mGy/h. The data showed a decrease of RBE follow increase of dose, these reflected correctly to dose rate of investigator source (125 mGy/h) lower than dose rate of control source (150 mGy/h).

3. The Experimental Curve of Distribution Dose-effect

3.1. Relationship Coefficiencies, General Distribution Equation of Dose-effect

- *The Linear Relationship Coefficincies Of Distribution Dose –effect:* The general equation of the distribution dose-effect will be decided by the relationship coefficiencies implied linear or square. The line relationship coefficiency $r(y,d) = [(\sum_i^n DiYi - n \cdot D \cdot Y)] / [(\sum_i^n Di^2 - D^2)^{1/2} \cdot (\sum_i^n Yi^2 - Y^2)^{1/2}]$, in this formula D-average obsorbed dose, y-average frequency of dicentric, Di-obsorbed dose at point i and yi –frequency of dicentric at point i, n-number of points. The linear relationship coefficiencies of five combinations were $r_a(y,d) = 0.985$; $r_b(y,d) = 0.986$; $r_c(y,d) = 0.983$; $r_d(y,d) = 0.987$ and $r_e(y,d) = 0.954$. The average linear relationship coefficiency was $r(y,d) = 0.979 \pm 0.014$.

- *The Square Relationship Coefficiencies Of Distribution Dose-effect:* The square relationship coefficiencies of distribution dose-effect $r(y,z) = [(\sum_i^n ZiYi - n \cdot Z \cdot Y)] / [(\sum_i^n Zi^2 - Z^2)^{1/2} \cdot (\sum_i^n Yi^2 - Y^2)^{1/2}]$, in this formula $Z = D^2$, Z-average square obsorbed dose, y-average frequency of dicentric, Di-obsorbed dose at point i and yi –frequency of dicentric at point i, n-number of points. The square relationship coefficiencies of five combinations were $r_a(y,z) = 0.991$; $r_b(y,z) = 0.984$; $r_c(y,z) = 0.989$; $r_d(y,z) = 0.979$ and $r_e(y,z) = 0.980$. The average square relationship coefficiency was $r(y,z) = 0.985 \pm 0.005$.

- *The General Equation Of Distribution Dose –effect:* The average square relationship coefficiency of five combinations was nearly more 1 than the average linear relationship coefficiency of five combinations, the general equation of distribution dose-effect was correctly to $y = \alpha D + \beta D^2 + C$.

3.2. Experimental Recurrent Equation of Distribution Dose-effect

The experimental recurrent equation of distribution dose-effect was determined by considering the experimental recurrent coefficiencies of the general equation of distribution dose-effect. The square equation $y = \alpha D + \beta D^2 + C$ can write in linear form with $z = (y_i - C) / Di = \alpha + \beta D$ and the coefficiencies $\alpha = [\sum[(yi - C)/Di] - \beta\sum Di] / n$; $\beta = \{\sum(yi - C) - [\sum Di \cdot \sum[(yi -C)/Di]] / n\} / [\sum Di^2 - (\sum Di \cdot \sum Di)/n]$. In these Yi(%) – frequency of dicentric at obsorbed dose Di(Gy); C – control frequency of dicentric; n – number of point.

The experimental recurrent coefficiencies from solving general equation $y = \alpha D + \beta D^2 + C$ were $\alpha_a = 0{,}393 \cdot 10^{-2}.Gy^{-1}$; $\alpha_b = 0{,}585 \cdot 10^{-2}.Gy^{-1}$; $\alpha_c = 0{,}340 \cdot 10^{-2}.Gy^{-1}$; $\alpha_d = 0{,}707 \cdot 10^{-2}.Gy^{-1}$; $\alpha_e = 0{,}435 \cdot 10^{-2}.Gy^{-1}$ and $\beta_a = 3{,}628.10^{-2}.Gy^{-2}$; $\beta_b = 2{,}789.10^{-2}.Gy^{-2}$;

$\beta_c = 3{,}303.10^{-2}.Gy^{-2}$; $\beta_d = 2{,}577.10^{-2}.Gy^{-2}$; $\beta_e = 2{,}972.10^{-2}.Gy^{-2}$. The private equation of five combinations presented follow: $Y_a = 0{,}393D + 3{,}628D^2 + C$; $Y_b = 0{,}585D + 2{,}789D^2 + C$; $Y_c = 0{,}340D + 3{,}303D^2 + C$; $Y_d = 0{,}707D + 2{,}577D^2 + C$ và $Y_e = 0{,}435D + 2{,}972D^2 + C$. The experimental recurrent equation of distribution dose-effect was $Y = 0{,}492D + 3{,}054D^2 + C$.

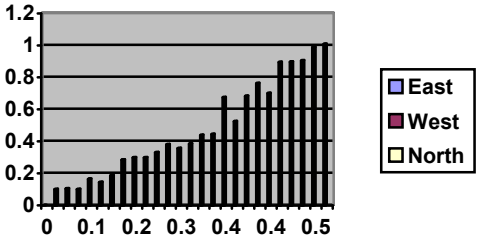

Diagram of the experimental dose-effect distribution

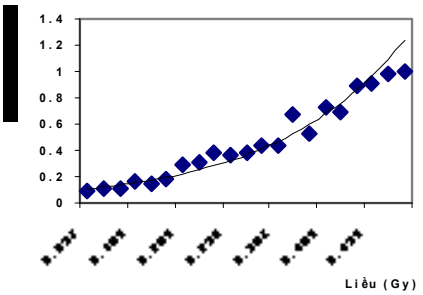

The calibration curve of the experimental dose-effect distribution

All the linear coefficiencies were below 1 and there was according to the Tranque data with calibration of gamma rays in dose rate 150 mGy/h. All the square coefficiencies were bigger than 2, it meaning that almost double strand breaks (DSB) lead to dicentrics were produced from indirect DSB. Bender, Preston, Savage proved that the indirect DSB were produced from unrepair or miss repair of ADN base damages. Natarajan, Preston, Sankaranarayanan, Van Zeland showed that the ratio α/β depended on LET (linear energy transfer), the observed experimental coefficiencies were according to low LET radiation. This result was also according to the reports of calibration curves at Biodosimetry group, Nuclear Research Institute.

Conclusion

1. Gamma rays in dose rate 125 mGy/h produced chromosome aberrations in the range of doses from 0.1Gy to 0.5Gy and there were increased follow doses. The Relative Biological Efficiencies in the range of doses from 0.1 Gy to 0.5 Gy were according to low LET radiation.

2. The generation equation of the experimental recurrent distribution dose-effect with Co60 activity 592 Ci (9/1985), dose rate 125 mGy/h was $y = \alpha D + \beta D^2 + C$, the square relationship coefficiencies was $r(y,z) = 0{,}985 \pm 0{,}005$ ($z = d^2$).

3. The calibration equation of the experimental recurrent dose-effect distribution with Co^{60} activity 592 Ci (9/1985), dose rate 125 mGy/h was $y = 0{,}492D + 3{,}054D^2 + C$, the experimental recurrent coefficiencies $\alpha = 0{,}492 \pm 0{,}151 \,.\, 10^{-2}\, .Gy^{-1}$; $\beta = 3{,}054 \pm 0{,}417 \,.\, 10^{-2}\, .Gy^{-2}$.

References

[1]. Bauchinger M. (1983), "Microdosimetric aspects of the induction of chromosome aberrations Radiation induced chromosome damage in Man". Alan R. Liss, Inc.,1-22

[2]. Bender M. A. et al. (1988), "Current status of cytogenetic procedures to detect and quantity previous exposures to radiation". Mutation research 196, 103-159.

[3]. Camparoto ML, Ramalho AT, Natarajan AT, Curado MP and Sakamoto-Hojo ET (2003), "Translocation analysis by the FISH-painting method for retrospective dose reconstruction in individuals exposed to ionizing radiation 10 years after exposure". Mutat Res 530:1-7.

[4]. Dugle DL, Gillespie CJ, Chapman JD. (1976), DNA strand breaks, repair, and survival in x-irradiated mammalian cells. Proc Natl Acad Sci U S A.73(3):809-12

[5]. Edwards A. A, D C Lloyd, P.R. Martin, R.E. Berdychevski, U. Subramanian, W.F. Blakely, and P.G.S. Prasanna, (2007), "Sample Tracking in an Automated Cytogenetic Biodosimetry Laboratory for Radiation Mass Casualties", Radiat Measurment. 1119–1124.

[6]. Fabry L. et al. (1985), "Induction of chromosome aberrations in Go human lymphocytes by low dose of ionizing radiations of different quality". Radiation Research 103, 122-134.

[7]. Fenech M and Morley AA (1985), "Measurement of micronucle in lymphocytes". Mutat Res 147:29-36

[8]. IAEA - International Atomic Energy Agency (1986), Biological Dosimetry Chromosomal Aberration in Analysis for Dose Assessment. Publication n. 260, Vienna

[9]. IAEA biodosimetry training course lectures at RERF, Hiroshima, Japan, Oct. 1997.

[10]. IAEA - International Atomic Energy Agency (2001) Cytogenetic Analysis for Radiation Dose Assessment. Technical Report Series n. 405, Vienna

[11]. IAEA biodosimetry training course lectures at KIRAM, Seoul, Korea, 2007.

[12]. Iwashita J, Kodama S, Nakashima M, Sasaki H, Taniyama K, Watanabe M., (2005), Induction of micronuclei in CHO cells by bleomycin but not by X-irradiation is decreased by treatment with HMG-CoA reductase inhibitors. J Radiat Res (Tokyo). pp 191-195.

[13]. Hamadeh HK, Trouba KJ, Amin RP, Afshari CA, Germolec D, (2002), Coordination of altered DNA repair and damage pathways in arsenite exposed, Toxicol Sci. 2002 Oct; 69(2):306-16

[14]. Hayata I., (2005), "Chromosomal mutants by low dose radiation vs. those by other mutagenic factors", Elservier, International Congress Series1276,17-20.

[15]. Lloyd DC, Edwards AA and Prosser JS (1986) Chromosome aberrations induced in human lymphocytes by *in vitro* acute X and gamma radiation. Radiat Prot Dosim 15:83-88.

[16]. Lloyd D. C. (1990), "Biological dosimetry by cytogenetic methods". I Reunion Internacional Sobre Dosimetria Biologica, Madrid, 59-73.

[17]. Lloyd DC, Edwards AA, Moquet JE and Guerero-Carbajal YC (2000), "The role of cytogenetics in early triage of radiation causalities". Appl Rad Isot 52:1107-1112

[18]. Lucas JN (1997), "Dose reconstruction for individuals exposed to ionizing radiation using chromosome painting". Radiat Res 148:33-38.

[19]. MMRC-Handbook (2003), Medical management of radiological casualties, Military Medical Operations, Armed Forces Radiobiology Research Institute Bethesda, Maryland 20889-5603.

[20]. Obe G. and B. Beck (1984), "Human peripheral lymphocytes in mutation research. Mutation in man", Springer-Verlag, 177-197.

[21]. Parveen, B., Preston, D. L., Doody, M. M., Hauptmann, M., Kampa, D., Alexander, B. H., Petibone, D., Simon, S. L., Weinstock, R. M., Bouville, A., Yong, L. C., Freedman, D. M., Mabuchi, K., Linet, M. S., Edwards, A. A., Tucker, J. D. and Sigurdson, A. J., (2007), " Retrospective Biodosimetry among United States Radiologic Technologists". *Radiat. Res.* 167, 727–734.

[22]. Preston R. J. (1984), "Radiation damage to DNA and its repair in the formation of chromosome aberrations", *Radiation induced chromosome damage in man*, Alan R. Liss, Inc., New York, pp 111-126.

[23]. Preston R. J. (1990), "Mechanisms of induction of chromosomal alterations and sister chromatid exchanges: presentation of genaralized hypothesis"*, In: A. P. Li and R. H. Heflich (ends) Genetic toxicology: A treatise. Telford Press, New York, in press.*

[24]. 24. Preston R. J. (1990), "Biological dosimetry: Mechanistic concepts", *I reunion internacional sobre, Dosimetria biologica, Madrid*, pp 21-34.

[25]. Sankaranarayanan K. (1982), "Genetic effects of ionizing radiation in multicelular eukaryotes and the assessment of genetics radiation hazards in Man". Elsevier Biomedicalpress. Amsterdam.

[26]. Sasaki M.S. (1983), "Use of lymphocyte chromosome aberrations in biological dosimetry: Possibility and limitations". Radiation induced chromosome damage in Man. Alan R. Liss, Inc., 585-604.

[27]. Savage J. R. K. (1976), "Classification and relationships of induced chromosomal structural changes", *Journal of medical genetic (13)*, Annotation, pp 103-122.

[28]. Screedevi B. et al. (1993), "Radiation induced chromosome aberration yields following an accidental non - uniform exposure". Radiation protection dosimetry vol. 50, 45-49.

[29]. Stephan G. and Oestreicher U., (1993), "Chromosome investigation of individuals living in areas of Southern Germany contaminated by fallout from the Chernobyl reactor accident", *Mutation research (319)*, Elservier, 189-196.

[30]. Tao Jiang, Isamu Hayata, et al., (2000), Dose effect ralationship of dicentric and ring chromosomes in lymphocytes of individuals living in the high background radiation area in China, J.Radiat. Res., 41, 63-68.

[31]. Tran Que, Hoang Hung Tien, Hoang Van Nguyen, Pham Ba Phong (2000), "Studies on epidemiology of chromosome aberrations induced in human lymphocytes for indicating contamination of radiation and radiomimetic chemical agents", *The effects of low and very low doses of ionizing radiation on human health, World Council of Nuclear Workers.* Elservier. 373-378.

[32]. 32. T. Que, H. T. T. Loan, T. D. Dat, P. V. Lap, P. B. Phong (2004), "Ionizing radiation or chemical mutagen induced chromosome aberration in lymphocytes from epidemiological data at Vietnam", *International Journal Low Radiation, Volum 1, No3. 309-317.*

[33]. 33. Voisin P, Benderitter M, Claraz M, Chambrette V, Sorokine-Durm I, Delbos M, Durand V, Leroy A and Paillole N (2001), "The cytogenetic dosimetry of recent accidental overexposure". Cell Mol Bio 47:557-564.

[34]. 34. Voisin P, Barquinero F, Blakely WF, Lindholm C, Lloyd DC, Luccioni C, Miller S, Palitti F, Prasanna PGS, Stephan G, Thierens H, Turai I, Wilkinson D, Wojcik A. (2002), "Towards a standardization of biological dosimetry by cytogenetics". *Cell Mol Biol.* 2002;48:501–4.

[35]. 35. Voisin P, Roy L, Benderitter M., (2004), Why can't we find a better

biological indicator of dose?, Radiation Protection Dosimetry, Vol. 112, No4: 465-469.

[36]. 36. Yamada K, Kakinuma K, Tateya H, Miyasaka C. (1992), "Development of an instrument for chromosome slide reparation". *J Radiat Res.* 242–249.

[37]. 37. Waselenko JK, MacVittie TJ, Blakely WF, Pesik N, Wiley AL, Dickerson WE, Tsu H, Confer DL, Coleman NC, Seed T, Lowry P, Armitage JO, Dainiak N. (2004), "Medical management of the acute radiation syndrome": Recommendations of the Strategic National Stockpile Radiation Working Group. *Annals of Internal Medicine.* 2004;15:1037–1051.

[38]. 38. Zombori P., Buglova E. (2007), IAEA role in response to radiation emergencies: IAEA response assistance Network (RANET), IAEA regional training course on biological dosimetry dose assessment immediately and retrospectively to an occupational and accidental overexposure, Soul, Republic of Korea.

[39]. 39. Xiao Y, Natarajan AT. (1999), Analysis of bleomycin-induced chromosomal aberrations in Chinese hamster primary embryonic cells by FISH using arm-specific painting probes. Mutagenesis, pp 357-364

[40]. 40. Wilding CS, Relton CL, Rees GS, Tarone RE, Whitehouse CA, Tawn EJ.(2005), DNA repair gene polymorphisms in relation to chromosome aberration frequencies in retired radiation workers. Mutat Res. 570(1):137-45.

1.8 - Radiation Technology

STUDY ON THE GAMMA IRRADIATION METHOD FOR FORMATION OF BIODEGRADABLE FILMS APPLIED IN PACKAGING AND PRESERVATION OF SOME PRELIMINARY PROCESSED AGRICULTURAL PRODUCTS

Tran Bang Diep[1], Le Thi Dinh[1], Nguyen Van Binh[1], Nguyen Quang Long[1]
Nguyen Van Toan[2], and Tran Minh Quynh[1]

Hanoi Irradiation Center, Minh Khai - Tu Liem - Hanoi
Institute for Nuclear Science and Technology, VAEC

Abstract: In this study, the different compositions of starch and polyvinyl alcohol (PVA) were irradiated by gamma radiation for preparation of biodegradable packaging films. The intact and smooth films were formed by irradiation treatment. The gelation of the starch-based films was significantly enhanced by radiation cross linking. Gel fractions of the irradiated films increased with the increasing of radiation dose from 5 to 15 kGy, whereas their enzymatic degradation rate and water vapor transmission rate decreased. The mechanical properties of these cross linked films were also measured and compared to PE films with the same dimension. The results indicated that the radiation treatment has induced the cross linking between starch and PVA and thus improved the functional properties of the conventional starch-based films.

Keywords: Biodegradable packaging film; Starch-based film; Irradiation; Mechanical Properties;Enzymatic degradation.

Introduction

The current global consumption of plastics is more than 200 million tones, with an annual grow of approximately 5%. Petrochemical-based plastics such as polyethylene terephthalate (PET), polyvinylchloride (PVC), polyethylene (PE), polypropylene (PP), polystyrene (PS) and polyamide (PA)... have been increasingly used as packaging materials, because of their availability in large quantities at low cost and favourable functionality characteristics such as good tensile and tear strength, good barrier properties to O_2 and aroma compounds and heat seal-ability. On the contrary they have a very low water vapour transmission rate and most importantly they are totally non-biodegradable, and therefore lead to environmental pollution, which poses serious ecological problems. For these reasons, the development of novel plastics for packaging that could be degraded by microorganisms in soil and seawater has recently been emphasized.

Starch is considered as one of the most promising natural polymers for packaging application because of its low cost, renewability, biodegradability, and its envisaged great potential for food packaging edible films. Since 1970 starch was incorporated into synthesized polymer matrix and in the past decades several efforts have been made to convert starch into a thermoplastic material. However, there are some limitations in developing starch-based products due to its poor mechanical properties and high moisture sensitivity, so polysaccharide-based films have not found extensive applications in the food industry yet. Polyvinyl alcohol (PVA) is a versatile polymer with many industrial applications, and it may be the only synthesized polymer,

whose backbone mainly composed of C-C bond, that is absolutely biodegradable. PVA samples with average molecular weights as high as 100,000 have been reported to be completely degraded by soil bacteria, especially by Pseudomonas.

Various physical methods have been developed to improve the mechanical properties of films including a dehydrothermal treatment, ultraviolet, and a gamma irradiation. Of these methods, a gamma irradiation has become well known as a very convenient tool for modification of polymer materials through a crosslinking, grafting and degradation techniques. In this study, the different compositions of starch and PVA were irradiated by gamma radiation for preparation of biodegradable packaging films. Glycerol and polyethylene glycol (PEG) were selected also . Gel fractions, mechanical properties, water vapor transmission rate and enzymatic degradation rate of starch-based films were investigated.

Radiation crosslinked starch-based film

The experimental solution containing 5% PVA, 0.2% PEO, 2.5% starch (or modified starch) was heat at 80^0C for 2 h to form homogeneously mixture. 5 ml of 1% chitosan solution in 1% acetic acid was blended and heated for 30 minutes. 0.5 ml glycerol and PEG was added as plasticizer. The total compositions were adjusted until pH 6. The films were prepared according to the casting technique, by dehydrating 160 ml of the film forming solution over a plastic mould (10x20 cm) in vacuum oven at 50^0C for 8 h. After that, wet starch-based plastic films (humidity about 15%) were irradiated at range doses from 0-15 kGy by Co-60 source at Hanoi Irradiation Center. After irradiation, the starch-based plastic films were dried and kept in desiccators for the next experiments.

In order to elucidate the crosslinking reaction between starch and PVA under irradiation, gel fraction of starch-based plastic film was determined. Starch-based plastic films were put into stainless net of 200 meshes and immersed in distilled water for 48 h at room temperature to extract the sol part. After that, the samples were dried to constant weigh at 50^0C. Gel fraction was calculated as:

Gel fraction (%) = (W_g/W_0) x 100

Where W_g is the weight of dry gel after extraction and W_0 is the inital weight of dry films.

Gel fraction of starch-based plastic films at different irradiation doses was showed in Fig. 1. The gelation of the starch-based films was significantly enhanced by radiation cross linking. Gel fractions of the irradiated films increased with the increasing of radiation dose from 5 to 15 kGy. The film created

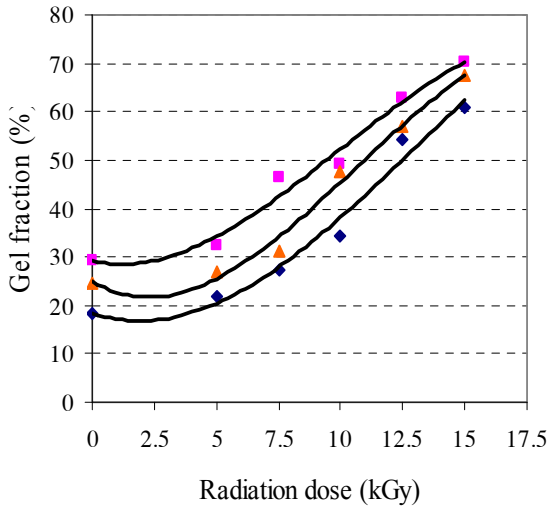

Fig. 1. Gel fraction of starch-based plastic films at different irradiation doses (♦ PVA/ PEO/ chitosan film, ■ PVA/PEO/Starch/chitosan film and ▲PVA/PEO/Modified Starch/chitosan film)

from the composition containing starch (or modified starch) has higher gel fraction compare with non-starch film.

Mechanical properties of starch- based plastic films

Tensile strength and the percent elongation each film were measured using Lloy Instrument (Enghland) according to ASTM-D 638. The results showed that tensile strength of all irradiated starch-based plastic films were lower than that of PE films. The results are similar in case of percent elongation of irradiated starch-based plastic films. However, tensile strength of starch-based plastic films treated at dose of 12.5 kGy is 14.07 MPa and percent elongation is 75,4%. These values were insignificantly lower than that of used PE films so investigational irradiated starch-based plastic films have the requested mechanical properties for packaging ready-to-eat fruits.

Water vapor transmission rate (WVR) of starch-based plastic films

Starch films have been reported to be ineffective moisture barriers due to their hydrophilic nature. Therefore, to improve the water-resistance properties of the starch films, the gamma irradiation treatment were implemented in this study. Water vapor transmission rate (WVR) of the film was measured according to the ASTM E96-95 with some modifications. The results in Fig. 2. show that WVR of the all starch-based film decreased significantly by irradiation. WVR of starch-based plastic films are not so high compare with other membranes for preservation and suitable for purpose of this study due to resistance water evaporability of ready-to-eat fruits.

Enzymatic degradation rate of starch-based plastic films

Fifty milligrams of film was hydrolyzed in a 50 ml tube with 16 ml of an acetate buffer (0.05M; pH = 4.8). After a 10 min pre-equilibration at 50^0C in an incubator shaker, 10 µl of Tecmamin was added. The different film- enzyme solution was incubated at 50^0C with 150 rpm by a rotary shaker. At least 3 film samples were used for every one data point. After predetermined incubation periods, the film was taken out, washed thoroughly with distilled water, and freeze – dried to a constant weight in vacuum. The enzymatic degradation rate was evaluated by weight loss value (mg) per unit area (cm^2) of film sheet with incubation time.

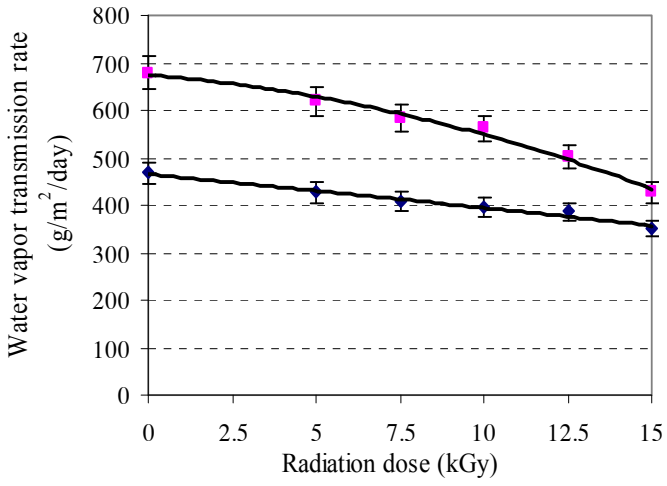

Fig. 2. Effect of irradiation doses to water vapor transmission rate of starch-based plastic films (♦ PVA/PEO/Starch/chitosan film and ■ PVA/PEO/Modified Starch/chitosan film)

Enzymatic degradation rate of 2 kinds of starch-based plastic films at dose of 12.5 kGy was showed in

Fig. 3. and enzymatic degradation rate of PVA/PEO/Starch/chitosan film at different irradiation doses was showed in Fig. 4.

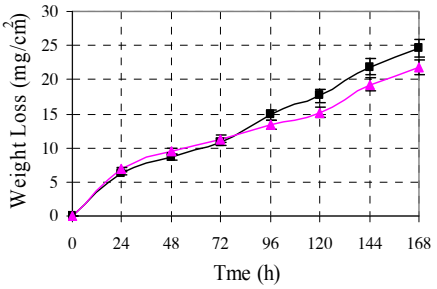

Fig. 3. Enzymatic degradation rate of starch-based plastic films at dose of 12.5 kGy (▲PVA/PEO/Starch/chitosan film, ■ PVA/PEO/Modified Starch/chitosan film)

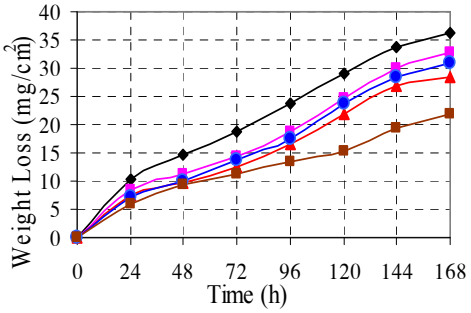

Fig. 4. Enzymatic degradation rate of PVA/PEO/Starch/chitosan film at different doses (♦ 0 kGy, ■ 5 kGy, ●7.5 kGy, ▲10 kGy, ■12.5 kGy)

Conclusion

The gelation of the starch-based films was significantly increased by radiation crosslinking. Gel fractions of the irradiated films increased with the increasing of radiation dose from 5 to 15 kGy, whereas their enzymatic degradation rate and water vapor transmission rate decreased. Mechanical properties of starch-based plastic films treated at dose of 12.5 kGy were insignificantly lower than that of used PE film with the same dimension so irradiated starch-based films met a demand for packaging ready-to-eat fruits.

References

[1]. C. Jo et al, Radiation Physics and Chemistry, 72(6), 745-750, 2005.

[2]. G. M. Glenn & J. Hsu, Industrial Crops and Products, 7, 37-44, 1997.

[3]. H. Kang et al, Carbohydrate Polymers, 60, 547-551, 2005.

[4]. J. K. Kim, C. Jo, H. J. Park & M. W. Byun, Food Hydrocolloids, 22, 248-254, 2008.

[5]. M. J. Kirwan & J. W. Strawbridge, Food Packaging Technology, 174-240, 2003.

[6]. M. Zhai, F. Yoshii, T. Kume, Carbohydrate Polymers, *52*, 311-317, 2003.

[7]. O. Martin, E. Schwach, L. Averous & Y. Coutrier, Starch, 53, 372-380, 2001.

[8]. R. W. Lenz, Advances in Polymer Science, 107, 1-40. 1993.

[9]. T. Kume, N. Nagasawa & F. Yoshii, Radiation Physics and Chemistry, 63, 625-627, 2002.

Papers Published In Relation To The Project

Màng phân huỷ Sinh học trên cơ sở khâu mạch bức xạ các polysaccharide sử dụng để bao gói rau quả chế biến sẵn. Báo cáo tại hội nghị Khoa học và Công nghệ Hạt nhân toàn quốc lần thứ VIII, Nha Trang, 20-22/2009.

CREATION OF WATER -NUTRIENT ABSORPTION PRODUCT BY GAMMA IRRADIATION

Le Thi Dinh[1], Nguyen Van Toan[2], Tran Bang Diep[1]
Nguyen Van Binh[1] and Hoang Thi Minh[3]

[1]Hanoi Irradiation Centre, [2]Institute for Nuclear Science and Techniques,VAEC
[3]Soil and Fertilizer Institute

Abstract: Water-nutrient absorption materials will be soure keeping and supplying water, nutrient for plants. Therefore efficiency of fertilizer using will be higher and pollution of water source will be decreased. In this study, water - nutrient absorption products created base on radiation crosslinked starch, polyvinylalcohol (PVA) and hydropolyacrilamind (HPA) is introduced. The results showed that swelling of products in water and in nutrient solution is decreased with increasing dose. Swelling of this material is higher than that of AMS-1 produced in Chemical Institute, National Technology and Science Centre that has been commercialized Vietnam. Ability of keeping water in room temperature (about 25^0C), (N, P and K) absorption in nutrient solution and (N, P and K) release in distilled of product were investigated.

Keywords: Irradiation; Radiation crosslinked; Gel fraction; Swelling; Nutrient absorption; Nutrient release.

I. Introduction

Water absorption polymers have been applied widely in agriculture. The field of this research has been developed rapidly. Many kinds of water absorbents such as SAP, Sky-gel, Aqua-sorb etc in USA, England, South Africa, Australia and Japan have been commercialized throughout the wolrd. Up to now, there are not much of studies about production of materials that has characteristic not only with water absorption but also with nutrient carrier. Application of materials having these characteristics will be very useful, because they can keep moisture for soil and supply nutrient for plants. In the VAEI, there are some kinds of radiation crosslinked water absorbents such as Gam.sorb.S. and Gam.sorb.P. In Chemical Institute, National Technology and Science Centre, there is AMS-1 product that has been commercialized in our country. They are water absorbents, but their ability of nutrient carrier has not been investigated. In this study, water-nutrient absorption products created base on radiation crosslinked starch, polyvinylalcohol (PVA) and hydropolyacrilamind (HPA) were investigated.

II. Materials

1. VL2-Product was created with PVA, HPA and starch. The matrix was irradiated with gamma ray at doses of 2.5, 5, 7.5 and 10 kGy in Co-60 source in Hanoi Irradiation Centre.

2. VL4-Product was created with PVA, HPA, starch, $(NH_4)_2SO_4$, KNO_3, and KH_2PO_4. The matrix was irradiated with gamma ray at doses of 2.5, 5, 7.5 and 10 kGy in Co-60 source in Hanoi Irradiation Centre.

3. VL6-Product was created based on VL2 absorbed $(NH_4)_2SO_4$, KNO_3 and KH_2PO_4.

4. AMS-1-Product was supplied by Chemical Institute - National Technology and Science Centre.

5. Murashige & Skoog solution was prepared by method in [2].

6. N, P and K - Portion solution included $(NH_4)_2SO_4$, KNO_3 and KH_2PO_4 with concentration as following:

I: 16.4 mg N -17.7 mg P -68 mg K/l - **II:** 36.4 mg N -37.7 mg P -88 mg K/l - **III:** 56.4 mg N – 57.7 mg P-108 mg K/l - **IV:** 76.4 mg N -77.7 mg P-128 mg K/l - **V:** 96.4 mg N – 97.7 mg P-148 mg K/l

III. Method

1. Swelling S (g/g) and gel fraction G (%)were calculated by methods and equation in [5, 7, 8]

$$S(g/g) = (W_w - W_d)/W_d$$

Whereas: W_w-Mass of wet sample after soaking

W_d-Mass of dry sample after soaking

$$G(\%) = G_d/G_i \times 100$$

Whereas: G_d-Mass of dry sample after soaking

G_i-Mass of initial sample before soaking

2. Keeping water ability of products was determined by following method: soaking 0.2g product VL2, VL4 in 200 ml distilled water until saturated state. Then take products out, weight their mass and keep in room temperature (about 25^0C). After 24, 120, 240, 360 and 480 h weigh their mass and compare with their mass in saturated state respectively.

3. N, P and K absorbed ability of products was determined by Disunphophenic and Vanadomolypdate and flame-able photometer methods in [3].

IV. Results and Discussion

1. Radiation Effect On Swelling of Products

Radiation effect on swelling of VL2 and VL4 products is showed in Fig. 1. The results indicate that swelling of products in distilled water is reduced with increasing dose. The result is same with results of studies of B. Fel and et al, R. A. Wach and et al, L. Q. Cao and et al and N. Nagasawa and et al in production of radiation crosslinked hydrogel from polyvinylalcohol (PVA), polyethylene oxide (PEO), polyvinylpyrrolidone, CMC, starch, CMS and derivatives of CMC [4, 7 and10]. The results also indicated swelling of VL2-product is higher than that of VL4-product. The swelling of Vl2 and VL4 products irradiated with dose from 5 to 10 kGy was lower than that with dose 2.5 kGy but the gel in stable state. This character is useful for absorbing water again.

2. Radiation Effect On Gel Fraction of Products

Radiation effect on gel fraction of VL2 and VL4 products is showed in Fig. 2. The results indicate that gel fraction of products is increased with increasing dose. The result is same with results of studies of B. Fel and et al**,** R. A. Wach and et al**,** L. Q. Cao and et al and N. Nagasawa and et al in production of radiation crosslinked hydrogel from polyvinylalcohol (PVA), polyethylene oxide (PEO)**,** polyvinylpyrrolidone**,** CMC,

starch, CMS and derivatives of CMC [4, 7 and10]. The results also indicated gel fraction of VL2-product is higher than that of VL4-products. Gel fraction of VL2 and VL4 products irradiated with dose 5 kGy is higher than that with dose 2.5 kGy and less than that with dose 10 kGy. The increase of gel fraction is due to the increase density of polymer chain with an increase of radiation dose, thus resulting in higher gel fraction.

3. Investigate Keeping Water Ability of Products

Keeping water ability of VL2 and Vl4 products is showed in Fig.3. The results indicate keeping water ability of both products in room temperature (about 25^0C) is decreased from 24-480 h. After 480 h amount of water residues in products is very little. It indicates there is water transfer permission in products and products can keep water in 480 h.

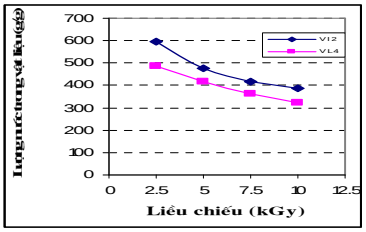

Fig. 1. Radiation effect swelling of products

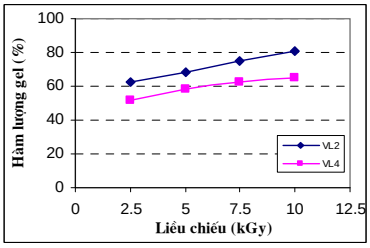

Fig. 2. Radiation effect on gel fraction of products

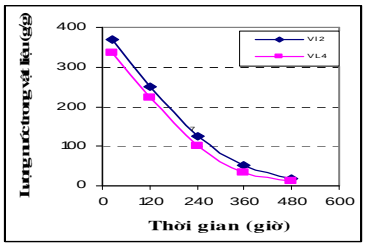

Fig. 3. Ability of water keeping on of products

4. Investigate swelling of products in Murashige & Skoog solution

Swelling of VL2, VL4 and AMS-1 products in Murashige & Skoog solution is showed in table 1. The results indicate that swelling of products less than that in water. Swelling of VL2 and VL4 products in Murashige & Skoog solution is higher than that of AMS -1 product that has been commercialized in our country. The result is same with results of studies of B. Fel and at al., L. Q. Cao and at al. and N. Nagasawa and at al. in production of radiation crosslinked hydrogel from starch, CMC, CMS and derivatives. The swelling of products in 0.9% NaCl is also less than that in water.

Tab 1. Swelling of Products in water and Skoog nutrient solution (g/g)

Solution	**Products**		
	VL2	VL4	AMS-1
Distiled water	47.29 ± 21.91	415.12 ± 19.7	182.72 ± 3.2
Murashige & Skoog	252.32 ±11.32	197.53 ± 7.54	159.13 ± 5.2

5. Investigate N, P and K Absorption Ability of Products In Nutrient Solution

N, P and K absorption ability of VL2-product in nutrient solution is showed in Fig. 4. The results indicate that it is increased with increasing concentration of N, P and K in nutrient solution from (16.4 mgN – 17.7 mgP – 68 mgK/l) to (96.4 mgN - 97.7 mgP – 148 mgK/l). The result is same results of studies of M. S. Chiou and at al. and L. Q. Cao and at al. in production of radiation crosslinked hydrogel from chitosan, CMC PVA, PEO, HPA when the products were absorbed in NaCl solution [7].

6. Investigate (N, P and K) Releasing Ability Of Products

N, P and K releasing ability of VL4 and VL6 products in water is showed in Fig. 5. The results indicate that N, P and K releasing ability of VL4 - product is better than that of VL6-product. N, P and K amount of products is reduced from 24 – 480 h in distilled water.

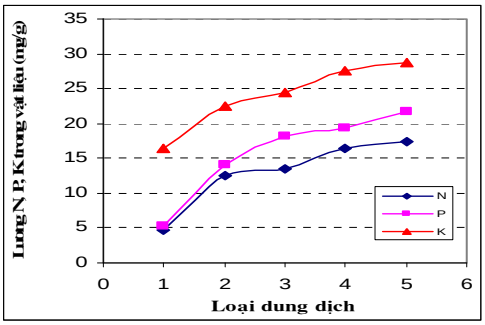

Fig. 4. Ability of N, P and K absorption of products in nutrient solution

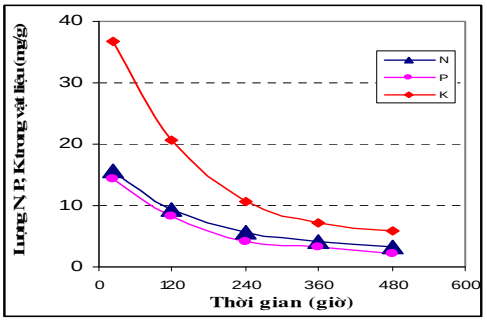

Fig. 5. Ability of N, P and K release of products in water

IV. Conclusion

Formulation of VL4-product and irradiation dose with 5 kGy are suitable for creating water-nutrient radiation crosslinked absorption product by gamma ray irradiation method. Ability of keeping water in room temperature (about 25^0C) and (N, P and K) releasing in distilled water of product is about 480 h.

References

[1]. http://www.phanbonmiennam.com.vn
[2]. B. Fel et al, Applied Polymer Science, vol. 78, 278-283, 2000
[3]. F. Yoshi, R. A. Wach, N. Nagasawa, H. Mitomo, T. Kume, B 208, 320-324, 2003.
[4]. http://msncares.com
[5]. L. Q. Cao, S. Meixu, S. Feig, J. D. Wang,Wiley Interscience, 2392-2397, 2004.
[6]. L. Zhao et al, Carbohydrate Polymers 51, 169-175, 2003.
[7]. M.S. Chiou, H.Y.Li, Pergamon, Chemosphere 50, 1095-1105, 2003.
[8]. N. Nagasawa, T. Yagi, T. Kume, F. Yoshi, Cabohydrate Polymers 58, 109-113, 2004
[9]. R.A. Wach, H. Mitomo, F. Yoshi, T. Kume, Macromol. Mater.Eng, 285-295, 2002.
[10]. R. W. Lenz, Advances in Polymer Science., 107, 1-40. 1993.

Papers Published In Relation To The Project

Nghiên cứu tạo vật lưu giữ nước và giữ dinh dưỡng (N, P, K) bằng phương pháp chiếu xạ gamma. Báo cáo tại hội nghị Khoa học và Công nghệ Hạt nhân toàn quốc lần thứ VIII, Nha Trang, 20-22/2009.

DOSE CALCULATION FOR FOOD IRRADIATION BY UERL-10-15T AT RESEACH AND DEVELOPMENT CENTER FOR RADIATION TECHNOLOGY

Tran Van Hung, Cao Van Chung and Nguyen Anh Tuan

Research and Development Center for Radiation Technology

Abstract: The depth-dose profile and dose uniformity in product irradiated by electron accelerator UERL-10-15T were calculated by using MCNP code and ModeRTL 2.6 software. The irradiation mode and the velocity of the conveyer for individual case were given. In addition, the effect of irradiation product width to dose uniformity, the dose distribution at product edge and the electron, photon spectrum in irradiation product were also studied.

1. Calculation Code

Both MCNP code version 4C and ModeRTL 2.6 software were used to calculate the dose profiles in irradiated product. The results of them have a good agreement with the difference less than 5%.

2. Results

2.1 Depth-Dose and Width-Dose Profiles

The depth-dose and width-dose profiles produced by 10-MeV electron beam normally incident onto the surface of product were calculated by ModeRTL 2.6. The calculated results show in Fig.1.The absorbed dose in depth-dose profile increases from about 23 kGy at the surface of product to a maximum at a matter depth of about 2.7 g/cm^2, before decreasing essentially zero. In case of width-dose profile, it's showed that the absorbed dose symmetric about the middle land of the product and decreasing when attacks the edge of product.

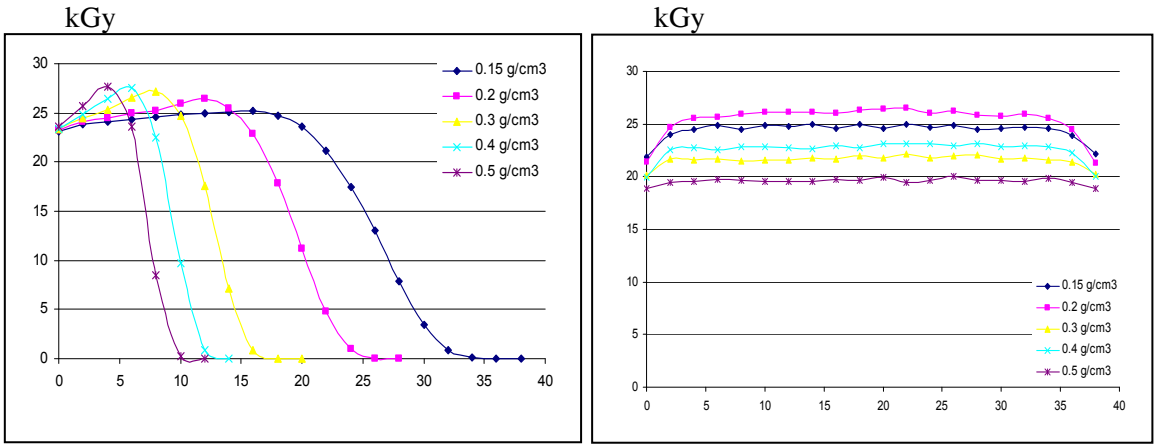

(a) (b)

Fig. 1. Depth-dose (a) and width-dose (b) profile for any densities for electron 10-MeV in matter.

2.2 Dose Uniformity and Optimum Thickness

For single-sided irradiation, the max:min ratio increasing from 1 at surface to less than 1.7 at product thickness about 4.1 g/cm^2, then increasing rapidly when increasing thickness product (Fig.2a).The dose-uniformity in double-sided irradiation product show in Fig.2b, it show that the dose-uniformity is excellent for densities less than 4.5 g/cm^2, and is good in the region between 8.1 and 9.2 g/cm^2.

From the calculation, the optimum thickness follows the power equation:

For single-sided irradiation:

$$d_{opt}(cm) = 8.3562\rho^{-0.9952} \quad (1)$$

For double-sided irradiation:

$$d_{opt}(cm) = 3.5803\rho^{-1.0288} \quad (2)$$

Fig.2 Max:min ratio for single-sided irradiation of matter using 10-MeV electrons

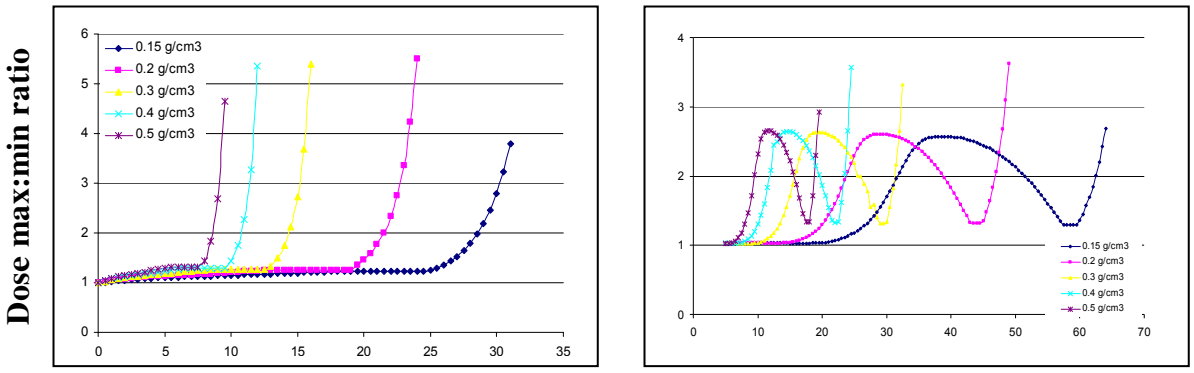

Fig. 2. Max:min ratio for single sided
(a), double-sided (b)irradiation using 10-MeV electrons

2.3 Chosen Irradiation Mode, Average Dose for Particular Product

Choosing between single-side or double-sided irradiation mode appropriate for particular product and correlative average dose show in table 1, 2, 3, 4.

Tab 1. Irradiation mode and average dose for Petri disk

COMPANY	**Irradiated product**	**Density** (g/cm^3)	**Heigh** (cm)	**Single-sided**	**Double-sided**	**Dose** (kGy.mA) (cm/s)	**Dose-demand** (kGy)	**Conveyer's velocity** (cm/s)
NAM KHOA	Petri disk	0.11	44	-	2.02	38.34	18	2.13
HUNG_DL	Petri disk	0.12	23	1.27	1.17	20.51	18	2.31
	Petri disk	0.14	24	1.55	1.29	41.49	18	2.31
BONNIE FARM	Petri disk	0.17	46.5	-	1.49	26.78	18	1.46
HONG-TAM	Petri disk	0.12	29.5	1.79	1.36	42.30	18	2.35

Tab 2. Irradiation mode and average dose for pharmaceutical product and medical herbs

COMPANY	**Irradiated product**	**Density** (g/cm^3)	**Heigh** (cm)	**Single-sided**	**Double-sided**	**Dose (kGy.mA)** (cm/s)	**Dose-demand** (kGy)	**Conveyer's velocity** (cm/s)
DUC THO SANH	MH	0.31	29	-	-	-	10	-
DN DUONG	MH	0.37	24	-	2.02	20.52	10	2.05
HOA T DUONG	MH	0.40	28	-	-	-	10	-
Pharmacy – Q3	MH	0.37	22	-	1.35	22.37	10	2.24
Pharmacy – TW25	Agar	0.25	22	-	-	-	10	-
	Uphagel	0.47	22	-	-	-	10	-
	Rheumatin	0.29	22	-	AL	-	10	-
BINH MINH	HTP	0.37	23.5	-	1.69	20.91	10	2.09
BEPHARCO	EDNYT	0.13	47	-	AL	-	10	-
	MH	0.13	12	1.12	1.05	18.57	10	1.86
HUNG PHAT	Clover	0.29	35.5	-	-	-	10	-
	Clover	0.26	28	-	1.89	25.35	10	2.54
VAN AN	ĐND	0.24	28	-	AL	-	10	-
MEDIPLANTEX	Antesik	0.45	23	-	-	-	10	-
Hau Giang Pharmacy	KTT	0.46	27	-	-	-	10	-
	Chiliver	0.37	34	-	-	-	10	-
	MH	0.52	32.5	-	-	-	10	-
NATA-HL	MH	0.25	21	-	AL	-	10	-

Tab 3. Irradiation mode and average dose for dried food

COMPANY	**Irradiated product**	**Density** (g/cm^3)	**Heigh** (cm)	**Single-sided**	**Double-sided**	**Dose (kGy.mA)** (cm/s)	**Dose-demand** (kGy)	**Conveyer's velocity** (cm/s)
ANH LONG	Dried fish	0.18	48	-	1.98	28.73	10	2.49
CHO LON	Dried fish	0.54	12	-	AL	-	10	-
THONG NHAT	Dried fish	0.37	28	-	-	-	10	-
MERIA	Dried fish	0.52	13	-	AL	-	10	-
CT HL MIEN NAM	Pig meal	0.53	23	-	-	-	4,5	-
	Pig meal	0.33	23	-	1.74	23.64	4,5	6.76

KIM SON	Dried cuttlefish	0.36	22	-	1.39	22.52	4,5	6.53
	Dried shrimp	0.38	19	-	AL	-	4,5	-
VINH LOC	Crisp shrimp pastry	0.26	36	-	-	-	3,5	-
LIPTON	Lipton Ice Tea	0.16	19.5	1.64	1.3	20.31	6	8.50
VINH HAO	Seaweed	0.24	36	9.31	2.07	33.93	8	3.63
TAN DONG	Shrimp paste	0.17	20	1.72	1.34	20.44	4,5	5.69
	Dried shrimp	0.24	32	-	1.43	24.65	4,5	6.41
	Dried shrimp	0.20	37	-	1.46	25.67	4,5	6.51
UNI-PRESIDENT	Gold-noodles	0.24	33	-	1.47	23.5	10	2.82

Tab 4. Irradiation mode and average dose for: frozen food

COMPANY	**Irradiated product**	**Density** (g/cm^3)	**Heigh** (cm)	**Single-sided**	**Double-sided**	**Dose** (kGy.mA) (cm/s)	**Dose-demand** (kGy)	**Conveyer's velocity** (cm/s)
CAFATEX	Shrimp	0.24	26	-	AL	-	3,5	-
	Shrimp	0.24	14	1.62	1.32	19.85	3,5	7.99
	Shrimp	0.37	24	-	-	-	3,5	7.80
VIET LINH	Shrimp	0.79	20	-	-	-	3,5	-
	Shrimp	0.38	16.5	-	2.05	25.42	3,5	7,26
	Shrimp	0.28	15	4.23	1.86	36.81	3,5	>10
	Shrimp	0.23	26	-	AL	-	3,5	-
	Seafood	0.49	22	-	-	-	3,5	-
	Farci	0.23	30	-	AL	-	3,5	-
	Frozen food	0.49	17	-	-	-	3,5	-
	Shrimp	0.38	18	-	AL	-	3,5	-
	cuttle-fish	0.45	13	-	AL	-	3,5	-

KIM ANH	Shrimp	0.79	23	-	-	-	3,5	-
	Shrimp	1.34	16	-	-	-	3,5	-
	Crab	0.27	27	-	1.52	24.08	3,5	8.18
	Yuzana	0.86	20	-	-	-	3,5	-
	Pangasius Fillets	0.50	14	-	AL	-	3,5	-
	Pangasius Fillets	0.47	22	-	-	-	3,5	-
	Exkimo	0.74	5	2.79	1.7	35.6	3,5	>10
	Frozen food	0.46	24	-	-	-	3,5	-
	Main Carton	0.79	20	-	-	-	3,5	-
	Shrimp	0.19	24	10.17	2.06	36.64	3,5	>10
	Anova	0.79	18	-	-	-	3,5	-
	Frozen food	0.74	20	-	-	-	3,5	-
	King Prawn	0.43	26	-	-	-	3,5	-
HAI THACH	Frog	0.31	20	-	AL	-	3,5	-
	Frog	0.35	20	-	1.66	23.71	3,5	8.06
	Crab	0.32	17	-	AL	-	3,5	-
	Crab	0.41	26	-	-	-	3,5	-

"-": the max:min ratio excess of 2

"AL": thickness of product is in region between 4.5 and 8.1 g/cm^2 and can be irradiated with addition density piece.

2.4 Study The Effect of Product Width To Dose Max: min Ratio

The max:min ratio to product width from 10 to 80 cm (20 cm thickness, density of 0.15 g/cm^3, irradiated by 10-MeV electron) were showed in Fig.3. The max:min ratio decreases when the product width increases for both single-sided and double-sided irradiation but the utilization efficiency increases form 5.6 % at a product width of 10 cm to 48.5% at 80 cm product width. The calculated results are the same for another case.

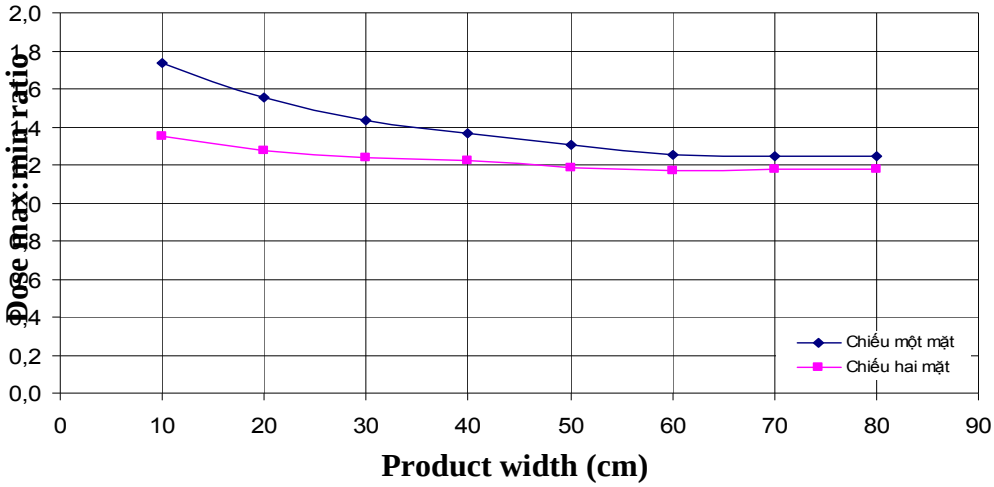

Fig. 3. Max:min ratio for 10-MeV electrons in matter with varies product width (20 cm product thickness, product density of 0.15 g/cm^3)

2.5 Electron-photon Spectrum In Irradiation Product

Using MCNP to calculate the spectrum of electron and photon produced in matter were showed in Fig.4a and Fig.4b respectively. Electrons promptly lose all of his kinetics when enter in the matter; at product depth about 6g/cm^2, almost of them are absorbed in the matter. As photon produced by bremsstrahlung by energetic electron proportional to Z^2; with low Z matter in irradiation product, the photon produced in matter has low energy too.

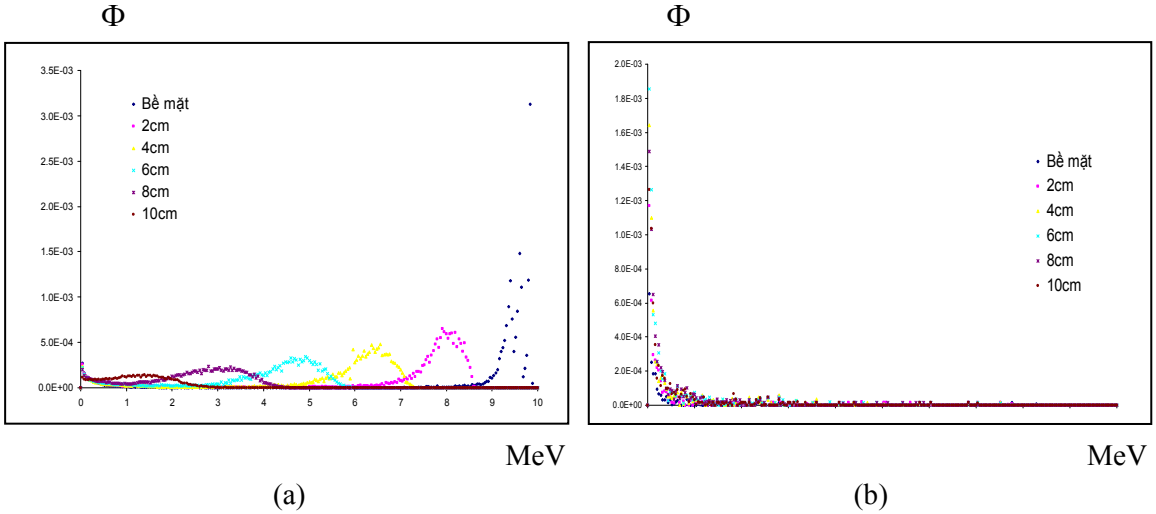

Fig. 4. Electron energy (a) and photon produced (b) in matter spectrum for initially mono-energetic 10-MeV electron

Reference

[1]. R. B. Miller, *Electronic Irradiation of Food, An Introduction to the Technology*, Springer, New Mexico 2005.

[2]. Commercial Offer for Delivery of Facility for Treatment by Electron Beam, CORD Service.

[3]. J.F.Briesmeister, *MCNP- A General Monte Carlo N-Particle Transport Code Version 4C2*, Transport Methods Group, Los Alamos National Laboratory, 1997.

[4]. R. B. Miller, *Food Irradiation Using Bremsstrahlung X-ray*, Radiation Physics and Chemistry 68, 963-974, 2003.

[5]. G.F. Popov, V.T Lazurik, Y.V. Rogov, KHNU Khakov, RT-office Electron beam, http://accelcinf.web.cern.ch/accelconf/e04/HTML/CLASO013.HTLM.

[6]. A.Kolchuzhkin, S.Korenev, O. Krivosheev, I. Tropin, *Distribution os Absorbed Dose in The Materials Irradiated by "Rhodotron" Electron Accelerator: Experiment and Monte-Carlo Simulation*, Process ding of the 2001 Particle Accelerator Conference, Chicago.

PREPERATION OF GLUCOSAMINE HYDROCHLORIDE AND GLUCOSAMINE SULFATE FROM IRRADIATED CHITIN

Nguyen Tan Man, Tran Thi Tam, Tran Thu Hong, Pham Thi Sam
Pham Thi Le Ha and Tran Thi Thuy

Nuclear Research Institute, VAEC

Abstract: Glucosamine hydrochloride is an amino sugar which is incorporated into the structure of body tissues. It comprises about 80% glucosamine, a compound helpful in maintaining joint health in individuals suffering from degenerative conditions such as arthritis. When orally ingested, it is selectively taken up by joint tissues to exert beneficial effects. Glucosamine may also have other therapeutic effects such as antiviral, anti-cancer, anti-aging, immune boosting or cholesterol lowering activity.

Glucosamine may be obtained by hydrolysis and deacetylation of chitin, a polymer of N-acetyl glucosamine with hydrochloric acid.

In this work we prepare glucosamine hydrochloride and glucosamine sulfate from irradiated chitin in order to produce high-purity product with good yield.

The method consists of the following steps:

1. Grinding the chitin
2. Irradiation the chitin using gamma Co-60 source at 30 kGy.
3. Digesting the chitin with prewarmed, concentrated HCl, by mixing the chitin with the HCl, and heating to 95^{o}C for 2hrs to produce a slurry.
4. Cooling the slurry to room temperature and filtering the precipitate
5. Dissolving the precipitate in hot water with activated charcoal at room temperature.
6. Filtering the solution and discarding the solids.
7. Evaporating the solution to recover glucosamine solids.
8. Washing the glucosamine solids with ethanol
9. Drying the glucosamine solids.

Glucosamine sulfate is very hygroscopic and degrades rapidly when exposed to moisture. To avoid this problem, glucosamine sulfate is made from glucosamine hydrochloride by adding potassium sulfate and co-crystallizing the resulting mixture.

The method comprising the following steps:

1. Dissolving 25.9g of glucosamine hydrochloride in 84g of distilled water with stirring.
2. Adding 10.6g of potassium sulfate and stirring was continued for about one hour at temperature of from 35^{o}C to 45^{o}C to complete the reaction.

3. Precipitating the stable crystalline form by addition of a liquid precipitating agent which is miscible with water and in which the crystalline form has a solubility no greater than 0.1% (w/v), with stirring or evaporation under vacuum.

4. Completing the precipitating by reducing the temperature of the mixture.

5. Recovering the precipitated crystalline form.

The liquid precipiting agent is selected from the group consisting of acetone, ethanol, isopropanol… and the liquid precipiting agent is added in a proportion of from 4 to 5 parts by volume relative to the volume of aqueous solvent, over the period of from 3 to 4 hours. The stable crystalline form recovered is dried at a temperature of from 45^{o}C to 60^{o}C.

I. Experiment and Results

I.1. Study The Degradation Effect of Chitin By Gamma Radiation

Chitin was irradiated with doses from 10 kGy to 70 kGy on gamma Co-60 source and then deacetylated by 47% NaOH solution for obtaining chitosan. The molecular weight of chitosan (Mv) was measured by viscosimetry decreased with increasing dose.

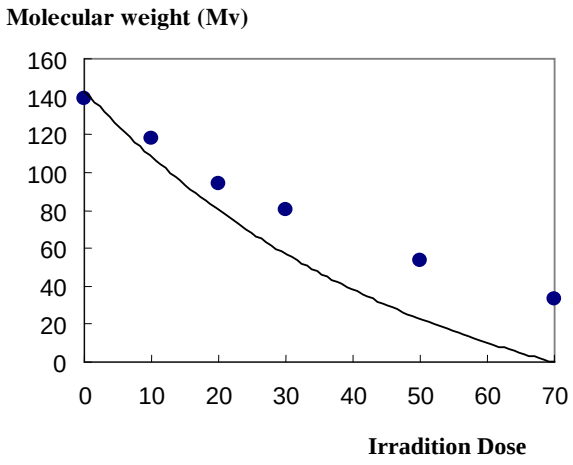

Fig. 1. The dependence of molecular weight (Mv) on irradiation dose

I.2. Preparation Process of Glucosamine Hydrochloride From Irradiated Chitin

Glucosamine hydrochloride was obtained by hydrolysis and deacetylation of chitin, a polymer of N-acetyl glucosamine with hydrochloric acid.

The parameters of hydrolysis reaction such as reaction temperature, reaction time, HCl concentration and reactant ratio have been investigated.

I.3. Preparation Process of Glucosamine Sulfate From Glucosamine Hydrochloride

Glucosamine sulfate is made from glucosamine hydrochloride by adding potassium sulfate and co-crystallizing the resulting mixture. The liquid precipitants such as ethanol, acetone, isopropanol or evaporation under vacuum have been carried out.

I.4. Evaluation of Product Quality

Molecular weight of glucosamine hydrochloride was determined by gel permeation chromatography (GPC). The contents of C, H, and N of glucosamine hydrochloride and glucosamine sulfate potassium chloride have been analyzed according to ASTM D 5373-02. The content of heavy metal and microbial index of glucosamine hydrochloride and glucosamine sulfate potassium chloride have been tested.

Tab I. Molecular weight of glucosamine hydrochloride was determined by (GPC).

Molecular weight (g/mol)	**Glucosamine.HCl** (Sigma-Aldrich)	**Glucosamine.HCl** (from non-irradiated chitin)	**Glucosamine.HCl** (from irradiated chitin)
	215.63	239	238

Tab II. Test results of C, H, and N contents of glucosamine hydrochloride.

TT	**Characteristic**	**Glucosamine.HCl** (from non-irradiated chitin)		**Glucosamine.HCl** (from irradiated chitin)	
		Theoretical	Found	Theoretical	Found
1	Carbon content (C), % (m/m)	33.4	33.6	33.4	33.4
2	Hydrogen content (H), % (m/m)	6.3	6.2	6.3	6.1
3	Nitrogen content(N), % (m/m)	6.3	6.0	6.3	6.0

Tab III. Test results of heavy metal content and microbial index of glucosamine hydrochloride.

TT	**Characteristic**	**Test method**	**Test result**
1	Total ash content, %	FAO FNP 14/7	0.03
2	Insoluble content, %	FAO FNP 5/REV.1	Not detected
3	Moisture content, %	FAO FNP 14/7	0.2
4	pH of 1% solution	Foodstuffs-EC 1994	4.2
5	Specific rotation, [α]D	FAO FNP 5/REV.1	72.8
6	Arsenic content, mg/kg	AOAC 2007	Not detected
7	Mercury content, mg/kg	AOAC 2007	Not detected

8	Lead content, mg/kg	AOAC 2007	0.13
9	Antimony content, mg/kg	AOAC 2007	Not detected
10	Cadmium content, mg/kg	AOAC 2007	Not detected
11	Total aerobic plate count, CFU/g	AOAC 2007	Less than 10
12	Coliform, CFU/g	BS 5763, 1991	Less than 10
13	*E. coli*, CFU/g	ISO 16649-2	Less than 10
14	*Staphylococcus aureus*, MPN/g	AOAC 2007	Less than 3
15	*Clostridium perfringens*, CFU/g	AOAC 2007	Less than 10
16	Salmonella/25g	AOAC 2007	Negative
17	*Vibrio cholerae*/25g	BS 5763, 1991	Negative
18	Total yeasts & moulds, CFU/g	FAO FNP 14/4	Less than 10

II. Conclusions

II.1 The effect of degradation of chitin with doses from 10kGy to 70kGy has been studied. The result shown that the molecular weight of chitosan decreased with increasing dose.

II.2 The yield of glucosamine hydrochloride increases about 15% and reaction time is two hours when using irradiated chitin at dose of 30kGy compared to four hours when using non-irradiated chitin.

II.3 The optimal parameters of operating conditions for the preparation process of glucosamine hydrochloride from irradiated chitin are:

- Chitin irradiated at 30kGy
- Reaction temperature: 95^{o}C
- Reaction time: 2 hours
- HCl concentration: 12N
- Reactant ratio (chitn/HCl, w/w): ½

II.4 The process for preparation of the glucosamine sulfate has been carried out by using liquid precipitants such as ethanol, acetone and isopropanol or evaporation under vacuum. The results shown that the method of evaporation under vacuum gives the highest yield.

II.5 Molecular weight of glucosamine hydrochloride is 238 gram/mol. The contents of C, H, N, heavy metal and microbial index of the products meet the requirements.

References

[1]. Horton, Derek; Wander, J.D.(1980). The Carbohydrates Vol IB. New York: Academic, 727-728.

[2]. Marine Nutraceuticals and Functional Foods.

Edited by Colin J. Barrow, Fereidoon Shahidi, CRC Press.

[3]. Website" http://www.thuocbietduoc.com.vn

[4]. Lê Hữu Tư, Lê Hải, Nguyễn Tấn Mân và Phạm Thị Lệ Hà.
Khảo sát hiệu ứng chiếu xạ chitin lên hiệu suất Glucosamine.HCl.
Hội nghị Khoa học và Kỹ thuật Hạt nhân lần thứ VI, Đà lạt 26-27/10/2005.

[5]. Nguyen Quoc Hien et al, Radiation Processing Technology for Production of Plant Growth Promoter from brown seaweed and Plant Protector from shrimp shell, International Symposium on Radiation Technology in Emerging Industrial Applications, 6-10 November 2000, Beijing, China.

[6]. Nguyễn Thi Phương Nhi, Nghiên cứu cắt mạch chitin bằng các tác nhân hóa học khác nhau để điều chế Glucosamine.
Luận văn cử nhân khoa học, Khoa Hóa, Trường Đại học Khoa học Huế, Khóa 1997-2001.
Journal of Food and Drug Analysis, 2000.8(2): 75-83.

[7]. V. Yu. Novikov and Ivanov, Synthesis of D(+)-Glucosamine Hydrocholride, Russian Journal of Applied Chemistry, Vol.70, No.9, pp.1467-1470, 1997.

[8]. V. Yu. Novikov, Kinetics of Formation of D(+)-Glucosamine by acid hydrolysis of chitin, Russian Journal of Applied Chemistry, Vol.72, No. 1, 1999, pp.156-161.

[9]. Zhou, et al, Preparation and properties of Glucosamine Hydrochloride. Journal of Shuichan Xuebao 2000, Vol. 24, No. 1, pp 76-80.

[10]. CAO, Preparation of Glucosamine hydrochloride from chitin. Journal of Huaxue Shijie 1998, Vol. 39, No. 5, pp. 250-253.

[11]. US Patent No. 6, 486, 307. Preparation of glucosamine hydrochloride.
Issued on November 26, 2002.

[12]. US Patent No. 5,843,923. Glucosamine sulphate potassium chloride and process of preparation.
Issued on December 1, 1998.

[13]. Chen, et al, Preparation of D-Glucosamine hydrochloride. Journal of Shipkin Kexue (Beijing), 2000 Vol. 21, No. 9, pp. 34-36.

[14]. Aslak Einbu, Characterisation of Chitin and a Study of its Acid-Catalysed Hydrolysis, Thesis for the degree of philosophiea doctor.
Norwegian University of Science and Technology.
Faculty of Natural Sciences and Technology.
Departement of Biotechnology, Trondheim, April, 2007.

[15]. Roberts, G.A.F., and Domszy, J.D., Determination of the viscometric constants for chitosan, Int. J. Biol. Macromol., (1982) 4, 374-377.

[16]. US Patent No. 4,642,340. Stable compounds of glucosamine sulphate.
Issued on Feb. 10, 1987.

[17]. US Patent No. 5,847,107. Method of preparating mixed glucosamine salts. Issued on Dec. 8, 1998.

[18]. Ke Liang B. Chang, John Lee and Wen-Rong Fu.
HPLC Analysis of N-acetyl-chito-oligosaccharides during acid hydrolysis of chitin.
Journal of Food and Drug Analysis, 2000.8(2): 75-83

STUDY ON THE SYNTHESIS OF COLLOIDAL SILVER NANOPARTICLES BY γ-IRRADIATION USING CHITOSAN STABILIZER

Dang Van Phu[1], Vo Thi Kim Lang[1], Doan Thi The[1], Nguyen Thi Kim Lan[1]
Bui Duy Du[2] and Nguyen Quoc Hien[1]

[1]Research and Development Center for Radiation Technology, VAEC
[2]Institute of Applied Material Science, Vietnam National Institute for Sci. and Technology

Abstract: Radiation-induced synthesis of colloidal silver nanoparticles using chitosan as a stabilizer and free radical scavenger is feasible and according to green method. The saturated conversion dose (Ag^+ to Ag^0) was determined by Uv-vis spectroscopy and silver nanoparticles size was characterized by transmission electron microscopy (TEM). The average diameter of silver nanoparticles is smaller than 10nm with narrow size distribution and the colloidal silver nanoparticles has good stability for a long time of storage. The effect of Ag^+ and chitosan concentration and molecular weight of chitosan on diameter and size distribution of silver nanoparticles was investigated. Silver nanoparticles of about 7nm stabilized by chitosan showed high antimicrobial effect. The inhibition of *Staphylococcus aureus* is more than 99.9% (from 10^7 CFU/ml to 10^3 CFU/ml at 5ppm). The antifungal effect particularly on *Corticium salmonicolor* attains to medium level (ED_{50} = 27.16ppm) and the inhibition percent is of 70-80% for silver nanoparticles concentration from 40 to 100ppm.

1. Introduction

During the last decades, developments of surface microscopy, materials science, biochemistry, physical chemistry and computational engineering have converged to provide remarkable capabilities for understanding, fabricating and manipulating structures at the atomic level. The rapid evolution of this new science and the opportunities for application promise that nanotechnology will become one of the dominant technologies of the 21st century [1]. The preparation and study of metal nanoparticles is of interest in both research and technology. Silver nanoparticles (Agnano) have attracted considerable interest because of their novel properties and their potential application [2, 3]. Different methods have been used for the synthesis of Agnano from Ag^+ solution such as chemical, electrochemical, gamma and electron beam irradiation,.. [3]. Methods of preparing Agnano by exposure to ionizing rays are provided several advantages because sizes and size distribution of the particles are easily control and the manufacturing process carries out at room temperature and purely colloidal silver nanoparticles can be obtained. Also, preparation process is simple and therefore mass production is possible at reasonable cost [3, 4]. It is well known that Ag^+ in solution could be reduced by γ-rays to Ag atoms while they would agglomerate if there is no protection. Hence an effective stabilizer is the key factor to fabricate densely dispersed Agnano using irradiation method [5]. Many workers used polymers having functional groups such as -NH_2, -COOH and -OH that are high affinity for Ag atom [2] to stabilize Agnano, such as PVA and PVP [3, 6], gelatin and CMC [7], oligochitosan [8]. Chitosan, a natural polysaccharide with excellent biodegradable and biocompatible

characteristics is a renewable polymer. Owing to the interaction with -NH_2 groups of chitosan chain, the Agnano is enveloped by chitosan fragments and so the nanoparticles could be kept from agglomerating during irradiation reduction process [5]. Using chitosan as free radical scavenger and stabilizer for colloidal silver nanoparticles prepared by γ-irradiation is appropriate to green method [5, 8, 9]. In addition, Agnano stabilized by chitosan is positive charge enrichment in surface so that antimicrobial property is significantly improved [10, 11]. Therefore, preparation of Agnano/chitosan by γ-irradiation and antimicroorganism properties have been carried out in this project.

2. Experiments

2.1. Chemicals: $AgNO_3$ was obtained from Shanghai Chemical Co., Absolute ethanol was a product of Vietnam. Polyvinyl pyrrolidone: PVP-K90 (M_w 10^6Da) was obtained from BASF, Germany. Chitosan (DDA 70%) with M_w 3.5-460kDa was prepared at VINAGAMMA Center. Deionized water for chromatography was used throughout in this study. Two microorganism strains namely *Staphylococcus aureus* ATCC 6538 and *Corticium salmonicolor* were supplied by University Medicine Pharmacy, Ho Chi Minh City and Rubber Research Institute of Vietnam, Binh duong Province, respectively.

2.2. Methods: The solutions containing chitosan, ethanol and Ag^+ in glass tubes, which were deaerated by bubbling with N_2. The γ-irradiation was carried out on a Co^{60} irradiator with dose rate of 1.3kGy/h at VINAGAMMA center. Uv-vis spectra of silver nanoparticles of water diluted solution to 0.1mM calculated as Ag^+ concentration were recorded on an UV-2401PC, Shimadzu, Japan. TEM images were taken with a JEM 1010, JEOL, Japan. The diameter of Ag nanoparticles was statistically processed using Photoshop software [3, 6, 12]. The antimicroorganism activity of Agnano was tested against *S. aureus* and *C. salmonicolor* by culture medium toxicity methods [10, 13, 14]. The Luria Bertani or Malt Extract agar plate containing the test sample and control were incubated at 37^0C for *S. aureus* and 27^0C for *C. salmonicolor*. The antibacterial effect was calculated using the equation: $\eta(\%)=(N_0-N)\times100/N_0$, where N_0 and N are survival number of bacteria in the control and studied samples, respectively. The antifungal effect was measured by diameter of colony growth and calculated as follows: Inhibition, $\%=(d_0-d)\times100/d_0$, where d_0 and d are diameter of the colony of the control and test sample, respectively.

3. Results and Discussion

3.1. The Influence of Ag^+ Concentration The Characteristics of Agnano

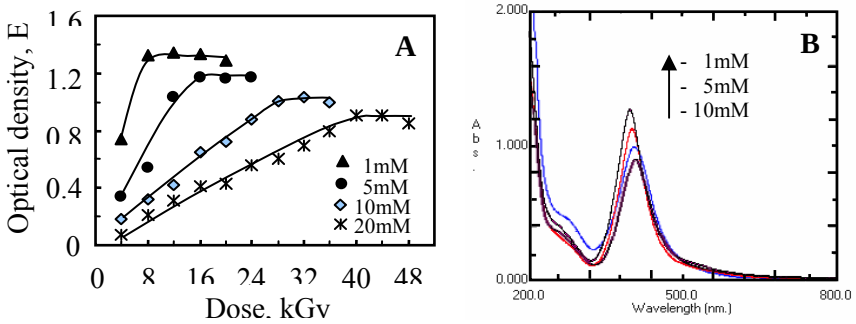

Fig. 3. 1. A) The relationship between E and dose of solution of CTS1%/ethanol 5% with different Ag^+ concentration. B) Uv-vis spectra of CSN at D

Tab 3.1. The characteristics of CSN from CTS1% (M_w120kDa)/ethanol 5% with different Ag^+ concentration

Samples	**E**	**λ_{max},** nm	**D,** kGy	**d,** nm (*)
[Ag^+] 1mM	1.33	397.0	8	4.6 ± 1.0 c
[Ag^+] 5mM	1.17	400.5	16	6.9 ± 1.5 b
[Ag^+] 10mM	1.01	403.0	28	10.4 ± 4.5 a
[Ag^+] 20mM	0.90	410.0	40	11.4 ± 1.6 a

(*) *On the same column, the values with same symbol do not have significant difference at P= 95%. LSD = 1.39*

The results from table 3.1 and Fig. 3.1 showed that the saturated converse dose (D) was of 8-40kGy for [Ag^+] 1-20mM. The optical density (E) decreased from 1.33 (1mM) to 0.90 (20mM) and maximum absorbed wavelength (λ_{max}) shifted from 397 to 410nm, respectively. The average diameter of Agnano (d) was of 5-7nm for [Ag^+] 1-5mM and ~11nm for [Ag^+] 10-20mM. The results obtained were in good agreement with other studies [2, 3, 6, 8] that when increasing [Ag^+] will increase D and d, simultaneously λ_{max} shifts to higher value.

3.2. The Effect of Chitosan Concentration

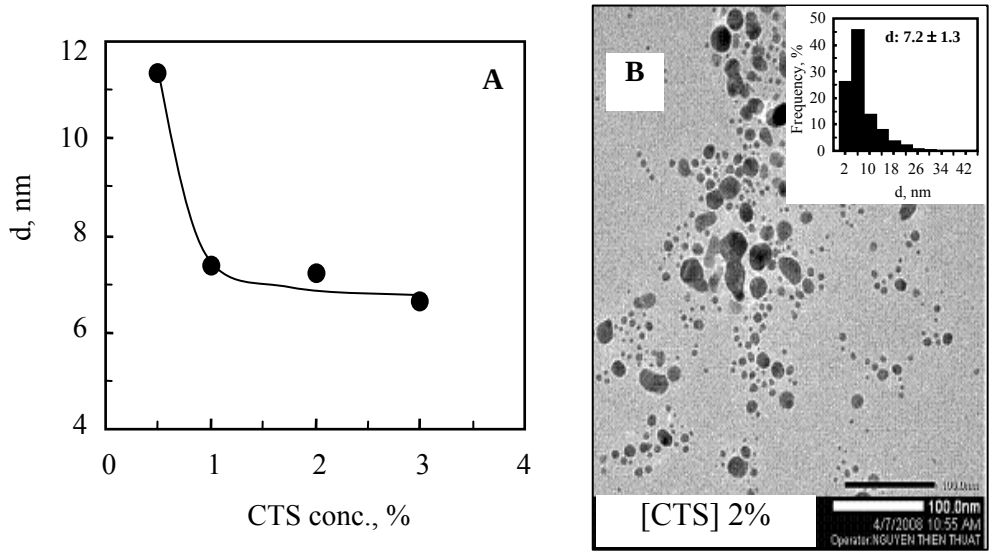

Fig. 3. 2: A) The relationship between d and CTS concentration. B) TEM image and size distribution of CTS stabilized Agnano from CTS 2%(M_w120kDa)/Ag^+ 5mM

From Fig. 3.2 showed Agnano stabilized by CTS 0.5% with weight ratio of $AgNO_3$/CTS = 1:6 had d ~11nm which was bigger than those stabilized by CTS 1%. There is no significant difference of Agnano size that stabilized by CTS 1-3% (d ~7nm). D of 16kGy for preparation colloidal silver nanoparticles did not change with [CTS] 0.5-3%. Agnano prepared with relatively high CTS conc. have better stability. The influence of CTS conc. was the same for PVA [6] with optimal ratio of PVA 2%/Ag^+ 10mM.

3.3. The Influence of Molecular Weight (M_w) of CTS

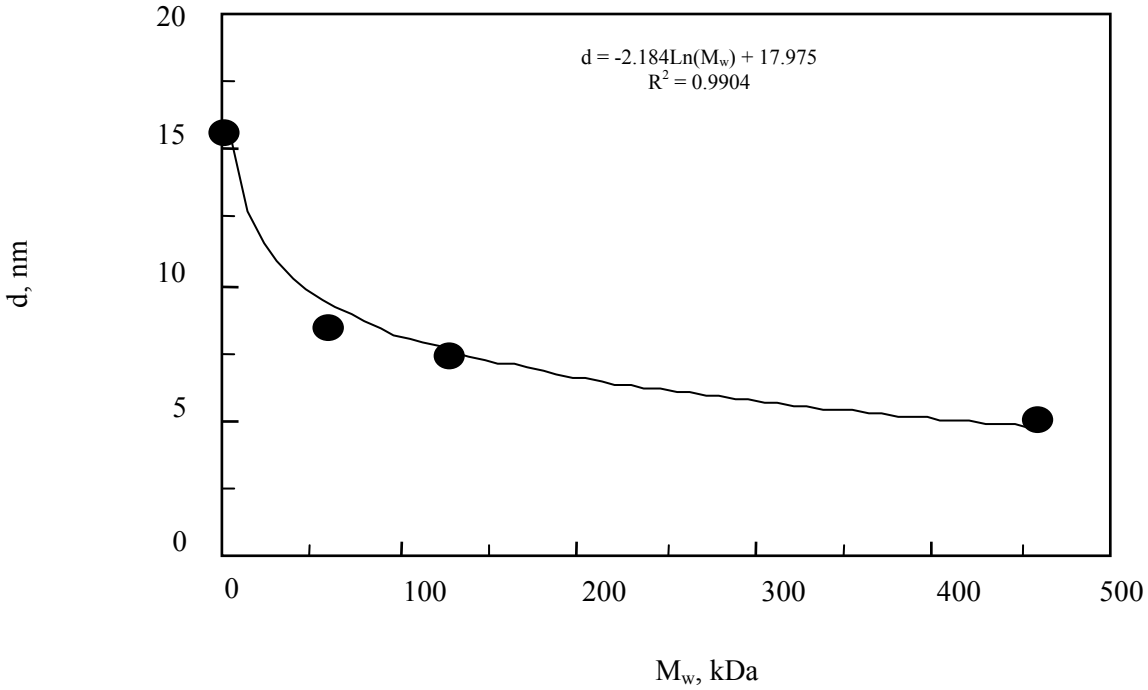

Fig. 3. 3. The dependence of d on M_w of CTS (Ag^+ 5mM/CTS1%)

Results showed that CTS with higher M_w, the stabilization of Agnano was better. d of 5-16nm for M_w 3.5-460kDa and the relationship is d(nm) = -2.184Ln(M_w) + 17.975. The stabilization of Agnano by CTS depends on electrostatic attractive force and space effects [3, 5]. A similar result was also observed by Huang et al., [9] using CTS as stabilizer for gold nanoparticles.

3.4. The Effect of Mixed Stabilizers

Tab 3.2. The E, λ_{max}, D and d of CNS from Ag^+ 5mM with different stabilizers

Samples	**D ,** kGy	**E**	**λ_{max},** nm	**d,** nm (*)
PVP 2%/Ethanol 5%	24	1.21	410.5	9.1 ± 2.6 a
CTS (M_w 120kDa) 2%	16	1.12	408.5	7.2 ± 1.3 b
PVP 1%/CTS 1%	16	1.12	415.5	8.7 ± 1.4 a

(*) *LSD = 0.8*

Results in table 3.2 showed that E and λ_{max} of three CNS are almost the same. D of PVP/Ethanol/Ag^+ is 24kGy and 16kGy for PVP/CTS/Ag^+, which proved CTS is a better scavenger than ethanol and D decreased 8kGy compared to ethanol. d of Agnano/PVP and Agnano/PVP/CTS was ~9nm, which was larger than of Agnano/CTS (~7nm).

3.5. The Stability of Colloidal Silver Nanoparticles/chitosan

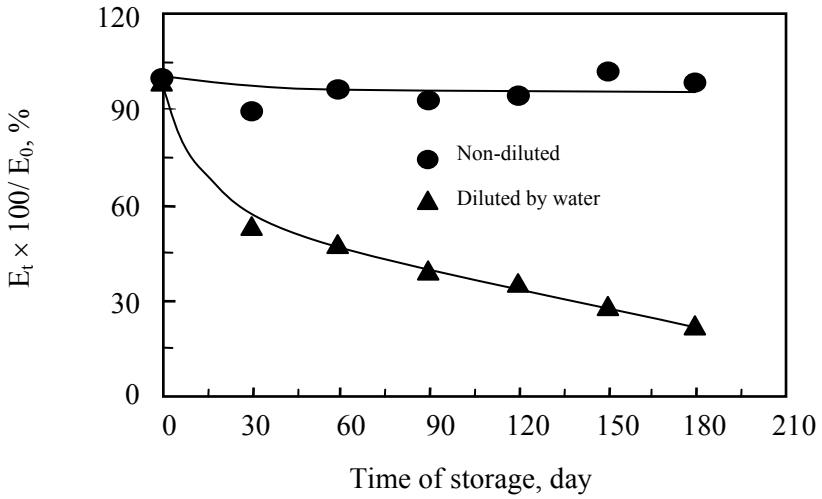

Fig. 3. 4. E of CSN from CTS2%/Ag^+ 5mM along with time of storage

Results in Fig. 3.4 revealed CSN from CTS 2%/Ag^+ 5mM without dilution was stable more than 6 months. However, when it was diluted by water with ratio 1/50 (v/v), E decreased to 36% after 3 months and 22% after 6 months. Furthermore, λ_{max} of the diluted sample shifted from 408.5nm to 423nm after 6 months. The decreasing of E and increasing of λ_{max} mean that there is aggregation to create larger particles [6, 8].

3.6. The Antibacterial Activity of Agnano /CTS For Staphylococcus Aureus

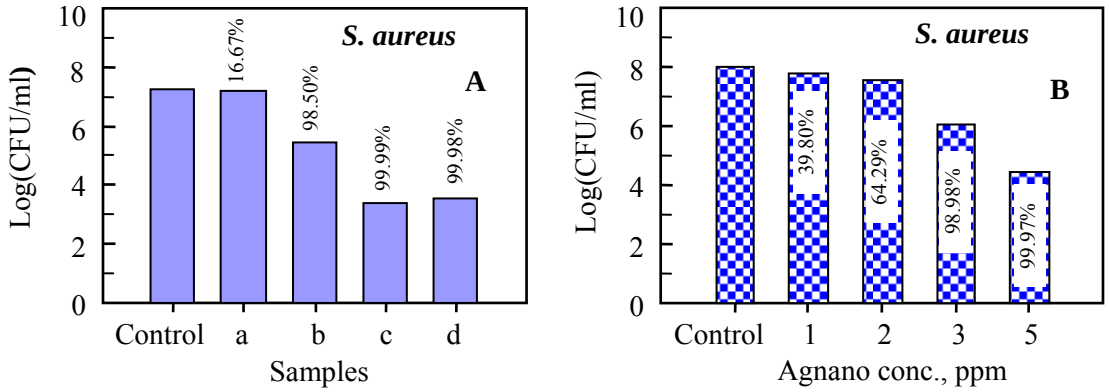

Fig. 3. 5. A) LB medium (cont.), a- CTS solution (diluted 1/50 by LB medium) and b, c, d are Agnano 5ppm of Agnano/PVP, Agnano/PVP/CTS, Agnano/CTS, respectively. B) Efficiency antimicrobial of Agnano/CTS with different concentration.

The CSN with d are 7-9nm have high antimicrobial with η ~99.99% at 5ppm. In particularly, with CTS (sample a) also inhibited *S. aureus,* η ~17%. Chen et al. [15] also determined minimum inhibitory concentration of CTS for *S. aureus* is 500ppm and for *Mucor kacilliformis* is 5.000ppm. The results from Sanpui [11] showed that antibacterial activity of Agnano/CTS is higher than CTS for *E. coli*. The antibacterial activity of Agnano/CTS increased with higher Agnano concentration, η reached to 39.8, 64.29, 98.98 and 99.97% for 1, 2, 3 and 5ppm of Agnano, respectively (Fig. 3.5 B).

3.7. The Antifungal Efficiency of Agnano /CTS On Corticium Salmonicolor

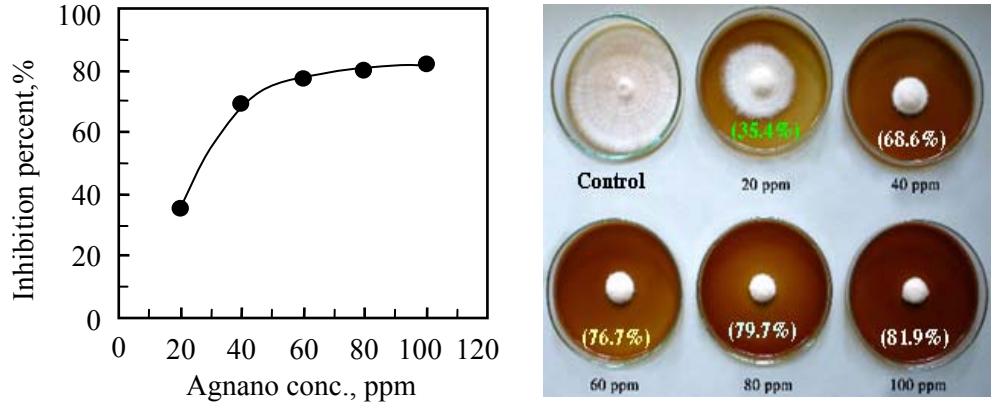

Fig. 3. 6: The % inhibition on *C. salmonicolor* with different Agnano conc.

The antifungal efficiency of Agnano/CTS increased with higher Agnano concentration. After incubation for 8 days, the inhibition was 35.4, 68.6, 76.7, 79.7 and 81.9% for Agnano 20, 40, 60, 80 and 100ppm, respectively. From the relationship between % inhibition and Agnano concentration, the ED_{50} (effect dose inhibited 50%) of Agnano/CTS on *C. salmonicolor* was found to be 27.16ppm. The above results, Agnano has antibacterial activity on *S. aureus* better than antifungal on *C. salmonicolor*. It may be because of differences of organization, structure and function of their cells [16, 17].

4. Conclusions

Colloidal silver nanoparticles were prepared by gamma-irradiation using chitosan as a stabilizer and free radical scavenger. The particles size was of 4.6 -11.4nm for Ag^+ concentration from 1 to 20mM. The particles size of ~7nm was obtained for CTS concentration 1-3% and that of ~11nm for CTS 0.5% ([Ag^+] 5mM). Chitosan with high M_w (460kDa - 5nm) was better in stabilization of silver nanoparticles compared with low M_w (3.5kDa - 15.5nm). The particles size was of 8.6nm for the mixture of stabilizer (PVP1%/CTS1%) which was less than that for PVP2% (9.1nm) and bigger than that for CTS2% (7.2nm). The colloidal silver nanoparticles stabilized by chitosan with particles size of ~7nm showed in good stability and strongly inhibition effect against *S. aureus* bacteria (>99.9%) at 5ppm and fungal *C. salmonicolor* with ED_{50} of 27,16ppm.

References

[1]. M. Singh et al., Nanotechnology in medicine and antibacterial effect of silver nanoparticles, *Digest J. Nanomaterials and Biostructures*, 3(3), pp.115-122, 2008.

[2]. S.P. Ramnani, J. Biswal, S. Sabharwal, Synthesis of silver nanoparticles supported on silica aerogel using gamma radiolysis, *Rad. Phys. Chem.*, 76, pp.1290-1294, 2007.

3]. B.D. Du et al., Preparation of colloidal silver nanoparticles in poly (N-vinylpyrrolidone) by γ-irradiation, *Journal of Experimental Nanoscience*, 3(3), pp.207-213, 2008.

[4]. H.J. Park et al., A new composition of nanosized silica-silver for control of

various plant diseases, *The Plant Pathology Journal*, 22(3), pp.295-302, 2006.

[5]. P. Chen et al., Synthesis of silver nanoparticles by γ-ray irradiation in acetic water solution containing chitosan, *Rad. Phys. Chem.*, 76, pp.1165-1168, 2007.

[6]. D.V. Phu et al., Study on the synthesis of colloidal silver nanoparticles by γ-irradiation for using as an antimicrobial substance, *The Report of Project,* code CS/07/07-02, 2007.

[7]. S. Kapoor, C. Gopinathan, Reduction and aggregation of silver, copper and cadmium ions in aqueous solutions of gelatin and CMC, *Rad. Phys. Chem.*, 53, pp.165-170, 1998.

[8]. D. Long, G. Wu, S. Chen, Preparation of oligochitosan stabilized silver nanoparticles by gamma irradiation, *Rad. Phys. Chem.*, 76, pp.1126-1131, 2007.

[9]. H. Huang, X. Yang, Synthesis of chitosan-stabilized gold nanoparticles in the absence/presence of tripolyphosphate, *Biomacromolecules*, 5, pp.2340-2346, 2004.

[10]. K.H. Cho et al., The study of antimicrobial activity and preservative effects of nanosilver ingredient, *Electrochimica Acta*, 51, pp.956-960, 2005.

[11]. P. Sanpui et al., The antibacterial properties of a novel chitosan-Ag-nanoparticle composite, *International Journal of Food Microbiology*, 124(2), pp.142-146, 2008.

[12]. K.C. Pingali et al., Silver nanoparticles from ultrasonic spray pyrolysis of aqueous silver nitrate, *Aerosol Science and Technology*, 39(10), pp.1010-1014, 2005.

[13]. W.K. Son, J.H. Youk, W.H. Park, Antimicrobial cellulose acetate nanofibers containing silver nanoparticles, *Carbohydrate Polymers*, 65, pp.430-434, 2006.

[14]. N.T. Hoan, Appling Agnano to eliminate *Corticium salmonicolor* which causing pink disease on the rubber trees, *The news Sci. Technol. Natural rubber*, No. 3, pp. 31-32, 2008.

[15]. S. Chen, G. Wu, H. Zeng, Preparation of high antimicrobial activity thiourea chitosan-Ag^{+} complex, *Carbohydrate polymers*, 60, pp.33-38, 2005.

[16]. S. Shrivastava et al., Characterization of enhanced antibacterial effects of novel silver nanoparticles, *Nanotechnology*, 18, pp.225103/1-225103/9, 2007.

[17]. D.K. Tiwari et al., Time and dose-dependent antimicrobial potential of Ag nanoparticles synthesized by top-down approach, *Current Science*, 95(5), pp.647-655, 2008.

Papers Published In Relation To The Project

1. Chế tạo keo bạc nano bằng phương pháp chiếu xạ sử dụng PVP /chitosan làm chất ổn định, *Tạp chí KH và CN*, T.46, số 3, Tr.81-86, 2008.
2. Preparation of colloidal silver nanoparticles in poly(N-vinylpyrrolidone) by γ-irradiation, *Journal of Experimental Nanoscience*, Vol.3, No.3, pp.207-213, 2008.
3. Nghiên cứu chế tạo bạc nano bằng phương pháp chiếu xạ: Kết quả bước đầu và triển vọng, *TT KH&CN Hạt Nhân*, số 15, Tr.32-34, 2008.
4. ảnh hưởng khối lượng phân tử chitosan và pH đến kích thước Agnano chế tạo bằng phương pháp chiếu xạ γ Co-60, *Hội nghị KH &CN HNTQ lần 8*, Nha trang, 8/2009.

1.9 - Radiochemistry and Materials Science Sciences

STUDY ON PREPARING ZIRCONIUM POWDER BY METAL-THERMIC METHOD USING CALCIUM

Nguyen Van Sinh[1], Tran Duy Hai[1], Tran Thanh Hien[1], Dam Van Tien[1]
Cao Phuong Anh[1], Ta Phuong Mai[1], Dao Truong Giang[1] and Nguyen Minh Duc[2]

1. Institute for Technology of Radioactive and Rare Elements, VAEC
2. Technology University

Abstract: Zirconium metal, especially in the state of powder, is a material that is widely used in lots of industrial fields.

The consumption of zirconium metal for nuclear industry is 90% of the total of zirconium that is produced in the world. The left (10%) is used in different non-nuclear industry fields such as metallurgy, chemistry, and national defense.

The reported results comprise: 1) A system of equipments made for metal-thermic reduction was well sealed to be able to reduce the pressure of the system to 10^{-2} atmosphere at 900-1000^{0}C. This system unit can give the yield of 100-300g/batch. 2) A technological procedure for reducing zirconium dioxide by metal-thermic method using calcium was determined in order to obtain Zirconium metal power which had efficiency 95-98%(meet the specifications according to standards in the world and General Department for Defense Industry, the Ministry of Defense.: zirconium content is 98.51%, total of damaging element content is less than 2%, self-combust temperature is lower than 200^{0}C, meant particle size is 4.891µm, particle size distribution range is from 0.06 to 19 µm). A very important part of the know-how that is vacuum distilling refinement of metal powder at 800^{0}C in the high-vacuum refining furnace VRS-15G was successfully employed to obtain high quality zirconium powder.

The obtained products have been used to prepare pyrotechnic MC1 for detonator fuse heads at General Department for Defense Industry, the Ministry of Defense.

Key words: Zirconium Powder, metal-thermic, calcium-thermic method.

I. Preface

Zirconium metal is a special material with some typical properties, which no other metals have, such as low cross-area of thermal neutron capture (0.185 to 0.2 barn), high melting point (1855^{0}C), high thermal resistance, high corrosion resistance, good conductivity of heat and electricity, high plasticity and good machinability. Thanks to such merits, zirconium alloy has been used as a structural material for fuel rode cover. Nowadays, about 90% of obtained zirconium metal in the world is employed in nuclear field; the other 10% is used in different industries such as electronics, electricity, machine fabrication, aeronautics, space, metallurgy and chemistry.

Some following alloys of zirconium have been used to make the cover of fuel rods and pressure resistant tubes/pipes of heat-exchange:

- Zircalloy-2 containing 1.2-1.7% tin, 0.07-0.20% iron, 0.05-0.15% chromium, 0.03-0.08% nickel.

- Zircalloy-4 containing 1.2-1.7% tin, 0.18-0.24% iron, 0.07-0.13% chromium.

- Alloy of zirconium added 2.5% zinc having very high strength.

Zirconium has been employed to remove oxygen, nitrogen and sulfur from additive steel. It has been also used as a constituent to alloy some type of steels such as armor, stainless and heat-resistant steel. Zirconium has been added to copper to enhance the strength of the later many folds while its electric conductivity almost remains. Magnesium alloy added with 4-5% Zn and 0.6-0.7% Zr has twofold strength in comparison with that of magnesium alloy having no additions. Furthermore, this alloy can retain its strength at 200^0C.

The present of Zr in aluminum alloy helps much increase the alloy's quality.

Besides, zirconium powder has some special characteristics such as strong activity, low self-combustion/ignition temperature, high energy combustion and, especially, the ability of combustion without releasing gas. Because of such distinguish merits, zirconium is used in defense industry to produce firing chemicals for pyrotechnics, delayed-action fuses, timer fuses, and differential detonators. In addition, it is used in gas-producers for automatic gas bags. Like zirconium metal, zirconium powder is largely used in other industrial branches such as metallurgy, chemical, electricity, electronics, aeronautics, space, etc.

Based on the broad application and the need of zirconium in different industries as mentioned above, we have chosen the method of metal-thermic reduction of Zr using Ca as the theme of this work.

II. Overview and Theory

There are a lot of methods for producing zirconium metal and zirconium powder. Five following methods are popular:

1. Reduction of zirconium dioxide with Ca, Al, Mg or C
2. Reduction of $ZrCl_4$ with Ca, Na, Mg or Al
3. Reduction of $Na_5Zr_2F_{13}$, K_2ZrF_6 with Na, K, Al
4. Electrolysis of melting mixture of K_2ZrF_6 and electrolytes
5. Hydrogenation of zirconium spongy or zirconium lump.

The first and the fifth methods are the most popular for production of zirconium powder because of some reasons such as the high efficiency of the methods, entire obtained products in the state of fine powder, good quality of powder. If we use the fifth method, we can produce a large amount of zirconium powder, leading to lower powder cost but this method requires spongy zirconium, an intermediate product for preparing zirconium powder, which is too difficult to prepare in countries without nuclear power. As a result, this method is used mainly in counties having produced nuclear material. If we use the first method, we can obtain zirconium powder with high quality when using Ca as a reducer. Though the cost of the products made by this method is high due to the high cost of Ca metal, this method has been widely used because it is the only method giving whole product in state of fine zirconium powder. In addition, this method has other advantages such as being easily carried out in any scale, giving high efficiency and the product with stable quality. The method is the most appropriate in Vietnam, so we have chosen the method of metal-thermic reducing ZrO_2 with calcium including designing and self-making equipments to produce zirconium powder as the theme of this work.

III. Experiment and Result

III.1 Equipment Design

III.1.1 Equipment for Metal-thermal Reducing

Zirconium metal, especially in the state of powder, has a very strong activity and fierce chemical affinity for oxygen, nitrogen and hydrogen, so that it must be prepared and processed in severe technological conditions such as high vacuum, and atmosphere of extra-pure inert gas. Accordingly, building up an equipment of a trivial leakage to satisfy the above severe requirements became an indispensable part of our work. The equipment shown in the figure 1, which has efficiency of 100-300 g/ batch, has been made up in our laboratory. It can be easily adapted to become another having larger efficiency whenever needed based on the theory of similarity.

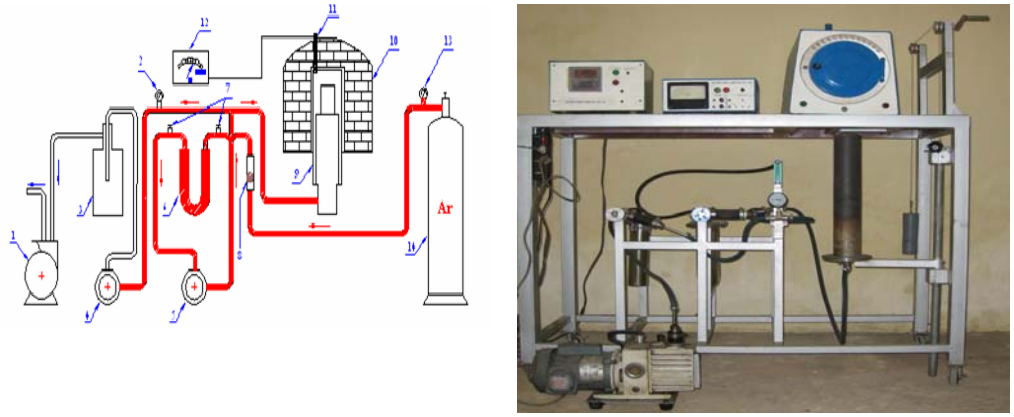

Fig. 1. Metal-thermic reduction equipment

III.1.2 Crucible for Metal-thermic Reduction

III.1.2.1 Open Crucible

This kind of crucible made of SS 304 steel, which releases little/trivial amount of gas and does not cause high pressure has been used for the system of Ca-addition-ZrO_2. Its structure is shown in the fig.2

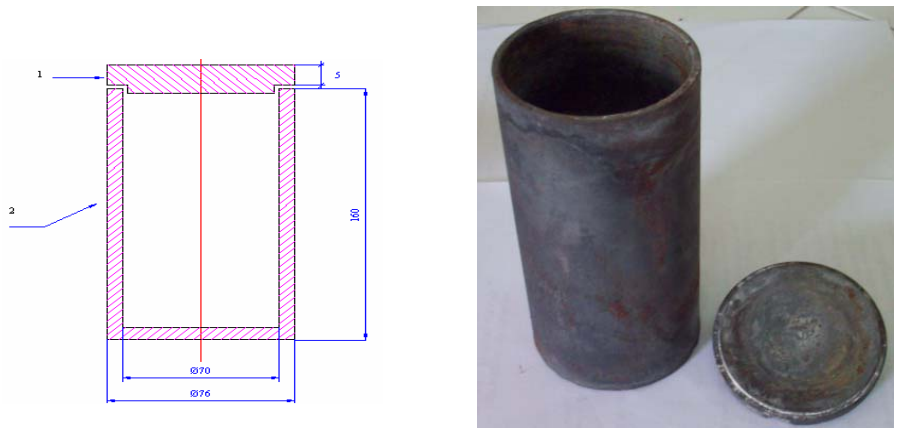

Fig. 2. Open crucible for metal-thermic reduction

1. Crucible made of SS 304, 2- cap made of SS 304

With this instrument, it is simple to cover the crucible with the cap and put it into the metal-thermic reduction bomb after loading material.

III.1.2.2 Pressure Resistance Sealed Crucible

This kind of crucible shown in the fig. 3 can resist high pressure at high temperature. It has been used for the systems of $ZrCL_4$-Ca-TrD, $ZrCL_4$-Na-TrD and $ZrCL_4$-(Na+Ca)-TrD, which releases much gas and causes generates high pressure. Its structure is shown in the fig.3.

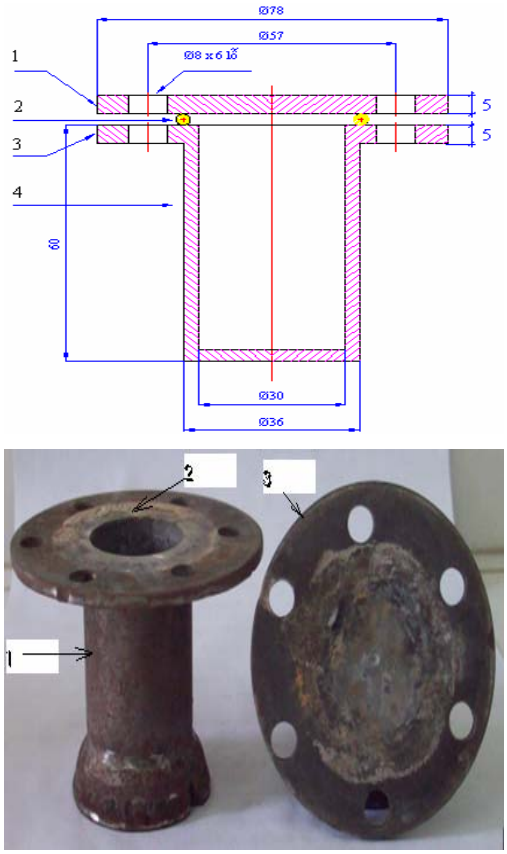

Fig. 3. Pressure resistant sealed crucible

1- Crucible body, 2- alloy seal, 3- crucible cap

With this crucible, material must be inserted under the condition of argon atmosphere. Right after loading material, the crucible must be covered with the cap and tightened by 6 screws before being inserted into a metal-thermic reduction bomb.

III.1.3 Bomb for Metal-thermic Reduction

The bomb which determines the quality of Zr powder is a very important part like a heat of the system for metal-thermic reduction. It has to work under severe conditions of high temperature and high pressure. So it must be tightly sealed to retain vacuum atmosphere throughout the reaction. The bomb (unit) made up in our laboratory is shown in fig. 4. It consisted of the body (1), which was made of SS 304 steel and has the thickness of 3-5 mm; two flanges (4) (one for the bomb and the other for the cap) with heat-resistance soft bearings (5). These bearings helped avoid leaking gas from the bomb during the reaction. The whole bomb unit was put into a high-temperature oven of 800-1000^{0}C.

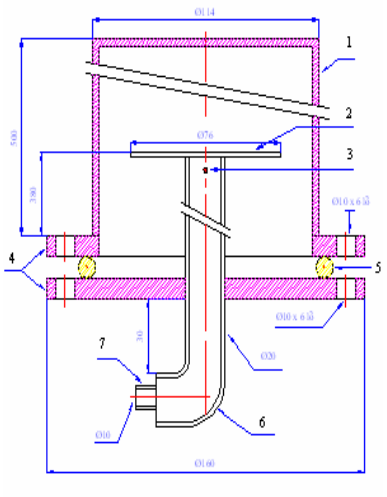

1- bomb body
2- crucible support,
3- tube/pipe for evacuating and loading Ar,
4- flanges,
5- bearing,
6- gas pipe,
7- end for joining

1
Body of bomb

2
Crucible support

Fig. 4. Bomb for metal-thermic reduction

III.2 Procedure for Preparation of Zirconium Metal

We have studied the following matters to determine efficiency of the reduction and quality of the obtained zirconium powder at our laboratory:

- The nature of components (ZrO_2, Ca, and additives), and their quantity in the metal-thermic reduction mixture;

- Technological parameters such as time and temperature of the reduction, the flow of argon, the detaining time in oven (to obtain the product in the state of powder);

- Conditions for treating the Zr product obtained from the metal-thermic reduction;

- Conditions for refining Zr powder;

- Necessary conditions for powder product storage.

- Choosing appropriate analytical methods for characterization of obtained Zr powder.

Based on the acquired results, we have determined a technological procedure for the metal-thermic reduction of zirconium dioxide, refining and storing obtained Zr powder as follows:

III.2.1 ZrO_2 Reduction

- Mix carefully the metal-thermic reduction mixture comprising 2-4 moles of Ca metal, 1 mole of ZrO_2, 1.1 moles of $CaCl_2$ (additive). Put the mixture into an open crucible.

- Insert the crucible into the oven, which is evacuated to 760.10^{-1} mmHg and filled with Ar at the flow rate of 80-120 milliliters per minute. The calcination is carried out at 950^0C for 90-120 minutes.

- Detain the metal product in the oven for 30-60 minutes.

III.2.2 Treatment of R Educed Product

- Product of the reduction is dissolved in water. Ratio of solid to liquid is 1/15;

- Drain the clear liquid, the left sludge is washed by adding HCl solution of 10-20% until no gas bubbles appear;

- Drain the clear liquid again; the left residue is Zr metal;

- Wash the product with water in a vacuumed funnel until the water coming out from the funnel does not contain Cl^- ions (tested with AgCl 1%);

- Repeat washing the product with absolute/surgical alcohol 3-5 times;

- Finally, wash the product three times with acetone.

III.2.3 Refining Zirconium Powder

The product obtained after washing contains about 2-3% ZrH_2. This substance is the principal causing gas- release (during firing) due to the reaction of

$ZrH_2 \xrightarrow{800^0 C} Zr + H_2 \uparrow$. That didn't satisfy the requirement of the Ministry of Defense. To remove ZrH_2 from Zr powder, our product was further treated by

evaluating impure elements under the condition of high temperature (800^0C) and high vacuum (760.10^{-6} mmHg) in the instrument of RVS-15G for 30 minutes.

III.2.4 Storage of Zr Powder

Zr metal, particularly in state of powder, is easily oxidized in the air, so it must be stored in non-oxidization media. The media that have been tested (at our laboratory) to store zirconium powder were the air, argon and distilled water. The result showed that in argon the speed of oxidizing zirconium was the lowest, 0.041% /month, while in distilled water and in the air these values were 0.042% and 0.046% respectively. So argon has been chosen the best medium to protect zirconium powder from oxidization.

III.2.5 Characterization And Application

The quality and specifications of our product and respective occupied analytical methods are shown as follows:

Specification	Value	Occupied analytical method
Zr metal content	98.55%	ICP-MS Plasma
Detrimental impurity (Si)	<0.15%	ICP-MS Plasma
Other impurities	<2%	ICP-MS Plasma
Activated Zr	>94.5%	Differential thermal analyzer DTG-DTA
Mean particle size	4.89 μm	Laze Dispersion Analyzer MASTERSIZER
Specific surface area	1.41-1.8m^2/g	COULTER- SA 310
Temperature of fire-catching	<200^0C	Pyrometer C700FK06 sensor K
Speed of combustion	5-8 cm/sec	Auto-recorder Canon Ixus 970 IS
Structure		X-ray diffraction BRUKER-D5005

With above specifications, our Zr powder became the material to prepare fuse MC1, which has been produced by the Institute of Explosive, General Department for Defense Industry, the Ministry of Defense. We finished the first order of 2 kg Zr powder and have filled the second order of 10 kg. This is the first time we, the Institute for Technology of Radioactive and Rare Elements (ITRRE), have been able to produce such a large amount of zirconium metal with stable quality.

IV. Conclusion

- We have self-designed and made necessary instruments and equipments for preparation of zirconium metal such as open and pressure resistant crucibles, a system of equipments for the metal-thermic reduction at the ITRRE.

- We have set up a suitable procedure for production of zirconium metal on the self-designed equipment system which gave the yield of about 300 g/batch.

- Zirconium powder prepared at the ITRRE has the same specifications as those of zirconium powder imported from some foreign companies. It has become a commodity and ordered by the Ministry of Defense.

Reference

[1]. T.S Krisnan & S. Chandra. Ductile zirconium powder by Hydride- dehydride process. Special Materials Plant-HDR- India 1976.

[2]. Ed Franknil, Adamsy. Zirconium in the Nuclear Industry. Sixth International Symposium. Philadelphia 1984.

[3]. Đỗ Ngọc Liên. Báo cáo thực hiện đề tài: Nghiên cứu công nghệ và thiết bị điều chế một số vật liệu có triển vọng ứng dụng trong ngành hạt nhân. Hà Nội năm 2003.

[4]. A.N. Gielicman; O.E.krayn. Luyện kim các kim loại hiếm. Moskva 1978 (Tài liệu Nga).

[5]. Nguyễn văn Sinh. Nghiên cứu thăm dò công nghệ điều chế $ZrCl_4$ bằng phương pháp clorua hoá ZrO_2. Hà Nội 2005.

[6]. Nguyễn văn Sinh. Nghiên cứu công nghệ điều chế $ZrCl_4$ bằng phương pháp clorua hoá ZrO_2 qui mô phòng thí nghiệm. Hà Nội 2006.

[7]. Iu. V. kariakin. Hoá chất tinh khiết. Nhà xuất bản Khoa học và Kỹ thuật Hà Nội 1990.

[8]. American Society for Metals Cleveland, Ohio. Zirconium and Zirconium alloys. American Society for Metals 1953.

[9]. D.Y. Kim, Moshutuka et al: Metall Review of Mmij, 10 (1993) P25 -45.

[10]. Z.L.K. Yasuda et al J Alloys and Comp. Vol 193 (1993) 26-28.

[11]. G. Radha Krishna, H. R. Ravindra, B. Gopalan and S. Syamsunder, Determination of iron in nuclear grade zirconium oxide by x-ray fluorescence spectrometry using an internal intensity reference, Analytica Chemica Acta Volume 309, Issues 1-3, 20 June 1995, Pages 333-338.

[12]. M. Al-Jobori, Determination of impurities in zircaloy clad by means of neutron activation analysis Journal of Radioanalytical and Nuclear Chemistry, Volume 120, Number 1/January, 1988.

[13]. Y.I. Wakoshi – Diễn đàn công nghiệp nguyên tử Nhật bản – Viện năng lượng nguyên tử Việt Nam. Hỏi & Đáp về năng lượng nguyên tử. Hà Nội, 5/2008.

[14]. United State Patent 4285724. Continuous production of finely divided zirconium powder – 2006.

[15]. Benjamin Lustman. The Metallurgy of zirconium. Megraw-Hill Book company, INC, 1955.

[16]. J.W. Mellor, D.Sc.,F.R.S. Inorganic and theoretical chemistry. Volume VII. Longmans, green and co. London. New york. Toronto.

[17]. Bùi Văn Mưu, Nguyễn Văn Hiền, Nguyễn Kế Bính, Trương Ngọc Thận. Lý thuyết các quá trình luyện kim. Hỏa luyện tập 1. Hà Nội -1997.

[18]. Phùng Viết Ngư, Phạm Kim Đĩnh, Nguyễn Kim Thiết. Lý thuyết các quá trình luyện kim. Hỏa luyện tập 2. Hà Nội -1997.

[19]. Zirconium metal powder Grrade AB, dry – Article Number 453085 – Special Metals Division.

STUDY ON ANALYSIS PROCEDURE OF U, Th, Ra, V, Fe, Ca, Mo AND COMPLETING ANALYSIS OF NUCLEAR GRADE URANIUM IN ORDER TO DETERMINE RATIO OF O/U MEETING ASTM STANDARD FOR MANUFACTURING UO_2 FROM URANIUM IN VIETNAM

Doan Thanh Son, Nguyen Xuan Chien, Nguyen Thi Kim Dung, Nguyen Thi Thuy, Nguyen Quoc Hoan, Dinh Cong Bot, Dao Nguyen, Pham Ngoc Khai, Tran Ngoc Diep, Bui Kim Ngan, Phung Vu Phong and Nguyen Hanh Phuc

Institute for Technology of Radioactive and Rare Elements, VAEC

Abstract: We have carried out this project for analyzing contents of Uranium and Th, Ca, Fe, V, Mo in Uranium ore by using X-ray fluorescence spectrometry method. We have also researched parameters of X-ray generator such as Cu, Mo secondary fluorescence target, exciting high voltage, current X-ray tube, procedure for preparing samples, measuring time, detection limit. By using standard samples which have contents known in advance and calculating based on fundamental parameters, we can determine contents of U, Th, Ca, Fe, V, Mo in the samples accurately. Uranium and other radioactive nuclei in the solid and liquid waste have been determined by using Gamma spectrometry and ICP mass spectrometry method. The specific energy lines and procedure for preparing and storing samples have researched. After storing experimental samples for a month to attain equilibrium, we have measured them by using Gamma spectrometry Digidard-10 on Gamma vision software.

Besides, we have carried out experiments to find out optimal parameters of conditions and time in vacuum heating for determining the ratio of O/U. Based on the received results, procedures for determining ratio of O/U have been set up according to ASTM standard.

Keyword: X-ray fluorescence, Gamma spectrometry, O/U ratio, U, Th in Uranium ore

I. Introduction

Analyzing contents of radioactive, rare elements and others in Uranium ore accurately plays an important role in prospecting for ores in order to estimate Uranium ore sources and choose an appropriate technology for separating Uranium from ore containing Uranium.

Nowadays, treating and managing radioactive waste are the first concern of many countries, which have nuclear technology. Up to now, analyzing contents of radioactive elements such as U, Th, Ra during treating radioactive waste has not been concerned properly, so that finding out an appropriate procedure for analyzing dangerous radioactive elements will meet the demands for managing radioactive waste of departments in ITRRE.

In addition, to determine the ratio of O/U is very important in estimating the quality of nuclear grade UO_2 because it is a norm for evaluating the regular composition of pellet UO_2. ITRRE has used the spectrometry method for researching and determining the ratio of O/U. However, accuracy degree of this method is not high, so it

was not used widely. Therefore, to research and apply the gravimetric method based on ASTM standard is necessary, meeting demand of high degree accuracy and standardization of method according to international standard.

II. Experiments and results

II.1 Equipment

The X-Ray Fluorescence Spectrometry System Includes:

- The excitation source: X-ray tube; Compact generator 3K5 with Mo anode and Mo secondary target;

- Si (Li) SL 30165 detector of 30 mm^2 and 25μm Be window with energy resolution of 180 eV (at 5.9 keV) of ^{55}Fe;

- Pre-amplifier Canberra Model 2008B, Canberra AFT Research Amplifier Model 2025, Canberra Multi port II Multi channel analyzer;

- Data acquisition software GENIE-2000, spectrum processing: Win Axil;

- High-Purity Germanium Spectrometry: Detector: p type;

- Detector Diameter: 54.95 mm; Detector Length: 63.5 mm. End Cap to Detector: 3 mm; Absorbing layers Aluminum 1.27 mm. Resolution (FWHM): 1.80 keV at 1332 keV, Co-60, Peak-to- Compton Ratio 52:1 at Co-60;

- A vacuum oven with possibility of maintaining and controlling temperature to 180^0C, equipped with double stopcocks and a vacuum gage with range from 0 to 102 kPa (0 to 30 in. Hg);

- Muffle furnace with possibility of maintaining and controlling temperature to 1000^0C.

II.2. Determine U and Other Elements Such As Ca, Mo, Si, V, Fe, Th In Uranium Ore By X - Ray Technique; Uranium In Solution Phases In Leaching Processing

II.2.1. Optimize Parameters of X -ray Generator

The purpose of this research is to compare fluorescence yields when using the Cu secondary target (energy: 8.05 keV) with using the Mo secondary target (energy: 17.48 keV) so that we can find out the highest fluorescence efficiency for each element of experimental samples. Besides, we have also researched parameters of X-ray generator such as voltage, current X-ray tube.

The experimental results show that when Uranium ore samples are excited by Cu secondary target, Ca, ,Si, V and Fe give higher X-ray intensity, and when U samples are excited by Mo secondary target, U, Th give higher intensity.

Tab 1. The X-ray intensity of U, Th in Uranium ore at high voltage U = 45(kV); U = 50 (kV) and different current values I (mA).

Number	**Element**	**X-ray Intensity of U, Th in uranium ore at high voltage U= 45, U = 50 (kV) and different current values I (mA).**			
		I=10 mA	*I=15 mA*	*I=20mA*	*I=25 mA*
1	U	26421	35555	47029	54943

2	Th	721	1009	1587	1353
Dead time (%)		8.32	12.56	15.56	22.41

Remark: The experimental results show that fluorescence intensity depends on exciting voltage (U), and current values (I) of X-ray generator. So U=45 kV and I=20 mA were selected for determining Si, Ca, V, Fe in Uranium ore to obtain the highest fluorescence intensity for each element. The same experiments with Cu secondary target, U=45 kV, I=20 mA were selected for determining U, Th in Uranium ore.

II.2.2. Determine Uranium In Solution Phases In Leaching Processing

Analyzing solid sample directly without dissolving is the best advantage of X-ray technique method. However, in some necessary cases, we can analyze samples in solution by XRF.

II.2.2.1. Study On Effect of Solvent On Determination of Uranium In Liquid Samples

The HNO_3 solvent is used to dissolve sample.

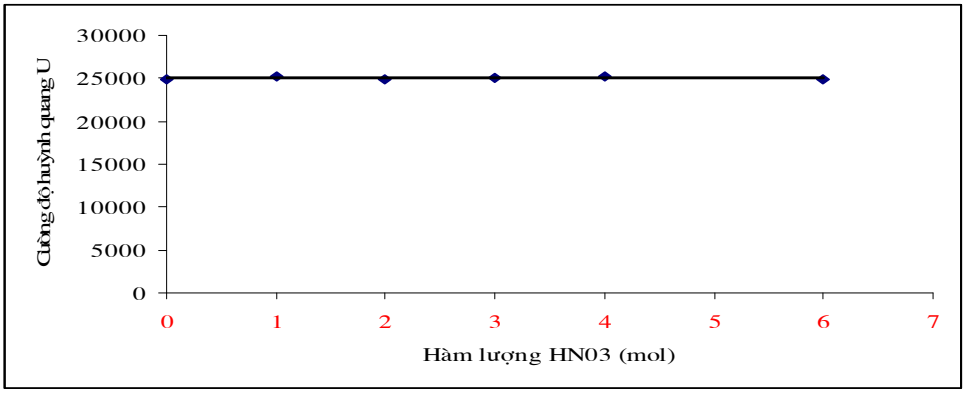

Fig. 1. The effect of different concentrations of HNO_3 solvent on determining U in liquid samples.

Remark: The figure 1 shows that concentration of HNO_3 solvent does not influence analysis of U in liquid samples.

II.3. Determine U, Th In Uranium Ore In Vietnam; U, Th and Other Radioactive Nuclei In Solid and Liquid Waste By Gamma Spectrometry Method

II.3.1 Research for Selecting Direct Energy Peaks

Determination of Uranium can be carried out by researching its direct as well as indirect energy peaks in the radioactive equilibrium range. It is not necessary to store radioactive non- equilibrium samples when amazing U and Th.

The 63.3 keV peak includes the 63.3 keV Gamma- ray (3.9%) (1^{st} peak) emitted from Th-234, the 63.9 keV Gamma-ray (0.023%) from Th-231(2^{nd} peak) and the 63.9 keV Gamma-ray (0.255%) from Th-232(3^{rd} peak). However, the 2^{nd} peak and the 3^{rd} peak can be neglected. The experimental results show that the ratio of Th-234/U-238 equals to 0.973. It means that the measurement of Th-234 activity can obtain activity of U-238. However, an important drawback of 63.3 keV line is its high self-absorption, which depends on the apparent density of the sample.

In general, the 63.3 keV line of U-238 and 1001 keV line of Pa-234 can be used for analyzing activity of U-238 in samples.

II.3.2. Study On Sample Store Processing and Radioactive Non- Equilibrium Samples

The represents of Rn-222 ($T_{1/2}$=3.8 day), which is noble gas and can migrate substance distanced from its source, in decay series of U-238 can make non-equilibrium between Ra and Rn. So, to analyze indirectly U by their daughters in equilibrium series, sample should be stored for 1 month to attain equilibrium between Ra-226 and Th-228 with their daughters.

Tab 2. Study the samples store process for waste samples

Radioactive waste	**Gamma-ray energy (keV)**				
	63.29 keV	*185.99 keV*	*609.32 keV*	*911.07 keV*	*1764 keV*
After 2 days	1872	37216	62265	924	24324
After 4 days	1890	36862	66213	914	29123
After 7 days	1869	37187	72314	930	32165
After 12 days	1875	37103	74313	910	34116
After 20 days	1860	36965	77982	905	35507
After 22 days	1880	37120	78431	925	35412

II.3.3. Study On The Efficiency of Detector for Different Energy Ranges

In this experiment, we use the references material standard RGU with activity 400 ppm and RGTh with activity 800 ppm.

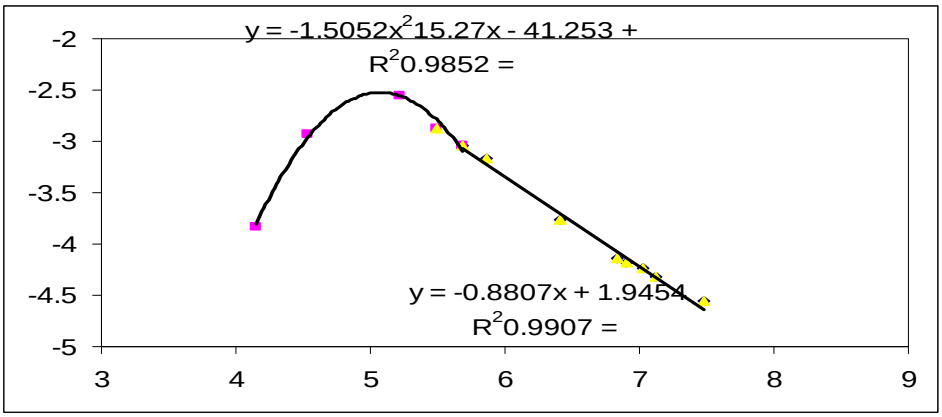

Fig. 2. The efficiency curve of measure geometry 3pi, mass: 180 g

II.4. Determine Uranium And The Ratio of Oxygen To Uranium (O/U)

There are two main stages in determine process of Uranium and the ratio of oxygen to uranium atomic (O/U), they are: heating and igniting samples. In the heating stage, UO_2 pellet received should be dry and valence of Uranium is not changed. UO_2 pellet is pressed at high pressure, so to ensure that the moisture content is run out of

pellet, the heating stage should be carried out in vacuum oven. In the igniting stage, the UO_2 pellet should be ignited by two stages to avoid strong reaction.

II.4.1. Study On Conditions and Range Of Time For Heating UO_2 pellet

Transfer approximately 5 ± 0.0001 g of UO_2 pellets to a platinum crucible. Place the crucible in a vacuum desiccators, and reduce the pressure to approximately - 0.04 Mpa. Close the vacuum valve and slowly flush the oven with dry argon until pressure around 0. Close the argon inlet and reduce the pressure to -0.04Mpa. Repeat the experiment 2 times. Then reduce the pressure to -0.07MPa. Set the temperature at 150^0C, and maintain this condition for 1h, 2h, 3h, 4h, 5h,etc. After that, turn off the heat and allow the oven temperature decrease to room temperature during reducing pressure. Turn off the vacuum valve and slowly introduce dry argon until the oven door can be opened. Transfer the crucible to desiccators and cool it. Remove the crucible and weigh it immediately. Time for heating samples at pressure - 0.07 MPa were showed in the Figure 3.

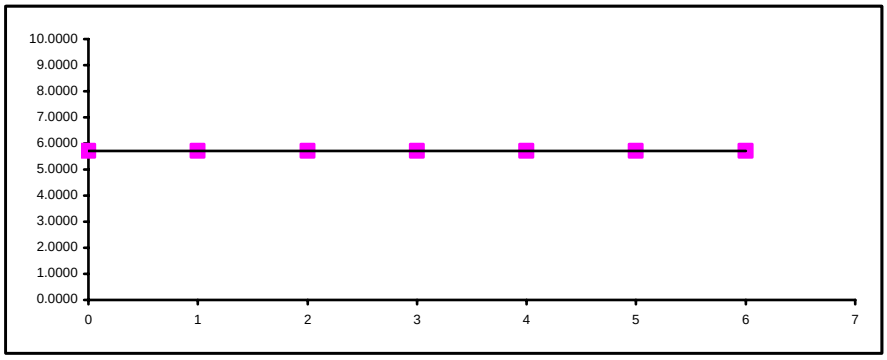

Fig. 3. Study the time for heating UO_2 pellet at pressure - 0.07 MPa

Remark: The results show that the mass of UO_2 pellet is almost constant after samples are heated at pressure - 0.07 MPa. It means that moisture content in UO_2 pellet is small and the loss when drying it is also small. To have confidence when determining the O/U ratio, we chose the conditions and range of time for the heating UO_2 pellet**:** p = - 0.07 MPa; time = 4 hour.

II.4.2. Study On Conditions and Range Of Time For Igniting UO_2 Pellet.

After heating UO_2 pellet samples in vacuum oven, they are ignited by two stages:

- Stage 1: samples are preheated at 500^oC for 3 hours.
- Stage 2: samples are then ignited at 900^oC for 1h, 2h, 3h,etc.

After that, remove the crucible from the furnace; cool it in the air for 2 to 3 min., then place it in desiccators and cool to room temperature and weigh it. The results show that the mass of UO_2 pellet increases after heating it at 500^oC for 3h and igniting it at 900^oC for 1h, but if we continue igniting it at 900^oC for 2h, 3h, 4h, its weight almost are constants. It proved that after igniting UO_2 pellet at 900^0C for 1h, it almost converts into U_3O_8.

To ensure accurately for igniting stage, we chose parameters: preheat samples for 3h at 500^0C and then ignite them for 3h at 900^0C.

III. Results and Discussion

III.1. Analyze Reference Material Standards By XRF Method

Tab 3. The Reference Material Standards RGU, UM, the U synthesized standard have been analyzed by using a fundamental parameter method

N°	Sample code	**U** (ppm)			**Th** (ppm)		
		Found Value by XRF	*Certified Value*	*Absolute Error*	*Found Value by XRF*	*Certified Value*	*Absol Error*
1	Reference Material Standards UM	4670±150	4800	150	14.5±3.2	12	2.5
2	Reference Material Standards RGU	426± 35	400	26			
3	Synthesized standard Uranium 2709a	43.5± 6.0	40	3.5	88.6±3.2	100	11.4

III.2. Analyze Uranium Ore In Vietnam and Compare With Gamma Spectrometry Method:

Tab 4. Analyze Si, Ca, V, Fe in Uranium ore in Vietnam by X-ray, using a fundamental parameter method compared with other analysis methods.

Sample code	**CPH** (%)		**BPH** (%)		**PH** (%)	
	XRF	ICP	XRF	ICP	XRF	ICP
Ca	1.21	0.931	0.37	0.232	0.016	0.02
V	0.054	0. 062	0.074	0.082	0.127	0.124
Fe	1.1	1.1	1.22	1.14	0.85	0.82
Mo	0.0018	0.0015	0.0017	0.0015	0.0017	0.0015

III. 3. Results Obtained When Analyzing U In Liquid Samples

Tab 5. Results obtained when analyzing some secondary standard samples.

Number	**Sample code**	**Certified Value (ppm)**	**Found Value** (ppm)	**Absolute Error**
1	R1	20	18.2± 3.2	1.8
2	R2	50	53.20± 4.0	3.2
3	R3	75	72.03± 4.6	2.03
4	R4	100	104.80±5.7	4.8
5	R5	150	146.36± 7.2	6.36

III.4. Results Obtained When Analyzing Solid Waste Samples By Gamma Spectrometry Method

Tab 6. Results obtained when analyzing solid waste samples by Gamma spectrometry method.

Number	**Radioactive**	**Radioactive waste 1** *(Bq/kg)*	**Radioactive waste 2** (Bq/kg)	**Radioactive waste 3** (Bq/kg)
1	K-40	965	972	1002
2	Tl-208	99.34	97.65	96.77
4	Pb-212	88.8	85.32	89.54
5	Pb-214	7091	6953	6987
6	Bi-214	7131	7018	6892
8	Ac-228	97.11	102.1	93.5
9	Th-234	1489	1236	1315
10	Ra-226	7120	7058	7087

Tab 7. Comparison of results analyzing liquid waste by Gamma spectrometry method and by ICP-MS method.

Sample code	**Gamma spectrometry method**		**ICP-MS method**	
	U (ppm)	Th (ppm)	U(ppm)	Th (ppm)
1	3± 0.3	1.5± 0.3	2.6	1.2
2	2.8± 0.3	1.2± 0.2	2.6	0.94
4	3.1± 0.3	0.16 ± 0.04	2.6	0.12

III.5. IAEA-CU-2006-03 Worldwide open proficiency test on the determination of Gamma emitting radio nuclides. Laboratory No 388)

Tab 8. Results of Worldwide open proficiency tests on the soil samples.

Analysis sample	**Energy** *(keV)*	**IAEA Value** *(Bq/kg)*	**Lab Value** *(Bq/kg)*	**Precision**	**Final Score**
Mn-54	834.1	48 ± 0.8	56.1 ±1.22	A	N
Co-60	1332.51	56.1± 1.7	56.7 ±1.29	A	A
Zn-65	1115.2	77.6 ±2.4	78.7 ±1.40	A	A
Cs-134	604.6	64.2 ±1.7	62.7±1.62	A	A
Cs-137	661.2	52.6 ±1.8	57.1± 1.36	A	A
Am-241	59.4	96.6± 2.7	88.5± 7.13	A	A

Tab 9. Results of World-wide open proficiency test on water sample.

Analysis sample	**Energy** *(keV)*	**IAEA Value** *(Bq/kg)*	**Lab Value** *(Bq/kg)*	**Precision**	**Final Score**
Mn-54	834.81	4.89±0.017	4.96±0.42	A	A
Co-60	1332.51	5.8±0.04	6.26±0.12	A	W
Zn-65	1115.52	7.27±0.075	6.31±0.25	A	N
Cd-109	88.04	19.62±0.1	26.15±0.47	N	N
Cs-134	604.66	13.03±0.1	13.88±0.36	A	A
Cs-137	661.62	16.72±0.08	18.25±0.64	A	A
Am-241	59.54	3.66±0.023	4.67±1.32	N	N

Tab 10. Results obtained when determining ratio of O/U in UO_2 pellet by using ignition gravimetric impurity correction method

Number	**Sample code**	**Ratio of O/U**	**Remark**
1	U1	2.0318	
2	U2	2.0355	
3	U3	2.0372	

IV. Conclusion

Some obtained results:

IV.1. Determine U and Other Elements Such As Ca, Mo, Si, V, Fe, and Th In Uranium Ore by X- ray Method

Parameters of X-ray generator have been chosen and optimized. Experimental results indicated that V, Si, Mo, Ca, Fe give higher in X-ray intensity when they are excited by Cu secondary target while X-ray intensity of U, Th is higher when they are excited by Mo secondary target.

For analyzing Uranium ore, the following parameters were chosen: high voltage U=45kV and current X-ray tube I =20mA for exciting by Cu secondary target; high voltage U=45kV, current X-ray tube I =25 mA for exciting by Mo secondary target

After studying some sample preparation methods, we found that sample pellets with density of 0.15 g/cm^2 at high pressure are optimistic. The time for counting sample is 1200s.

We have studied some quantitative analytical methods used in X-ray fluorescence such as calibration curve method, transition emission method and fundamental parameter method. We used the fundamental parameter method for analyzing because of its advantages: use only small amount of standard sample, calculate simply, can be used on a large scale.

We have also used Am-241 radioactive sources for exciting U in Uranium ore. The results indicated that the most optimal distance from sample to radioactive source is 2.2 cm; time for measuring samples is 3600s.

U was analyzed directly in solution from ore leaching process by XRF. The parameters of X-ray generator such as U=40 kV and I=20 mA were selected. HNO_3 and NH_4OH solutions with different concentrations were selected. The experimental results showed that different concentrations of these solutions don't affect determination of U in liquid solution.

IV.2. Determine U, Th and Other Radioactive Nuclei In Uranium Ore, In Solid and Liquid Waste By Gamma Spectrometry Method

We have chosen special energy lines for determining U, Th directly in non-equilibrium samples, for determining U, Th indirectly and other radioactive nuclei in radioactive equilibrium condition.

We have studied efficiency of detector for different energy ranges, calculated efficiency for different measured geometry such as 3pi 180 g, 240 g, 500 ml, 2pi: 200 ml, 250 ml, and 500 ml.

Based on the results, we have built the procedure for the determining U, Th and other radioactive nuclei in Uranium ore, in solid and liquid waste by Gamma spectrometry method. We have tested precision and accuracy of quantitative analysis meeting references material standard and compared with results of other laboratories in the World by analysis proficiency test.

IV.3. Determine U, Th In The Liquid Waste By ICP-MS

We have studied parameters, which influence the results of analysis of liquid waste by ICP-MS and found that intensity of spectrum line is maximum when sample depth is 6.5 mm, RF Power is 1420 W, and speed of carrier gas is 1.35 l/minute.

We have studied effect of some elements such as Na, K, Al, and Ca with large concentrations on analysis of U, Th. Based on the results; we have built the procedure for the determination of U, Th in the liquid waste by ICP-MS.

IV.4. Determine The Ratio of O/U By The Ignition (gravimetric) Impurity Correction Method

After studying pressure conditions: p = -0,04 MPa, p = -0,07 MPa and heating time: 1h, 2h, 3h and 4h, we have chosen the pressure p = - 0,07 MPa, heating time = 4 hour for determination of the ratio of O/U by the ignition (gravimetric) impurity correction method.

We have studied the conditions and range of time for igniting UO_2 pellet**.** The results showed that UO_2 pellets are ignited in two stages: preheating in 3h at 500^0C and then igniting in 3h at 900^0C, and UO_2 pellets well converted to U_3O_8.

We have set up the procedure for the determination of O/U by the ignition (gravimetric) impurity correction method to meet ASTM standard.

Reference

[1]. ASTM C 696- 93 Standard test methods for chemical, mass Spectrometric, and spectrochemical analysis of nuclear-grade uranium dioxide power and pellets, 1994.

[2]. Analytical techniques in uranium exploration and ore processing, Vienna-International Atomic Energy Agency, 1992.

[3]. Ron Jenkins , X-ray Fluorescence Spectrometry. John Wiley &Son, Ed 1988.

[4]. IAEA- TECDOC-950. Sampling, storage and sample preparation procedures for X-ray fluorescence analysis of environmental material. IAEA June 1997.

[5]. IAEA. QXAS Quantitative X-ray Analysis System. Ver1.2 (1995-1996).

[6]. IAEA-TECDOC-1121, Industrial and environmental application of nuclear analytical techniques. Report of workshop, Vienna, September 1998.

[7]. Rene E.Van Grieken,. Handbook of X-ray Spectrometry. Second edition.2002.

[8]. Bertin Eugene P. Principles and practice of X-ray spec analysis 2nd edition, 1975.

[9]. P.Quittner, Peak Area Determination for Ge (Li) Detector Data, and Methods, 1969.

[10]. Peter M. Van Dyck and Rene E. Van Grieken, Absorption Correction via Scattered Radiation in EDXRF analysis for Samples of Variable Composition and Thickness, Anal. Chem (1980) 1859.

[11]. R. Tertian and F. Claisse, Principles of Quantitative X-ray Fluorescence Analysis, Heyden & Son LTD., London-Philadelphia-Rheine (1982).

[12]. V.Osorio, WinAxil Software Package. Manual Version 1.4, 12/2002

[13] Technical Reports series No-308: Construction and use of calibration facilities for radiometric field equipment. International Atomic energy Agency Vienna, 1989.

[14]. Nguyễn Hào Quang, Phóng xạ môi trường, tuyển tập các bài thực hành nâng cao dành cho cán bộ ngành năng lượng nguyên tử.

[15]. N.Q.Huy, T.V.Luyen , Appllied Radiation and Isotopes 61 (2004) 1419-1424 A method to determine U-238 activity in environmental soil samples by using 63.3- keV – photopeak-gamma HPGe spectrometer.

SETTING UP THE PREPARATION PROCESS OF THE POROUS POLYMERIC ADSORBENT SGS-NT8(H^+) FOR THE TREATMENT OF WASTEWATER WITH PRELIMINARY APPLICATION TO SEPARATING UO_2^{2+} FROM WASTEWATER IN THE URANIUM LEACHING PROCESSES

Nguyen Minh Thu, Nguyen Phuong Nam, Nguyen Minh Phuong and Pham Hong Ha

Institute for Technology of Radioactive and Rare Elements, VAEC

Abstract: A preparation process of the porous polymeric adsorbent SGS-NT8(H^+) set in the laboratory includes: (1) synthesizing the polymer SGS-NT8 by the polycondensation of resorcinol (R) and formaldehyde (F) with the molar ratio F/R = 2.75 in an acid medium (with the determinate time period and temperature in each reaction stages); and (2) chemically treating the polymer SGS-NT8 into the porous polymeric adsorbent SGS-NT8(H^+) (similar to an ion exchanger) by contacting with 5M H_3PO_4 solution at 110° C or 5M H_2SO_4 solution at 100° C for 2 hours. SGS-NT8(H^+) resins in the agglomerated powder or block form have a spatial globular structure like SGS-NT8, the microglobule surface is coated with acid functional groups with the content in the range of 2.290 - 2.578 meq H^+/g. The SGS-NT8(PH^+) resin, i.e. SGS-NT8 treated with H_3PO_4, has not only the higher total ion-exchange capacity than that of SGS-NT8(SH^+), i.e. SGS-NT8 treated with H_2SO_4, but also a selective adsorption capability to UO_2^{2+} from the study solution as well as from the wastewater in the Uranium ore leaching processes, particularly in a H_2SO_4 solution at pH 6, the Uranium recovery efficiency reached 98%.

Key words: SGS - polymer, adsorption, Uranium

I. Introduction

Numerous great progresses have been recently achieved in the field of ion exchange and adsorption technology thanks to the development of macroreticular pore or spatial globular structure of polymeric material (named SGS polymer) since the seventies of the last century [1-5]. The advantages of this material include a large inner surface area and a high pore volume. Effective synthesis processes are therefore in need to improve in the pore and inner surface area parameters of a large range to meet specific application purposes [6, 7].

Recently, the industrial production has been increasingly developed and the nuclear power plant will be built in Vietnam in the near future; as a result, the treatment of industrial and radioactive wastewaters is becoming a particularly urgent issue that draws a great attention from environmental engineering and sciences. Studying the preparation of new materials for cleaning wastewater before releasing to the environment is thus extremely necessary. The aim of this subject is setting up a preparation process of the porous polymeric adsorbent SGS-NT8 in the laboratory by which the product will be applicable to separating UO_2^{2+} from the study solution and the wastewater in the Uranium leaching processes. The results of this subject will allow us to assess the domestically initiative preparation of a new adsorbent material used in the treatment technology of radioactive wastewater in particular, and of industrial wastewater in general.

II. Experiment

1. Preparation Process of SGS-NT8(H^+)

A series of the experiments were set up to determine the optimal condition involving mol ratio F/R, pH, T^o and τ for the synthesis reactive stages of SGS-NT8. Subsequently, these optimal parameters were combined together in further synthesis to provide an acceptable polymer SGS-NT8 having the characteristics most similar to that of the control sample SGS-81 available (USR) [5-21].

The optimal condition for the chemical treatment is determined by contacting 5 g of a suitable SGS-NT8 sample with H_2SO_4 or H_3PO_4 solution of a concentration (1.5-7.5M) in a controlled temperature (80-120^{o}C) for a definite period of time (1-4 hrs) [19, 27-30]. After being neutralized, the quality of the dry treated sample was evaluated by the total static cation exchange capacity Q_o (meq H^+/g) [20-22]. The typical characteristics of SGS-NT8 and SGS-NT8(H^+) were analyzed and compared with SGS-81, therein the form of the network structure, the microglobule size and the pore size were determined on the stereo microscope LABOMED or the scanning electron microscope (SEM).

2. Adsorption of UO_2^{2+} on SGS-NT8(H^+)

2.1. Adsorption of UO_2^{2+} In The Study Solution

2.1.1. Batch Operation

The experimental conditions used for studying the sorption of UO_2^{2+} under static conditions are summarized on Fig. 4, 5, 6 and 7. After a given period of time (i.e. 10; 30; 60; 90; 120 and 150 minutes) the equilibrium UO_2^{2+} concentration was determined either by spectrometrically with H_2O_2 at 375 nm on the UV-1601 Shamash (Japan) or by ICP-MS method. The UO_2^{2+} adsorption capacity of the resin (q) was like a function of pH, C_o and τ, and calculated by:

$$q = (C_o - C) \cdot V/m, \text{ [mg } UO_2^{2+}/g] \quad (1)$$

when C_o and C are the initial and equilibrium UO_2^{2+}concentrations, [mg/mL], respectively; V is the solution volume, [mL]; m is the amount of dry resin, [g] [22 - 26].

The distribution factor K_d of UO_2^{2+} on two kinds of resin was calculated by:

$$K_d = [(C_o/C) - 1] \cdot V/m, \text{ [mL/mg]} \quad (2)$$

2.1.2. Column Operation

A glass column (ϕ = 1.8 cm, l = 20 cm) with a down top valve, holding a tablet of SGS-NT8(PH^+) (m = 2.945 g, d = 0.386 g/cm^3) in the block form (ϕ = 1.8 cm, l = 2.85 cm, wet resin volume V = 7.6 mL) was examined.

a) Dynamic Exchange Capacity: Before an experiment the resin column was washed by passing 20 mL H_2SO_4 solution at the same pH of the UO_2^{2+} solution. The experiment conditions are summarized on Fig. 8, 9. The UO_2^{2+} concentration in each 20 mL of the eluate (C) was determined, then the breakthrough curve was set up [20, 26-30]. The amount of adsorbed UO_2^{2+} was eluted with the solution containing 10 g

Na_2SO_4 in 1L 2M H_2SO_4 and washed by water. The resin was regenerated by 20 mL 1M H_2SO_4 solution and washed with water until the wash water became neutral.

b) Elution of UO_2^{2+}: The experiment conditions were summarized in Table 1. The same amount of adsorbed UO_2^{2+} was deadsorbed by using one of three solutions containing 10g Na_2SO_4, respectively in 1L of destilated water, 1L 1M H_2SO_4, 1L 2M H_2SO_4 and washed by water, those in the minimum volumes. The UO_2^{2+} concentration in the eluate was determined to calculate the elution efficiency (η_{rg}) by:

$$\eta_{rg} = (m_{rg}/m_{hp}) \cdot 100, [\%] \quad (3)$$

where m_{hp} and m_{rg} are the adsorbed and deadsorbed UO_2^{2+} amounts, [mg].

c) Regeneration of SGS-NT8(PH^+): The experiment conditions were summarized in Table 2, the adsorbed UO_2^{2+} amount was the same in each cycle. The eluated UO_2^{2+} concentration was determined to calculate the recovery efficiency (η_r) by:

$$\eta_r = (m_r/m_o) \cdot 100, [\%] \quad (4)$$

where m_o and m_r are the adsorbed and eluted UO_2^{2+} amounts, [mg]. This sorption-elution procedure was repeated 8 times, in there after three consecutive cycles the resin was regenerated.

2.2. Separation of UO_2^{2+} From The Real Wastewater By The Column Operation

Two liters of the wastewater from the Uranium ore leaching processes containing UO_2SO_4 (supplied by ITRRE) had pH~1. After being neutralized and filtered to reject a majority of U, Fe and other metals present in the solution, 1250 mL of the filtrate (feed solution) was adjusted pH = 6 and passed through the column holding a tablet of SGS-NT8(PH^+) changed in Na^+ form (m = 1 g, the wet volume V = 2.85 mL) at the flow rate of 3.1 SV/h. The concentration of some metal elements in the feed and the effluent were determined by the ICP-MS method (ITRRE). The separation efficiency (η_t) was calculated by:

$$\eta_t = [(C_o - C_r)/C_o] \cdot 100, [\%] \quad (5)$$

where C_o and C_r are the UO_2^{2+} concentrations in the feed and out stream, [mg/mL], respectively, and K_d of each metal element was calculated by the formula (2).

III. Results

1. Preparation Process of SGS-NT8(H^+)

A stable preparation process of SGS-NT8(H^+) with the optimal condition has been set up as illustrated by the diagram in Fig. 1. The product is SGS-NT8(H^+) in two forms: SGS-NT(SH^+) and SGS-NT8(PH^+), which have the characteristics similar as of SGS-81: Black brown color, soft, easy cut; Network structure including microglobules connected to each other at the point of contact forming inter-connected micropores, micropoints are attached on the microglobule surface (Fig. 2 and 3); Size of microglobules: 5-7 μm; Pore size: 5-10μm; Porosity: 75-82%; Total cation exchange capacity (or content of functional group) reached 2.290 meq H^+/g for SGS-NT8(SH^+) and 2.578 meq H^+/g for SGS-NT8(PH^+); while this value for SGS-81 is of 1.5-1.7 meq H^+/g [5].

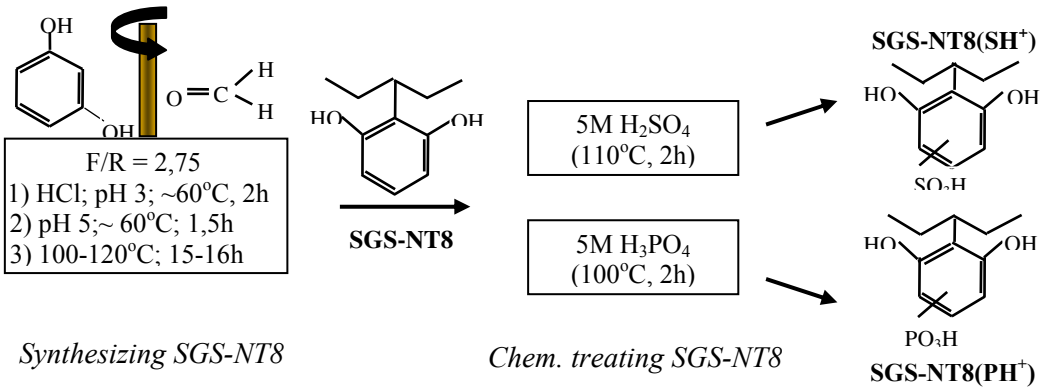

Fig. 1. Preparation process of SGS-NT8(H^+)

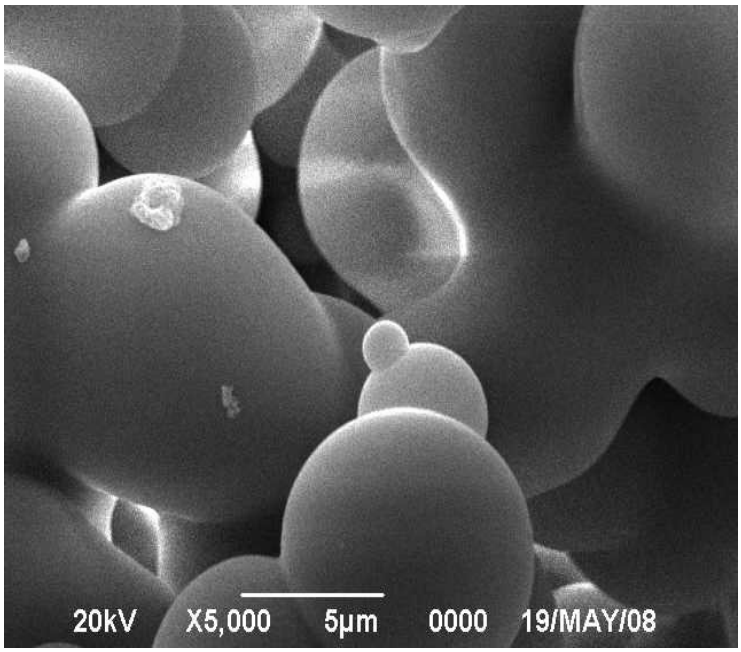

Fig. 2. SEM: SGS-NT8 microglobules before the chemical treatment

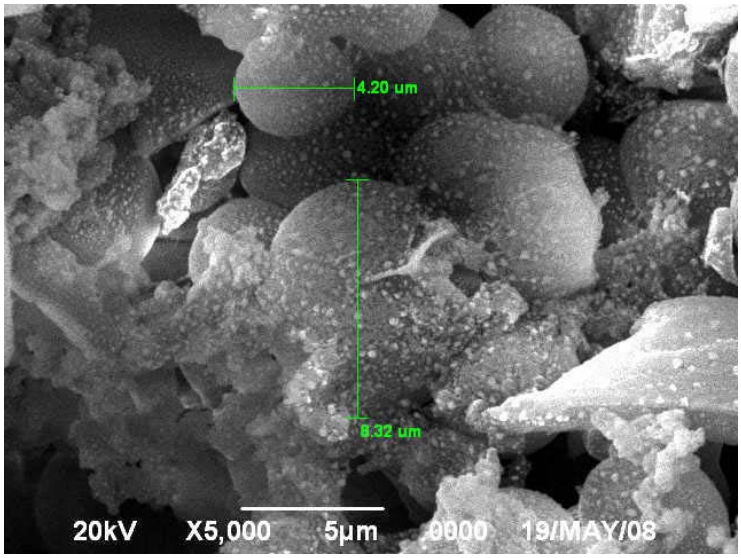

Fig. 3. SEM: SGS-NT8 microglobules treated by H_3PO_4

2. Adsorption of UO_2^{2+} on SGS-NT8(H^+)

2.1. Adsorption of UO_2^{2+} In The Study Solution

2.1.1. Batch operation:

Both SGS-NT8(SH^+) and SGS-NT8(PH^+) exhibit the UO_2^{2+} adsorption ability and influenced by pH, C_o and τ (Fig. 4, 5 and 6); SGS-NT8(SH^+) has the best adsorption at pH 4 while SGS-NT8(PH^+) at pH 5 (Fig. 4). The UO_2^{2+} adsorption of SGS-NT8(PH^+) is increased with the increase of C_o and τ, becoming saturated when $C_o \geq 0{,}5$ mg UO_2^{2+}/mL or $\tau \geq 2$ hrs when all of the active places of the function groups are completely replaced by ion UO_2^{2+} (Fig. 5 and 6). SGS-NT8(PH^+) had the better UO_2^{2+} adsorption than SGS-NT8(SH^+) at any pH (Fig. 4), that also shown by the K_d on SGS-NT8(PH^+) that is always higher than on SGS-NT8(SH^+) (Fig. 7).

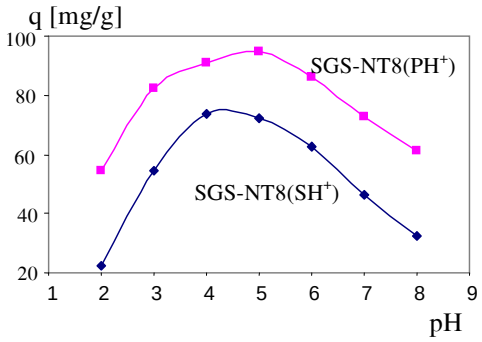

SGS-NT8((SH$^+$), SGSNT8(PH$^+$): 0.5 g; size: 0.125-0.147 mm; V = 50 mL; C_o= 0.01M (2.7mg UO_2^{2+}/mL); τ = 24 h; 25^{o}C.

Fig. 4. Effect of pH on the adsp. capacity

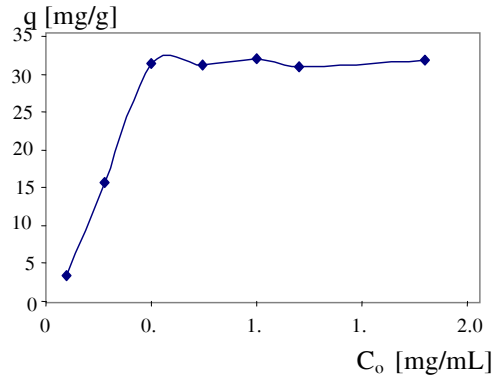

SGS-NT8(PH$^+$): 0.5 g; size: 0.125 - 0.147 mm; V = 50 mL; $C_o(UO_2^{2+})$= 0.37 - 6.67mM; pH 5; τ = 24 h; 25^{o}C.

Fig. 5. Effect of C_o on the adsp. capacity

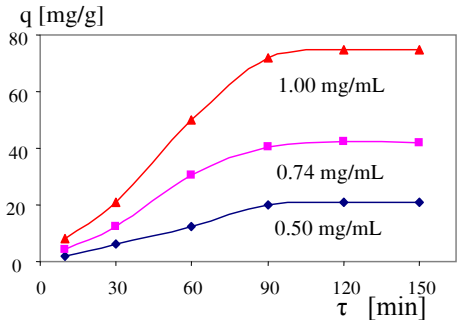

SGS-NT8(PH$^+$): 0.5 g; size: 0.125 - 0.147 mm; V = 50 mL; $C_o(UO_2^{2+})$ = 1.85; 2.74; 3,8mM; pH 5; T^o = 25^{o}C.

Fig. 6. Effect of C_o and τ on the adsp. capacity

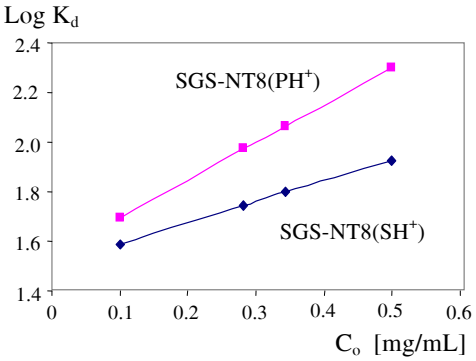

SGS-NT8SH, SGS-NT8(PH$^+$): 0.5g; size: 0.125 -0.147mm; V =50 mL; $C_o(UO_2^{2+})$= 1.85; 2.4; 3,8mM pH 5; τ = 2 h; 25^{o}C

Fig. 7. K_d depends on C_o

2.1.2. Column Operation:

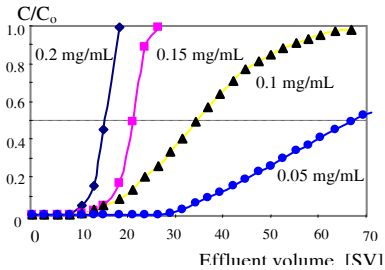

SGS-NT8(PH$^+$): 7.6 mL; V = 250 - 550 mL; pH ~ 5; v = 3.1 SV/h (0.4 mL/min).

Fig. 8. Effect of C_o on the breakthrough capacity

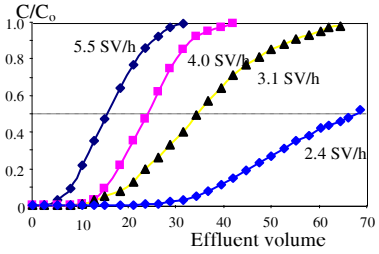

SGS-NT8(PH$^+$): 7.6 mL; V = 250 - 550 mL; C_o= 0.1 mg UO_2^{2+}/mL; pH ~ 5.

Fig. 9. Effect of *v* on the breakthrough capacity

a) Dynamic Ion Exchange Capacity: According to the breakthrough curves (Fig. 8 and 9), at the point C/C_o = 0.5: the breakthrough capacity is more increasing when C_o and the flow rate *v* was lowering. The reason was that in the range of the study solutions the major adsorption mechanisms is particle-diffusion, where the adsorption is dependent upon the initial uranyl concentration and the contact time [7].

b) Elution of UO_2^{2+}: In 3 different elution conditions the elution efficiency of UO_2^{2+} by the 10 g Na_2SO_4+ 1L 2M H_2SO_4 solution always reached the highest value compared to two other solutions (Table 1). Therefore, the elution solution chosen for the adsorbed UO_2^{2+} from SGS-NT8(PH$^+$) was the solution containing 10 g Na_2SO_4 in 1L 2M H_2SO_4.

Tab 1. Study of the elution condition

Elution condition	**10 g Na_2SO_4 + 1L H_2O Elut. Sol./H_2O η_{rg} [mL/mL] [%]**		**10 g Na_2SO_4 + 1L 1M H_2SO_4 Elut. Sol./H_2O η_{rg} [mL/mL] [%]**		**10 g Na_2SO_4 + 1L 2M H_2SO_4 Elut. Sol./H_2O η_{rg} [ml/mL] [%]**	
1	20/40	5	20/40	65	20/50	88
2	30/40	20	30/40	78	30/50	98
3	45/40	35	45/40	93	45/50	100

Column SGS-NT8(PH$^+$), V = 7.6 mL; Adsorption: 50 mL sol.; C_o= 0.15 mg UO_2^{2+}/mL; pH = 5; v = 0.4 mL/min; Elution: v = 2.1 SV/h (0.15 mL/min).

c) Regeneration of SGS-NT8(PH$^+$): The recovery efficiencies of UO_2^{2+} in all 8 of adsorption - elution cycles are almost unchanged (99.95 - 100%), indicating that SGS-NT8(PH$^+$) may be renewable and reused multifold (Table 2).

Tab 2. Cycles of UO_2^{2+} adsorption – elution

Cycles	**m_r (UO_2^{2+}) [mg] η_r [%]**		**Cycles**	**m_r (UO_2^{2+}) [mg] η_r [%]**	
1	3.750	100.00	5	3.748	99.95
2	3.745	99.87	6	3.749	99.97
3	3.745	99.87	7	3.750	100.00
4	3.750	100.00	8	3.748	99.95

Column SGS-NT8(PH^+), V = 7.6 mL; Adsorption: 25 mL sol.; C_o= 0.15 mg UO_2^{2+}/mL; pH = 5; v = 0.4 mL/min; Elution: 45 mL solution of 10 g Na_2SO_4+1L 2M H_2SO_4/50 mL H_2O; v = 0.15 mL/min;

Regeneration: 20 mL 1M H_2SO_4 then H_2O to pH 6 – 7.

2.2. Separation of UO_2^{2+} From The Radioactive Wastewater By The Column Operation

The data in Table 4 indicated that SGS-NT8(PH^+) has the separation ability for almost all of the metals present in the radioactive wastewater, where the effluent pH is about 7. Particularly, as the recovery efficiency of Uranium as well as its K_d reached the highest values (98% and 61.25 L/g), so that demonstrated the selective separation ability of SGS-NT8(PH^+) to UO_2^{2+} ion. Compared to the standards for the industrial wastewater in the Standard TCVN-2005, the concentrations of a majority of the heavy metals present in the effluent (except Mn and Zn) are reached within the allowed level.

Tab 3. Concentration of some metals present in the feed and in the effluent

No.	Element	C_o [mg/L]	C [mg/L]	C^* [mg/L]	η_t [%]	K_d [L/g]
1	Al	0.091	0.008	-	91.2	12.97
2	As	0.014	0.005	0.5	64.3	2.25
3	Co	0.638	0.551	-	14.0	0.20
4	Cu	0.100	0.07	5.0	30.0	0.54
5	Cd	0.106	0.097	0.5	8.5	0.12
6	Ce	0.831	0.248	-	70.2	2.94
7	Fe	1.666	1.252	1.0	25.0	0.41
8	Hg	0.050	0.011	0.01	78.0	4.43
9	K	432.533	404.126	-	6.6	0.09
10	La	1.221	0.528	-	56.8	1.64
11	Ni	0.929	0.844	2.0	9.1	0.13
12	Mn	72.763	68.043	5.0	6.5	0.09
13	Sr	11.303	10.786	-	4.6	0.06
14	Sn	0.013	0.008	5.0	38.5	0.78
15	Zn	25.749	21.143	5.0	18.0	0.27
16	Zr	0.004	0.002	-	50.0	1.25
17	Th	0.039	0.019	-	51.3	1.32
18	U	0.150	0.003	-	**98.0**	**61.25**

C_o: Metal concentration in the feed; C : Metal concentration in the effluent

C:* Metal concentration in Industrial wastewater following TCVN-2005 standards

η_t *:* Metal recovery efficiency on SGS-NT8(PH^+) column ; Effluent pH ~ 7.

IV. Conclusion

Our research group have successfully established a production process for the porous polymeric adsorbent SGS-NT8(H^+) in the laboratory. Two types of the porous polymeric adsorbents, i.e. SGS-NT8(SH^+) and SGS-NT8(PH^+), are shown to be capable of treating the wastewater containing heavy metals in general, and Uranium in particular. Of practical importance is that by the efficient synthesis process of the porous polymer SGS-NT8 with other derivative chemical agents enables to create suitable adsorbent materials for a wide variety of wastewater treatment applications.

References

[1]. R. Kunin, The use of macroreticular polymeric adsorbents for the treatment of waste effluents, *Pure &Appl. Chem.*, 46, 205-211, Perg. Press., 1976.

[2]. K. H. Lieser, New Ion Exchangers, Preparation, Properties and Application, *Pure & Appl Chem.*, 51, 1503-1517, Perg. Press., 1979.

[3]. N. J. Ljubman, G. K. Imangazieva, Sintez vysokopronicaemych polimernych filtrujuscich izdelij prostranstvennoj globuljarnoj struktury; *"KAZMECHANOBR*", No. 23, Alma-Ata, 1980.

[4]. N. J. Ljubman, G. K. Imangazieva, Uskov A. I., New polymer and ion - exchange filtering materials for the purification of technical solutions and waste waters, *Cvet. metallurgija*, 9, 36-39, (russ.), 1981.

[5]. N. J. Ljubman, G. K. Imangazieva, T. C. Sydykova, Polymer and ionexchanging filtration elements for purification from waste and circulating water, *Sci. reports "KAZMECHANOBR"*, 5-12, Alma-Ata 1986.

[6]. Licence documentation, Polymer filtering and ionexchanging materials, synthesis, properties, applications; *"KAZMECHANOBR"*, Alma-Ata 1989.

[7]. "SGS - Polymers "(Information), *Www.stud.uni-_leipzig.de/~che94beq/pwaterbr.htm.*

[8]. IAEA – TECDOC - 1336: Combined methods for liquid radioactive waste treatment *Final Report of a co-ordinated research project, 1997-2001*; IAEA, Feb. 2003.

[9]. "Phenol formaldehyde resin "*www.en.wikipedia.org/wiki/ Phenol _formaldehyde _resin*

[10]. L. D. Pennington, Chelating Ion Exchange Resin*, Indus. Eng. Chem.,* 51(6), Jun 1959.

[11]. NEA Nuclear Science Committee, Actinide Separation Chemistry in Nuclear Waste Streams and Materials, *NEA/NSC/DOC* (97), Dec. 19, 1997.

[12]. N. M. Hassan, K. Adu- Wusu, J. C. Marri, Resorcinol-Formaldehyde Adsorption of Cesium (Cs^+) from Hanford Waste Solution - Part 1: Batch Equilibrium Study, *WSRC-MS - 2004-00250, 2004.*

[13]. C. S. Tyberg, Void-Free Flame Retardant Phenolic Network: Propetrties and Processability, Blacksburg, Virginia, March 22, 2000.

[14]. S. L. Gibson, Cresol novolac/ epoxy network: Synthesis, properties, and processability, Blacksburg, Virginia, April 12, 2001.

[15]. J. Zheng, Studies of PF resol/isocyanate hybrid adhesives, Blacksburg, Virginia, Dec. 17, 2002,

[16]. I. Poljansek, M. Krajnc, Characterization of Phenol - Formaldehyde Prepolymer Resins, *Acta Chim. Slov.* 238-244, 2005.

[17]. J. Wolfrum, G. W. Ehrenstein, Interdependence between the curing, structure, and the mechanical properties of phenolic resins, J. App. Polym. Sci., 74, 3179-3186, June 3, 1999.

[18]. Astarloa-Aierbe G., Echeverria J. M., Vazquez A. , Mondragon I., Influence of the amount of catalyst and initial pH on the phenolic resol resin formation, *Polymer*, 41(9), 3311-3315, 2000.

[19]. Ion Exchange – Novasep Process/ Applexion' expertise, 2005.

[20]. IAEA, Appliction of Ion Exchange Processes for the Treatment of Radioactive Wastes and Management of Spent Ion Exchangers, *Technical Report Series no 408*, Vienna, 2002.

[21]. L. Yankov, S. Philipova, I. Zlatanov and L. Ivanova, Studies of phenolic resin - based microporous separator materials, Sofia, Bulgaria, Oct. 25, 1982.

[22]. B. Gorski, Nguyen Za Hung, N. Ya. Ljubman, Use of spatial-globular polymer sorbents to separate radioact. contaminants from water, Isotopenpraxis, *Environ. Health Stud.*, 29, 275-282, 1993.

[23]. Y. Zinmermann, A. Eilfield, A. Weiske, U. L. Kretzschmar and J.A.C Broekaert, Eval. of SGS- polymer for the purif. of expl. contam. surface and groundwater with square-wave-voltametry, Univ. Hamburg, Germany, 2005.

[24]. N.T. P. Nam và ccs., Nghiên cứu, đánh giá hiệu quả ứng dụng polyme đã qua xử lý hóa học để tách một số nguyên tố k. loại từ d. dịch thải c. nghiệp, *Báo cáo tổng kết đề tài cơ sở 2005*, VCNXH - VNLNTVN, 2006.

[25]. N.T. P. Nam, N. M. Thư, N.T. M. Phượng, P.T. H. Hà, Nghiên cứu khả năng hấp phụ Ni^{2+}, Cu^{2+} và Zn^{2+} trên polyme xốp SGS-NT8, *Tuyển tập báo cáo khoa học Hội nghị KHCN Hạt nhân toàn quốc lần thứ VII"*, NXB KHKT, Đà Nẵng, 8-2007.

[26]. H. Maeda, H. Egawa, Studies on Selec. Adsorp. Resins. XXIII. Preparation and Properties of Macroretic. Chelat. Ion Exch. Resins Containing Phosphoric Acid Groups, *J. App. Polym. Sci.*, 29, 2281-2287, 1984.

[27]. H. Egawa, T. Nonaka, Studies on Selec. Adsorp. Resins. XXI. The Influence of Porosity of Macroretic. Chelat. Resin on Adsorp. of H. Metal Ions in an Aq. Solution, *J. App. Polym. Sci*., 30, 3239-3247, 1985.

[28]. J. R. Kaczvinsky Jr., J. S. Fritz, D.D. Walker and M. A. Ebra, Synthesis and development of porous chelating polymers for the decontamination of nuclear waste, *J. Radioanal. Nucl.Chem.*, 91(2), 349-360, Sep. 1985.

[29]. S. Kobayashi, T. Tanabe, T. Saegusa, and R. Mashio, Resins: Phosphonomethylated Polyethylennimine Resin for Recov. of Uranium from Seawater, *Polym. Bull.,* 15, 7-12, 1986.

[30]. V. Strelko Jr., M. Streat and O. Kozynchenko, Preparation, characterisation and sorptive properties of polymer based phosphorous-containing carbon, *Reac. Func. Polym,* 41(1-3), 245-253, July 15, 1999.

RESEARCH THE METHOD FOR SEPARATING SOME RADIOACTIVE CONTAMINANTS FROM OIL SLUDGE

Le Xuan Huu, Nguyen Ba Tien, Ngo Van Tuyen, Vu Thi Thao
Pham Kim Thoa and Doan Thu Hien

Institute for Technology of Radioactive and Rare Element,VAEC

Abstract: According to documents in the world, oil sludge and scale pollute environment because it contains not only organic substances but also radionuclide. We have researched a method for separating directly radionuclide oil sludge and scale by using hydrochloric acid 5%. After that, we used the gamma spectrometry method to analyze obtained samples. The results showed that the treated oil scale and sludge are safe from radiation.

Keywords: Oil sludge, oil scale, hydrochloric acid.

I. Introduction

I.1. Origin and composition of radioactive elements in oil scale and sludge

The geologic information shows that deposits which often contain oil, natural gas along with radionuclide which are referred to as "NORM"(Naturally-Occurring Radioactive Materials)[1, 2, 6]:

- uranium (and its decay products)
- thorium (and decay products)
- radium (and decay products)
- lead-210

Geologists have recognized the presence of four above elements since the early 1930s and used it as a method for finding deposits [1]. As a result, petroleum deposits often occur in aquifers containing brine (salt water). Radionuclide, along with other minerals, dissolve in the brine, precipitate (separate and settle) out and form different substances. When we mine the oil, that waste often comes with the oil.

I.2. Oil scale in Vietnam

Tab 1. Concentration of NORM in oil, gas and byproducts [2, 5].

Radionuclide	**Crude oil** (Bq/g)	**Natural gas** (Bq/m3)	**Produced water** (Bq/L)	**Hard scale** (Bq/g)	**Sludge** (Bq/g)
U-238	10^{-7}–0.01		3.10^{-4}–0.1	0.001–0.5	0.005–0.01
Ra-226	10^{-4}–0.04		0.002–1200	0.1–15 000	0.05–800
Po-210	0–0.01	0.002–0.08		0.02–1.5	0.004–160
Pb-210		0.005–0.02	0.05–190	0.02–75	0.1–1300

Rn-222		5–200 000			
Th-232	3.10^{-5}–0.002		3.10^{-4}–10^{-3}	0.001–0.002	0.002–0.01
Ra-228			0.3–180	0.05–2800	0.5–50
Ra-224			0.5–40		

We have analyzed three basic components of oil scale: crude oil, water and mechanical impurities in many different samples. The results are shown in the table 2 [3.4].

Tab 2. Composition of oil scale in Vietnam

	Components of impurities (calculated for 100% scale of oil)
Crude oil	75 – 80
Water	5 – 10
Mechanical impurities	10 – 15

I.3. We Have Studied Some Samples of Oil Scale As Following

We take samples of oil scale in Ba Ria-Vung Tau province at two different places. The first sample is taken at Research Center of the crude oil, VietXo Petro, Ba Ria-Vung Tau (we call it M1); the second is taken at Dinh mountain, Ba Ria-Vung Tau province (we call it M2). Two samples have different characteristics. The sample M1 which is taken right after scraping traces off the vessels contains much oil. Conversely, only 3 kg of sample M2 along with much soil and small rocks which is taken when scale of oil has already been transported out of the tank is not a representative sample.

I.4. Methods for Managing and Treating Oil Scale In The United States

Steps are carried out for treating oil scale containing radioactive elements in the U.S. [1, 3, and 5]

+ The first step: Liquid extraction

Liquid extraction by hydrocarbon solvent.

Extraction by thermal pretreatment with vaporized hydrocarbon at 600^0C.

+ The second step: Volume reduction and radioactivity verification.

Extracted materials are separated into two categories by high-speed sorting machine.

+ The third step: Radionuclide extraction.

Radioactive materials (NORM) are dissolved by aqueous solvents.

Separate solid from liquid by using Hydro-cyclones

+ The fourth step: Radioactivity verification in solid and radioactive injection in solution.

Materials below regulatory level are returned for disposal as a non hazardous waste.

The NORM- containing solution is injected into injection wells.

II. Experiments, Results And Discussion

II.1. Determining Radioactivity of Scale of Oil In Vietnam

Two samples of oil scale taken in Ba Ria - Vung Tau province have been analyzed by using analytical technique of low font gamma spectrometer. The results are shown in the table 3.

Tab 3. Concentration of basic radioactive elements in oil scale in Vietnam

N	**Symbol sample**	**Concentration of basic radioactive elements** (Bq/kg)				
		K	**U**	**Th**	**Ra**	**Total radioactivity**
1	M1	155.22	7.32	5.52	17.52	322.8
2	M2	942	30.56	56.25	55.5	1606

Looking at the results shown in the table 3, we can see the levels of radiation in oil scale are too low, so the sample taken cannot be a fully represent for oil scale in Vietnam. Therefore, according to the standard of processing and managing radioactive waste in Vietnam (TCVN 6868: 2001) [6], safety guide RS-G-1.7 of IAEA and documents [5] on criteria for regulation for NORM, it is usually unnecessary to regulate materials below: [5, 6]:

Tab 4. The exemption limit of NORM

Radionuclide	**Exemption level** (Bq/g)	**Exemption level** (pCi/g)
U; Th	5.5	150
Ra-226	1.1	30
Ra-228	1.1	30
Pb-210	0.2	5
Po-210	0.2	5
K-40	10	270

These values can also be used as clearance levels for releasing residues from NORM at present.

Therefore, according to our initial assessment, radioactivity of oil scale in Vietnam is lower than radioactivity of scale in other countries. This is explained that collected samples may be not representative and some more basic researches are needed.

II.2. Studying Capability of Separating Radioactive Elements In Oil Scale In Vietnam By Using Agent Hydrochloric Acid (HCl)

II.2.1. Studying methods

Use a technical balance with degree of accuracy 0.01 gram for weighing 300 grams of oil scale, put it into a heat-resistant glass with volume 1000 ml, and then add 300 ml of 5% hydrochloric acid (HCl). Heat it slowly up to nearly 100^0 C for 2 hours and stir. Then, cool it, at that time, the self-phase separation takes places; crude oil floats on the top; water with radioactive ions is in the bottom. Eliminate water from the glass. Next, clean acid off the crude oil by putting pure water into the glass (with crude oil), heat it up to about 90^0 C and stirring. Cool it, eliminate water from the glass again, (wash 5 times). Analyze radioactive elements by using analytical technique of low font gamma spectrometer. The similar experiments are carried out with changing content of acid from 10% to 15%.

II.2.2. Results. After analyzing, the results are presented in the table 5.

Tab 5. Influence of acid (HCl) content on capability of separating radioactive elements in oil scale.

Content of HCl acid (%)	**Activity of radioactive elements left** (Bq/kg)			
	U	**Th**	**Ra**	**K**
0	7.32	5.52	17.52	155.22
5	2.60	2.46	9.01	95.3
10	2.38	2.39	9.01	101
15	2.30	2.38	9.10	97.1

II.2.3.Discussion

The results in the table 5 show that: in general, with the low content of HCl acid, the separation capability radioactive elements in oil scale have is high. When content of acid is higher than 5%, separation capability of radioactive elements does not changed significantly. Therefore, according to the standards for radioactive safety in Vietnam as well as in the world, we selected content of HCl acid about 5% for treating radioactive elements in oil scale.

II.3. Surveying Influence of Time On Optimal Separation Capability for Removing Radioactive Elements From Oil Scale In Vietnam

II.3.1. Experimental method

Weigh 300 grams of oil scale, put it into a heat-resistant glass with volume 1000 ml, and add 300 ml of 5% hydrochloric acid. Heat it slowly up to nearly 100^0 C, when the temperature reaches about 100^0 C, stir it for 30 minutes. Then, cool it, at that time, the self-phase separation take places, crude oil floats on the top, and water with radioactive ions is at the bottom. Eliminate water from the glass. Next, clean acid off the crude oil by putting pure water into the glass (with crude oil); heat it up to about 90^0 C and stirring it at the same time. Cool it, eliminate water from the glass again, and (wash 5 times). Bring crude oil to analyze radioactive elements by using analytical technicality low font gamma spectrometer. Similar experiments are carried out with changing the time: 1 hour, 1.5 hours, 2 hours, 2.5 hours and 3 hours. The results are shown in table 6.

II.3.2. Results

Tab 6. Dependence of time and cleanness of the radioactive elements in scale of oil in Vietnam when content of HCl acid is 5%.

Separation time (hour)	**Total activity of remaining in scale oil** (Bq/kg)	**Separation time** (hour)	**Total activity of remaining in scale oil** (Bq/kg)
0.0	322.8	2.0	183.5
0.5	298.0	2.5	182.6
1.0	256.7	3.0	183.2
1.5	191.3		

II.3.3. Discussion

Results in the table 6 shown that: a total of concentrations of radioactive elements in oil scale decrease when we increase separation time. However, when separation time increases to two hours, almost radioactive elements don't dissolve. Therefore, we have chosen heating and stirring time 2 hours for the separation technology of radioactive elements in oil scale.

III. Conclusion

We have analyzed, surveyed and determined the basic chemical – physical properties of oil scale in Vietnam such as: radioactive activity; concentration of impurities and melting temperature.

We also studied, chosen some parameters: content of hydrochloric acid is 5%; optimal separation time for removing radioactive contaminants from the oil scale is 2 hours.

We have some suggestions: more study on oil scale in Vietnam is needed, according to the methods in the world.

References

[1]. www.epa.gov/rpdweb00/tenorm/oilandgas.html.-Oil and Gas Production Wastes.

[2]. www.iaea.org - *Safety Reports Series* No.34. - Radiation protection and the management of radioactive waste in the oil and gas industry.

[3]. http://vietbao.vn/Xa-hoi/Chat-thai-dau-khi-de-doa-moi-truong/10775219/157/. Hiện trạng quản lý và xử lý chất thải rắn nhiễm dầu tại Việt Nam.

[4]. www.nea.gov.vn/tapchi/Toanvan/04-99-16.htm - Kết quả nghiên cứu tận dụng chất thải rắn từ quá trình súc rửa tàu dầu.

[5]. www.ogp.org.uk/pubs/412.pdf - Guidelines for the management of Naturally Occurring Radioactive Material (NORM) in the oil & gas industry - *Report No. 412 September 2008*

[6]. TCVN 6868: 2001- An toàn bức xạ - Quản lý chất thải phóng xạ - Phân loại chất thải phóng xạ.

STUSY ON DETERMINATION OF ISOTOPIC COMPOSITION OF URANIUM, THORIUM AND LEAD IN SINGLE ZIRCON

Le Hong Minh, Huynh Van Trung, Nguyen Xuan Chien
Nguyen Viet Thuc and Bui Thi Ngan

Institute for Technology of Radioactive and Rare Elements, VAEC

Abstract: The method for determination of isotopic compositions of uranium, thorium and lead in single zircon using ŸCP -MS has been studied. The effect of plasma operating parameters on the sensitivity of ŸCP -MS was investigated in detail and the optimal operating conditions were established to have the high sensitive measurement whereas the influence of polyatomic ions was minimized. Uranium, thorium, lead were separated from matrix and from each other well by ion- exchange chromatography on anionit resin Biorad AG 1x8, 200-400 mesh. Single zircons were decomposed in a Teflon vessel with a mixture of fluorhydric and nitric acids. Analytical results of reference material Plesovice Zircon were in good agreement with the recommended reference values.

Keywords: ICP-MS, Biorad AG 1x8, content, isotopic composition, age dating, ion-exchange chromatography.

I. Results and Discussion

I.1. Research On Optimal Conditions For Determination of Isotopic Compositions of Uranium, Thorium And Lead By ICP -MS

To investigate optimal plasma operating parameters of the device, we measured ^{238}Œ, ^{235}Œ, ^{232}Th, ^{206}Pb, ^{207}Pb and ^{208}Pb by ICP -MS at mode **ISOTOPE ANALYSIS**

Mix standard solution of uranium, thorium and lead with concentration of 20 ppb of each element was used for measurement on ICP -MS when peripump rate - PR was fixed at 0.1 rps and other parameters were changed.

The optimal parameters were chosen based on the measurements that have the large signal intensity and the smallest ratios of oxides and hydroxides as follows:

RFP = 1300 W, CGFR = 1.2 L/min., SDe = 6 mm, PR = 0.1 rps

Figures from 1 to 4 show the correlation between sensitivity of the device and the change of one parameter whereas three others were fixed at their optimal values.

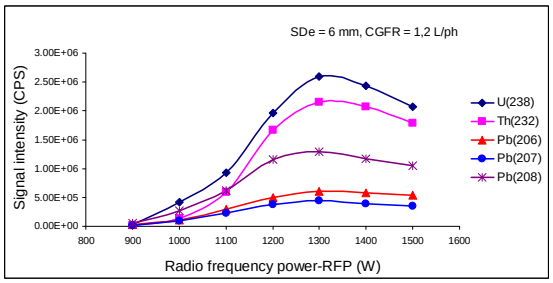

Fig. 1. Correlation between sensitivity and RFP

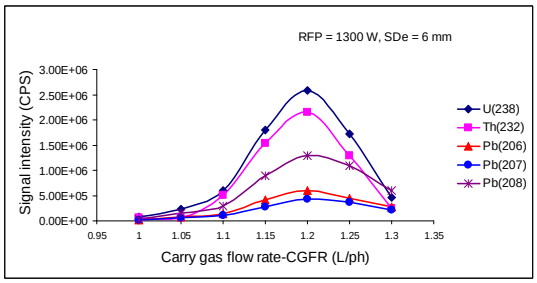

Fig. 2. Correlation between sensitivity and CGFR

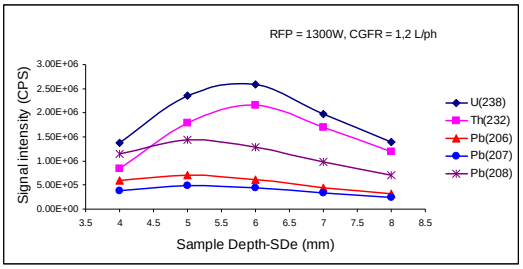

Fig. 3. Correlation between sensitivity and SDe

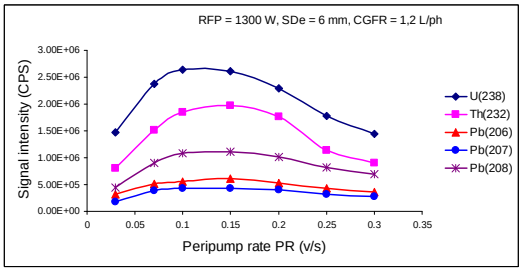

Fig. 4. Correlation between sensitivity and PR

HNO_3 acid solution was the best choice for sample medium and samples in 0.3M HNO_3 medium were used for measurement on ICP -MS.

I.2. Study On Separation Of Uranium, Thorium and Lead

Separation of uranium, thorium and lead was carried out on a quartz-glass chromatography column with the internal diameter of 8 mm and 200 mm height, filled with 5 gr. of previously washed Biorad AG1x8, 200-400 mesh. The medium of resin in the column was equilibrated with HCl or HNO_3 acid solution that has suitable concentrations.

I.2.1. Study On Separation Of Uranium, Thorium and Lead In HCl and HNO_3 media

Mix standard solution of uranium, thorium and lead in 1.0M HCl; 2.0M HCl; 3.0M HCl medium (5 microgram of each element) was loaded onto the column. This solution passed through the column at the rate of 0.6 ml/min. Uranium and lead were absorbed to the resin best in 3.0M HCl medium while thorium was not washed out from the column.

Lead was best eluted with 6.0M HCl solution and its recovery efficiency was 92% (fig. 5).

Just after lead being eluted, uranium was best eluted with water and its recovery efficiency was 90% (fig. 6).

Thorium standard solution in 7.0M HNO_3 medium was loaded onto the column. Thorium was absorbed to the resin well and best eluted with 6.0M HCl solution, its recovery efficiency was 90% (fig. 7).

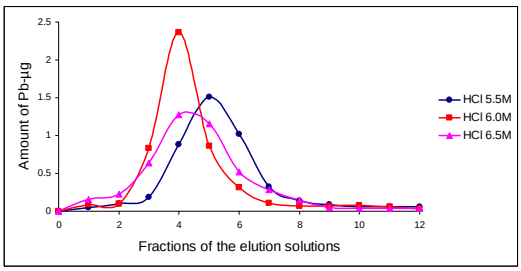

Fig. 5. Elution curves for lead

I.2.2. *Study On Separation of Uranium, Thorium and Lead From Matrix*

Multi-element standard solution in 3.0M HCl medium (5 microgram of each element) was loaded onto the column. Zirconium and hafnium with the large amounts in solution were not absorbed to the resin and washed out from the column. Thorium and other elements were not absorbed and washed out (solution A). Some

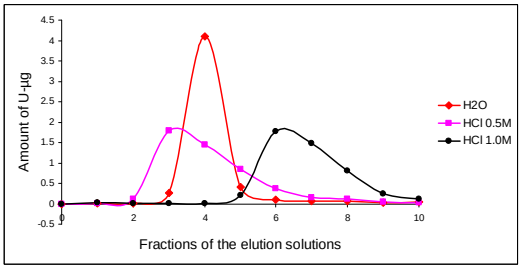

Fig. 6. Elution curves for uranium

elements such as zinc, cadmium, neodymium, and samarium were absorbed to the resin together with uranium and lead.

Lead was eluted with 6.0M HCl solution. Zinc, cadmium, neodymium, samarium and uranium were remained on the column.

Uranium was eluted with water. Zinc, cadmium were eluted together with uranium (Fig. 8). Cadmium was eluted after the elution of uranium had finished. There was only a small amount of zinc in the final elution aliquots of uranium.

Solution A was converted to 7.0M HNO_3 medium and loaded onto the column. Thorium was absorbed to the resin well while zirconium, hafnium, Ô were not absorbed and washed out from the column. Thorium was eluted as described above.

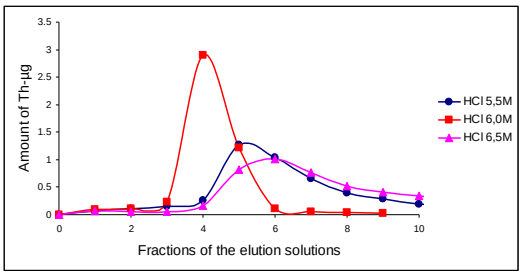

Fig. 7. Elution curves for thorium

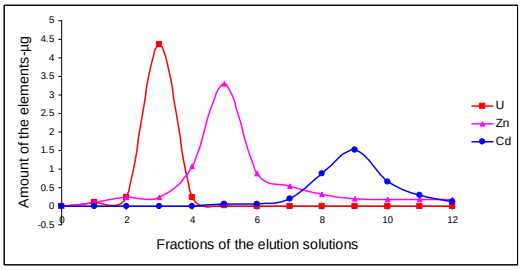

Fig. 8. Elution curves for elements

I.3. Study On Decomposition of Single Zircon Sample

Samples were decomposed with HF acid and a mixture of HF + HNo_3 acids.

I.3.1. Study On Influence of Acid Mixture With Different Volume Ratios

10 mg of single zircons was taken and put into the teflon vessels. The sample in the first vessel was decomposed by concentrate HF only and other samples were decomposed by mixture of HF + HNO_3 with different volume ratios.

The sample in the acid mixture with volume ratio $HF/HNO_3 = 4/1$ was completely dissolved after 4 days. The sample was best decomposed by the acid mixture with this ratio, compared with HF only and the acid mixture with any ratio else (Fig. 9).

I.3.2. Study On Influence of Temperature

Effect of temperature on the sample decomposition was investigated: 10 mg of single zircons in the acid mixture with volume ratio $HF/HNO_3 = 4/1$ was decomposed at 160^0C, 180^0C and 200^0C.

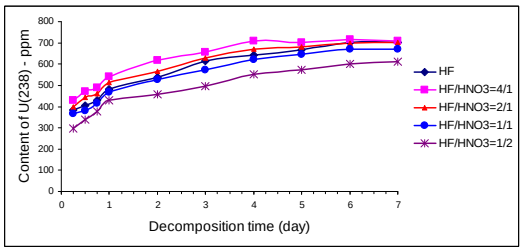

Fig . 9. Correlation between U content found and decomposition time with different acid mixture

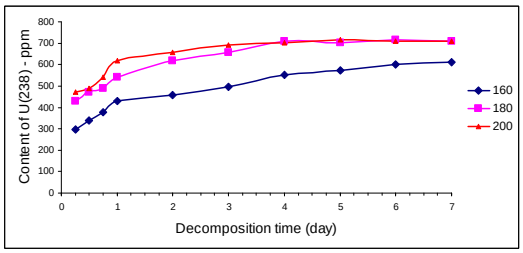

Fig. 10. Correlation between U content found and decomposition time with different temperature

The sample was decomposed best at 200^0C and worst at 160^0C (Fig. 10). The decomposition effectiveness at 180^0C and 200^0C had no marked difference.

I.4. Analysis of Reference Material - Plesovice Zircon

The precision of the analytical method was evaluated by analysis of reference materials. Isotopic compositions of uranium, thorium and lead in Plesovice Zircon were determined; the results were obtained as follows:

N^0	**Item**	**Recommended values**	**Found values**	**Bias** (%)
1	Œ	755 (465-1106) (ppm)	743 ± 3 (ppm)	- 1.6
2	Th	78 (44-183) (ppm)	85.1 ±2.1 (ppm)	+ 9.1
3	Pb	39 (21-55) (ppm)	44.5 ± 2.2 (ppm)	+ 14.1
11	$^{207}Pb/^{206}Pb$	0.0532	0.0562	+ 5.63
12	$^{208}Pb/^{206}Pb$	0.0291	0.0317	+ 8.93
13	$^{207}Pb/^{235}Œ$	0.3942	0.4035	+ 2.35
14	$^{206}Pb/^{238}Œ$	0.0536	0.0554	+ 3.35

The results had bias of + 14.1% for the content of isotopes and + 8.93% for the isotopic ratios.

II. Conclusion

II.1. The effect of plasma operating parameters on the sensitivity of ICP -MS was investigated. The optimal parameters were chosen for measurement of the isotopes of uranium, thorium, lead as follows:

RFP = 1300 W, CGFR = 1.20 L/min., SDe = 6.0 mm, PR = 0.1 rps.

The measurements had high sensitivity and the formation of polyatomic ions was minimized as the device run in this condition.

II.2. The separation of uranium, thorium, and lead by ion-exchange chromatography was studied with anionit resin Biorad AG1x8, 200-400 mesh on the quartz-glass column. Uranium and lead were separated from matrix (zirconium, hafnium, etc.) and also from thorium in 3.0M HCl medium. Thorium was separated from zirconium, hafnium, etc. in 7.0M HNO_3 medium.

II.3. Single zircons were decomposed by HF acid and mixture of HF and HNO_3 acids with different volume ratios. The sample was best decomposed in the mixture with ratio: HF/HNO_3 = 4/1. The suitable temperature for sample dissolution was 180^0 C.

II.4. The procedure for analysis of isotopic compositions of uranium, thorium, and lead in single zircons was proposed and its precision was evaluated by analysis of isotopes in Reference Material Plesovice Zircon from Bergen University, Norway. The precision of the analytical method was compliant with recommended requirement (-10% to +20%). The method could be applied for analysis of isotopic composition of uranium, thorium, and lead in single zircons.

Refference

[1]. Aronne, C.C., Godoy, J.M., and Godoy, M.L.D.P., Study of the application of inductively coupled plasma quadruple mass spectrometry for the determination of monazite ages by lead isotope ratios, IV South American Symposium on Isotope Geology.

[2]. Gunter Faure, Principle of isotope geology, John Wiley & Son, 1986.

[3]. K. Tagami and S. Uchida, 2004, Use of TIVA resin for the determination of U isotopes in water samples by Q -ICP-MS, Applied Radiation and Isotopes, vol. 61, pp. 255-259.

[4]. Krogh, T. I., 1973, a low contamination method for hydrothermal decomposition of zircon and extraction of U and Pb for isotopic age determinations, Geochim. Cosmochim. Acta, vol. 37, pp. 485-494.

[5]. Paqette JL and Pin C., 2001, a new miniaturized extraction chromatography method for precise U -Pb zircon geochronology, Chem. Geol., vol.176, pp. 311-319.

[6]. Parrish RR, Roddick JC, Loveridge WD and Sullian RW., 1987, Uranium-lead analytical techniques at the geochronology laboratory, Geological Survey of Canada, Radiogenic age and isotopic studies, Report 1, Geological Survey of Canada, Paper 87-2, pp. 3-7.

[7]. Yokoyama et al., 1999, Separation of Thorium and Uranium from Silicate Rock Samples Using Two Commercial Extractions Chromatographic Resins, Anal. Chem., vol. 71 pp. 135-141.

[8]. Yokoyama et al., 2001, Uranium Isotope Analysis by TIMS, Chem. Geol., vol. 181, pp. 1-12.

SELECTION OF PROCESSING FLOWSHEET AND EQUIPMENTS FOR URANIUM ORE HYDROPROCESSING PLANT (AS A PART OF EXPLORATION PROJECT 8.000 TONS OF U_3O_8 IN THANH MY AREA, QUANG NAM PROVINCE)

Cao Hung Thai, Than Van Lien, Cao Dinh Thanh
Nguyen Ba Tien, Pham Quang Minh and Phan Van Dung

Institute for Technology of Radioactive and Rare Elements, VAEC

Abstract: We have proposed the processing flowsheet with equipments and the testing plant layout for technological samples testing in order to carry out hydroprocessing investigations as a part of exploration project 8.000 tons of U_3O_8 in Thanh My area, Quang Nam province.

Keyword: uranium, hydroprocessing, technological sample, exploration project.

I. The Flow Diagram of Uranium Ore Processing Testing

The conclutions obtained from the office study allow us to propose the following flowsheet for technological samples testing (Fig.1), in order to carry out investigations as a part of exploration project 8.000 tons of U_3O_8 in Thanh My, area Quang Nam province.

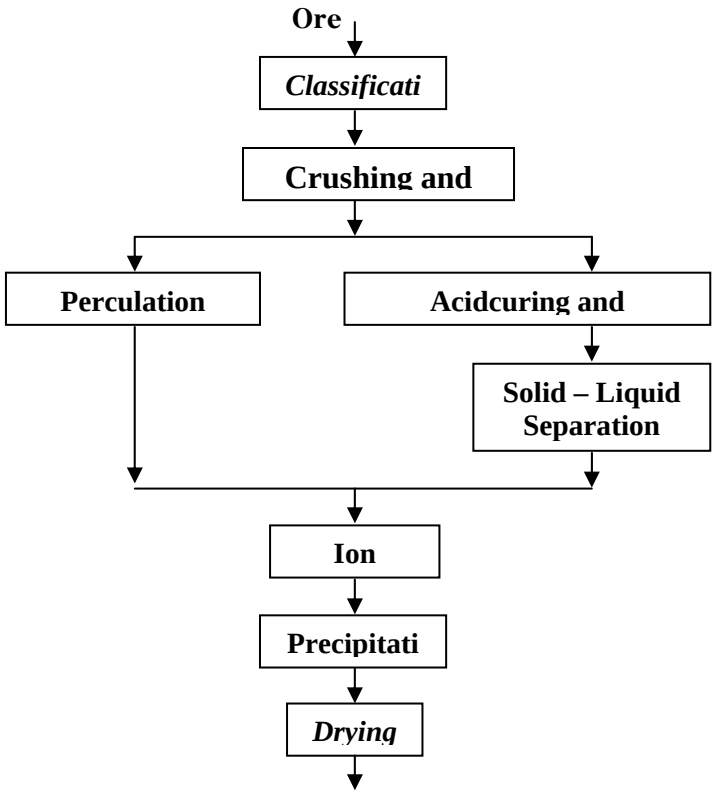

Fig. 1. The flow diagram of uranium ore processing testing

II. The Testing Plant Layout For Thanh My Uranium Ore Processing

The testing plant for Thanh My uranium ore processing consists of following sections:

1. Section for raw materials and reagent preperation: includes two crushers , two millers , two screeners, two mixers, a container for feed ore (4 m^3), a container for ore after grinding (2 x 2 m^3), a container for incubated ore (2 x 2 m^3), intermediary containers, elevators, hand-carts ...

Area of section: 450 m^2.

2. Section for leaching: includes two tanks for perculation leaching , five stirred reactor, five thichkeners, a pressure filter, a tank contains pregnant solution (3 m^3), pumps, intermediary containers, elevators, hand-carts ...

Area of section: 630 m^2.

3. Section for ion exchange: includes two ion exchange colum systems, a tank contains solution (2x 1m^3), pumps, intermediary containers ...

Area of section: 180 m^2.

4. Section for precipitation and drying: includes three reactors for impurities precipitation, two reactors for yellowcake precipitation, five thichkeners , a vacuum filter, a dryer, product packing equipments, a tank contains solution (1m^3), pumps, intermediary containers..

Area of section: 450 m^2.

5. Section for radioactive waste processing and management: includes five stirred reactors, two mixers of solid phases, three reactors for precipitation, five thichkeners, a pressure filter, a concrete mixer, a container for waste (4m^3), a module for testing of disposal and recycle, pumps, intermediary containers, elevators, hand-carts ...

Area of section: 540 m^2. Testing disposal field: 1.000 m^2.

The figure 2 shows the testing plant layout for Thanh My uranium ore processing with area of 6.000 m^2.

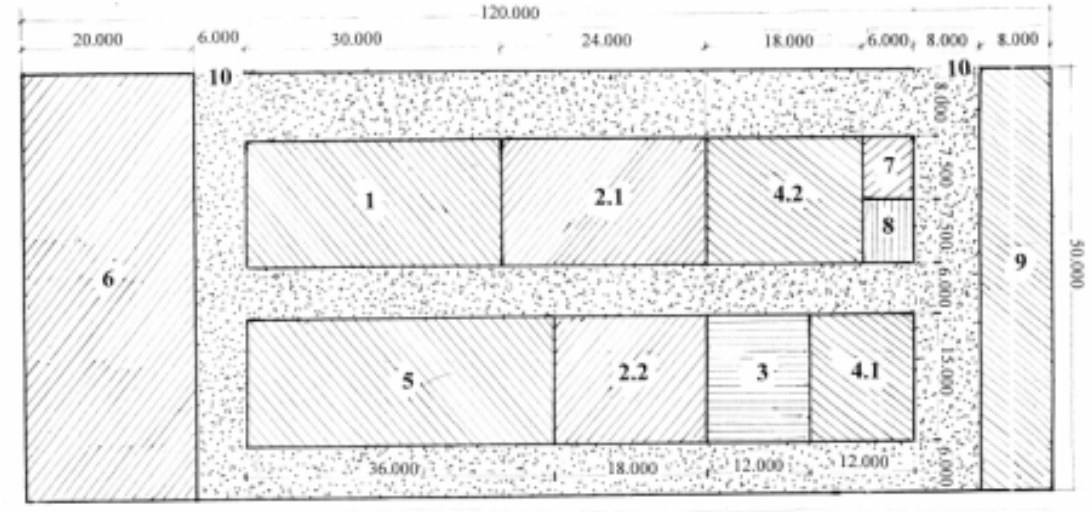

Fig. 2. The testing plant layout for Thanh My uranium ore processing

1. Section for raw materials and reagent preperation.

2.1. Section for perculation leaching.

2.2. Section for Acidcuring and Agitatorwashing.

3. Section for ion exchange.

4.1. Section for impurities precipitation.

4.2. Section for yellowcake precipitation and drying.

5. Section for radioactive waste processing and management.

6. Area for disposal testing.

7. Analyze Division.

8. Repair Plant.

9. Area for Administration and Washing & W.C.

10. Enter and Exit.

Reference

[1]. Collection of science works 1985 – 2000, ITRRE, VAEI, Hanoi, 2002

[2]. Manual on Laboratory Testing for Uranium Ore Processing, Technical Reports. IAEA 1990.

[3]. Manual on Pilot Testing for Uranium Ore Processing, Technical Reports. IAEA 1990.

[4]. Smirnov,U.V., Efimova, J.I., Skorovarov, D.I., Ivanov, F., Gidrometallurgitreskaia Pererabotka Uranorudnovo Suria, Moskva, Atomizdat 1979.

1.10 - Computation and Other Related Topics

DESIGN OF NEW MECHANICAL PRODUCT TRANSPORTATION SYSTEM FOR IRRADIATOR SVST-Co60/B

Le Minh Tuan*, Tran Van Hung*, Cao Van Chung*
Nguyen Anh Tuan*, Phan Phuoc Thang*, and Nguyen Tat Toan**

** Research and Development Center for Radiation Technology, VAEC*
***Technical Teachers' University, Ho Chi Minh City*

Abstract: The calculated physical parameters of tote boxes of irradiator SVST-Co60/B with different dimensions by using MCNP code are presented. Optimal project for new tote box based on obtained calculation results are chosen and then design of a new mechanical product transportation system for irradiator SVST-Co60/B are suggested.

1. Introduction

After more than 9 years of operation, the mechanical product transportation system of irradiator SVST - Co60/B is downgraded because of corrosion and rust. Simultaneously, the irradiator was not designed appropriately for frozen sea foods irradiation. To surmount above inadequacy, design of new mechanical product transportation system is needed. In addition, this design will increase processing productivity of the irradiator and enhance safety, confidence in operation too.

Especially, through this design will help technical staff of Research and Development Center for Radiation Technology (VINAGAMMA) have more practical knowledge for designing of an industrial irradiator. In the short time, the irradiator will be modified and upgraded to serve the actual needs of market. In the future, a domestic industrial irradiator will be designed and fabricated by technical staff of VINAGAMMA.

2. Calculation Code

The MCNP code is used to calculate physical parameters of tote box with three different dimensions. On basis of irradiated statistic, three different dimensions of tote box with 50x50x90, 50x67x90 and 50x80x90 cm are chosen to calculate.

3. Results

3.1 Calculation Physical Data of Optimal Tote Box

The model and irradiated direction of tote box are shown as follows:

Calculated data with dummy density of 0.4 g/cm^3, Co^{60} source capacity 335 kCi, the MCNP gives results of calculation as follows:

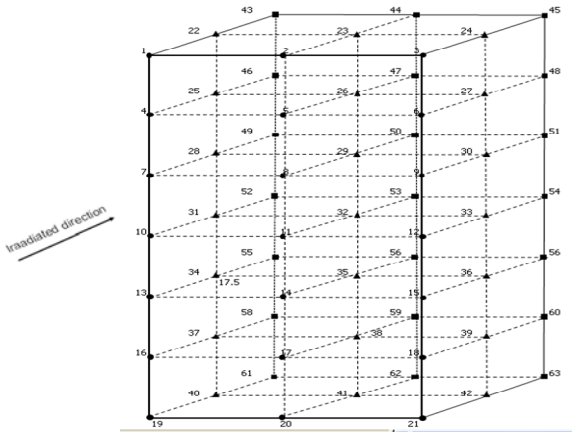

Fig. 1. Model of tote box and irradiated direction

Tab 1. Calculation results with three different dimensions of tote box

Parameters \ Tote box dimension	50x50x90	50x67x90	50x80x90
D_{min}	15.83	15.54	15.59
D_{max}	24.98	26.87	26.90
D_{max}/D_{min}	1.53	1.73	1.89
Total dose (kGy)	1,322	1,337	1,241
Product contain volume (m^3)	0.21	0.29	0.34
Weight of a tote box (kg)	85	115	137.5
Weight of 68 boxes (kg)	5,782	5,968	6,051
Average irradiated dose on a point (kGy)	1.49	1.51	1.41
Processing productivity at 1 hour (kg.kGy/h)	17,920	17,920	17,920
Practical productivity at 1 hour (kg.kGy/h)	8,667	9,047	8,514
Irradiator performance at density 0.4 g/m^3 (%)	48.37	50.49	47.51

3.2 Design of New Tote Box

Through above calculation results, the project with tote box dimension of 50 x 67 x 90 cm is optimal. This box has maximum average irradiated dose, highest practical processing productivity at 1 hour and highest used performance of the irradiator too. Meanwhile, ratio of D_{max}/D_{min} is in permission. So, an aluminum tote box with dimension of 50 x 67 x 90 cm is chosen. The following is a drawing of aluminum tote box.

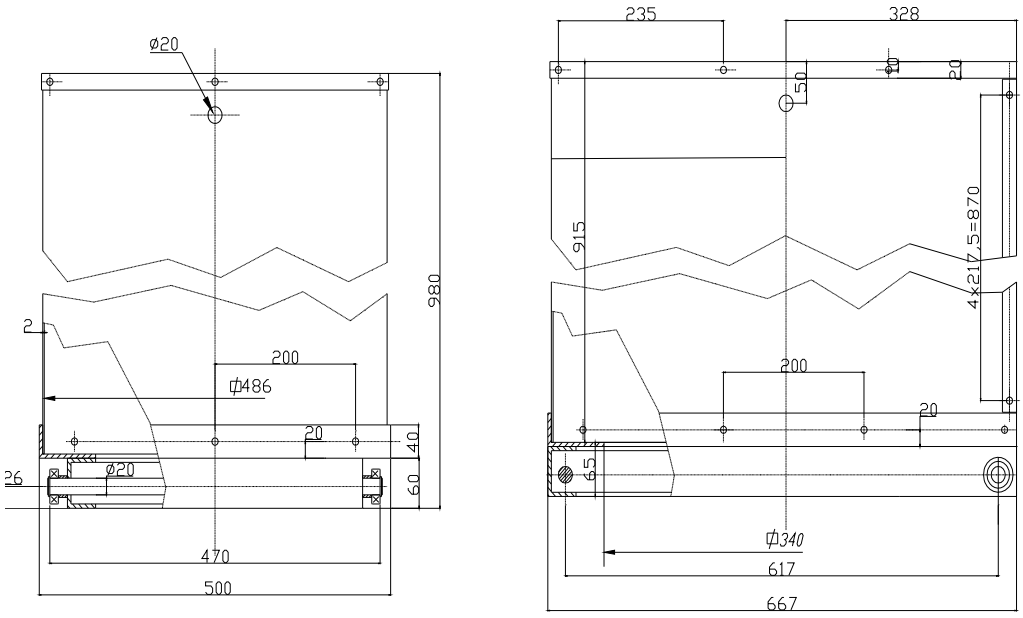

Fig. 2. Aluminum box with dimension 50 x 67 x 90 cm

The aluminum box is calculated mechanical structure and loading capacity with 200 kg. From calculated results and machinery parts handbook, bearing of 6004 is chosen. Two horizontal axles are permitted.

3.3 Design of New Mechanical Product Transportation System

At the same time with change of box dimension, the replacement of worn and rust parts and modification of new mechanical product transportation system are carried out. The purpose of modification aims at increase in processing speed and decrease in minimum irradiation time. The fastest current irradiation time for a cycle is 2 hour and 45 minutes.

The operation model of current product transportation system is shown as follow:

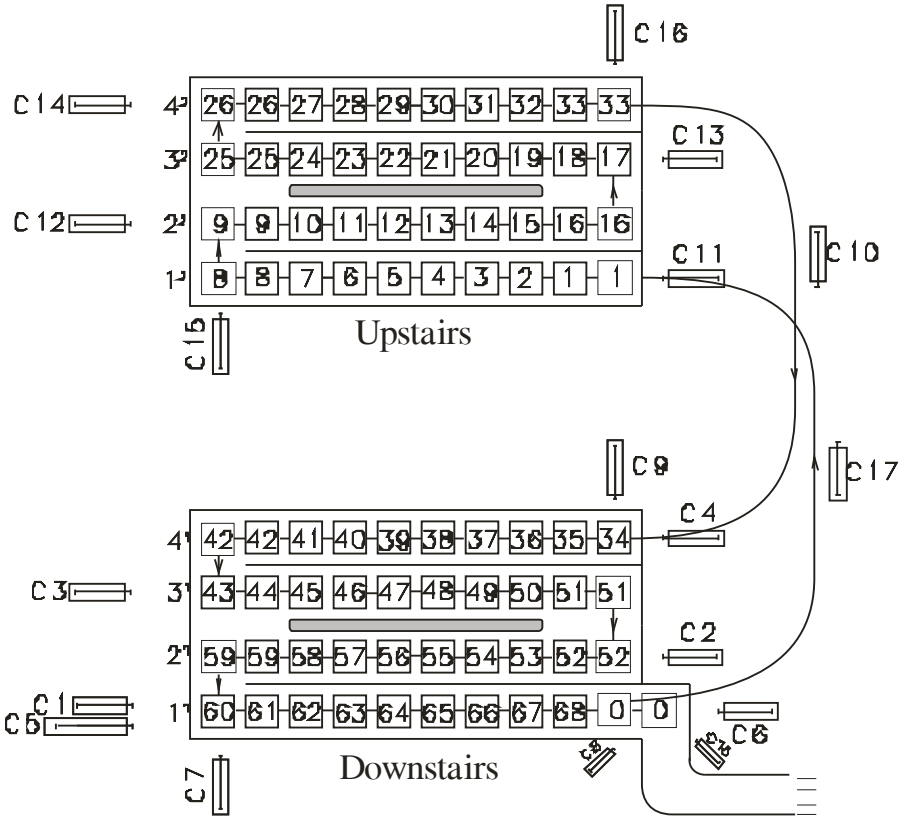

Fig. 3. Moving order of current product transportation system

Moving order of current product transportation system has a weak point, which is moving time of tote box car being not joined in moving time of cylinders in irradiation room. With specific reason, new product box has to move upstairs and then cylinder C17 has to move downstairs to put up a bridge for irradiated box passing through. So, it looses so time for this processing.

To overcome above weak point, the new product transportation system is designed to receive immediately the irradiated box into tote box car when the new box coming in irradiation room. Moving order of new product transportation system is shown as follows:

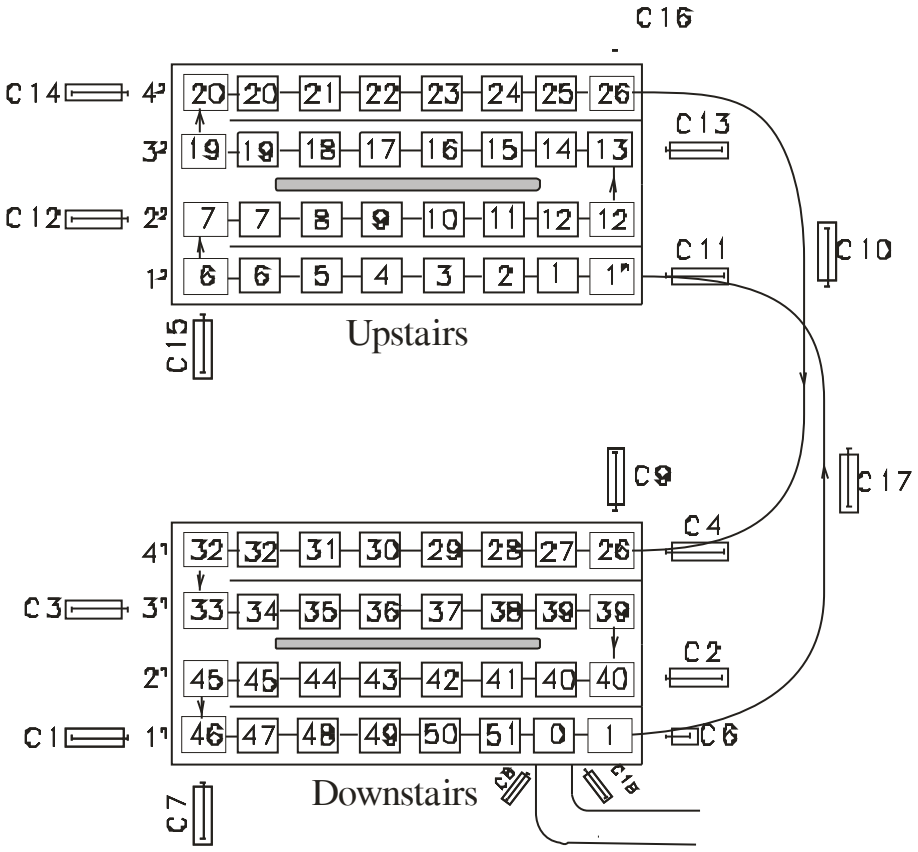

Fig. 4. Moving order of new product transportation system

The new product transportation system has some innovations as follows:

- Tote box passes only 51 positions in continuous mode and only 52 positions in batch mode.
- Without using long cylinder C5 but only using short cylinder C6.
- The rail of tote box car is moved to the left about 70 cm.

The innovation has the advantage of being quick and effective, namely the fastest new irradiation time for a cycle is 2 hour and 05 minutes for continuous mode and 1 hour and 48 minutes for batch mode.

References

[1]. Tran Khac An, fundamental subject report with code CS/00/02-04 “Research on innovating method for irradiator SVST – Co60/B to improve processing productivity and serve irradiation needs”, 2000.

[2]. Gamma sterilization and their applications, Naarri Bulletin, Vol.XI, No.4, August 2003.

[3]. Radiation safety of Gamma and Electron Irradiation facilities, Safety series No. 107, IAEA, 1992.

[4]. Gamma sterilization fact book, Nordion Marketing Communications, 1994.

[5]. Safety design and use of Panoramic, wet source storage gamma irradiators (Category IV), American National Standard N43.10, July 1984.

[6]. Training manual on operation of food irradiation facilities, First edition, Vienna, 1992.

[7]. Operation and Maintenance Manual for SVST-Co60/B type irradiator, Vol. 1, 2, 3, Institute of Isotopes Co. Ltd., 2nd Edition, May 1999.

[8]. Nghiem Hung, common steel and iron handbook, Polytechnic University, Hanoi, 1997.

[9]. Nguyen Trong Hiep, Design of machinery parts, Education edition, 1999.

[10]. Bui Trong Luu, Strength of materials, University and Technical college edition, Hanoi, 1973.

[11]. Tran Huu Que, Mechanical engineering drawing, Education edition, 2004.

2. IAEA TC Projects and Research Contracts

2.1- LIST OF VIE PROJECTS IMPLEMENTING IN 2008

Code	Project	Implementing Institute	Counterpart	Budget (USD)
VIE0011	Human Resource Development and Nuclear Technology Support	VAEC	Vuong Huu Tan	**896,960.00**
VIE4014	Modification of the Dalat Reactor Control System	NRI	Nguyen Nhi Dien	**243,220.00**
VIE5015	Enhancement of Quality and Yield of Rice Mutants Using Nuclear and Related Techniques, Phase II	CNT	Le Xuan Tham	**376,692.00**
VIE8014	Upgrading the Irradiation Facility at Hanoi Irradiation Centre	Hanoi Irradiation Center	Ho Minh Duc	**34,300.00**
VIE8017	Upgrading the Irradiation Facility at Hanoi Irradiation Centre	Hanoi Irradiation Center	Ho Minh Duc	**391,350.00**
VIE8018	Applying Electron Beam Technology for Processing Biomaterials	VINAGAMMA	Tran Khac An	**304,650.00**
VIE9008	Establishment of a National Radiation Safety Training Centre	NRI	Dang Thanh Luong, Nguyen Nhi Dien	**131,666.00**
VIE9009	Formulation of Atomic Law	VAEC	Vuong Huu Tan	**88,410.00**
VIE/2/008	Development of Nuclear Analytical Techniques for Application and Research Purpose	CNT	Nguyen Duc Thanh	**380,552.00**
VIE/8019	Establishment of Tracer Technique to Study Processes in the Gas Industry	Center of Nucl. Tech. for Industrial Applications	Nguyen Huu Quang	**123,362.00**
VIE/3/005	Upgrading Capacity of Waste Processing and an Interim Storage Facility for Low and Intermediate Level Radioactive Waste	ITRRE	Le Ba Thuan	**239,351.00**

VIE0010	Technical Support for Training in Nuclear Engineering at the Hanoi University of Technology	Hanoi Technology Univ	Phung Van Duan	**203,340.00**
VIE6023	Establishment of National Cyclotron Facilities and Centres for Medical and Research	Health Ministry, Defence Ministry	Pham Minh Bao, Truong Van Viet	**350,620.00**
VIE/9/010	Strengthening the Technical Capacity of the Regulatory Body for Radiation and Nuclear Safety	VARANSAC	Ngo Dang Nhan	**312,588.00**

2.2 LIST OF NON - RCA PROJECTS IMPLEMENTED IN 2008

Code	Project	Year of Commencement	Implementing Institute
RAS/0/036	Country and Regional Programme Review	2003	VAEC
RAS/0/037	Support to Member States on Design and Formulation of Project Proposals	2003	VAEC
RAS/0/046	Support towards Self-Reliance and Sustainability of National Nuclear Institutions	2007	VAEC
RAS/0/047	Supporting Web-Based Nuclear Education and Training through Regional Networking	2007	VAEC
RAS/0/049	Pre-project Assistance	2007	VAEC
RAS/0/050	Human Capacity Development for Technology Dissemination	2007	VAEC
RAS/0/051	Country and Regional Programme Review	2007	VAEC
RAS/2/013	Good Radiopharmacy Practice and Good Manufacturing Practice	2007	VAEC
RAS/3/009	Strengthening Infrastructure for Radioactive Waste Management	2007	VAEC
RAS/4/027	Test procedures for Quality Control in the Maintenance and Refurbishment of Nuclear Instruments	2007	VAEC
RAS/4/028	Integrated Management Systems for Expanding Nuclear Power Programmes	2007	VAEC
RAS/4/029	Strengthening Nuclear Power Infrastructure and Planning	2007	VAEC
RAS/5/049	Sharing Regional Knowledge on the Use of the Sterile Insect Technique within Integrated Area-Wide Fruit Fly Pest Management Programmes	2007	Ministry of Agriculture and Rural Development
RAS/6/034	Quality Assurance Programme for Molecular-Based Diagnosis of Infectious Diseases	2007	Health Ministry
RAS/6/043	Regional Screening Network for Neonatal Hypothyroidism	2007	Health Ministry
RAS/6/050	Control and Prevention of Childhood Malnutrition in Asia	2007	Health Ministry

RAS/6/051	Supporting Education and Training in Medical Physics	2007	VAEC
RAS/7/014	Monitoring of Food Fortification Programmes Using Nuclear Techniques	2007	Health Ministry
RAS/7/017	Application of Nuclear Techniques to the Management of Hazardous Algal Blooms	2007	Institute of Oceanography, Nha Trang
RAS/9/043	Using the Asian Nuclear Safety Network to Raise Nuclear Safety Levels	2007	VAEC + VARANSAC
RAS/9/045	Strengthening National Regulatory Infrastructure for the Control of Radiation Sources	2007	VARANSAC
RAS/9/046	Strengthening Technical Capacities for Occupational Exposure Control	2007	VARANSAC
RAS/9/047	Strengthening Radiological Protection of Patients and Protection from Medical Exposure	2007	Health Ministry
RAS/9/048	Strengthening National Capabilities for Public Exposure Control	2007	VARANSAC
RAS/9/049	Establishment of National Capabilities for Response to Radiological and Nuclear Emergencies	2007	VARANSAC
RAS/9/050	Education and Training in Support of Radiation Protection Infrastructure	2007	VAEC + VARANSAC
RAS/9/051	Awereness Raifsing and training for Nuclear Security	2007	VARANSAC

2.3- LIST OF RAS PROJECTS IMPLEMENTING IN 2008

Code	Project	Year of Commencement	Implementing Institute	Counterpart
RAS0045	Evaluation of Sustainable Energy Development Strategies for Addressing Climate Change Issue	2007	VAEC	MSc.Mr. Le Doan Phac
RAS0048	Management of TCDC	2007	VAEC	VAEC
RAS4026	Increasing material value by neutron irradiation	2007	VAEC	Dr. Nguyen Nhi Dien, Director
RAS5043	Sustainable Land Use and Management Strategies for Controlling Soil Erosion and Improving Soil and Water Quality (RCA)	2007	Ministry of Agriculture and Rural Development	Tran Duc Toan
RAS5044	Integrated Approach for Improving Livestock Production Using Indigenous Resources and Conserving the Environment (RCA)	2005	Ministry of Agriculture and Rural Development	Tran quoc Viet
	Integrated Approach for Improving Livestock Production Using Indigenous Resources and Conserving the Environment (RCA)			*Doan Duc Vu*
RAS5045	Improvement of Crop Quality and Stress Tolerance in for sustainable crop production using mutation Selected Crops by Mutation Techniques and Biotechnology	2007	VAEC	Associate Prof. Dr. Le Xuan Tham
RAS5046	Novel application of Food Irradiation Technology for Improving Socia-Economic Development	2007	VAEC	MSc. Tran Khac An
RAS6029	Upgrading Nuclear Medicine Technologist Training	2007	Health Ministry	Tran Xuan Truong
RAS6038	Strengthening Medical Physics through Education and Training Phase II	2007	Health Ministry	Phan Sy An

RAS6040	Improvement in QA for Brachytherapy of Frequent Cancers in the Region	2007	Health Ministry	To Anh Dung
RAS6041	Prevention of Osteoporosis and Promotion of Bone Mass in Asian Populations using a Food-based Approach	2007	Health Ministry	Vu Thi Thu Hien
RAS6042	Tumor Imaging Using Radioisotopes	2007	Defence Ministry	Le Ngoc Ha
RAS6048	Application of 3D conformal radiotherapy for predominant cancers in the RCA region	2007	Health Ministry	Mr. Nguyen Xuan Cu
RAS6049	Upgrading of Sustainability of PET technology in RCA Member States	2007	Defence Ministry	Ms.Pham Thi Minh Bao MD
RAS7015	Characterization and source identification of Air Particulate Pollution in the Asian Region	2007	VAEC	MSc. Vuong Thu Bac
RAS7016	Establishment of a benchmark for assessing the radiological impact of nuclear power activities on the marine environment in the Asia-Pacific region	2007	VAEC	MSc. Nguyen Trong Ngo
RAS8084	Isotope Use in Managing and Protecting Drinking Water (RCA)	1999	VAEC	Dang Duc Nhan
RAS8095	Improving Regional Capacity for Assessment, Planning, and Response to Aquatic Environmental Emergencies (RCA)	2003	Ministry of Agriculture and Rural Development	Dang Dinh Phuc
RAS8097	Isotope Techniques for Groundwater Contamination Studies in Urbanized and Industrial Areas (RCA)	2003	VAEC	Nguyen Kien Chinh
RAS8099	Radioisotope Technology for Natural Resource Exploration and Exploitation (RCA)	2005	VAEC	Nguyen Huu Quang
RAS8100	Advanced Industrial Radiography (RCA)	2005	VAEC	Vu Tien Ha

RAS8104	Assessment of trends in freshwater quality using environmental isotopes and chemical techniques for improved resource management	2007	VAEC	Nguyen Kien Chinh
RAS8105	Improvement of production quality and safety in steel, petrochemical and civil industries using Advanced Industrial Radiography and Tomography Techniques	2007	VAEC	Vu Tien Ha
RAS8106	Consolidation of Radiation Processing Applications for Health and Environment	2007	VAEC	1. Dr. Hoang Hoa Mai
	Consolidation of Radiation Processing Applications for Health and Environment	*2007*		*2.MSc. Le Hai*
RAS8107	Intensification of Productivity in Coal, Minerals and Petrochemical Industries using Nucleonic Analysis Systems (NAS) and Radiotracers	2007	VAEC	1.Khuong Thanh Tuan
	Intensification of Productivity in Coal, Minerals and Petrochemical Industries using Nucleonic Analysis Systems (NAS) and Radiotracers	*2007*		*2. Mr. Nguyen Huu Quang*
RAS9042	Sustainability of Regional Radiation Protection Infrastructure	2007	VARANSAC	Le Chi Dung

2.4- FNCA PROJECTS IMPLEMENTING IN 2008

Coordinator: Prof. Dr. Vuong Huu Tan, Chairman of the VAEC

	Project Title	Implementing Institute	Counterpart
1.	Research Reactor Technology (RTT Project):	NRI	Dr. Nguyen Nhi Dien
2.	Neutron Activation Analysis (NAA)	NRI	Dr. Nguyen Ngoc Tuan
3.	Mutation Breeding	Agricultural Institute	Dr Le Huy Ham
4.	Bio-fertilizer	MARD	Dr. Pham Van Toan
5.	Electron Beam Application	VINAGAMMA	Dr. Nguyen Quoc Hien
6.	Radioactive Waste Management	ITRRE	Dr. Le Ba Thuan since Sep. 2008, (Former Project Leader was Dr. Cao Dinh Thanh)
7.	Nuclear Safety Culture	NRI	Pham Van Lam
8.	Public information	VAEC	Dang Thi Hong
9.	Human Resources Development	VAEC	Vu Dang Ninh
10.	Radiation Oncology	K Hospital	Prof. Nguyen Ba Duc
11.	Application of Cyclotron and Positron Emission Tomography (PET) in Medicine	108 Hospital	Pham Thi Minh Bao (Imaging) and Dr. Le Ngoc Ha (Diagnosis)

2.5- INTERNATIONAL RESEARCH CONTRACTS IN 2008

Code	RC Tittle	Institution	Chief Investigator	Start date
12951/R3/RB	Tracers in hight temperature and fractured basement rock reservoir	Center of Nucl. Tech. for Industrial Applications	Nguyen Huu Quang	1/12/2007
12951/R3/RB	Interaction between water from Red River and groundwater in catchment of the river.	Hanoi University of Mining and Geology	Bui Hoc	1/13/2007
13013/R3/RB	Determination of genetic diversity in Vietnamese indigenous goat breed based on molecular marker	National Inst. of Animal Husbandry	Le Thi Thuy	15/12/2007
13003/R3/RB	Validation and pyramiding of drought resistants/genes	Inst of Biology	Nguyen Thanh D.	1/12/2007
13027/R3/RB	Development of rearing techniques for Bactrocera pyrifoliae in Vietnam	Plant Protection Research Insitute (PPRI)	Le Duc Khanh	15/10/2007
13429/R2/RB	Comparision of the various calibration methods of diagnostic kVp meters	INST	Tran Ngoc Toan	1/12/2007
14077/R1/RB	Role of ECG-gated Tc-99m MIBI SPECT imaging in evaluation of asymptomatic diabete patients	108 Hospital	Le Ngoc Ha	15/12/2007
14/78/R1/RB	Value ofECG-gated TC-99m MIBI SPECT imaging in patients with acute chest pain	108 Hospital	Vu Dien Bien	15/12/2007
14700/R0/RB	Assessment of left ventricular function in coronary artery diseases with nuclear Techniques	Cho-Ray Hospital	Truong Van Viet	15/9/2007
14085/R1/RB	Application and evaluation of real time PCR in diagnosis on avian influenza	Veterinary Institute	Nguyen Tien Dung	15/12/2007
14465/R0/RB	Improvement of water use efficiency through Isotopic Techniques for the Scarce Water Resources in the Tay	Inst. for Research of Water Source	Duong Hai Sinh	15/9/2007

	Nguyen Plateau, Central part of Vietnam			
14819	Trial and Development of New Verieties in Central Highlan of Vietnam	Inst. of Agricultural Science	Do Khac Thinh	1/7/2007
13850/R1/RB	Assessment of Source Term, Radionuclides Transport within Containment/Confinement and Release to the Environment for Dalat Nucelar Research Reactor	NRI	Luong Ba Vien	15/04/2008
14773/R0/RB	Preparation of Biotic Elicitor from Chitosan for Rice and Sugarcane by Gamma-Irradiation Method	VINAGAMMA	Nguyen Quoc Hien	1/12/2007
14834/R0/RB	Priclical Evaluation of Peptides and Antibodies Radiopharmaceuticals Labeled with Generator Produced 90Y for potential clinical use	NRI	Nguyễn Thị Thu	1/4/2008
14316/R0/RB	Assessment of uptake and bioacccumulation of Cadmium in Benthic Organisms raised in the Red River's mouth area using Radio-cadmium and Radioassy Technologies	INST	Dang Duc Nhan	15/09/2007

3. Scientific Papers Published Abroad and in Vietnam

3. SCIENTIFIC PAPERS PUBLISHED ABROAD

3.1 International Journal

1. Kyota KAMIKUBO, Satoshi AKASAKA, Hirokazu HASEGAWA and Hai LE, Nanoporous Membranes via Bicontinous Mirodomain Structures of Block Copolymers, Polymer Preprints, Japan Vol. 56, No. 2 (2007).
2. D.T. Khoa and D.C. Cuong. Missing monopole strength of the Hoyle state in the inelastic α+ ^{12}C scattering. *Physics Letters*, 2008, **B660**, 331.
3. D.T. Khoa, W. von Oertzen and H.G. Bohlen. Probing the equation of state of nuclear matter in the nuclear rainbow scattering. *International Journal of Modern Physics*, 2008, **B22**, 4684.
4. D.T. Khoa and D.C. Cuong. Mean-field description of the nucleus-nucleus optical potential. *Nuclear Physics*, 2008, **A805**, 412.
5. D.T Khoa. Probing the isoscalar excitations of 12C in the inelastic alpha scattering. *Journal of Modern Physics E,* vol 17, No10, 2055 (2008).
6. Tran Huu Phat, Nguyen Van Long, Nguyen Tuan Anh, and Le Viet Hoa. Kaon condensation in the linear sigma model at finite density and temperature. *Phys. Rev.* **D78**, 2008, 105016.
7. Tran Huu Phat, Nguyen Tuan Anh, and Nguyen Van Long. Determination of nuclear symmetry energy in the Cornwall-Jackiw-Tomboulis approach. *Phys. Rev.* **C77**, 2008, 054321.
8. Physical group: Upper Limit on the Cosmic-Ray Photon Flux Above 10^{19} eve Using the Surface Detector of the Pierre Auger Observatory*, Astroparticle Physics* 29 (2008), 243.
9. Physical group: Upper Limit on the Diffuse Flux of Ultrahigh Energy Tau Neutrinos from the Pierre Auger Observatory, *Physical Review Letters* 100 (2008), 211101.
10. Physical group: Observation of the Suppression of the Flux of Cosmic Rays above $4x10^{19}$ eV, Physical *Review Letters* 101 (2008), 061101.
11. Physical group: Correlation of the highest-energy cosmic rays with the positions of nearby active galactic nuclei, *Astroparticle Physics,* 29 (2008), 188.
12. Physical group: *Comments on moon counting in the FADC traces of the Auger Surface Detector (SD)*, *Auger GAPNOTE,* number 136 (2008).
13. Larsen F. P. Q. Nhan, D. D. Nhan, D. Postma, S. Jessen, N. V. Hoan et al.,. Controlling geological and hydro geological processes in an arsenic contaminated aquifer in the Red River flood plain, Vietnam, *App. Geochem.* 23: 3099-3115, 2008.
14. S. Jessen, F. Larsen, D. Postma, P. Q. Nhan, D. D. Nhan, et al.,. Paleo-hydrogeological control on groundwater As level in Rd River delta, Vietnam, *App. Geochem.* 23: 3116-3126*,* 2008.
15. J. Norrman, C. J. Sparrenbom, M. Berg, D. D. Nhan, P. Q. Nhan, H. Rosqvist et al. Arsenic mobilization in a new well field for drinking water production along the Red River, Nam Du, Hanoi, *App. Geochem., 23: 3126-3142*, 2008

16. F. Carvalho, J-P. Villeneuve, C. Cattini, I. Tolosa, D. D. Nhan, D. D. Thuan. Agrochemical and polychlorinated biphenyl (PCB) residues in the Mekong River delta, Vietnam. *Marine Poll. Bul., 56: 1476-1485*, 2008.

17. Philip K. Hopke, D.D. Cohen, B.A. Begum, S.K. Biswas, B.Ni, G.G. Pandit, M. Santoso, Y.S. Chung, P. Davy, A. Markwitz, S. Waheed, N. Siddique, F.L. Santos, P.C.B. Pabroa, M.C.S. Seneviratne, Wanna W., S. Bunprapob, Thu Bac Vuong, Pham Duy Hien, Andrzej Markowicz. *Urban air Quality in the Asian Region*. Science of the Total Environment, 404 (2008) 103-112

18. Nguyen Duc Thanh, Tran Quoc Dung and Luu Anh Tuyen, *"Semi-empirical Formula for large pore-size estimation From o-Ps Annihilation Lifetime"* Int. J. Nuclear Energy Science and Technology, Vol. 4, No. 2, 2008

19. Zs. Kajcsos, C. Kosanovic, S. Bosnar, B. Subotic, P. Major, L. Liszkay, D. Bosnar, K. Lázár, H. Havancsák, A. T. Luu, N. D. Thanh , *"Monitoring the Crystallization Stages of Silicalite by Positron Lifetime Spectroscopy"* Materials Science Forum Vol. 607 (2008) pp 173-176.

20. Truong Binh Nguyen, Le Xuan Tham. *Inter-subspecies hybrid dikaryons of Oyster mushroom independently isolated in Vietnam and Japan*. Biosci. Biochem. Biotech. Vol. 72(1): 216-218, 2008.

21. Truong Binh Nguyen, Le Xuan Tham *Changes in texture of the post-harvest fuitbodies of an abalone mushroom, Pleurotus cystidiosus subsp. abalonus, cultivated on different agro-forestry wastes*. Mushroom Sci. Biotech. Vol. 16(3): 109-116, 2008.

22. N. Q. Hien, B. D. Du, D. V. Phu, N. N. Duy, N. T. K. Lan, V. T. K. Lang, et al. *Preparation of colloidal silver nanoparticles in poly(N-vinyllpyrrolidone) by gamma irradiation*. J. of experimental Nanoscience, Vol. 3, No 3, September 2008, 207-213.

23. T. M. Quynh, Hiroshi Mitomo, Long Zhao, Shigeo Asai. *The radiation cross linked films based on PLLA/PDLA stereo complex after TAIC absorption in supercritical carbon dioxide*. J. Carbohydrate Polymer, Vol. 72, No 4, 2008, 673-681.

24. T. M. Quynh, Hiroshi Mitomo, Long Zhao, Masao Tamada. *Properties of a poly (L-lactic acid)/poly (D-lactic acid) stereo complex cross linked with trially isocyanurat by irradiation.* J. of Applied Polymer Science, Vol 110, No 4, 2008, 2358-2365.

3.2 Domestic Journal

25. Nguyen Xuan Chien, Huynh Van Trung, Tran Kim Hung, Determination of Rare Earth Elements in tea, soybean, vegetable and environmental samples by using ICP-MS method. Journal of Chemical, Physical and Biological Analysis. Vol. 13, No 1, 2008.

26. Tran Tu Hieu, Le Hong Minh, Nguyen Viet Thuc. Determination of trace concentration of some heavy metals in shellfish in West Lake in Hanoi by using ICP-MS method. Journal of Chemical, Physical and Biological Analysis. Vol. 13, No 2, 2008.

27. Nguyen Van Ri, Nguyen Xuan Chien, Tran Kim Hung, Nguyen Thi Thu Phuong. Study on Molecular absorption spectrometry for simultaneous determination of Ce,

Cu and Ca in coasting of black metal protection using artificial neutron network. Journal of Chemical, Physical and Biological Analysis. 2008.

28. Huynh Van Trung, Nguyen Xuan Chien, Doan Thanh Son. Study on elements in ancient coins by using X ray fluorescence method with basic parameters. Journal of Chemical, Physical and Biological Analysis. , 2008.
29. Huynh Van Trung, Nguyen Xuan Chien, Le Hong Minh, Study on decomposition of Zircon single mineral for determining isotope content and concentration of elements by using ICP-MS. Journal of Chemical, Physical and Biological Analysis, 2008.
30. Tran Thi Ngoc Diep, Nguyen Thi Kim Dung, Pham Luan, Simultaneous determination of *As(III) and As(V) in underground water samples by using CV-AAS*, Journal of Chemical, Physical and Biological Analysis, 2008.
31. Le Minh Tuan, Nguyen Trong Uyen, Nguyen Dinh Bang. Study on complex formation of some lanthanides (Pr, Nd, Eu, Gd) with L-isoleucine by pH meter titration method. Journal of Analytical Science, Vol. 13, No 2, 2008
32. Le Minh Tuan, Nguyen Trong Uyen, Nguyen Dinh Bang. Synthesis and study on the complexes of some rare earth elements (La, Pr, Nd, Sm)) with L-isoleusine. Journal of Science and Technology, Vol. 45, No 5, pp. 87-91, 2008
33. Hoang Nhuan et al. Synthesis and study on characteristics of complexes of Ni (II) and benzoyltrifloaxetat, Journal of Chemistry, Vol.46 (2A), pages 164-168, 2008.
34. Hoang Nhuan et al. Synthesis and study on characteristics of complexes of iridium (III) and benzoyl trifloaxetat. Journal of Chemical, Physical and Biological Analysis, Vol. 13 No 2, 2008.
35. Pham Quang Minh, Vu Thanh Quang, Cao Dinh Thanh, Pham Van Thiem, Percolation leaching of uranium ore and calculation for scale change. Journal of Chemistry, Vol. 46, 2A, pages 188-193, 2008.
36. Nguyen Viet Long, Le Ba Thuan, Nguyen Van Hai, Pham Thanh Binh, An investigation of Er3+ doped silica glasses: processing, properties and potential application, Journal of Chemistry, Vol. 46(2A), P.398-405, 2008.
37. Nguyen Viet Long, Le Ba Thuan, Nguyen Van Hai, Pham Thanh Binh, Chemico-physical properties of Er3+ doped SiO2-Al2O3 glasses from sol-gel process, Journal of Chemistry, Vol. 46(2A), P.406-413, 2008.
38. Nguyen Viet Long, Le Ba Thuan, Nguyen Van Hai, Pham Thanh Binh, Improvement of optical properties of Er3+-Yb3+ codoped SiO2-Al2O3 glasses by co-doping method with Al3+ ion for optical fiber amplifiers, Journal of Chemistry, Vol. 46(2A), P.414-420, 2008.
39. Nguyen Viet Long, Le Ba Thuan, Nguyen Van Hai, Pham Thanh Binh, SiO2-Al2O3 glasses co-doped with Er3+-Yb3+ and their application for optical amplifiers and upconversion lasers, Journal of Chemistry, Vol. 46(2A), P.421-428, 2008.
40. Le Ba Thuan, Nguyen Van Hai, Pham Duc Roan, Tran Ngoc Ha, Purification of Yttrium by solvent extraction technique using the extractant aliquot 336, Journal of Chemistry, Vol. 46(2A), P.440-445, 2008.
41. Le Ba Thuan, Nguyen Van Hai, Pham Duc Roan, Tran Ngoc Ha, Development a

computer simulation program for determination the parameters of the rare earths separation, Journal of Chemistry, Vol. 46(2A), P.446-452, 2008.

42. Le Ba Thuan, Nguyen Van Hai, Pham Duc Roan, Tran Ngoc Ha, Verification the assumptions used for development of simulation program for rare earths separation technique using the acidic phosphor extractants, Journal of Chemistry, Vol. 46(2A), P.453-458, 2008.
43. Le Ba Thuan, Nguyen Trong Hung, Luu Xuan Dinh, Doan Thi Mo, Removal arsenic from water using rare earth based materials, Journal of Chemistry, Vol. 46(2A), P.459-462, 2008.
44. Le Ba Thuan, Nguyen Trong Hung, Nguyen Duc Vuong, Study on light-convertible polyethylene film containing complexes of Ln(III) with 1,10-phenanthroline, Journal of Chemistry, Vol. 46(2A), P.463-470, 2008.
45. La Ba Thuan, Cao Duy Minh, Nguyen Trong Hung, Study on preparation of denaturized diatomite with CeO in nanometer dimension and application for treatment of Asen in water. Journal of Chemical, Physical and Biological Analysis, 2008.
46. Than Van Lien, Application of Bentonite in atomic energy field and results of studying uranium adsorption in Vietnamese bentonite. Journal of Chemistry, Vol. 46, No 2A, pages 158-163, 2008.
47. Nguyen Trong Nghia, Ngo Sy Luong, Than Van Lien, Production of organic clay from Binh Thuan bentonite and xetyl trimetylamoni bromua, Journal of Chemistry, Vol. 46, No 2A, pages 200-205, 2008.
48. Than Van Lien, Summary on application of bentonite. Information of Nuclear Science and Technology, No 15, 8/2008.
49. Pham Quang Trung, Status of research and development on reproduction for recovery of zinc from secondary materials. Information of Nuclear Science and Technology, No 15, 8/2008.
50. Nguyen BaTien, Draft estimation on natural radioactivites situation along the HCM road. Information of Nuclear Science and Technology, No 15, 8/2008.
51. Phan Sơn Hai, Nguyen Thanh Binh, Tran Van Hoa, Tran Dinh Khoa, Nguyen Dao, Nguyen Thi Mui, Trinh Cong Tu. Evaluation of erosion rate and efficiency of solutions for soil protection by using radioisotop method and experimental cell method. Journal of soil science, No 27, pp. 154-159.
52. Phan Son Hai, T. D. Khoa, Nguyen Dao, N. T. Mui, T. V. Hoa, T. C. Tu. Application of Cs-137 and Be-7 to assess the effectiveness of soil conservation technologies in the Central Highlands of Vietnam. *Journal of Nuclear Science and Technology* 10/2008.
53. N.T. Ngo, N.T. Binh, Truong Y, N.V. Phuc, L.N. Siêu, M.T. Huong, N.T. Linh, P.S. Hai, N.M. Sinh, L.N. Chung. Radioactive content in main foods in some ecological areas in Vietnam. Journal of Chemical, Physical and Biological Analysis, 2008.
54. Truong Y, N.T. Binh, N.T. Ngo, L.N. Siêu, N.T. Linh, N.V. Phúc. Application of calculation model of radioactive gas emission for site evaluation of nuclear power plant. *Journal of Nuclear Science and Technology* 10/2008.

55. Nguyen Ngoc Tuan, Nguyen Giang, Nguyen Thanh Tâm, Le Nhu Ton, Trương Minh Tri. Determination of concentration of some heavy metals Cu, Pb, Cd, Hg, and Se in water, sediment and some animals (shellfish) in Nha Phu ragoon, Khanh Hoa province. Journal of Chemical, Physical and Biological Analysis, Vol. 13, No 1, pp.100-105, 2008.
56. Nguyen Ngoc Tuan, Nguyen Duc Thinh. Evaluation of excess content of antibiotics Tetracycline and Cloramphenicol in food samples by using High Pressure Liquid Chromatography (HPLC). Journal of Chemical, Physical and Biological Analysis, Vol. 13, No 1, pp39-40, 2008.
57. Nguyen Giang, Nguyen Ngoc Tuan, Truong Minh Tri, K. Shiraishi. Daily penetration leval of Ca, Cu, Fe, Mg, Mn and Zn via food. Journal of Chemical, Physical and Biological Analysis, Vol. 13, No 2, pp.122-127, 2008.
58. Tran Huu Phat, Le Viet Hoa, Nguyen Tuan Anh, Nguyen Van Long. High Temperature Symmetry Non-Restoration And Inverse Symmetry Breaking in the $Z_2 \times Z_2$ Model. *Vietnam Communications in Physics*, **18**, No 1 (2008).
59. Tran Huu Phat, Nguyen Tuan Anh, Nguyen Van Long, Le Viet Hoa. On the phase transition in stable quark model. J of Nuclear Science and Technology, No 2, 2008.
60. Vuong Huu Tan, Tran Tuan Anh, Nguyen Canh Hai, Pham Ngoc Son. Neutron capture cross section measurement of ^{69}Ga, ^{71}Ga and ^{160}Gd on filtered neutron beams. J of Nuclear Science and Technology, No 1, 2008.
61. Vuong Huu Tan, Tran Tuan Anh, Nguyen Canh Hai, Pham Ngoc Son, Tokio, Fukahori. Measurement of Neutron capture cross sections of ^{139}La, ^{152}Sm and ^{191,193}Ir at 54kEV. J of Nuclear Science and Technology, No 2, 2008.
62. Le Xuan Tham. The first time two musrom species: *Lignosus sacer (Fr.) Ryv. And accocephallum hartmannii (Cooke) Nunez & Ryv. were found in Vietnam. Journal of Biology, special number.* .
63. Hoang Thi My Linh et al. *Estimation of genetic changes in rice mutants after gamma irradiation using RAPD and RAMP markers***.** Journal of Nuclear Science and Technology.
64. Nguyen Duc Thanh, Le Thi Bich Thuy, Dang Thi Minh Lua. Selection of drought resistant mutant in rice using DNA markers. J of Nuclear Science and Technology, No 1, 2008.

3.3 International Conference

65. Nguyen T.K.D., Nguyen P.T., Pham N.K., Pham L., "Determination of toxic trace elements in Curcuma-longa using ICP-MS", accepted for publishing in the 3rd Conference IUPAC on "Trace Elements in Food", Roma, Italy, April (1-4) 2009.
66. R.Ludwig, and Nguyen T.K.Dz. "High Temperature HPLC Stationary Phases for Molecular Recognition based on metal Oxides, Workshop on the Development of Modern Analytical Methods", Institute for Energy and Environ. Technology, Duisburg, Germany, 23rd April, 2008.
67. Nguyen Tien Thinh, Le Van Thuc, Vo Quoc Bao, Use of in vitro flowering system in combination with irradiation technique for the study of plant mutation breeding, Proceeding of the FNCA 2008 International Workshop on Mutation Breeding, October 27-31, 2008, Dalat city, Vietnam, NSRA (Japan), VAEC, MEXT (Japan),

VAAS.

68. Phan Son Hai. Estimation of the concentration level of radionuclides and elements in coastal marine sediments at some areas in south of vietnam. *RCA/UNDP Project Final Meeting on Post-tsunami Environment Impact Assessment, 3-7 Nov 2008, Xiamen, China.*
69. Heetaek Chae, Chulgyo Seo, Jonghark Park, Cheol Park, Vinh L. Vinh. Conceptual Thermal Hydraulics Design of 20MW Multipurpose Research Reactor. Proceeding of the 16th International Conference on Nuclear Engineering ICONE-16, 11-15/5/2008, Orlando, Florida, USA.
70. H.S. Than, D.T. Khoa, N.V. Giai, E. Khan. Continuum properties of the Hartree-Fock mean field with finite-range interactions. *Proc. of Intern. Symp. on Phys. of Unstable Nuclei*, World Scientific, Singapore, 2008, p. 457.
71. D.C. Cuong and D.T. Khoa. Microscopic study of the inelastic alpha+12C scattering. *Proc. of Intern. Symp. on Phys. of Unstable Nuclei*, World Scientific, Singapore, 2008, p. 469.
72. V.T.Bac. Vietnam Country Report. Progress Assessment Meeting on the IAEA /RCA/RAS/7/015 Project "*Characterization and Source Identification of Particulate Air Pollution In the Asian Region*" Colombo, Sri Lanka, 25-29 August, 2008.
73. PHILIP K. HOPKE, David D. Cohen, Bilkis A. Begum, Swapan K Biswas, Bangfa Ni, Gauri Girish Pandit, Muhayatun Santoso, Yong-Sam Chung, Perry Davy, Andreas Markwitz, Shahida Waheed, Naila Siddique, Flora L Santos, Preciosa Corazon B. Pabroa, Manikkuwadura Consy Shirani Seneviratne, Wanna Wimolwattanapun, Supamatthree Bunprapob, Thu Bac Vuong, and Andrzej Markowicz. Urban Air Quality in the Asian Region. **2008** AAAR Annual Conference. October 20–24, 2008 • Rosen Shingle Creek • Orlando, Florida.
74. Nguyen Kien Chinh et al. *Use of Isotope Techniques to study the Interaction between reservoir water and shallow groundwater*. RAS/8/104 Mid-term Review Meeting, Chiangmai, Thailand, 3-2008.
75. Le Xuan Tham. *The speciation of Tomophagus in Ganodermataceae. Proc. The 5th Meeting of East Asia for Collaboration on Edible Fungi*. September 17-20, 2008. Kyushu University Research and International Exchange Plaza, Fukuoka, Japan.
76. Nguyen Van Mai et al. *Study and establish testing procedures to ensure radiation safety & technical quality criterions of radio-therapy machines of radio-therapy hospitals of Hochiminh City*. 8th Asia – Oceania congress of Madical Physics & 6th South – East Asian Congress of Medical Physics, ChoRay Hospital October, 2008.

3.4 Domestic Conference

77. N. T. Ngo, N. T. Binh, N. V. Phuc, Truong Y, L. N. Sieu, N. M. Sinh and L. N. Chung. Preconcentration procedure of sea-water samples at the field for the simultaneous determination of radionuclides activity of Sr-90, Cs-137, Ra-226, ^{239,240}Pu, U and Th. Science Conference in Dalat University, 2008.
78. Pierre Darriulat. Black holes: recent advances, Proceeding of Theoretical Physics in Da Nang 2008.

TUYỂN TẬP
BÁO CÁO CÁC CÔNG TRÌNH KHOA HỌC
NĂM 2008

BAN BIÊN TẬP